DEVELOPMENT OF A 3-DIMENSIONAL CHEMICAL TRANSPORT MODEL BASED ON OBSERVED WINDS AND USE IN INVERSE MODELING OF THE SOURCES OF CCl_3F

by

Natalie Marie Mahowald

B.S. Physics, A.B. German, Washington University
(1988)

M.S. Natural Resource Policy, University of Michigan
(1993)

Submitted to the Department of Earth, Atmospheric and Planetary Sciences
in partial fulfillment of the requirements for the degree of

DOCTOR OF PHILOSOPHY
IN METEOROLOGY

at the

MASSACHUSETTS INSTITUTE OF TECHNOLOGY

March, 1996
[June 1996]

@Massachusetts Institute of Technology 1996
All rights reserved

Signature of Author_____
Center for Meteorology and Physical Oceanography
March, 1996

Certified by_____
Ronald G. Prinn
Professor of Atmospheric Chemistry
Thesis Supervisor

Accepted by_____
Thomas H. Jordan
Head, Department of Earth, Atmospheric and Planetary Sciences

MASSACHUSETTS INSTITUTE OF TECHNOLOGY
WITHDRAWN
APR 26 1996
MIT LIBRARIES

DEVELOPMENT OF A 3-DIMENSIONAL CHEMICAL TRANSPORT BASED ON OBSERVED WINDS AND USE IN INVERSE MODELING OF THE SOURCES OF CCl_3F

by

NATALIE M. MAHOWALD

Submitted to the Department of Earth Atmospheric and Planetary Sciences on April 4, 1996 in partial fulfillment of the requirements for the degree of Doctor of Philosophy in Meteorology

Abstract

The surface fluxes of many radiatively and chemically important species are uncertain to a factor of 2-3, e.g. carbon dioxide or methane [IPCC, 1994]. In order to gain more information about the sources and sinks, inverse methods have been used in combination with chemical transport models and observations of the concentrations of the trace gases at the surface [e.g.Hartley and Prinn, 1993]. These inverse methods rely critically upon the ability of the chemical transport model to accurately simulate the transport in the atmosphere. The goal of the thesis was the development of a chemical transport model (CTM) based on analyzed observed winds capable of simulating the transport of trace gases accurately enough to use an inverse method to determine the surface sources of important gases. The model was developed to be used with forecast center winds, either European Center for Medium-Range Weather Forecasting (ECMWF) or National Meteorological Center (NMC) reanalyses. These winds represent a combination of meteorological observations as well as numerical weather prediction model outputs, and represent the best information we have about the state of the global atmosphere at a given time. Unfortunately, the forecast centers do not archive mixing coefficients for important sub-grid scale mixing processes, so that the CTM must be capable of deriving both boundary layer mixing and moist convective transports. In the model developed here, which we name the MATCH model (Model of Atmospheric Transport and CHemistry), there is the ability to derive moist convective transport using one of three schemes: Hack [1992], Tiedtke [1989] or the Pan [NMC, personal communication, 1995] schemes. The non-local boundary layer scheme from Holtslag and Boville [1992] is used. The model is capable of model simulations at either T42 (approximately 2.8 by 2.8 degrees), with 19 layers for the ECMWF data or at T63 (approximately 1.8 by 1.8 degrees) with 28 vertical layers for the NMC reanalysis data.

The ability of the model to simulate interhemispheric transport, the seasonal cycle in transports and synoptic scale events is explored by comparing simulations of ^{222}Rn and CCl_3F with observations at surface stations (and upper level data where available). The model in general compares quite well with observations using either the ECMWF or NMC data. However, the ECMWF-based model results indicate too strong of an interhemispheric gradient in the CCl_3F, which is not seen in the NMC-based model results.

The model is used in conjunction with an inverse method (recursive weighted least squares) to

determine the sources of CCl_3F using in the model either the ECMWF or NMC meteorological data. Here, the emissions of CCl_3F are reasonably well known for the period considered (1990-91) and global CCl_3F measurements are available from two networks, so that this serves as a test of the ability of the model to be used in such an inverse methodology. The results showed mixed success: the inverse method and the model, using NMC winds, could deduce the correct global total emissions, and hemispheric total emissions, but was unable to distinguish between emissions from similar latitudes.

Acknowledgments

Completing my doctorate at MIT was not only a good educational experience, but also an enjoyable way to spend 4 1/2 years. This is due in a large part to my advisor Ron Prinn, who managed to provide me with scientific motivation as well the freedom to make and learn from my own mistakes. I would like to thank him for his unrelenting support of me and for his scientific guidance. I also benefited greatly from the insight and guidance from Phil Rasch, my mentor at NCAR, without whose collaboration this thesis would have not been the same, and certainly my enjoyment of it would have been less. I was lucky enough to be provided with an excellent committee and I would like to thank them for their contribution to my education: Guy Brasseur, Kerry Emanuel, and Alan Plumb.

Numerous colleagues at MIT and NCAR helped make my graduate education scientifically more interesting and generally enjoyable. All my fellow graduate students at MIT contributed in many tangible and intangible ways to my education, especially at Tea and Peer Hour, on the volleyball court, soccer field and hockey rink. At NCAR, lunch time discussions with my colleagues under the flatirons were truly inspiring. Trying to thank each of my friends and family members for their support would double the size of this already too long document, but I could not have done this without their companionship.

I would like to thank Brian Eaton for his computer guidance and sense of humor. I would like to thank the scientists at NCAR for allowing me to use the online and offline CCM2. I would like to thank Kerry Emanuel for his suggestions regarding the inverse thermodynamic scheme. I would also like to thank Martin Heimann for copies of the Tiedtke-TM2 model; Max-Planck-Institut fur Meteorologie in Hamburg for a copy of the EC-Tiedtke scheme; Kerry Emanuel for copies of the Emanuel scheme; Chien Wang for 2-dimensional model results; Bert Holtslag for a copy of the new non-local boundary layer scheme; and W. Pan at NMC for a copy of the NMC reanalysis moist convective algorithm. Discussions with Dana Hartley, Bert Holtslag, Jim Hack, Byron Boville, Chien Wang, Brian Eaton, Kevin Trenberth, Mark Lawrence, Paul Crutzen, Martin Heimann, Hans Feichter, John Mulquiney, Carl Wunsch, W. Pan, and Jeff Berry were also very useful. Data was provided by European Center for Medium Range Weather Forecasting and the National Meteorological Center. Data for CEPEX was very kindly provided by the Center for Clouds, Chemistry and Climate at the Scripps Institute of Oceanography. Constituent observations were kindly provided by J. Elkins, R. Larsen, G. Polian, and Stuart Whittlestone.

Part of this work was conducted while at the National Center for Atmospheric Research and the Center for Climate, Clouds and Chemistry, both supported by the National Science Foundation. This work was supported by a NASA Global Change Science Fellowship to N.M.M., the National Science Foundation (ATM92-16340 to MIT and ATM 9405024 to the Center for Clouds, Chemistry and Climate at Scripps Institution of Oceanography), and NASA (Grant NAGW474).

Table of Contents

Chapter 1:
Introduction

Substantial scientific efforts are currently directed towards understanding the effect of human activity on the earth's atmosphere. These efforts revolve around two main issues: (1) the possibility of warming of the planet due to the anthropogenic emissions of gases which change the radiative budget of the atmosphere and (2) the depletion of the ozone layer due to industrial emissions of chlorofluorocarbons. In both cases, the cause of concern is that the relevant trace gases are observed to be increasing in the atmosphere, apparently due to anthropogenic emissions.

Unfortunately, the surface sources of several important trace gases (e.g. carbon dioxide, methane, nitrous oxide) are not well constrained. Many of the these species can be directly emitted by human activity, or their emissions can be indirectly affected by human action, such as land use. In both cases the sources are highly variable in space and time and accurately estimating regional and global emissions is a major challenge in atmospheric chemistry.

Broadly speaking, there are two methods of determining the global surface sources of important trace gases. First, the more traditional *in situ* flux measurements are used to estimate surface fluxes (e.g. for methane and nitrous oxide: Bartlett et al. [1985), Cicerone et al. [1981, 1983], Crutzen et al.[1986], Holzapzel-Pschorn et al. [1986], Seiler et al. [1984, 1984], and Schutz et al.[1989]). The measurements are made at individual sites, and then global emissions are estimated from industrial or land cover information. This method has very large uncertainties. For example to estimate the emissions from wetlands, flux measurements are taken at one or more sites, estimates are made of the total amount of wetlands in a region, and the total emissions from wetlands are estimated. Unfortunately, emissions from wetlands are highly variable, and this type of methodology results in uncertainties of 50% in the total emissions from wetlands [IPPC, 1994]. As a example of the estimates of the global emission sources for methane are shown in Table 1.1. Uncertainties can be as large as a factor of two in different sources.

The second method is more global in nature and potentially more accurate: observed concentrations of the trace gases are used as well as information about the chemistry and transport of tracers to deduce the emissions. This is commonly referred to as an inverse problem, and recent studies have used this approach to estimate emissions of important trace gases using two-dimensional models(e.g. Cunnold et al, [1983, 1986], Prinn et al. [1990], Enting and Mansbridge [1989] and Brown, [1993]) as well as three-dimensional models [e.g. Hartley and Prinn, 1993, Mulquiney, 1995]. The Hartley and Prinn [1993] study demonstrated the importance of accurate transport in chemical transport models in conducting the inverse modeling. Deducing the source of atmospheric gases raises questions of error growth and the well-posedness of the question, since the atmosphere is diffusive in nature [Enting and Newsam, 1990; Plumb and Zheng, 1996] In addition, there have been several studies using trial and error approaches, which lack the rigor of inverse methods, but are simple to apply and understand [Tans et al., 1989; Fung et al., 1990]. There is considerable literature on inverse methods and their application to atmospheric sciences [e.g. Gelb, 1988; Daley, 1992]

Table 1.1: Emission Estimates for Methane

Source Description	Estimated Source Strength (Tg Methane/year)
Natural Sources	
Wetlands	115 (55-150)
Termites	20 (10-50)
Oceans	10 (5-50)
Other Natural Sources	15 (10-40)
Anthropogenic Sources	
Fossil fuel related	100 (70-120)
Entermic fermentation	85 (65-100)
Rice paddies	60 (20-100)
Biomass burning	40 (20-80)
Landfills	40 (20-70)
Animal Waste	25 (20-30)
Domestic sewage	25 (15-80)
Total	535 (410-660)

The three-dimensional inverse method approach is very appealing, due to the availability of high temporal resolution measurements of concentrations, capable of resolving pollution events. For example, Figure 1.1 shows data from the Macehead, Ireland site with the mean annual increases in concentration removed. Notice that the concentrations of all three species rise and fall at the same time. Wind direction analyses show that the low concentrations of species correlate with winds coming from the Atlantic Ocean, while high concentrations correlate with winds from Europe (referred to as pollution events). Pollution events of seven day duration are not uncommon and three-dimensional inverse methods should be capable of determining emissions of trace gases from the European continent, if the transport model can resolve and accurately simulate such events.

Unfortunately, currently available climate models, although able to resolve these synoptic scale events, do not get the right magnitude or seasonality. An analysis done by Hartley, et al. [1994] shows that the National Center for Atmospheric Research's (NCAR) Community Climate Model (CCM2) does not adequately simulate these high temporal resolution events. Although one would never expect a climate model to correctly predict the winds on any one day, climate models should behave correctly in a climatological sense and one would expect that seasonal averages of

tracer transport would be correctly simulated. Notice, in Figure 2, that not only is the magnitude of the pollution events incorrectly simulated, but the seasonality of the events is wrong as well. This is apparently due to this model's placement of the storm track too far north [Hartley, et al. 1994].

Because inverse methods heavily rely on accurate transport [Hartley and Prinn, 1993; Mulquiney, 1995], a model which more accurately predicts concentrations at monitoring sites is crucial. Another approach to determining the transport of the tracers is to use actual observations of winds rather than climate model winds to calculate advection. This is made possible by the availability of analyzed wind fields from forecast centers. These analyzed wind fields incorporate observations from radiosondes, satellites and surface observations, as well as integration of primitive equation models. Because the forecasts are constantly being compared to actual conditions and the initial conditions are very important for adequate forecasts, the procedure which calculates the analyzed wind fields should be fairly accurate and certainly superior to climate models.

However, no chemical transport model can expect to simulate the atmosphere perfectly. In addition, there is substantial dilution occurring in the atmosphere, reducing the ability of the model to determine the distribution of emissions. Thus, it is not clear that inverse methods will be able to derive emissions which are unique and correct. This thesis will consider the sensitivity of the inverse method to errors in the transport model, and attempt to determine the sources of a constituent whose emission are relatively well known (CCl_3F), thus testing the combination of the transport model, inverse method and observational network.

The goal of this thesis is to develop a chemical transport model capable of simulating tracer transport using observed winds with an accuracy sufficient to do inverse modeling studies of the sources of radiatively and chemically important trace gases. While the best information we have about the state of the atmosphere comes from forecast center analyses, these analyses do not include information about the transport in subgrid-scale mixing in the boundary layer or in cumulus convection. Thus, Chapter 2 addresses the issue of how to choose a moist convective scheme for inclusion in a chemical transport model based on observed winds. Chapter 3 describes the development of the model in collaboration with the National Center for Atmospheric Research. Once the model was developed, simulations with the model using ^{222}Radon are compared to observations in Chapter 4, while CCl_3F observations are compared to model simulations in Chapter 5.

Next, we considered the application of the model to inverse modeling studies of the regional magnitudes of surface sources of trace gases in the atmosphere. In order to test an inverse methodology, we used the CCl_3F simulation from Chapter 5. For CFC-11, the sources are relatively well known, and we can evaluate whether the model and inverse method in combination can calculate sources for CFC-11 which are consistent with our current best estimates. Chapter 6 describes the inverse method used for this study and applies it to the sources of CFC-11 to test the consistency of the inverse method. A summary of, and conclusions from this thesis are given in Chapter 7.

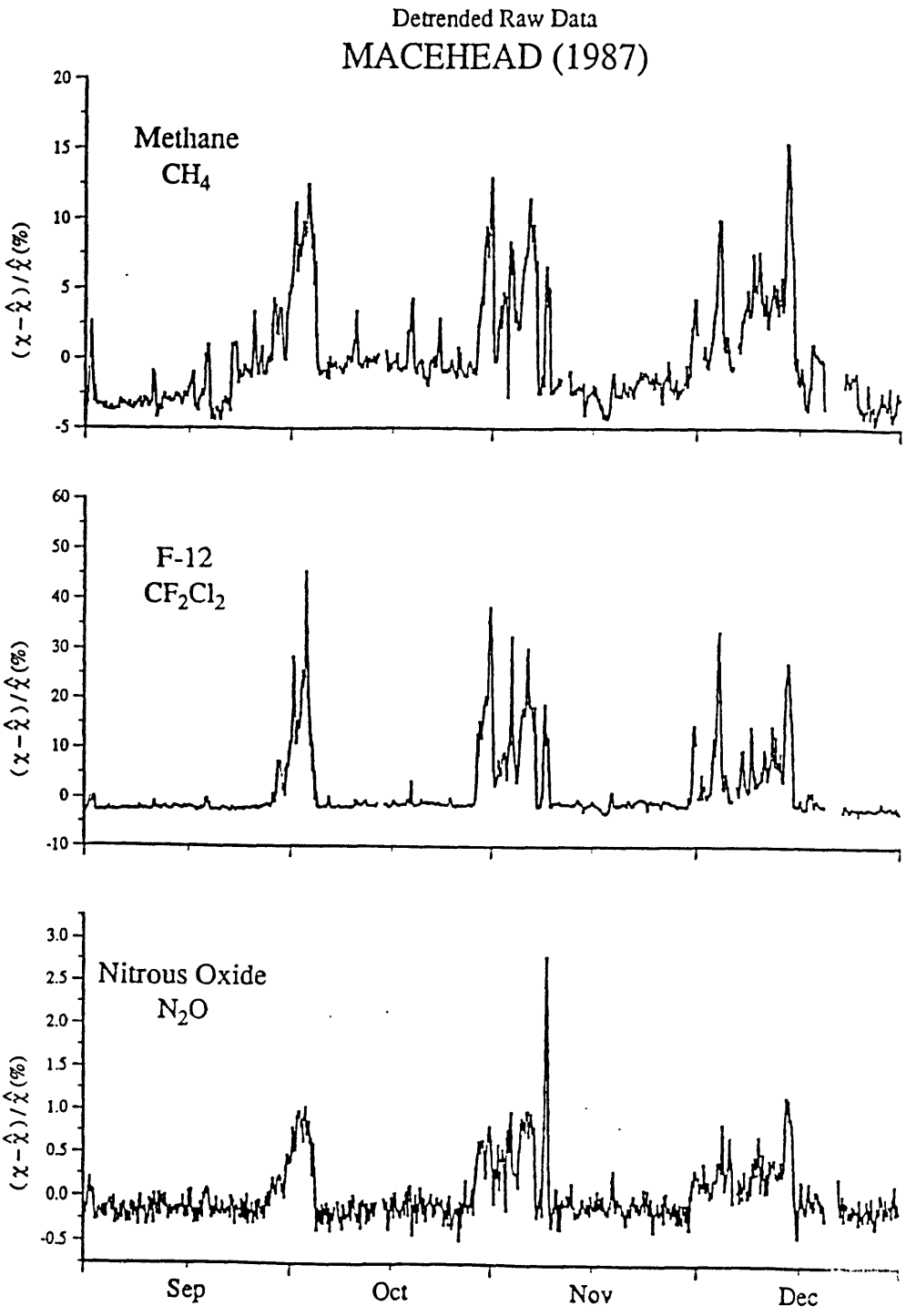

Figure 1.1: Detrended raw data from Macehead, Ireland measured during 1987 for the ALE/ GAGE network. Individual synoptic pollution events due to circulation of air off Europe can be seen as peaks in the concentrations. In between pollution events is relatively clean air circulated off the North Atlantic [Cunnold, et al., 1994, Prinn, et al., 1983].

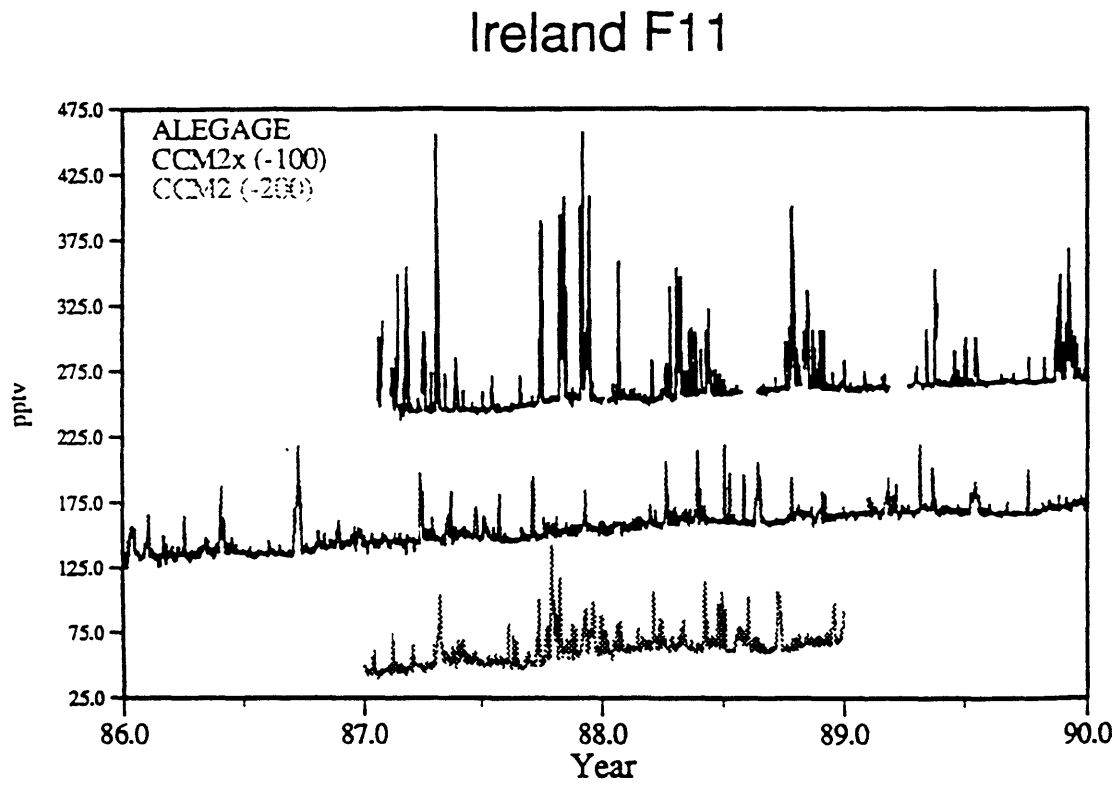

Figure 1.2: Comparison of ALE/GAGE observations to modeled output from two versions of the CCM2. The model results have been shifted down by the amount in the legend to allow for an easier visual comparison. Taken from Hartley [1992].

Chapter 2:
Cumulus Parameterizations in Chemical Transport Models

2.1.0 Introduction

In this chapter we report the results of a study of several convective schemes elucidating their strengths and weaknesses for use in three-dimensional transport models. Most of the work in this Chapter has been published [Mahowald, et al., 1995, copyright American Geophysical Union, included with permission of American Geophysical Union]. Some new unpublished material appears in section 2.2.5. Three-dimensional global chemical transport models (CTMs) are increasingly being used in the study of a variety of important scientific questions (for example, global radiative forcing by trace gases and aerosols). A large uncertainty in these models is the vertical transport due to subgrid scale processes such as boundary layer mixing and convective transport. These processes can move highly polluted surface air parcels into the upper troposphere within minutes, while the polluted parcels might take months to reach the same altitude (or isentropic surface) if only adiabatic processes (such as the adiabatic portion of frontal action in the mid-latitudes) or turbulent diffusion were operating. This is because adiabatic processes cannot, by definition, move parcels to a different isentropic surface. The importance of subgrid scale transports, especially moist convection, in redistributing trace gases in the vertical is shown to be important from both observations as well as model studies [e.g. Chatfield and Crutzen, 1984; Dickerson, et al., 1987; Brost and Heimann, 1991; Pickering, et al., 1992]. While there is agreement that subgrid scale processes are important, there is little agreement on an appropriate method of parameterizing these processes, especially moist convection [e.g. Emanuel and Raymond, 1993]. Much of the work on parameterizing moist convection has emphasized the transport of heat and moisture, without considering the effectiveness of these schemes for other trace gases.

There are several different global chemical tracer models currently being used in the scientific community, some using the winds generated by GCMs [e.g. Prather, et al., 1987 and Rasch et al., 1994], while others use the winds from the forecast centers [e.g. Heimann and Keeling, 1989]. The chemical transport models using winds from forecast centers have the advantage that they can recreate the tracer transport for specific days. In addition, the transport by winds generated by climate models is often not representative of the atmosphere [Hartley, et al 1994]. Using analyzed data from forecast centers should increase the accuracy of the large scale transport. Unfortunately, fields such as convective mass flux are not currently archived as a standard product. In order to include the transport of convective mass fluxes in a chemical transport model based on meteorological observations, two approaches can be taken: either to reanalyze the winds from the original observations and archive the mass fluxes, or recreate the mass fluxes from the available data. We are attempting to do the latter.

In attempting to recreate mass fluxes from the data available from the forecast centers, we have the advantage of not having to integrate a forecast model and assimilate data, which is a time-consuming process. We also have substantial amounts of data already available to us. However, the process of recreating mass fluxes is not without hazards. The winds, temperature and humidity structure available from the forecast centers may be very dependent on the convection scheme

used in the original forecast model and the assimilation model. This paper will also consider how well we can recreate mass fluxes from the available data.

Although the CTMs use different convective parameterizations, few studies have attempted to intercompare the sensitivity of the results of a CTM to the convective scheme used [exceptions are Brost and Heimann, 1991; Brost and Chatfield, 1989]. In 1993, the World Climate Research Programme (WCRP) sponsored a workshop to intercompare a large number of CTMs, many of which differed in their formulation of convective transport. They found substantial differences in the vertical profiles of radon calculated using the different models [*Prather,* personal communication, 1993].

The purpose of this study is two-fold: 1) to choose a moist convection scheme for use in a new CTM driven by forecast analyses (with its numerics based on the off-line version of the CCM2 (Community Climate Model) developed in Rasch, et al., 1994) and 2) to examine the uncertainty in the vertical profiles of trace gases to the moist convective parameterization chosen. We also consider two boundary layer schemes and the sensitivity of the tracer concentrations to them.

The process of choosing a "better" moist convective scheme is not straightforward, since different schemes have different advantages. Here, we attempt to chose a convective scheme based on three criteria: 1) quality of the results relative to observations, 2) realism of the physics and related considerations, and 3) computational efficiency. The computational efficiency is calculated by the amount of time it takes to run the simulations, and is the most straightforward criterion. More subjective are considerations such as how physically based a scheme is, what scheme was used in the forecast center's model, etc. The most important criterion is the quality of the results as judged by comparisons with observations, and most of this paper will discuss the tests used to examine the quality of the moist convective transports from the different schemes.

The quality of the results from the different schemes is not an easy issue to characterize. Obtaining tracer distributions as similar as possible to observations is an obvious goal in choosing a subgrid-scale parameterization for a CTM. The best test of the different schemes in combination with the model would be to compare results of 3-dimensional computer simulations with observations. However, 3-dimensional simulations are costly, and high quality 3-dimensional observations are in short supply. Therefore, 1-dimensional simulations are used here to document the relevant basic characteristics of the different schemes. In future studies, 3-dimensional simulations are intended to be conducted with the two most promising moist convective schemes, chosen from the larger set considered here. In addition, there is a lack of adequate observations to determine definitively which parameterization is better. A single vertical profile of a constituent does not provide enough information for a complete examination, even if the chemical sources and sinks of the trace constituent are known exactly.

The tests used in this study are described in detail in the later sections. Briefly, we look at mid-latitude summer convection, tropical oceanic convection and tropical continental convection. For each type of convection, we compare the behavior of the different schemes against each other and the observations. We also conduct two sensitivity tests. The first uses transport fields archived from the NCAR CCM2 to drive the 1-dimensional column model for transporting tracers with a surface source and a range of atmospheric lifetimes. This calculation also provides some insight into how difficult it is to reproduce the convective rates computed in a comprehensive

atmospheric model (e.g. a numerical weather prediction model (NWP) or a general circulation model (GCM)) using another model driven by the GCM or NWP output. The second calculation uses forecast center fields from the National Meteorological Center (NMC) and European Center for Medium-Range Weather Forecasting (ECMWF) to provide information on the simulation sensitivity to different driving fields.

2.2.0 Description of Subgrid Scale Parameterizations

We incorporate seven different convection schemes into our 1-dimensional trace constituent model. Most of these parameterizations have been used elsewhere for the convective transport of trace constituents. We have examined schemes with closures as varied as moisture convergence, conditional instability, and the potential temperature budget. The cloud models used in the convective parameterizations range from quasi-"diffusive" (moving tracers only one or two levels at a time, like the Hack [1994] scheme), to "entraining plume" types which can move a parcel from near the surface through the depth of the troposphere (e.g. the Tiedtke [1989] scheme, the Feichter-Crutzen [1990] scheme and the inverse thermodynamic scheme (described in this paper)), to "episodic mixing" schemes [Emanuel, 1991]. Thus, although this study does not include every different parameterization currently used or proposed, it does include a wide variety of schemes. Several of the schemes (Emanuel, Hack and Tiedtke-EC) considered here are meant to be used in an interactive GCM as opposed to an offline CTM as our 1-dimensional model. The Emanuel and Hack schemes are especially sensitive to the stability of the meteorological input and they are implemented in our model somewhat differently than in a GCM as described in Sections 2.1 and 2.3. The Tiedtke scheme was less sensitive to the stability of the fields, as discussed in Section 4.0.

While the emphasis of this study is to evaluate moist convective parameterizations, we have also compared two boundary layer schemes: a complicated non-local model and a simple model assuming adiabatic mixing within the boundary layer. A thorough investigation of boundary layer schemes is beyond the scope of this paper, but inclusion of these two very different schemes gives additional information on the sensitivity of trace constituent calculations to subgrid-scale parameterizations.

In the following sections we briefly describe the convective parameterizations used in the study, with references to more thorough descriptions for those schemes which have previously appeared in the literature.

2.2.1 Emanuel

The Emanuel episodic mixing scheme [Emanuel, 1991] is based on the idea that clouds are not homogeneous in nature, with a single entraining and detraining updraft. Instead, the more basic elements of convective transport are the subcloud-scale drafts, rather than the clouds themselves.

The updrafts within a grid-box are considered to originate in the lowest layer of the model and they are lifted unmixed up to a level i, which lies between the lifted condensation level and the level of neutral buoyancy for the undiluted parcel. A portion of the condensed water is assumed to precipitate, and can reevaporate into an unsaturated downdraft. The remaining cloudy air mixes at

level *i* and is moved to its level of neutral buoyancy, which can lie above or below level *i*. The updraft mass fluxes are determined so that they drive the mass fluxes toward a state of quasi-equilibrium with the large scale forcing. The downdraft mass fluxes are unique functions of the updraft mass fluxes.

The parameterization is driven by the initial temperature and moisture profiles, as well as the large scale forcing terms for these fields. The large scale terms considered in this study are the horizontal and vertical advection of temperature and moisture, and their surface fluxes. The radiative forcing term for temperature should be included, but was not available from the forecast center analyses, and thus was only used when CCM2 archived fields were used as input to the 1-dimensional model.

Because this parameterization is meant to be run interactively in a climate model, and the stability of the temperature/humidity profile is very important, it is necessary to "destabilize" these profiles to produce non-zero convective mass fluxes. This is done by "time-stepping" through a six hour period, and allowing the temperature and humidity profiles to be modified by the large scale forcing and convective scheme. This parameterization is still in the development stage, and the free parameters in the scheme have not yet been tuned (Emanuel, personal communication, 1994).

2.2.2 Feichter-Crutzen

An empirically based scheme using a simple plume-type cloud model was developed by Feichter and Crutzen [1990] for moist convective transport in the "MOGUNTIA" model. This scheme uses an empirically derived vertical structure for the updrafts and the amount of precipitation to deduce what the mass fluxes must have been to produce the specified amount of rainfall [Austin and Houze, 1973]. The parameterization is driven by the temperature and moisture profiles and the precipitation. Basically, the Feichter-Crutzen scheme calculates the amount of precipitation clouds of different heights with a unit mass flux could produce, weighted by the forecasted amount of precipitation for that gridbox and a statistical distribution of cloud heights.

This scheme assumes that the most important questions for identifying the impact of convection on tracer distributions are the following: 1) when and where do convective events occur? 2) what is the vertical extent of the clouds?, and 3) what is the magnitude of the vertical mass flux? This scheme assumes that most of the mass flux due to convection occurs in clouds which precipitate.

The parameterization assumes that convection can be represented as a set of entraining plumes. The profile for the mass fluxes are a function of plume height, and is prescribed following Austin and Houze [1973]. Entrainment rates are also prescribed. The mass fluxes for each plume is scaled to account for a fraction of the prescribed precipitation rate (as described below).

The precipitation efficiency is the portion of condensed water which precipitates and is a free parameter in the scheme. In this study the precipitation efficiency is assumed to be 100%, since this achieved results that appeared to be the most consistent with the CCM2 archived fields, although this may be related to the fact that CCM2 has a 100% precipitation efficiency. Feichter and Crutzen used 33% efficiency, which is in the recommended range (10-50%) of Austin and Houze [1973]. Based on our sensitivity studies, changing the precipitation efficiency to 33% should quantitatively but not qualitatively change the results of this study.

An important parameter in the model is the depth of convection, which is implemented slightly differently here than in Feichter and Crutzen [1990]. In this implementation of the model, the top of the deepest convection is set to approximately the tropopause height in mid-latitudes (200 mb), and the input precipitation is divided statistically between clouds of different height. The precipitation is originally divided amongst the various cloud heights by a formula which assigns most of the precipitation to the highest clouds, similar to Feichter and Crutzen [1990] and as observed in Austin and Houze [1973]. For example, in a typical case in the mountains where the surface pressure is 880 mb and there are 19 levels (where the 19th level is the surface level), the convection extends between levels 18 and 9. Clouds having their cloud top at level 9 are assumed to have produced 25% of the precipitation. Clouds having their cloud top at level 10 and 11 are assumed to have produced 16% of the precipitation each, while clouds with cloud tops between levels 11 through 16 are assumed to have produced 8% of the precipitation each. For each cloud of a given height, a calculation is made of how much precipitation could be produced from that cloud. If no, or very little, precipitation could be generated by that cloud, then that cloud is not considered to have existed in the atmosphere, and the precipitation is redistributed between the remaining cloud heights.

To determine trace gas transport, the convective mass fluxes calculated as described above are used in a simple "entraining plume" cloud model. Mass is considered to be entrained into the cloud when the mass fluxes are increasing with height and detrained when the mass fluxes are decreasing. To improve computational efficiency, only one bulk plume is considered when transporting the trace gases, and it has the sum of the mass fluxes from all the clouds calculated using the above described method.

2.2.3 Hack

The Hack scheme [Hack, 1994] is a stability-dependent mass flux representation of moist convective processes that is used in the NCAR CCM2. This scheme redistributes heat, moisture, and trace constituent mass through a set of idealized cloud elements each consisting of three levels. In the bottom level, only entrainment can occur; in the middle level, condensation and detrainment occurs; and in the top level, detrainment may occur. The cloud elements act to produce convective mass fluxes when there is conditional instability and when saturation will occur if the parcel is lifted up one level. The scheme is successively applied to each level in the model. Because the scheme lifts a parcel at most two levels and mixes it completely with the environment, it is not possible for mass to be transported from the bottom level to the top level without substantial dilution. For this reason we characterize it as a "diffusive" scheme (as opposed to the "entraining plume" schemes).

The CCM2 data used to drive our 1-dimensional model is archived immediately following the operation of the convective parameterization in CCM2. Because of this, mass fluxes calculated by us from this archived data are expected to be much weaker than were present in the original model, despite the fact that the same scheme is used in both cases. The Hack scheme also produces very weak convection when driven by analyzed data, perhaps for similar reasons. In order to produce mass fluxes using this scheme from CCM2 output or forecast center analyses, some modifications were therefore made. The first modification studied was to add perturbations to the cloud updrafts in the scheme at every level, to add instability. These perturbations were

calibrated using the CCM2 archived fields so that the 1-dimensional model mass fluxes were similar to the CCM2 calculated mass fluxes from the same time step.

An alternate modification of the code was to use the Hack scheme in a "time-stepping" mode, as described above for the Emanuel scheme. The large scale forcings such as advection and surface fluxes are allowed to destabilize the temperature and humidity profiles. In a later section we will discuss how these two modified Hack schemes compare to the original Hack scheme.

2.2.4 Inverse Thermodynamic

In this approach, the evolution of a conserved variable is used to determine what convective mass fluxes the forecast model predicted between each set of 6 hourly data as a residual in the thermodynamic equation. This approach has previously been used to calculate mass fluxes for observational data using moist static energy and water as the conserved variable [Emanuel, 1994; Yanai et al., 1973]. In this paper, virtual potential temperature has been used to determine what the convective mass flux would have to have been between the last time step and the current one. The virtual potential temperature is a conserved quantity (unless condensation occurs) and serves as a good proxy for density. The virtual potential temperature(θ_v)is defined by:

$$\theta_v = T\left(\frac{p}{p_s}\right)^{0.286}(1 + 0.608r) \tag{2.1}$$

where T is the temperature, p is the pressure, p_s is the surface pressure and r is the water vapor mixing ratio.
The equation for the conservation of virtual potential temperature is (similar to Arakawa and Schubert [1973], eq. 74):

$$\frac{\partial\theta_v}{\partial t} = -\hat{v}\cdot\nabla_H\theta_v - w\frac{\partial\theta_v}{\partial z} + R + M_c\frac{\partial\theta_v}{\partial z} + D\,(\theta_v(\text{cloud}) - \theta_v(\text{env}) - Ll) \tag{2.2}$$

where t is the time, $\hat{v}$ is the horizontal velocity, ∇_H is the horizontal La Placian, w is the vertical velocity, R is the radiative heating, M_c is the upward convective mass flux, D is the detrainment mass flux, $\theta_v(\text{cloud})$ is the potential temperature at the edge of the cloud, $\theta_v(\text{env})$ is the potential temperature of the environment, and Ll is the evaporative cooling due to detrainment of liquid water. Here, we assumed that the region of the gridbox where the virtual potential temperature differs significantly from the environment is very small. Thus, even though the cloud might cover a large area of the gridbox, the cloud's virtual potential temperature will differ significantly from the environmental virtual potential temperature only in the area of the updraft, which is a small fraction of the total gridbox area [Emanuel, 1994]. The latent heat of condensation does not appear in this equation, since the equation originated from looking at the thermodynamic balance *outside* of the cloud, which is assumed to be most of the area in a gridbox.

Several terms are ignored in this representation of a cloud that represent processes included in the forecast models: the heating from stratiform precipitation, and subgrid scale mixing by vertical turbulent diffusion outside of clouds. The inverse thermodynamic approach assumes that all the

heating is due to convective overturning and will over-predict the mass fluxes where these processes are important. With the CCM2 archived fields, our analysis shows that the contributions from stratiform precipitation and diffusion are small for the cases considered here. Also neglected is the reevaporation of falling rain, but this process is often neglected in climate and forecast models, and thus right or wrong, will not introduce errors when trying to recalculate the mass fluxes from the archived fields from the CCM2 output or ECMWF and NMC forecast analyses.

If we follow Emanuel [1994], we assume that the boundaries of the cloud include any area where there is liquid water. This definition of the cloud boundaries allows the last term (representing evaporative cooling) in equation (2) to become a part of the cloud virtual potential temperature term, without affecting the other terms. By defining the cloud differently than in Arakawa and Schubert [1974] (who assumed that liquid water could exist outside the cloud), we can avoid explicitly treating the liquid water in this equation. This gives the following equation:

$$\frac{\partial \theta_v}{\partial t}^v = (-\hat{v}) \cdot \nabla_H \theta_v - w\frac{\partial \theta_v}{\partial z}^v + R + M_c\frac{\partial \theta_v}{\partial z}^v + D(\theta_v(\text{cloud}) - \theta_v(\text{env})) \tag{2.3}$$

Next we define the edge of the cloud such that the virtual temperature at the edge of the cloud is close to the virtual temperature of the environment [Arakawa and Schubert, 1974, Emanuel, 1994]. This definition implies that the cloud updrafts are detraining at the level of neutral buoyancy, which is consistent with observations [Emanuel, 1994]. With this definition, the heating by convection can be considered to be due to the compensated subsidence which occurs outside of the convective cloud. The latent heat of condensation serves to make the updrafts buoyant, which forces the subsidence outside the clouds. We do not need to explicitly calculate the latent heat release to know the mass fluxes. This results in the following equation:

$$\frac{\partial \theta_v}{\partial t}^v = (-\hat{v})\,\nabla_H \theta_v - w\frac{\partial \theta_v}{\partial z}^v + R + M_c\frac{\partial \theta_v}{\partial z}^v \tag{2.4}$$

By knowing or estimating all the terms but the last, M_c can be calculated.This scheme is appealing in its simple approach to convection, but may not produce accurate mass fluxes for three reasons: 1) the terms which are ignored in the above equations may not always be small; 2) only net mass fluxes can be determined (updrafts and downdrafts may cancel) and 3) numerical errors may be large. The magnitude of the errors in using this scheme can be assessed by using data where the mass fluxes which produced the meteorological fields are known. In this paper this assessment is done using archived fields from the CCM2 model, where the mass fluxes are known. However, the mass fluxes represented here are the net mass fluxes, thus if there were an updraft and downdraft of equal magnitude, the mass transports would sum to zero, and M_c would be zero, but the tracers were transported by the updraft and downdraft mass fluxes. Because it calculates updrafts only, the Hack scheme used in CCM2 has a good chance to be accurately represented using equation (4), but the Tiedtke scheme used in the ECMWF forecast model does have downdrafts, which may therefore cause errors in the mass fluxes computed using (4).

Once the mass fluxes have been determined as described above, the tracer transport is accom-

plished using a simple plume-type cloud model, where entrainment occurs when the mass fluxes increase, and detrainment occurs when the mass fluxes decrease, as used in the Feichter-Crutzen scheme.

2.2.5 Pan Version of the Arakawa-Schubert Scheme

The NMC reanalysis model uses a simplified Arakawa-Schubert scheme developed at NMC by Pan and Wu [1995]. (Note that this is a different scheme than that used for the operational analyses used in this 1-dimensional study.) The original Arakawa-Schubert scheme is based on the quasi-equilibrium hypothesis, stating that the time rate of change of convective available potential energy (CAPE) is roughly zero. The original Arakawa-Schubert scheme had several different cloud types, indicating different heights to which moist convection would occur, and there was detrainment along the sides of the clouds, with a detrainment rate dependent on the depth of the cloud. The scheme required an inversion of a matrix, and was fairly computationally expensive.

The Pan scheme follows the work of Grell [1993] and Lord et al., [1982]. The closure for the scheme is that the CAPE relaxes back to a reference profile (from Lord, et al. [1982]) during one time step. Only one type of cloud, or cloud top height is included in this implementation, and there is entrainment only before cloud base, and detrainment at cloud top. The cloud base is chosen as the level with the largest virtual static energy, and the height of the cloud is determined by buoyancy. A modification was made to the scheme to insure that the convective mass fluxes out of a gridbox during one timestep could not exceed the mass in the gridbox. The cloud model type is a non-entraining plume.

2.2.6 Tiedtke

Two implementations of the Tiedtke scheme [Tiedtke, 1989] were included in the study. The first version derives from the formulation found in the ECMWF forecast model and the ECHAM3 model [Roeckner et al., 1992], and the second version is from the TM2 model [Heimann personal communication, 1992]. Hereafter, we refer to the former as the Tiedtke-EC version, and the latter as the Tiedtke-TM2 version. The EC version of the scheme has three types of convection: deep, shallow and mid-level, and includes an unsaturated downdraft. Deep convection is driven by moisture convergence in the entire column. Shallow convection is driven by moisture convergence in the boundary layer, and the mid-level convection will occur when there is upward motion creating conditional instability. A bulk entraining plume type cloud model is used for all convective types, and different entrainment and detrainment rates are used for the different types of convection. The updraft mass flux is proportional to boundary layer moisture convergence for the shallow and deep convection and the upward motion in the mid-level convection, while the height of convection is dependent on the buoyancy of the plume. A modification was made to the scheme so that the convective mass flux out of a gridbox during one time-step could not be greater than the total mass in the gridbox.

The TM2 version of the scheme is much simpler and more computationally efficient, with only deep and shallow convection, and without a downdraft. As in the EC version, the mass fluxes are

determined by boundary layer moisture convergence and the cloud extends upward until the plume is no longer buoyant.

2.2.7 Non-Local Boundary Layer Scheme

The non-local boundary layer scheme from CCM2 [Holtslag and Boville, 1993] calculates diffusion coefficients based on the diagnosed boundary-layer height and a turbulent velocity scale. The boundary layer height is determined by solving iteratively for the height at which the bulk Richardson number is a critical value. Because the assumption that the scale of the eddies is much smaller than the gradient scale is not a good approximation in large portions of the planetary boundary layer under unstable conditions, the non-local boundary layer scheme includes a counter-gradient term [Holtslag and Boville, 1993], which attempts to emulate the counter-gradient transport due to eddies as:

$$\overline{w'C'} = -K_c\left(\frac{\partial C}{\partial z} - \gamma_c\right) \tag{2.5}$$

where $\overline{w'C'}$ is the vertical constituent flux due to turbulent eddies, K_c is the coefficient of diffusion, $\frac{\partial C}{\partial z}$ is the vertical gradient of the constituent, and γ_c is the counter gradient term.

The counter gradient term is neglected in stable conditions, but under unstable conditions, the counter gradient term is dependent on the surface flux of the constituent, vertical velocity scale and the boundary layer height.

2.2.8 Adiabatic Boundary Layer Scheme

A simple mixing scheme is also investigated, in which the boundary layer when unstable is considered well mixed. The height of the boundary is defined by the highest level at which the virtual potential temperature is equal to the virtual potential temperature in the lowest level. The virtual potential temperature is a conserved quantity (unless condensation occurs) and serves as a good proxy for density. The virtual potential temperature(θ_v) was defined in equation (2.1). The scheme is formulated to mix trace constituents to a state of uniform mixing ratio when the boundary layer is diagnosed as unstable.

2.3.0 Modeling Studies

In order to identify the sensitivity of trace constituent vertical profiles to the fields used to drive the convective and boundary layer parameterizations, and to the parameterizations themselves, we have performed two sensitivity and three modeling studies. For reference these five studies are summarized in Table 2.1. A brief description follows to motivate the studies. The calculations are described in more detail in the following sections. First, we have conducted a sensitivity study using archived fields from the CCM2. This study seeks to identify the differences between mass

Table 2.1 Summary of Model Studies

Test	Purpose	Trace Species	Meteorological Dataset
Sensitivity Test with CCM2 archived data	1. Compare on-line and off-line mass fluxes 2. Estimate sensitivity of vertical profile to convective scheme 3. Test implementation of Hack and Inverse thermodynamic	4 species with surface sources and lifetimes of 11 years, 1 year, 1 month and 1 day.	10 days of CCM2 data at 3 locations (Venezuela, western Pacific and Nebraska) iterated over 365 times (total of 10 years of integration).
Sensitivity Test with ECMWF and NMC Datasets	Test sensitivity of vertical profile to the dataset chosen. (only 3 schemes were used).	Radon-222 (surface source and 5.5 day lifetime).	5 datasets at 3 locations (New Mexico, Indonesia and Kalahari): 1. T106 ECMWF hybrid, 2. T42 ECMWF hybrid, 3. T42 NMC sigma, 4. T42 ECMWF on pressure surfaces, 5.T42 ECMWF pressure data interpolated onto hybrid system. Use 10 days of data (June 1-10, 1991) and iterate 365 times.
Mid-latitude Summer Convection	Compare Rn-222 profiles to each other and Liu, et al. [1984] vertical profile.	Radon-222	T42 ECMWF hybrid dataset at 8 locations in western U.S.
Tropical Oceanic Convection (CEPEX)	Compare height of convection in modes to height of convection observed.	Look at Mass fluxes not species.	T42 NMC dataset at 4 closest locations during the entire day of the March 8 and April 3, 1993 storms in Central Equatorial Pacific.
Tropical Continental Convection (ABLE2A)	Compare Transport of tracer gas during 6 hour period	Carbon Monoxide (CO)--inert on this time scale	T42 ECMWF dataset at 4 closest locations and 2 times to the August 3, 1985 storm over Brazil.

fluxes calculated within a general circulation model and those calculated after the fact (in our 1-dimensional model for example). At the same time we illustrate the range in predicted trace constituent profiles resulting from the choice of convective scheme in the 1-dimensional model. In

the second sensitivity study we have used five different sets of forecast center analyses for the same period to examine the differences in the predicted convective mass transports when the model is driven with different forecast center analyzed datasets. In the subsequent three modeling studies, we compute and compare the mass transport of trace constituents using the eight convective and two boundary layer parameterizations under three different meteorological conditions: mid-latitude summer, tropical oceanic and tropical continental.

A simple one-dimensional column model is used to investigate the subgrid scale parameterizations. The trace constituent mixing ratios are calculated using the following equation

$$\left.\frac{\partial \chi}{\partial t}\right)_i = \left.\frac{\partial \chi}{\partial t}\right)_i^{\text{convection}} + \left.\frac{\partial \chi}{\partial t}\right)_i^{\text{diffusion}} \tag{2.6}$$

where χ is the mixing ratio of trace constituent, t is the time, and i is the vertical level in the model. Thus, the trace constituent mixing ratio is subject only to convective and diffusional processes in this 1-dimensional column model.
The column model reads in the fields required to drive the parameterizations. These fields are either extracted from CCM2 archived datasets or ECMWF or NMC analyzed datasets, and are typical of those distributed as standard products by operational forecast centers. The fields used by the 1-dimensional model are temperature, specific humidity, wind velocities, divergence of the winds, upward motion and the horizontal advection of temperature and specific humidity into that column. At the bottom level, orography (land or ocean), surface pressure, wind stresses, sensible and latent heat fluxes, temperature and specific humidity at 2 meters (10 meters for CCM2 archived fields) and precipitation are also available from the datasets.

2.3.1 Sensitivity to Meteorological Data

Off-line chemical transport models are typically driven by fields from either a general circulation climate model, or analyzed datasets from a forecast center. These datasets can differ substantially, because of differences both in the models, and whether and how the observations are used to improve the model output. Forecast centers routinely produce analyses, which are a combination of a previous forecast and observations. The procedures used at the forecast centers to combine the data and model forecasts attempt to optimize the analyses so as to match the observations and maximize forecast skill [Parrish and Derber, 1992, ECMWF Research Manual 1, 1987]. These datasets are not typically constructed to be optimal for driving an off-line transport model. Nevertheless they represent the most complete picture of the atmosphere that we have, and are therefore the best available data which can be used for this purpose. It is not clear how various analyzed datasets differ in their utility for driving an off-line model, and to the best of our knowledge, our study represents a first attempt to assess this issue

Historically, analyzed datasets have been distributed on a set of standard pressure levels. The datasets available on these standard pressure levels are not optimal for this type of modeling study for several reasons. First, the standard pressure levels intersect the surface, complicating the model formulation significantly. Most global models in use today utilize terrain following (so-called "sigma" or "hybrid") coordinates. Sigma coordinates follow the orography throughout the model, while hybrid coordinates follow the orography in the lower troposphere, but return to pressure surfaces far from the lower boundary. In addition the standard analyzed datasets do not provide sufficient resolution in the boundary layer to resolve many important atmospheric

features (e.g. see section 3.1b). Finally, previous studies of the ECMWF standard pressure level datasets have indicated problems with analyses on these surfaces [Trenberth, 1992].

Available to us were one year of ECMWF upper air data on "hybrid" surfaces, several years of ECMWF upper air data on standard pressure level surfaces, and approximately three years of National Meteorological Center (NMC) upper air data on "sigma" coordinates. Also available are surface datasets from both ECMWF and NMC for the last few years. The NMC surface datasets were preferred for this study, because they include all the variables necessary for all the seven chosen parameterizations. The upper air data are from the four-times-daily analyzed data sets, while the surface data set consists of the forecasted values for the next six hours as calculated by the NMC model.

In choosing the subgrid scale parameterization to be used in an off-line CTM, it might be considered desirable to use one which is consistent with that used in the original model which generated the driving meteorological data. ECMWF and NMC use different moist convective parameterizations, and the schemes used changed with time. Before 1989, they both used a Kuo [1973] type scheme, which does not provide a unique mass flux. In 1989, ECMWF switched to a Tiedtke [1989] scheme. The centers use different versions of the local-diffusion boundary layer schemes, where the diffusion coefficients rely on the local Richardson number [Kanamitsu, personal communication, 1993; ECMWF Research Manual 3, 1991].

The CCM2 archived fields used for the modeling studies are from the standard version of the CCM2, described in Hack, et al, [1993]. We used fields archived every 6 hours, representing instantaneous values. The standard version of the CCM2 has 18 vertical levels (using a hybrid coordinate system) and an equivalent horizontal resolution of 2.8 degrees by 2.8 degrees (T42 spectral resolution). The model uses semi-lagrangian transport of moisture [Rasch and Williamson, 1990], as well as the moist convective scheme from Hack [1994] and the non-local boundary layer scheme from Holtslag and Boville [1993].

2.3.1.a Sensitivity Tests with CCM2 input data

A sensitivity study indicating the differences between the various schemes was run using archived fields from the CCM2 model in the 1-dimensional model. The CCM2 convective mass transports have also been archived, and it is possible therefore to either use them directly within our 1-dimensional column model, or to compare the mass fluxes with those calculated from other archived fields. Our primary task in this sensitivity study is to see how accurately one can reproduce atmospheric behavior in an offline transport model using a dataset similar to that available from a forecast centers analyses.

We have combined this task with three others: 1) we have compared the profiles of trace constituents with different atmospheric lifetimes calculated with different parameterizations; 2) we have attempted to modify the Hack parameterization to be less sensitive to whether the driving fields are output before or after convection operates in the model; and 3) we have developed the inverse thermodynamic parameterization. The non-local boundary layer scheme is used with all the tests with the CCM2 data, with the exception of the tests of the Emanuel scheme and Hack scheme in the time-stepping mode which use the simple adiabatic boundary layer scheme due to

time constraints.

The driving fields come from a 10 day run from May 1 through 10 during a year of CCM2 integration. We consider three widely different locations -- at 9.8 N and 67.5 W over Venezuela (continental tropical convection), at 9.8 N and 135E over the western Pacific Ocean (marginal between tropical and sub-tropical convection) and at 42 N and 101 W over Nebraska (mid-latitude convection); and the input to the column model is 6 hourly instantaneous archived data at each location. Over this 10 day period within the CCM2, Venezuela had substantial convection, while the western Pacific and Nebraska locations had intermediate amounts of moist convection.

Four hypothetical chemical trace species were considered, each having a constant source at the surface, an initial vertical profile similar to that observed for methane; and chemical lifetimes of 11 years, 1 year, 1 month and 1 day, respectively. The surface fluxes of trace gases were calculated so the amount of trace gas mass stayed roughly constant. The column model was run out 10 years (by repeating over the same 10 days of meteorological data), so that the trace gases were approximately in equilibrium. The convective mass fluxes calculated by the models over a 10 day period and the average tracer profile over the last repetition of the 10 day period were used to compare the different moist convection formulations.

A 10 day period was chosen as appropriate for a sensitivity study of this nature. The CTM we plan to use with these parameterizations (with a 250 km horizontal resolution) will not be able to reproduce events on an hour by hour basis. However, this model should accurately reproduce events which have a week to 10 day ("synoptic") time scale.

Figure 2.1 shows the 10 day averaged vertical mass fluxes at Venezuela from the Hack scheme as archived from the CCM2 run and as derived using the identical Hack scheme run in the 1-dimensional column model. Significantly, the column model mass fluxes were derived using temperature and humidity fields archived after the CCM2 Hack convection scheme had operated. Despite using the same convective scheme, the mass fluxes from the column model are significantly smaller than the original CCM2 mass fluxes. This confirms our suspicion that the Hack scheme is very sensitive to conditional instabilities between two adjacent levels. Once the temperature and humidity profiles have been adjusted to be stable to moist convection, this scheme, not surprisingly, has difficulties in producing significant mass fluxes. It is not clear exactly how the moisture and temperature fields will be archived in analyzed datasets from forecast centers, but it is clear that this very strong sensitivity to relatively small changes in the column profile is an undesirable feature of the Hack scheme when applied our specific purposes. In an attempt to reduce this sensitivity we took two approaches.

In the first approach, perturbations to temperature and humidity in the updraft were added to produce an instability at the entrainment level of all the clouds in the column. Such perturbations are routinely added to the updrafts within the Hack convective parameterization to enhance the convection. (Recall that the Hack scheme uses a three level cloud that is consecutively is applied at each level in the column). The perturbations in the updraft at level i are proportional to the detrained cloud properties from the cloud originating at level $i+1$ (one level below level i). The second approach used a "time-stepping" approach, as described earlier in Sections 2.1 and 2.3, to produce instability in the column from the large scale forcing (advection, radiation and surface fluxes). Figure 2.1 shows the mass fluxes computed in the column model with these two

modifications to the Hack scheme. It shows for the column model that the mass fluxes using either modification are much closer to the mass fluxes derived in the CCM2 than those using the original scheme. Thus these two modifications are both used for further analysis.

The inverse thermodynamic scheme is a scheme based on the tendency equation for the virtual potential temperature (equation (4)). This scheme attempts to determine the mass fluxes calculated in the original model that produced the archived fields used to drive the off-line column model. The mass flux is equal to the residual of several comparable terms in this equation, and thus there exists potential for simple numerical error, as well as errors from neglecting terms. Using the CCM2 archived mass flux and other fields, it was possible to determine how large these errors might be and try methods for mitigating the errors. In analyzing individual times steps, it appeared that the mass fluxes tended to have errors that could be as large as 0.01 $kg/m^2/s$ at any one time, but tended to have opposite signs at different time steps. The approach used here to mitigate the numerical errors is to establish a minimum "threshold" mass flux, below which the calculated mass flux is considered to be equivalent to zero. This threshold was chosen to be 0.01 $kg/m^2/s$, based on the above assessment of error. Figure 2.2 shows the results with and without this threshold at the West Pacific location. Using this threshold the mass fluxes at specific time steps (not shown) and averaged over a 10 day period (shown) tend to look much more like the mass fluxes used in the CCM2 (and thus are the correct mass fluxes for the inverse thermodynamic scheme to determine).

The inverse thermodynamic scheme also has difficulty in the boundary layer, because we divide by the vertical derivative of virtual potential temperature, which is close to zero in the boundary layer. Since we are not interested in determining the overturning of the boundary layer with the inverse thermodynamic scheme, we only calculate the mass flux outside of the boundary layer in the scheme with a "threshold" value.

In Figure 2.2, which shows the 10 day average mass fluxes at the western Pacific location, notice that the CCM2 did not predict much convection, and no deep convection. The inverse thermodynamic scheme without a "threshold value" calculated non-zero mass fluxes in the middle to upper troposphere, while the inclusion of the threshold value reduced these mass fluxes significantly. The impact of these mass fluxes on trace constituent profiles is shown in Figure 2.3. Here, the vertical mixing ratio profiles are plotted for the four hypothetical gases discussed earlier. (Note that all these profiles use the bulk "entraining plume" cloud model (see section 2.2) not the "diffusive" cloud model described in Section 2.3.) Notice that the inverse thermodynamic scheme without a threshold value produces much more transport to the upper troposphere than the CCM2 mass fluxes (the "right answer"). However, the implementation of the threshold value in the inverse thermodynamic method improves agreement with the CCM2 mass fluxes so that now the profiles are very similar.

The trace constituent profiles resulting from all seven schemes are shown in Figures 2.4, 2.5 and 2.6 for the Venezuela, western Pacific and Nebraska locations, respectively. Each figure.shows the average equilibrium profile for the four different tracers with lifetimes of 11 years, 1 year, 1 month and 1 day, respectively. In a highly convective region, such as Venezuela, the vertical profiles of the long-lived species are not highly dependent on the convective parameterization used, but in a region that has intermediate convection such as over the western Pacific or Nebraska, the profiles vary considerably, even for long-lived species. In all locations, the tracer

profiles for the short-lived species, especially the 1 month tracer, display a high sensitivity to the parameterization chosen. The 1-day tracer remains mostly in the boundary layer, because due to the fact that convection does not occur every day, convection acts at time scales larger than 1-day in moving trace gases from the boundary layer to the middle and upper troposphere.

In summary, it seems possible to reproduce the convective behavior in an offline model that was seen in the original model if the off-line convection scheme is carefully constructed. This test shows that changing the moist convective scheme can produce very different trace gas profiles in a 1-dimensional column model. This has two implications for 3-dimensional models: 1) short lived trace gas profiles are likely to be highly sensitive to the moist convective parameterization chosen, and 2) long-lived tracers have less sensitivity, but may exhibit high sensitivity over intermediate convecting regions if the transport times of interest are short.

2.3.1.b Sensitivity to Different Forecast Center Analyses

Because there are several sets of forecast center analyses available to drive CTMs, a study of the sensitivity of the trace gas profiles to input meteorological data sets was conducted. A 10 day period in June, 1991 is used, since there is data available from 5 distinct forecast center datasets for the period. The datasets used in the study were 1) the ECMWF hybrid data at T106 horizontal resolution (1.8 degree by 1.8 degree), 2) the same data set truncated to T42 horizontal resolution (2.8 degree by 2.8 degree), 3) NMC sigma level data truncated to T42, 4) ECMWF pressure level dataset at T42 and 5) the ECMWF pressure level data set at T42 interpolated onto the ECMWF hybrid vertical coordinate system (thereby increasing the vertical resolution, especially in the boundary layer). The upper air data are available every 6 hours. The surface data used for all five simulations were the NMC surface data sets, also available every 6 hours. Three locations were simulated in this study: specifically sites in New Mexico (34N and 107W), Indonesia (0N and 120E), and the Kalahari desert (25S and 20E). A subset of the parameterizations were used to examine the sensitivity: the Feichter-Crutzen, Hack and Tiedtke-TM2 schemes. Due to time constraints, dataset 5 (ECMWF pressure level data interpolated onto hybrid coordinates) was only evaluated with the Tiedtke-TM2 model.

Radon (which is discussed in more detail below) was used as the trace gas for these sensitivity tests. Radon is assumed to have a constant surface source of 1 pCi/cm^2 and a lifetime of 5.5 days [Jacob and Prather, 1990]. The model was run enough to equilibrate, and the average, standard deviation, maximum and minimum radon concentration at each location calculated.

As an example, Figure 2.7 shows the radon profiles predicted for the location in Indonesia using the Tiedtke-TM2 scheme with the various input data sets. The mean and standard deviation values are shown on the Figure. In this example, each of the datasets result in vertical profiles which are statistically significantly different from each other for most of the troposphere. But qualitatively, the profiles are similar, except for the profiles generated in the column model using the pressure level dataset. In all of the cases considered in this study, the pressure level dataset (dataset 4) gave a result qualitatively and quantitatively different than the other datasets. At other locations or using the other schemes than that shown in Figure 2.7, the standard deviations are larger, and the differences between the profiles are more often of the same order as the standard deviations (except for the results derived using the pressure level dataset).

Overall, the results from the datasets (except for the pressure level dataset--dataset 4) are often statistically significantly different from each other, but qualitatively similar. An analysis of the vertical profiles of temperature and humidity at these sites shows that the temperatures are usually very similar, while the specific humidity varies slightly between the datasets. We examined whether there was one dataset which tended to have more convective events than the other datasets using the mass fluxes as well as the calculated CAPE (convective available potential energy), but we did not notice any strong bias in the datasets at the sites and times we examined in this study.

The differences between the predicted radon profiles resulting from the ECMWF hybrid level T42 and NMC datasets (datasets 3 and 4, respectively) indicate the uncertainty in vertical profiles due only to which forecast center dataset was used, since both of these datasets should be of roughly similar quality. These results suggest that trace gas profiles may be somewhat sensitive, but not highly sensitive, to the analysis procedure. This will be considered more in later sections.

The differences between the results in Figure 2.7 (and those not shown) for the T106 and the T42 resolutions of the ECMWF (datasets 1 and 2) illustrate the sensitivity of the parameterization to the resolution of the driving fields, and this sensitivity seems smaller or of the same size as the sensitivity due to origin of the datasets. Note that this does not imply that horizontal resolution is not critical in determining tracer gas distributions for many processes (e.g. advection), but rather that it may not be central in controlling the response of convective parameterizations.

As expected, this test indicates that the pressure level data on only 14 levels (dataset 4) gives results that are considerably different than the other datasets. Once interpolated onto a higher resolution vertical coordinate system (dataset 5), the ECMWF pressure level data and model level data (dataset 2) give vertical profiles that are often very similar, although often significantly different (in Figure 2.7 and results not shown). This implies that it is important to have sufficient vertical resolution, especially in the boundary layer, in order to determine the convective mass fluxes.

In summary, the input meteorological dataset does effect the resulting vertical profile of the radon tracer in this 1-dimensional study. Our study suggests that deriving mass fluxes using only the standard 14 pressure levels should probably be avoided for models such as our 1-dimensional column model. For the other 4 datasets, the differences between the profiles resulting from different datasets are often significantly different from each other, although qualitatively similar. Sensitivity studies such as this one could be used by modelers to estimate the uncertainty in their modeling results due to the forecast center analyses chosen for the scientific experiments, and use this information in error analysis estimates.

2.3.2 Comparison of Schemes with Observations

Three tests evaluate the ability of the convective schemes to reproduce the behavior of the atmosphere. The tests attempt to characterize the behavior of the schemes under three general convective regimes: mid-latitude continental summer convection, tropical continental convection and tropical oceanic convection. Choosing tests which could accurately evaluate the ability of the different schemes to simulate the atmosphere was not an easy task and the tests discussed here

cannot conclusively show that one scheme is better than another in a CTM. However, we feel that these tests give important information about the quality of convective schemes behavior in comparison with observations.

2.3.2.a Mid-latitude Continental Summer Convection

A good constituent for testing the convective parameterization in a chemical transport model is radon, which has been used previously in verifications of CTMs [e.g. Jacob and Prather, 1990, Feichter and Crutzen, 1991]. A comparison between model predicted radon and observed radon looks at the ability of different schemes to predict mid-latitude continental summer convection. The main advantages of radon are that the main source is known (decay of uranium and its radioactive daughters in the earth's crust and slow degassing from continental crust) and the sink is radioactive decay with a time-scale of 5.5 days. Disadvantages of using radon are that the source can vary depending on the geologic region and the amount of precipitation, and there are not sufficient measurements to adequately define climatologies of radon profiles for different locations. A useful set of data was compiled by Liu, et al. [1984], containing 16 radon profiles taken during the summer over the western U.S.A. The data come from Larson and Hoppel, [1973], Moore, et al. [1973], and Wilkening [1970] and these data were extracted from the above papers and averaged for this study of the sub-grid scale parameterizations.

Advection can be an important process in controlling the distribution of radon. To ameliorate this effect we have compared only composite observed or modelled radon data representing regional, long term estimates of the vertical distribution of radon. Eight different model locations were used to predict 3 months of radon profiles. These eight locations were chosen to be close to the location of the above measurements in the western U.S.A. and west of the measurement locations, since the predominant winds are from the west. However, with a column model we cannot, even by averaging, eliminate any contribution to the profiles from advection that varies with altitude. Hopefully, we have chosen enough locations that the average profiles are representative of how that convective scheme will behave in a three-dimensional model (We confirmed that removing any one of the locations does not significantly change the average profile). Any adiabatic movement of tracers due to large scale motions such as fronts should be averaged out by the use of 3 months of predictions.

The average concentrations of radon for all eight schemes (driven from the ECMWF T42 data on hybrid surfaces for the months of July and August, 1990, and June, 1991) are shown in Figure 2.8a for the adiabatic mixing boundary layer scheme, and for five schemes with the non-local boundary layer scheme in Figure 2.8b. A mean observed radon profile for the summer in the western U.S.A. is also shown in Figures 2.8a and 2.8b. The columnar mass in the atmosphere implied from the observations is about 50% of the radon mass predicted by the models. This could be due to three factors: 1) the emission rate used in the model over the western U.S.A. of 1.0 atom/cm^2/s could be too high (a lower value would be within the estimated uncertainty, but is not supported by the emission data [Turekian, et al., 1977]); 2) the observed profiles from Liu, et al. [1984] are not a large enough sample to truly describe the state of the atmosphere, or 3) the discrepancy is caused by advection of air from oceanic as well as continental regions.

It seems likely that the third factor is the most important. The emission of radon from the ocean is

two orders of magnitude smaller than from the continents, so air originating from the boundary layer west of the continental U.S.A. would be expected to have smaller concentrations of radon. It is uncertain how this would affect the overall vertical distribution of radon predicted here, although is it likely that the models will overpredict the radon concentrations in the middle to upper troposphere, especially, since the boundary layer needs less time to equilibrate with the surface source of radon than the middle and upper troposphere. However, the fact that the radon observed in the boundary layer is also lower than the model predicted values implies that the emission source may also be too high. Because we cannot be sure where the discrepancy between the modelled and observed columnar mass, we do not attempt to correct for the mass differences.

The substantial differences between predicted boundary layer values for the different subgrid-scale schemes is consistent with the large model and observed standard deviations there, but the differences between 4 and 14 km are larger than the natural variability. We will use these latter differences to compare the behavior of the different schemes.

The non-local boundary layer scheme seems to be able to simulate the observed average boundary layer gradient better than the adiabatic mixing scheme, but both overestimate the concentrations between 2 and 4 km. The planetary boundary layer heights are sometimes too large relative to observed values in the CCM2 [Holtslag, personal communication, 1994], and work is underway to improve this and other aspects of the non-local boundary layer scheme's behavior. Preliminary work shows that use of a new revised non-local boundary layer scheme results in lower predicted concentrations between 2 and 4 km with a stronger gradient in the boundary layer. This latter behavior is closer to that seen in the radon observations.

A summary of our assessment of the ability of each of the moist convective schemes to reproduce the observations appears in Table 2.2. The schemes are compared qualitatively, by identifying whether the predicted radon profiles have the same basic characteristics as the observed radon profile and quantitatively (whether the profiles lie within one observed or modeled standard deviation of each other).

For example, Figure 2.9 shows the results of the Tiedtke-EC scheme compared with observations. This predicted profile has the same shape as the observations throughout the troposphere. In addition, the profile predicted by the scheme is within one standard deviation (as calculated in the model) of the observations except between 1 and 3 km. This scheme is considered therefore to have done well qualitatively and adequately quantitatively and is labelled "good." Notice that the boundary layer scheme only affects the distribution of the mass in the boundary layer, and not the vertical distribution of the tracer in the middle and upper troposphere. This is true for all the cases considered here. Figure 2.10 shows the results for the Emanuel scheme, which by comparison we judge by the same criteria to perform "medium" qualitatively and "medium-poor" quantitatively. Before leaving this topic we caution that because the lifetime of radon is long enough to allow some advection from areas west of the continental U.S.A., this radon test should be repeated in a 3-dimensional model. This will be the focus of a future paper using a limited set of the moist convective parameterizations studied here.

Table 2.2 Convection Schemes versus Observations

Test	Emanuel	Feichter-Crutzen	Hack-Perturbations	Hack-Time-Stepped	Inverse Thermo-dynamic	Pan	Tiedtke-EC	Tiedtke-TM2
Radon Quality	Medium	Medium	Poor	Poor	Medium	Good	Good	Poor
Radon Quantity	Medium-Poor	Medium	Poor	Poor	Medium	Medium-Good	Medium-Good	Poor
Radon	Medium	Medium	Poor	Poor	Medium	Good	Good	Poor
CEPEX	Good	Medium	Poor	Poor	Good	Good	Good	Good
ABLE2A	Too High	Good	Too Low	Too Low	Good	Too High	Good	Too High
Summary	Medium	Medium	Poor	Poor	Medium-Good	Medium-Good	Good	Medium
Computer Time (s)	117	2.82	0.68	8.6	1.76	NA	6.55	2.30

2.3.2.b Tropical Oceanic Convection

One critical property of a convective parameterization is the ability to accurately diagnose from the grid-scale forcing the depth to which convection occurs. We have therefore used data gathered during the CEPEX (Central Equatorial Pacific Experiment) to assess the ability of the convective schemes to appropriately diagnose deep convection over the tropical oceans (where radon data is not useful). We specifically compare the height of convection predicted by the parameterizations to the height of convection observed and modelled during the CEPEX (Wang, et al, 1994). On March 8 and April 3, 1993 large convective events were observed in CEPEX which reached heights of 17 km. These two events were of sufficiently large proportions that they should substantially affect the trace constituent vertical profiles even within a global CTM grid-box with dimensions of 250 km.

However, a difficulty in interpreting this test is that it only checks convection at specific locations, not over a whole region. The results from both days, however, were very similar, so we feel that we have identified systematic differences between the schemes. In addition, it may be that the input meteorological dataset from the forecast centers may contain errors that inhibit the convection schemes, instead of an inherent problem in the convection schemes. In order to examine whether this might be a problem, we also conducted this simulation with radiosonde data taken very close to the convection events, and obtained similar results.

The events were modeled using the column model located at the nearest 4 grid-boxes (on a 2.8 degree T42 grid) to the convective event during the entire 24 hour period surrounding the event using the NMC upper air dataset. The calculated mass fluxes from each scheme were used to diagnose the depth of the convection from the parameterization and this was compared to the depth of convection seen from observations.

Both days show similar results. Figure 2.11 shows the height to which the different schemes diagnosed mass fluxes on March 8, 1993. Models which diagnosed deep convection (Emanuel, inverse thermodynamic, the Pan, and both versions of the Tiedtke) were assigned a "good" designation. Schemes which predicted convection, but not up to 16 km, were assigned a "medium" designation (Feichter-Crutzen), while the models which did not diagnose deep convection were assigned a "poor" designation for this test (both versions of the Hack scheme). Table 2. 2 summarizes the results of this CEPEX-based analysis.

2.3.2.c Tropical Continental Convection

In this section we have assessed the ability of the convective schemes to move mass to the levels seen in observations and detailed two-dimensional squall line modeling studies over the continent. We have used the Amazon Boundary Layer Experiment 2A (ABLE2A) over Brazil and a simulation the carbon monoxide distributions for the Aug 3, 1985 event [Garstang, et al., 1988; Pickering, et al., 1992] derived in part from those observations.

The events were modeled using the ECMWF pressure level data set, interpolated onto the ECMWF hybrid vertical coordinate. The surface data sets used were the 1985 ECMWF surface data sets for the same location and day (this dataset lacks a precipitation field, so a value of 0.6 mm/hour of precipitation was used, which is from a rain event at the same location on August 3, 1990). The closest 4 locations (on a T42 grid) and closest 2 times were chosen for testing the schemes. This was done because the forecast model could put the convective event in the adjacent gridbox, and we expect that often only one location and time will actually match the observations.

Although, comparing the 1-dimensional model to a 2-dimensional model of an observed event is in principle less rigorous than comparing to the observations themselves, the observations are in this case incomplete and we will use elements of the aforementioned two-dimensional modeling study which are consistent with the observations: in particular, the height to which the convective mass fluxes transfer the trace constituents. The initial trace gas profile for the 2-dimensional and our 1-dimensional models with the various schemes come from the observations. Since the final predicted profile from the 2-dimensional model is not representative of the entire grid-box, we have examined only to what level the models move the tracer mass, not how much mass has been moved, and the mass transport in the 2-dimensional model is consistent with observations (e.g. the height of the anvil). The quality of the simulation is identified using the labels "too high" (indicating the height of convection to be too high), "good" (indicating the transport of mass is close to the observed anvil height) or "too low" (indicating the height of convection to be too low) in Table 2.2.

Figure 2.12 shows the predicted carbon monoxide distributions for the Feichter-Crutzen scheme conducted at the 4 closest locations on a T42 grid and 2 closest times from the 6-hourly data set (designated cases 1-8) to the observations. Notice that the Feichter-Crutzen scheme has moved the carbon monoxide up from the boundary layer to between 3 and 13 km (marked "observed level of detrainment" in Figure 2.12), as seen both in the observations and the 2-dimensional model output. We therefore assigned this scheme a "good" assessment for this test. Note that we do not expect the column model to change the profile completely from the initial profile to the final 2-dimensional profile, since the final 2-dimensional profile is not representative of the

concentration over an area the size of a gridbox (250 km). All eight cases are shown on the same plot, making it difficult to distinguish each, but in this figure, we only wish to point out whether one case has managed to move mass to the right height. Figure 2.13 shows the CO predictions from the Tiedtke-TM2 scheme, which tends to transport this trace gas higher than observed in the observations or in the 2-dimensional model. We have labelled this result "too high" in Table 2.

2.3.3 Computational Expense

The last row of Table 2 identifies the CPU time in seconds required to run each convection scheme for the mid-latitude summer convection test, representing a six month integration at one location. Since the schemes were tested using one location they do not vectorize. For this reason they are not a realistic estimate of the amount of time required in a 3-dimensional model. Nevertheless, the differences are so large as to provide a rough assessment of computational cost. The Emanuel scheme takes an order of magnitude longer than the other schemes (even than the Hack scheme in the time-stepped mode). The Hack scheme with perturbations in the updraft is the fastest scheme, with the other schemes intermediate between these extremes in computer time required. The Tiedtke-EC model takes much longer to run than the inverse thermodynamic scheme, while both did about the same on the tests conducted here. We estimate that running the Tiedtke-EC scheme in the 3-dimensional chemical transport model (at T42 horizontal resolution and with 5 trace gases) will cause the entire model to run approximately twice as slow as with inverse thermodynamical scheme. No comparable information was available for the Pan scheme, so that information is not included in Table 2.

2.4.0 Summary and Conclusions

There were two goals of the current study: 1) to choose the most promising moist convective schemes for inclusion in a 3-dimensional chemical transport model, and 2) to estimate the uncertainty in 3-dimensional atmospheric chemistry models due to the choice of moist convective and boundary layer parameterizations. Computational considerations restricted this study to the use of a one-dimensional column model which we argue suffices for an approximate ranking and inter-comparison of the various schemes. To rigorously test the convective parameterizations, a 3-dimensional simulation is necessary, which we plan to carry out in future studies. All the conclusions of this study should be considered preliminary, because of the 1-dimensional nature of the study.

The summary of the results of the qualitative assessment of the schemes (not accounting for computational demand) is also shown in the second to last row in Table 2. The Pan, Tiedtke-EC and the inverse thermodynamic schemes rate the highest in our tests of convection. Both versions of the Hack scheme driven by the forecast center analyses tended to be unable to transport the trace constituent far enough upward to be consistent with the observations considered here. The Feichter-Crutzen model did an adequate job of determining the trace gas transports, but tended to form an exaggerated "C" shaped profile in the radon simulation. The Emanuel scheme had the most difficulty in the boundary layer, which may be due to the fact that we only tested this scheme with the adiabatic mixing scheme. However, the implementation of the Emanuel scheme used

here has a tendency to move all the trace gas out of the bottom level of the model, instead of taking some mass out of each layer in the boundary layer.

The Tiedtke-TM2 scheme tended to drive convection much higher than the other schemes, and (like Feichter-Crutzen) produced an exaggerated "C" shaped profile in the radon simulations. The difference in the behavior of the Tiedtke-TM2 and the Tiedtke-EC schemes lies in how detailed they are. The height of the convection in the Tiedtke-EC model is reduced relative to the Tiedtke-TM2 scheme by the downdraft in the former, which tends to reduce the upward mass fluxes, and by the many buoyancy checks in the EC parameterization that were omitted for the TM2 scheme. In addition, the version of the TM2 convective model used here never actually checks to make sure that an updraft is buoyant at the lifted condensation level, so that boundary layer air can be brought up several kilometers and then detrained at the lifted condensation level, without the updraft ever being buoyant. This lead to quite large trace gas fluxes over the Nebraska location in the sensitivity test with the CCM2 archived fields, which were not seen in the Tiedtke-EC parameterization (not shown in the Figures here). Future versions of the Tiedtke-TM2 scheme will make a check for buoyancy at the lifted condensation level (Heimann, personal communication, 1995).

The fact that the moist convective scheme that did the best in these studies, the Tiedtke-EC scheme, happens to be the moist convective scheme that was used to generate some of the data (the ECMWF hybrid data set) may be significant. Although our sensitivity study showed that the results for radon (or a radon-type species) species may not be highly sensitive to which forecast center analyses is used, this may only be true for a limited set of moist convective schemes (we used the Hack, inverse thermodynamic and Tiedtke-TM2 schemes for this sensitivity test). The Hack schemes tended to have extreme behavior when driven with the forecast center analyses, and this may indicate that the Hack scheme should not be used with driving fields from the NMC (Kuo scheme) or ECMWF (Tiedtke-EC scheme). On the other hand, the Tiedtke-EC scheme seemed to have very little difficulty with the CCM2 (Hack scheme) or the NMC (Kuo scheme) archived fields, which may indicate less sensitivity to driving fields with that scheme. Many of the other schemes, such as the inverse thermodynamic or the Feichter-Crutzen, seemed to do equally well with any of the input datasets.

The Pan, Tiedtke-EC and inverse thermodynamic schemes appear to reproduce the observations more closely in the tests conducted here with analyzed winds from the forecast centers. The Tiedtke-EC scheme did slightly better in our tests, but is computationally more expensive to run than the inverse thermodynamic scheme. The inverse scheme is prone to numerical errors, which we seem to have corrected using the threshold approach, and is less expensive to run than the EC model. In addition, the inverse scheme can only deduce the net mass fluxes, not both updraft and downdraft mass fluxes. The Pan scheme seemed to do a good job in the tests, but has a tendency to move mass slightly too high. All three of these schemes are therefore planned for further scrutiny in a 3-dimensional CTM. By testing a CTM with multiple convection schemes, we will also have sensitivity test of the importance of moist convective schemes in a CTM. Since the Tiedtke-EC schemes corresponds closely to that used in the ECMWF forecast model entering into the analyses after May of 1989, it has the advantage of being consistent with some of the analyses used to drive the CTM. The Pan scheme is consistent with the NMC reanalysis dataset also used by the 3-dimensional model.

Our comparison between two different boundary layer schemes implies that the middle- and upper-tropospheric concentrations of trace constituents are not sensitive to the boundary layer scheme chosen. For the moist convective schemes and cases examined here, the boundary layer scheme only serves to redistribute the trace gas in the boundary layer, rather than change the amount of trace gas which escapes to the middle-troposphere. For some schemes, this may be due to the scheme entraining throughout the boundary layer (Tiedtke-TM2 and Tiedtke-EC), but some of the schemes considered here entrain most of their trace gas in one level (Feichter-Crutzen and inverse thermodynamic).

A major difficulty in attempting to choose a parameterization for the vertical transport of the trace gases is the lack of observational data available to compare with predictions. Greater measurement frequent and more data field studies in different regions would be highly useful in future studies.

The results of this study show that different moist convective parameterizations can substantially change the amount of trace gas transported to the middle and upper troposphere. This can significantly change the vertical profile of the gas, which may result in substantially different scientific conclusions derived from CTM studies sensitive to vertical transport. In the worst cases, predicted concentrations in the upper troposphere can change by more than an order of magnitude depending on the scheme chosen.

The tests performed here are not all-encompassing, or (due to the column model used) conclusive. However, we feel that this analysis provides modelers of chemical transport some insight into the differences between and implications of choosing specific subgrid parameterizations. These tests may also be useful to climate modelers, since the reproduction of the transports of trace gases is another way to test a subgrid scale parameterization.

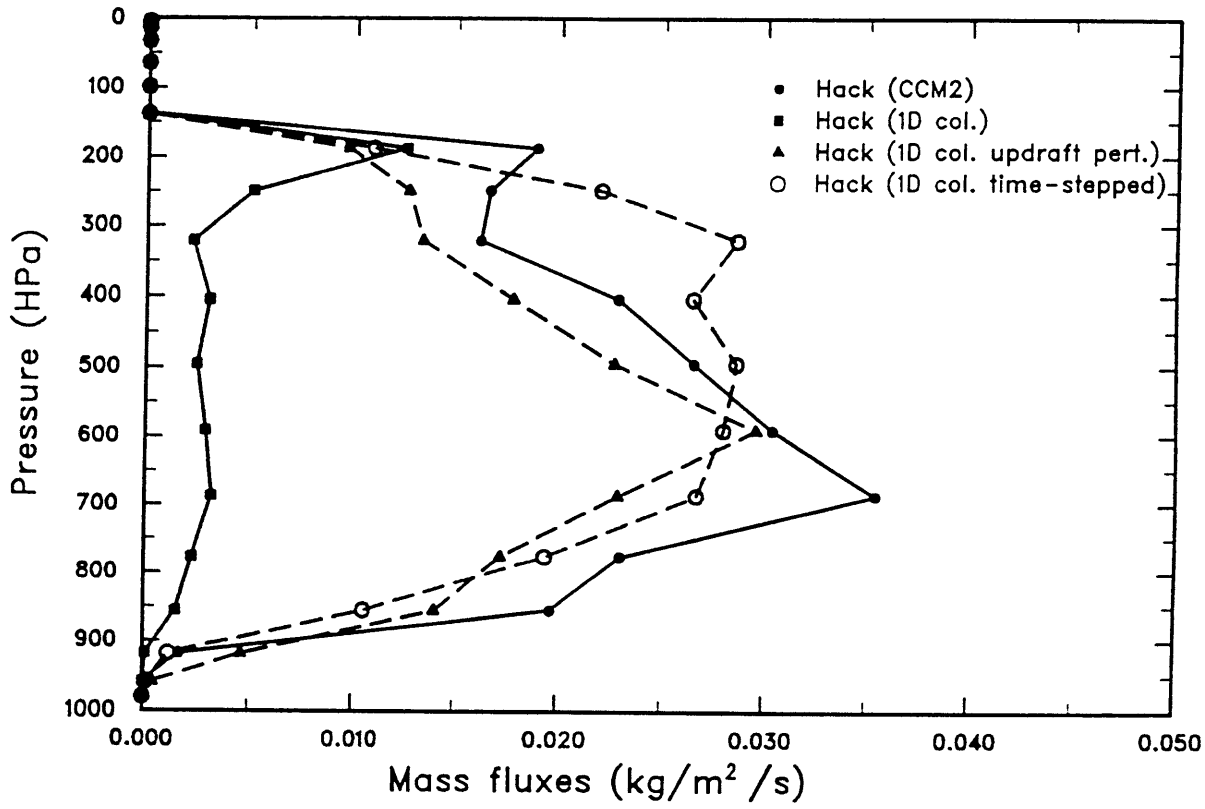

Figure 2.1. The 10 day average moist convective mass fluxes ($kg/m^2/sec$) as calculated at the Venezuela location: (1) in the CCM2 using the Hack scheme and (2) in the column model using the original Hack scheme, (3) in the column model with the Hack scheme with updraft based perturbations and (4) in the column model using the Hack scheme in a time stepping model.

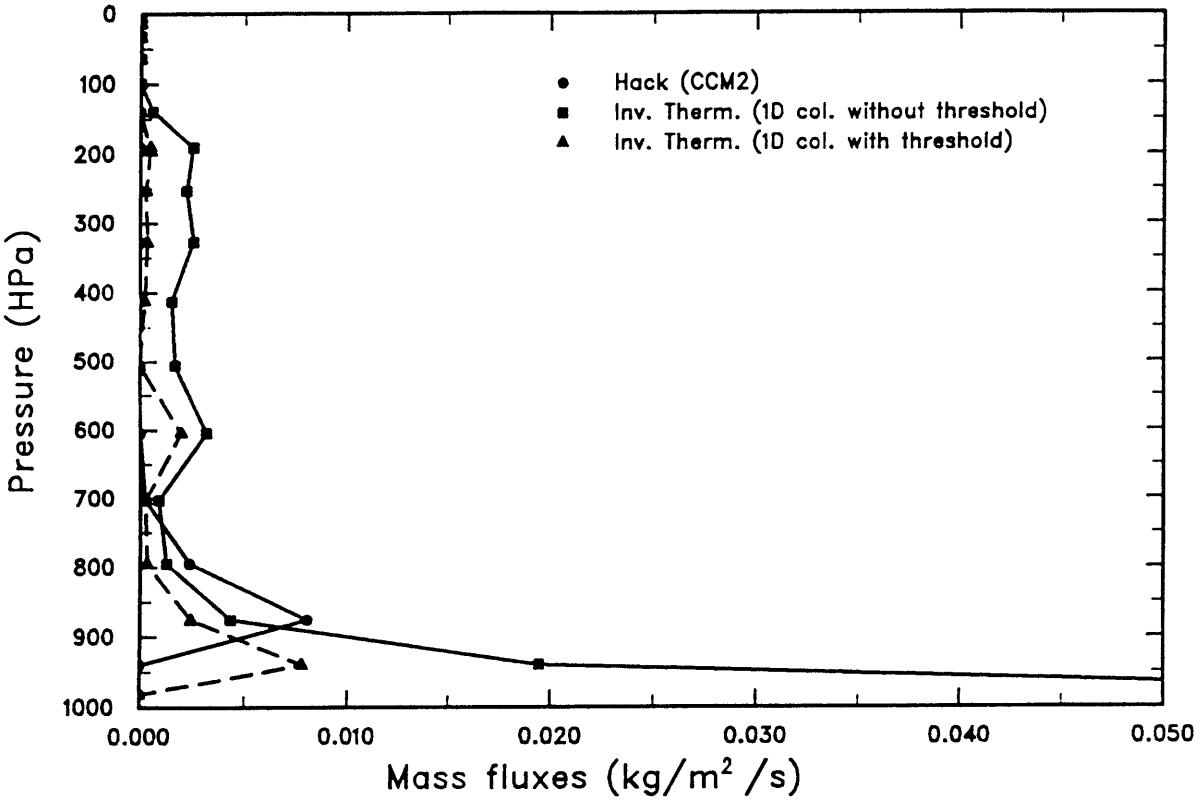

Figure 2.2. The 10 day average moist convective mass fluxes (kg/m2/sec) as calculated at the West Pacific location: (1) by the CCM2 model using the Hack scheme, (2) by the column model using the inverse thermodynamic scheme (without a threshold), and (3) in the column model with the inverse thermodynamic scheme with a threshold value. Note that because the column model is being driven by the archived fields from the CCM2, case (1) is the "correct" answer.

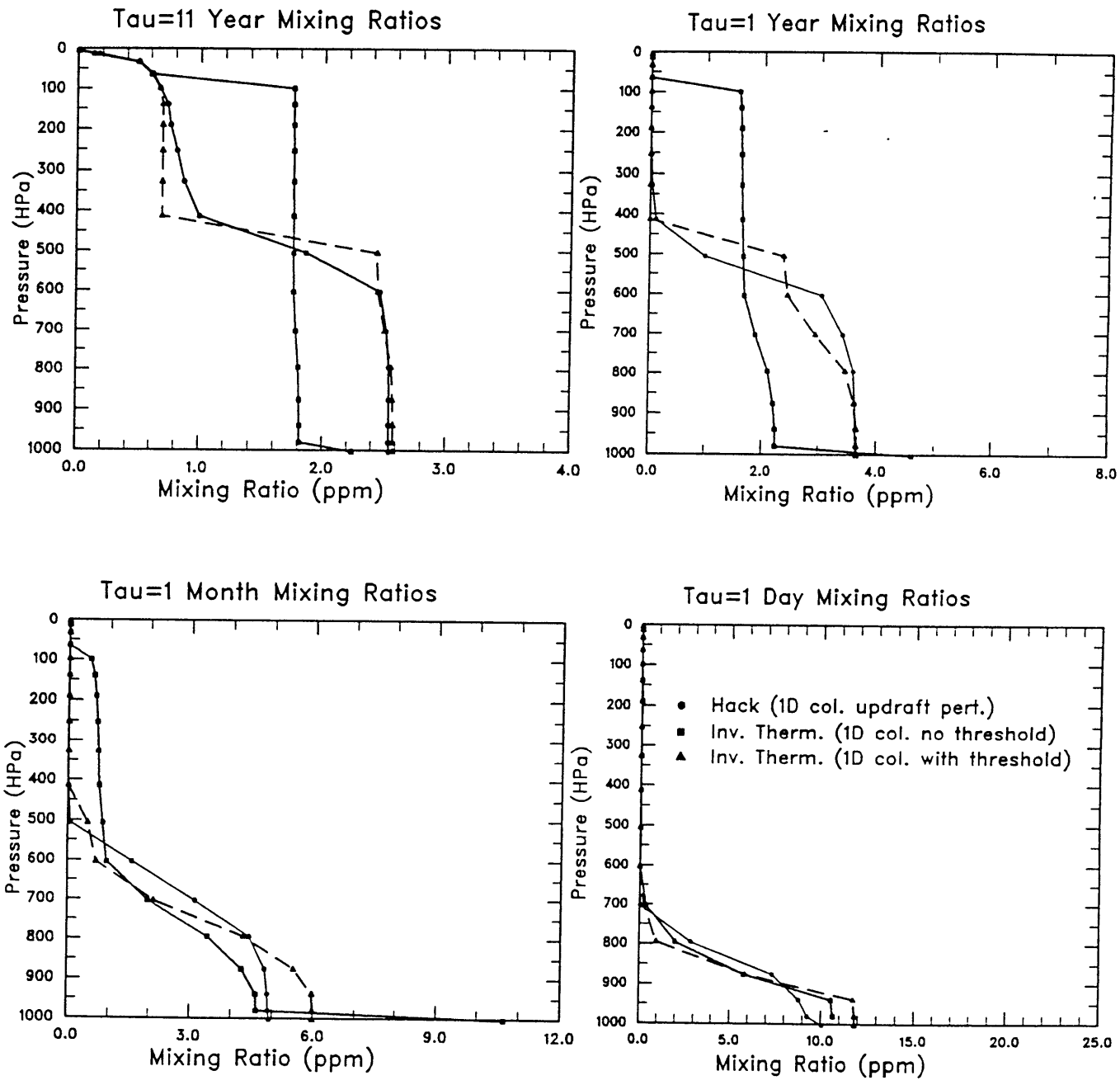

Figure 2.3a-d. The vertical profile (ppm) of a trace gas with (a) 11 year (like Methane) (b) 1 year lifetime, (c) 1 month, and (d) 1 day lifetime using the column model at the same location and the schemes shown in Figure 2.2.

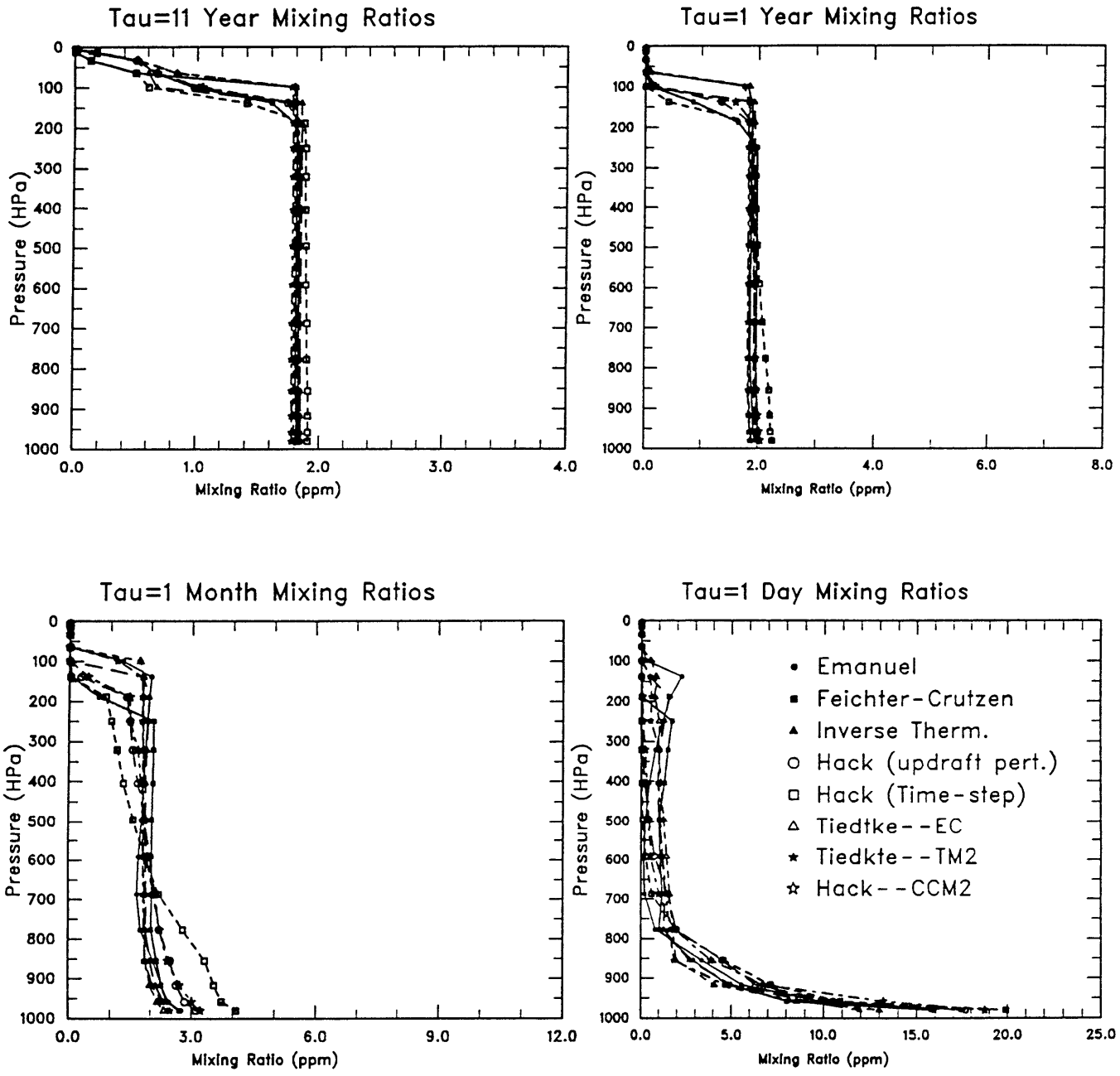

Figure 2.4a-d. The vertical profile (ppm) of (a) a trace gas with (a) 11 year (like Methane) (b) 1 year lifetime, (c) 1 month, and (d) 1 day lifetime at the Venezuela location for all 7 schemes: Emanuel, Feichter-Crutzen, inverse thermodynamic, Hack with updraft perturbations, Hack in time-stepping mode, Tiedtke-EC and Tiedtke-TM2. Also shown is the vertical profile derived from the mass fluxes archived from the CCM2 (with the Hack scheme).

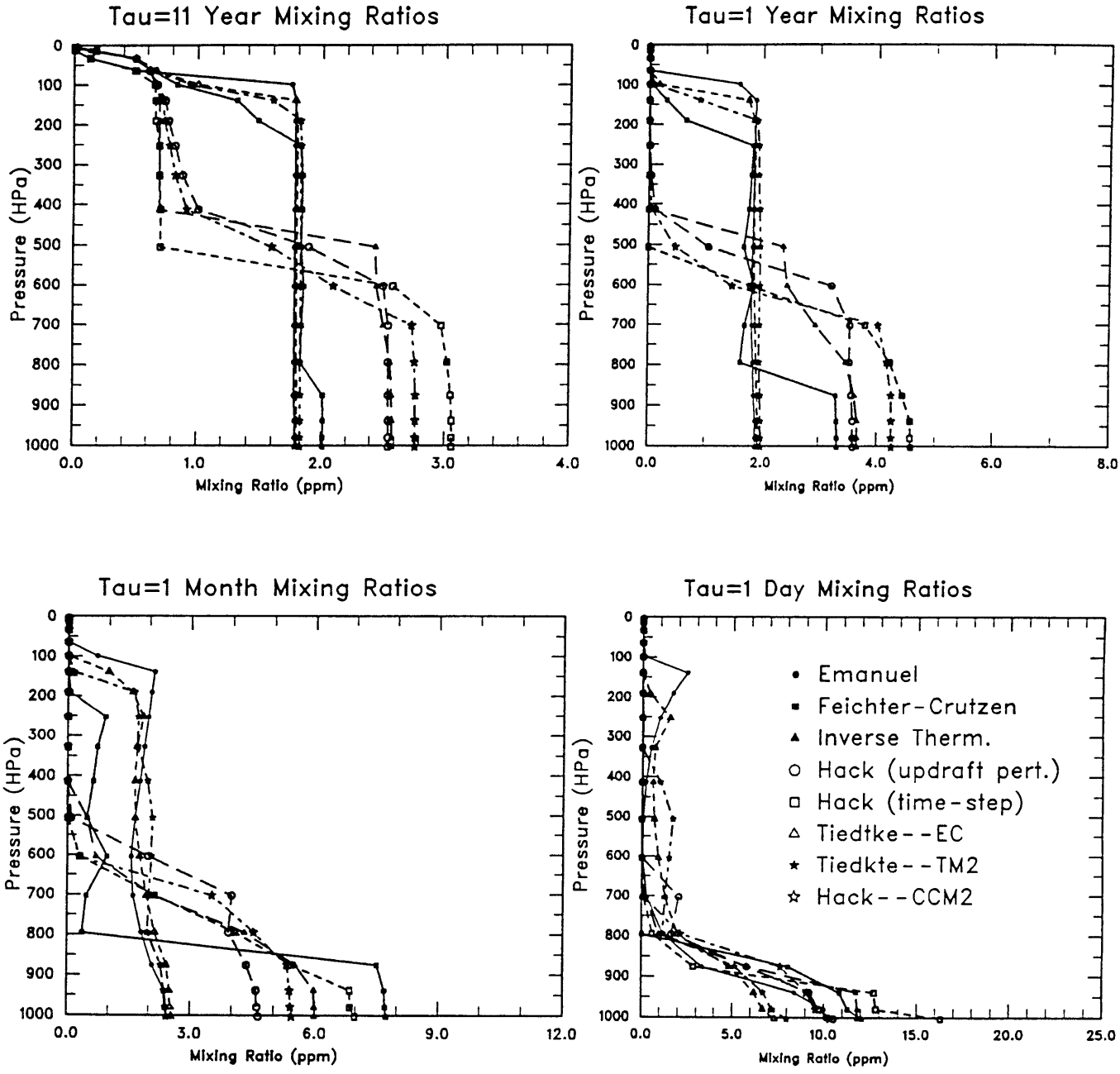

Figure 2.5a-d. As in Figure 2.4a-d except at the West Pacific location.

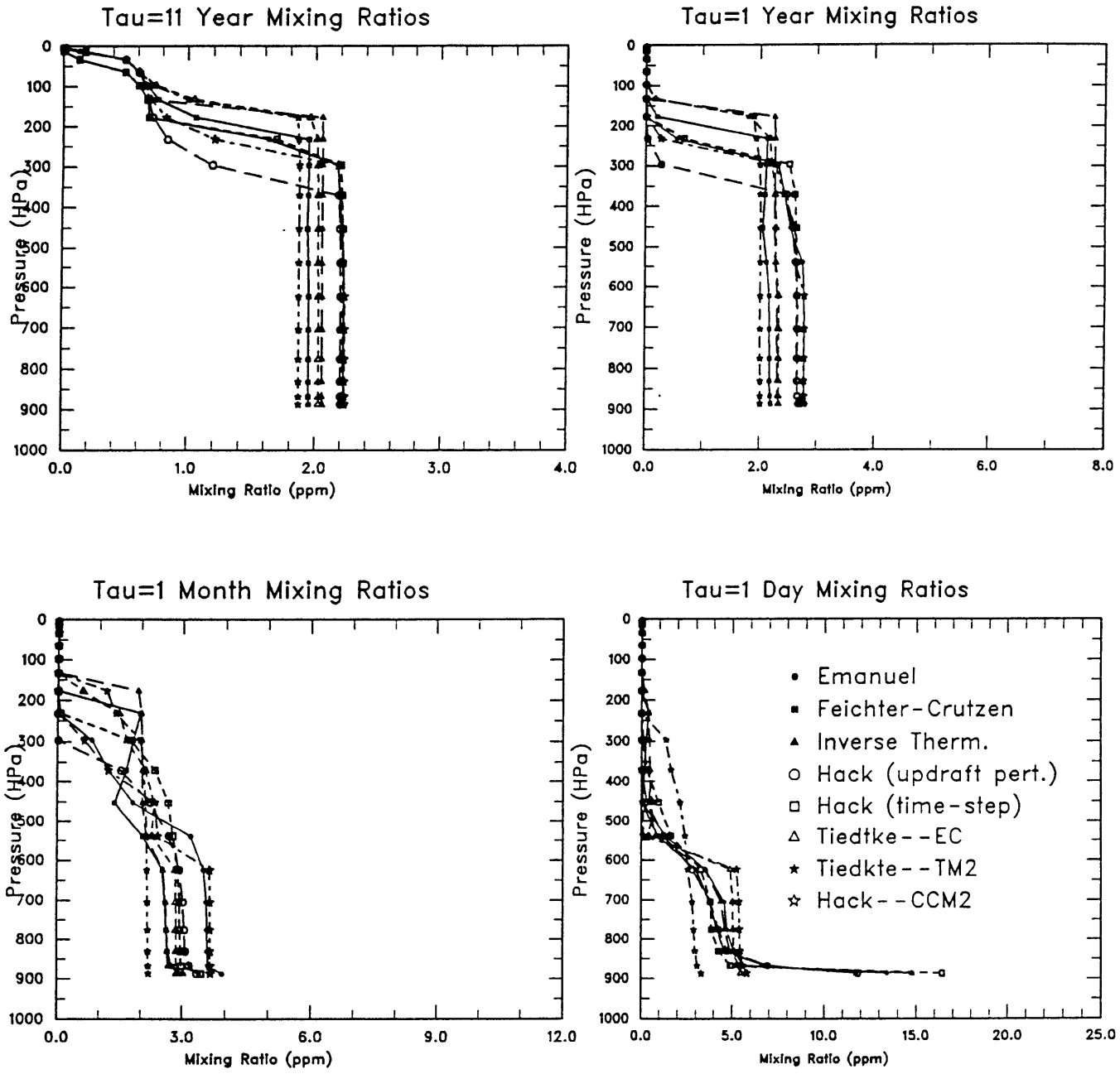

Figure 2.6a-d. As in Figure 2.4a-d except at the Nebraska location.

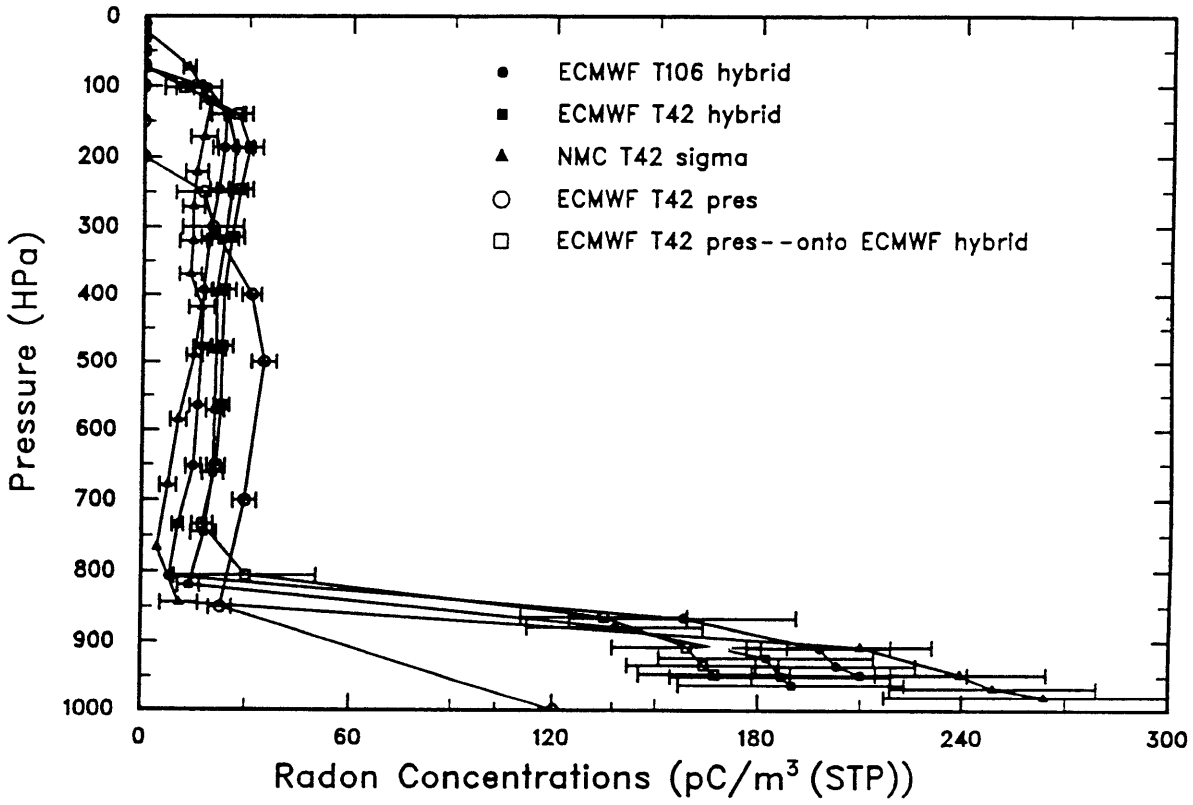

Figure 2.7. The vertical profile of Radon-222 (pCi/m^3) as modeled in the column model using the Tiedtke-TM2 scheme over Indonesia using archived fields from (1) the ECMWF T106 hybrid coordinate dataset, (2) the ECMWF T42 hybrid coordinate dataset, (3) the NMC T42 sigma coordinate dataset, (4) the ECMWF T42 pressure surface dataset and (5) the ECMWF T42 pressure level dataset interpolated on the hybrid vertical coordinate. Shown are the mean values, and an error bar indicating the standard deviation.

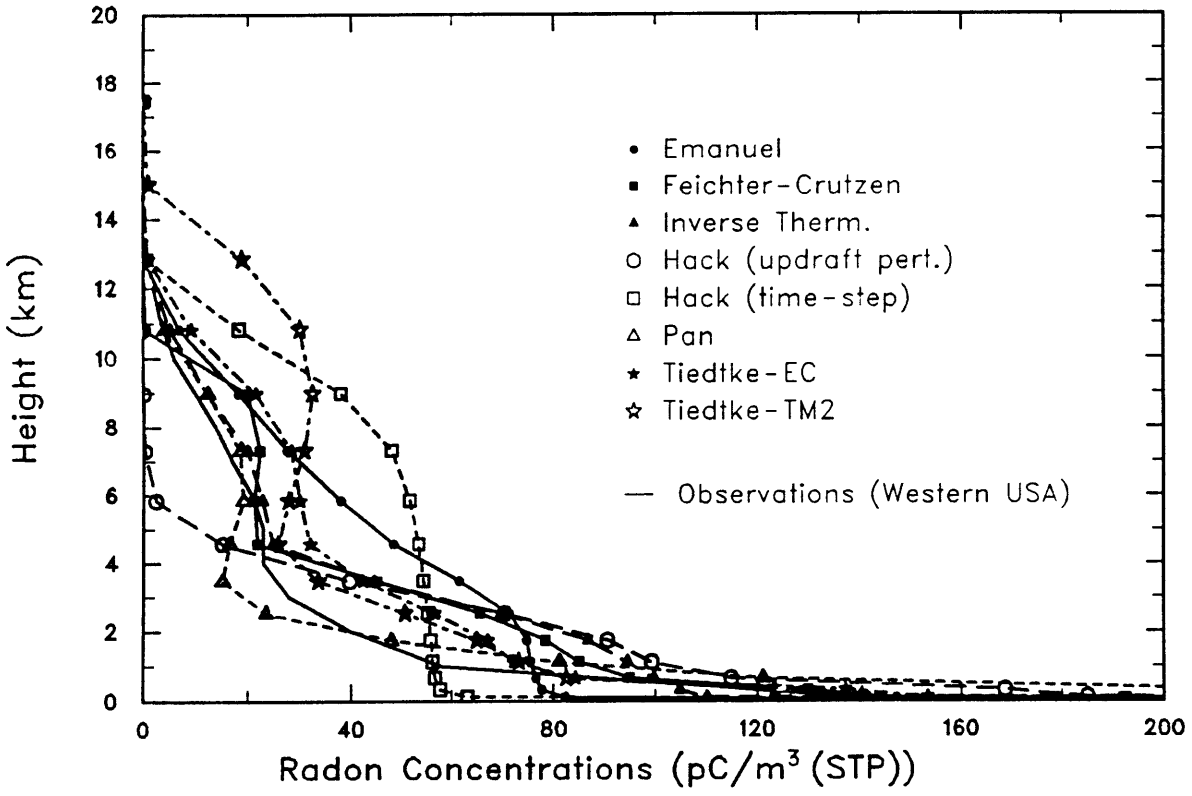

Figure 2.8a-b. The vertical profile of Radon-222 (pCi/m^3) as modeled in the column model using: (a) 8different moist convective schemes (Emanuel, Feichter-Crutzen, inverse thermodynamic, Hack with updraft perturbations, Hack in time-stepping mode, Pan, Tiedtke-EC and Tiedtke-TM2) and the simple adiabatic mixing boundary layer scheme. Also shown is the average of 16 vertical radon profiles for the western USA summer taken from Liu, et al [1984]; (b) 5 moist convective schemes (Feichter-Crutzen, inverse thermodynamic, Hack with updraft perturbations, Tiedtke-EC and Tiedtke-TM2) are used and the non-local boundary layer scheme are used.

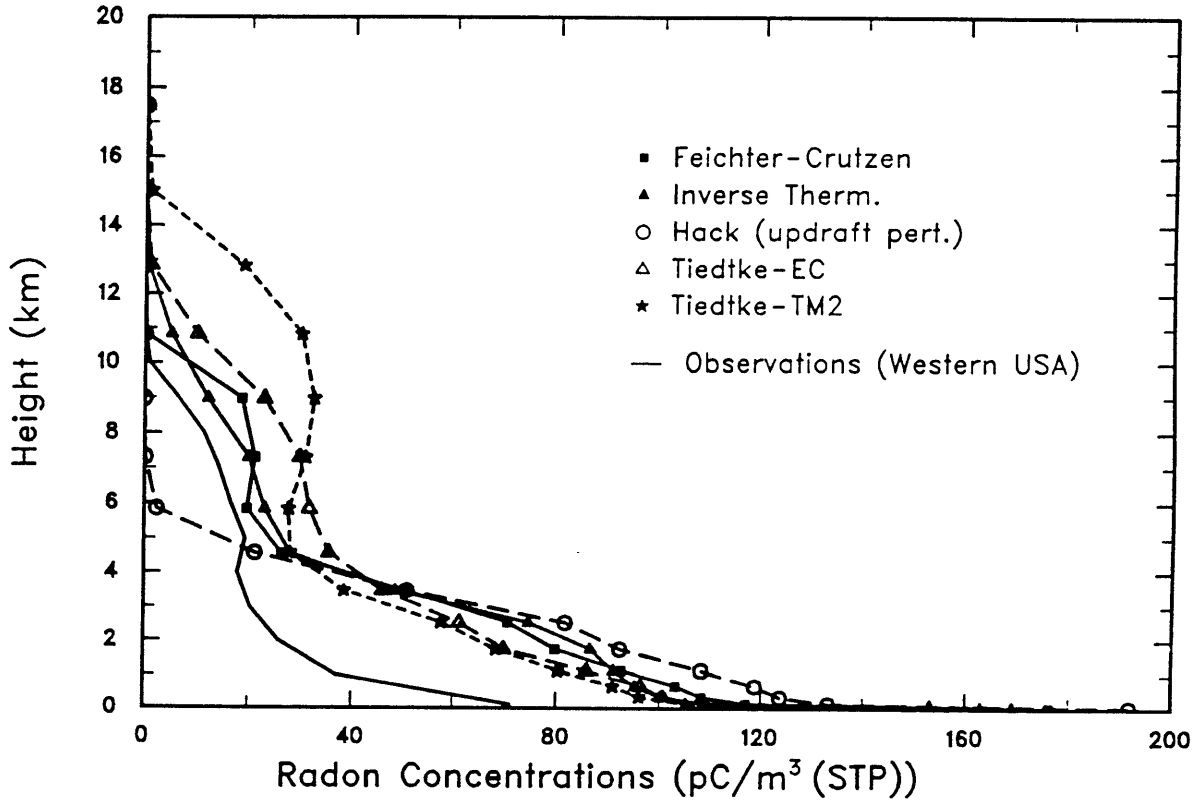
Height (km)
20
18
16
14
12
10
8
6
4
2
0
0
40
80
120
160
200
Radon Concentrations (pC/m³ (STP))
Feichter-Crutzen
Inverse Therm.
Hack (updraft pert.)
Tiedtke-EC
Tiedtke-TM2
Observations (Western USA)

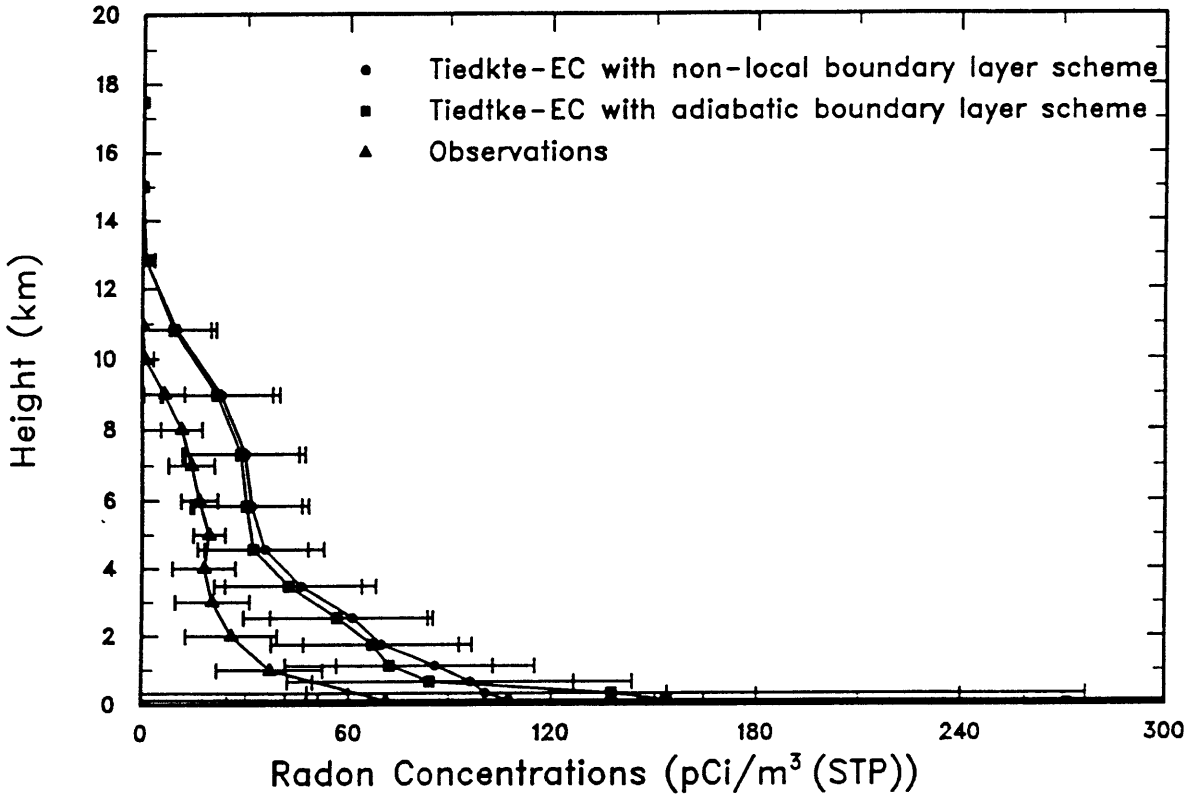

Figure 2.9. The vertical profile of Radon-222 (pCi/m^3) as modeled in the column model using the Tiedtke-EC scheme. Shown are results using the non-local boundary layer scheme and the adiabatic boundary layer scheme, as well as the observed profile from Figure 2.8. Shown are the mean values, and an error bar indicating the standard deviation.

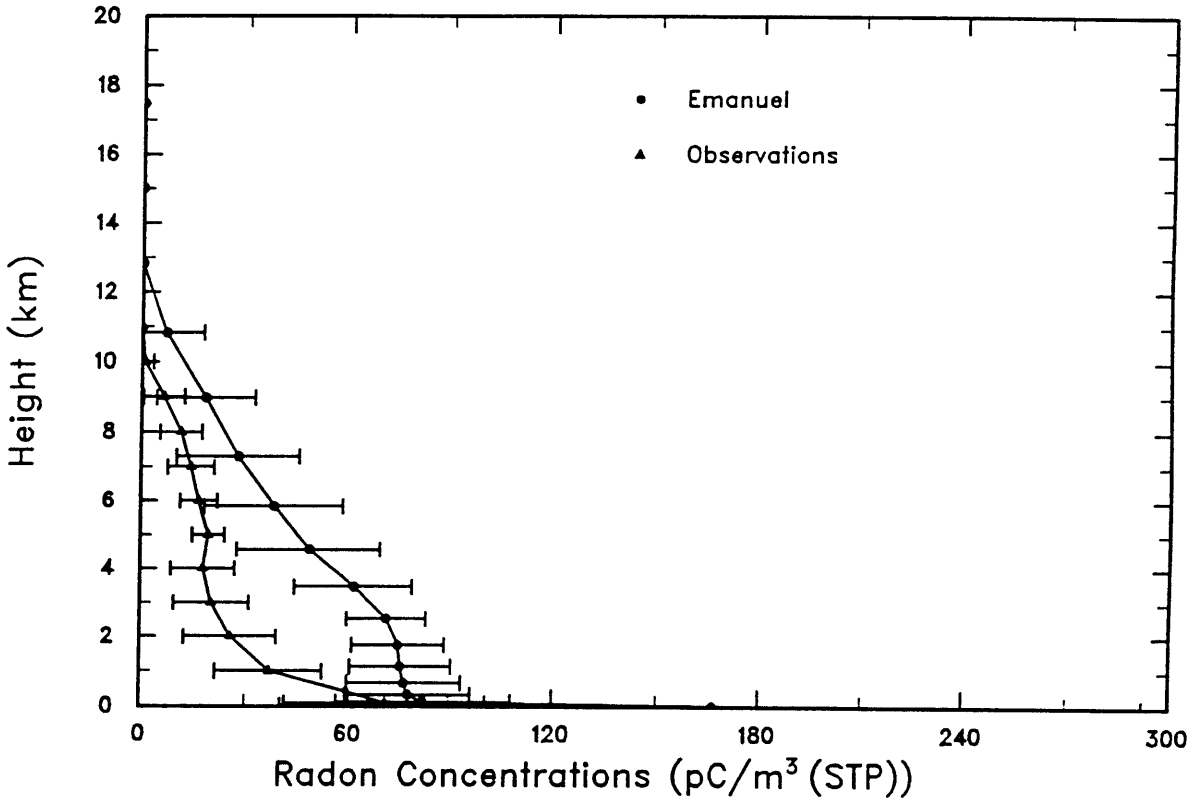

Figure 2.10. The vertical profile of Radon-222 (pCi/m3) as modeled in the column model using the Emanuel scheme and the adiabatic boundary layer scheme, as well as the observed profile from Figure 2.8. Shown are the mean values, and an error bar indicating the standard deviation.

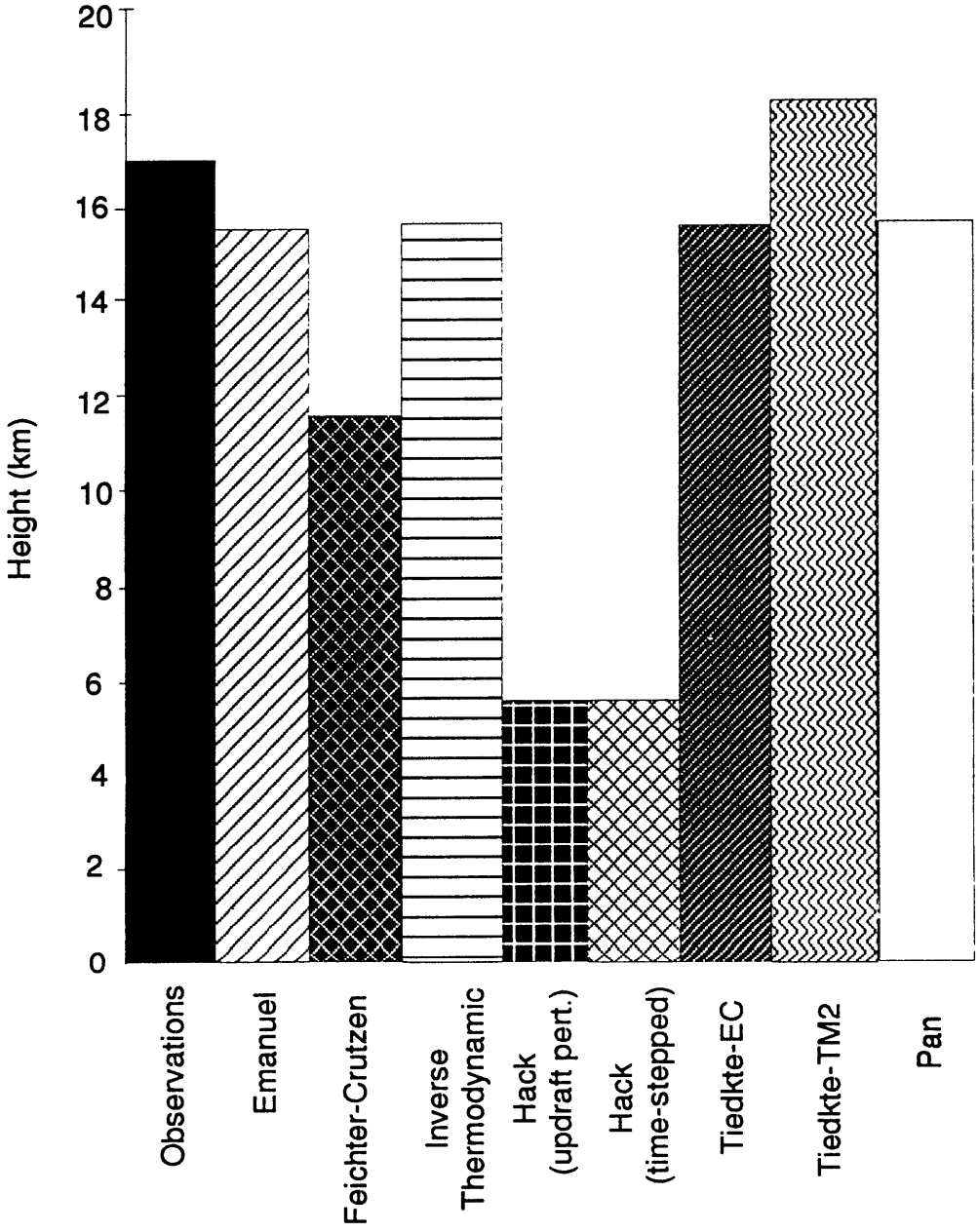

Figure 2.11. The height to which to convection penetrated during the March 8, 1993 event during CEPEX as observed and as calculated by the 8indicated moist convective parameterizations.

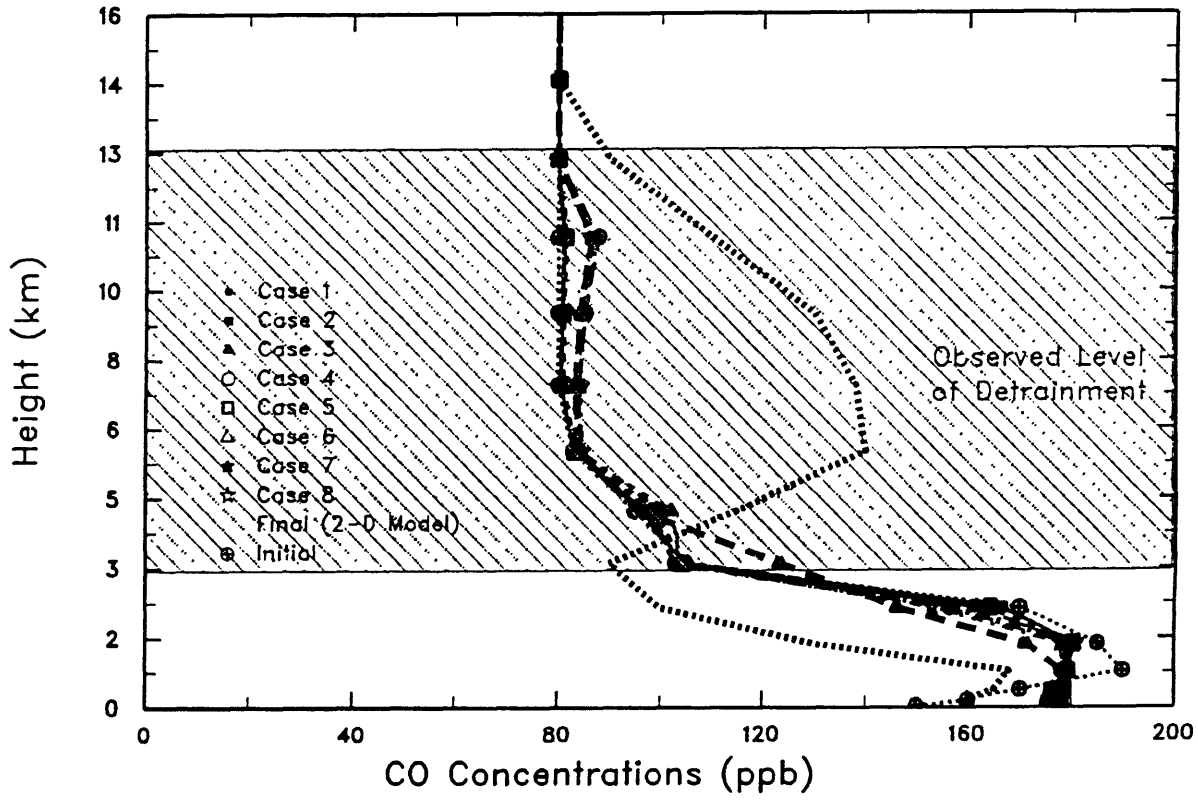

Figure 2.12. The vertical profile of the CO mixing ratio (parts per billion by volume) for the August 3, 1992 event over Brazil during ABLE2A as simulated by the Feichter-Crutzen scheme. The initial vertical profile and Final (2-D) profile come from a 2-dimensional simulation by Pickering, et al, [1992]. The 8 cases are driven by ECMWF analyses fields from the four closest locations and two closest times to the actual event. Notice that the tracers have moved from the initial profile towards the final profile (from the 2-D model), indicative of a "good" performance."

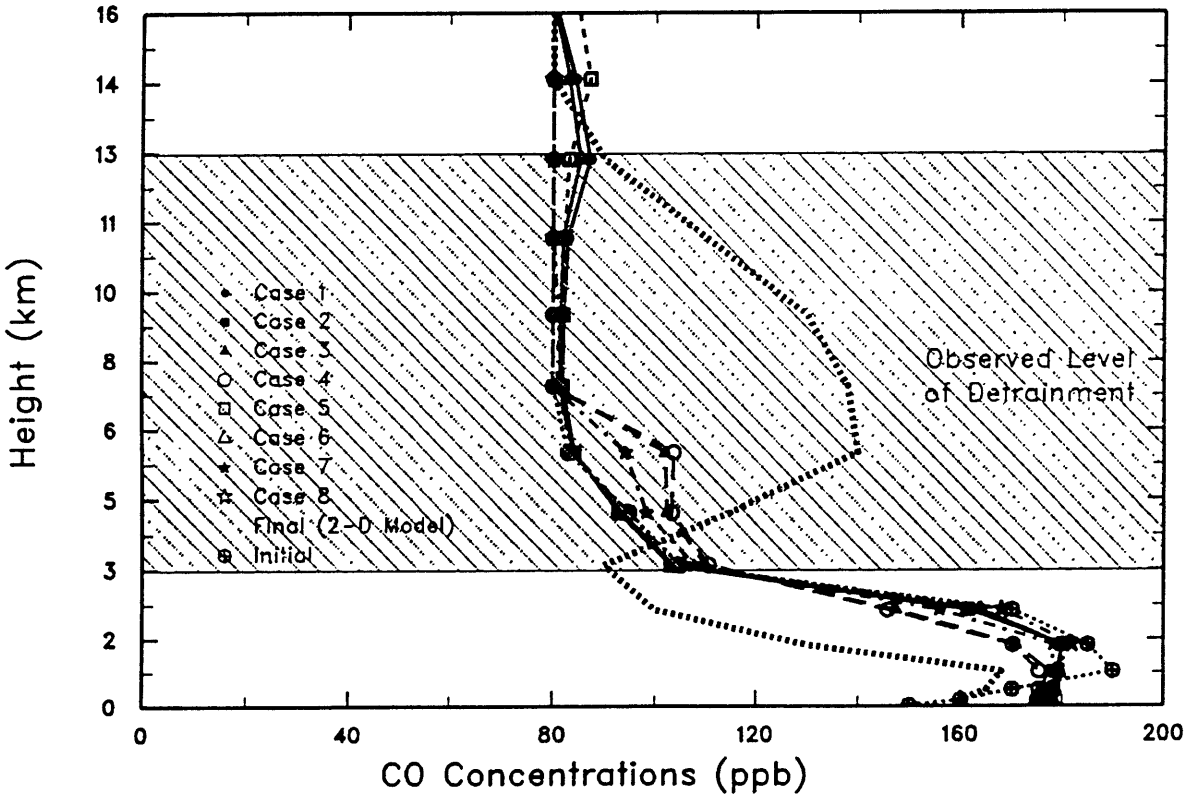

Figure 2.13. As in Figure 2.12, except for the Tiedtke-TM2 scheme.

Chapter 3: Development of 3-dimensional Chemical Transport Model Based on Forecast Center Winds

3.1.0 Introduction

This chapter is a "nuts and bolts" chapter, discussing the development of the 3-dimensional chemical transport model from a model able to advect tracers using CCM2 meteorology, to one able to derive moist convective and boundary layer mixing from either CCM2 or forecast center analyses.

3.1.1 Description of Model

A new chemical transport model using winds from the forecast centers is used in this study. The MATCH model and the use of off-line models has been described in a previous paper [Rasch, Mahowald and Eaton, 1996, manuscript in preparation). This model has been designed to run "off-line" (meaning that most of the meteorological fields are read as archived data, rather than calculated) from either GCM output or from forecast center analyses. Because the routine analyses available from the forecast centers does not contain subgrid scale mixing information such as the boundary layer mixing and moist convective mixing, the off-line model can calculate these fields or it can read them in.

The MATCH model contains the semi-lagrangian transport scheme developed by Rasch and Williamson [1990]. This transport scheme is shape preserving and allows the advection of strong gradients, but is not inherently mass preserving, so that a mass fixer must be applied to the tracer fields. The mass fixer weights the amplitude of the adjustment in proportion to the advection tendencies and the field itself. More discussion of the semi-lagrangian scheme and the fixer is in Rasch, et al.[1995]. In addition, some problems with advecting ozone (which resides predominantly in the stratosphere) have been observed [Lawrence, Max-Planck-Institute in Mainz, personal communication, 1995], but these problems have not appeared in the work presented in this thesis.

The non-local boundary layer scheme from the CCM2 [Holtslag and Boville, 1993] is used for the ECMWF, while the NMC run uses an updated version of this non-local scheme, which reduced the depth of the boundary layer to match observations better. More discussion of the non-local scheme appears in Chapter 2.

In this thesis, the MATCH model is used with meteorological driving fields from the ECMWF and the NMC reanalysis for the year from July, 1990 to June, 1991. The ECMWF upper air data is available at T106 horizontal resolution (equivalent to 1.1 by 1.1 degrees) and 19 vertical levels. Unfortunately, running the model at such high resolution is prohibitively expensive, so we chose to make the ECMWF model runs at a reduced horizontal resolution of T42 (equivalent to 2.8 by 2.8 degrees). Surface data from the same period is also available from ECMWF. The NCEP/NCAR reanalysis dataset (National Centers for Environmental Prediction/National Center for

Atmospheric Research) is used here [Kalnay, et al., 1996] is used in the 3-dimensional model, and is referred to as the NMC reanalysis dataset in this thesis. This dataset is available at NCAR at T63 (equivalent to 1.8 x 1.8 degree resolution) with 28 levels. NMC reanalysis surface datasets are available for 1985 to the present, and are used for the same 1 year period.

For the studies in this thesis, the meteorological input is available every 6 hours, and are interpolated to every 40 minute time step. Advection, moist convective mixing, boundary layer mixing and chemical transformations occur every 40 minute time step. If moist convective and boundary layer mixing coefficients are being derived, they are derived every 40 minutes.

In this chapter the modifications to the model which were made in order to make the model capable of deriving the mixing coefficients which are not archived by the forecast centers associated with subgrid scale mixing are described, Some of these modifications were made using CCM2 output, so that the ability of the offline model to rederive the coefficients could be verified.

Our original intention was to build a model capable of running with the ECMWF winds available at NCAR on model surfaces (19 hybrid levels) at T42 for July, 1990 to June, 1991. At the time of the inception of this project (May, 1992), these were the best winds available. Since that time, reanalyses winds from NMC have become available, and the model was modified to be able to simulate transport with the NMC reanalysis winds as well.

The chapter will consider the ability of the model to rederive mixing coefficients for the non-local boundary layer scheme, the Tiedtke moist convective scheme, and the Pan moist convective scheme, all described in more detail in Chapter 2.

3.2.0 Boundary Layer Mixing

The non-local boundary layer scheme from the CCM2 [Holtslag and Boville, 1993] has been implemented in the off-line code. This scheme requires the temperature and humidity profiles, wind stress at the surface, surface heat and moisture fluxes, the surface temperature, and the temperature and humidity at 10 meters. A modification to the code was to use the bottom level temperature and humidity instead of the temperature and humidity at 2 meters (or 10 meters), since the temperature and humidity at 10 meters were not easily available (and often wrong for NMC). This modification to the algorithm does not appear to have substantially degraded the performance of the scheme.

It was seen in one-dimensional model simulations that this diffusion subroutine seems quite capable of getting the same results off-line as online. The three variables we looked at are the K_v, γ_q and H_{pbl}, which correspond to the coefficient of eddy diffusion, counter gradient term and the boundary layer height.The formulation of the non-local boundary layer scheme is described in more detail in Chapter 2, and there the definition of these terms is given. In order to consider how well we could derive these variables from the forecast center winds, we first considered the ability of the offline model to rederive values seen in the online CCM2. The following table shows the spatial correlations, ratio of standard deviations and ratio of mean values for these three variables

at a particular time step using CCM2 standard model output:

Table 3.1: Boundary Layer Mixing Coefficients

Variable Name	Correlation	Ratio of Standard Deviation (off/on)	Ratio of Mean (off/on)
K_v	0.996	0.993	0.990
γ_q	0.726	1.133	1.134
$H_{pbl,}$	0.953	0.898	0.898

Thus, K_v is accurately diagnosed, while the boundary layer height is slightly lower than in the online model (probably due to the stabilization of the boundary layer potential temperature profile in the output from CCM2), which then causes the γ_q to be slightly higher. Overall, the diffusion is well recreated in the off-line model.

Using the ECMWF and NMC reanalyses winds, the mean boundary layer height is 690 m and 680 m in July, 1990 and 620 m and 640 m in January, 1991, respectively. In the CCM2 model average for one July and January, the mean is 1020m and 950 m. For CCM3, the mean boundary layer height is 605m and 570 m. Since values of the boundary layer were too high in the CCM2 and more realistic in the CCM3, it appears that the MATCH model is diagnosing reasonable boundary layer heights in the mean when used with forecast center winds.

A newer version of the non-local scheme was later implemented in the model (run with the NMC reanalysis winds) which derives from the CCM3 version of the scheme. This version of the scheme attempted to reduce the too-high boundary layer height seen in the CCM2.

3.3.0 Vertical velocity calculation:

There are two vertical velocity variables used in the model: ω (dp/dt) and $\dot{\eta}$ (dη/dt). $\dot{\eta}$ is the vertical velocity on η surfaces (used for vertical advection) and must be calculated since it is not on the ECMWF or NMC tapes.η surfaces are the vertical coordinates, and represent terrain following coordinates near the surface (similar to sigma coordinates) and gradually move to pressure coordinates in the free troposphere. ω is the vertical velocity at a pressure level and is used in the convection subroutine. Phil Rasch wrote the codes used to calculate $\dot{\eta}$ in a manner consistent with how they are calculated in the CCM2.

Within the model, we use an approximation to calculate ω for input to the convection scheme. That is: $\omega=\dot{\eta}$*surface pressure. As discussed under the Tiedtke scheme, the convection scheme does not appear highly sensitive to the ω variable, so we did not seek to improve this. Shown in Table 3. 2 is a comparison of the $\dot{\eta}$ calculation in the off-line model to the archived online value, and a comparison of the ω archived from the online model and calculated using the above method and the archived $\dot{\eta}$ value.

Table 3.2: Vertical velocity calculation

Variable Name	Correlation	Ratio of Standard Deviation (off/on)
$\dot{\eta}$	0.971	0.859
ω	0.871	1.066

The correlation and ratio of standard deviation are close to one in Table 3.2, indicating that the calculation is well recreated. The ratio of the mean values have not been included in the table, because the mean vertical velocity at a level should give zero or a very small number (or all the atmosphere would be moving away at once). Thus small errors in the off-line calculation or in the calculation of the mean would give large errors in the ratio of the means, rendering it useless. Overall, calculating the $\dot{\eta}$ and estimating ω from $\dot{\eta}$ seems to work in the model.

Note that when we are running with forecast analyses, we don't have any choice but calculate $\dot{\eta}$, but ω is available on the ECMWF data tapes (not on the NMC data tapes).

In simulating trace gases in the model, it was discovered that near the poles the particular numerical algorithm used in the model suffers from errors which cause too much mixing between the stratosphere and the troposphere. This was seen initially in tropospheric ozone simulations conducted by Mark Lawrence [Max-Planck-Institute in Mainz, Germany, 1995 personal communication] since stratospheric ozone is a large source of tropospheric ozone. He discovered that there are spuriously high and low values of $\dot{\eta}$ calculated in the MATCH model poleward of 60 degrees. He found he could reduce the problem, by using a mean value of $\dot{\eta}$ calculated along a latitude line. The same problem appears to be seen in the CFC-11 simulations, as discussed in Chapter 5 of this thesis.

3.4.0 Moist Convective Transports

The derivation of moist convective mixing offline is more difficult than deriving the boundary layer coefficients. Three different moist convective schemes are considered in this thesis to be run with forecast center analyses. In addition to these schemes, the MATCH model is capable of deriving moist convective mixing following the Hack scheme [1992] from the CCM2 or the Zhang scheme [1993] from the CCM3. These will not be discussed in this thesis.

3.4.1Tiedtke Convection

The ECHAM3 version of the Tiedtke mass flux convection scheme is implemented in the off-line model. This scheme is described in Tiedtke [1989] and briefly described in Chapter 2. It is a simple mass flux scheme, which divides convective events into three types: shallow, mid-level and deep. Deep convective events are those in which the column integral moisture converges (not including surface moisture fluxes). The mass flux in this case is proportional to the boundary layer convergence of moisture (including surface moisture fluxes). Shallow convective events are those events where deep convection does not occur, but there is boundary layer moisture convergence.

Mid-level convection occurs when neither shallow nor deep convection occurs, but there is upward vertical velocities, and conditional instability.

This scheme requires the temperature, humidity, vertical velocity (dp/dt), surface flux of moisture and the moisture tendency at every level. In order to calculate the moisture tendency, we chose to advect the moisture around in the model as the first tracer. We looked at several different ways of running the Tiedtke scheme:

The goal was to find the simplest way to recreate the mass fluxes from the forecast center analyses. Therefore we started with Case A, where we use the values of temperature (T) and specific humidity (q) read in from the tape as input to the Tiedtke scheme. In Case B, we use the value of T from the tape, and the advected value of q as input to the Tiedtke scheme. In Case C, we advect T as well as q and use both advected versions in the Tiedtke scheme. (Note that we actually advected potential temperature, and that we interface differently with the diffusion scheme in this case). Case D is similar to Case A, but we calculate $\dot{\eta}$ instead of reading it in. Similarly, Case E is the same as Case C, but we calculate $\dot{\eta}$ instead of read it in. And in Case F we but read in ω, instead of estimating it, but it is otherwise similar to Case C.

The above cases were run in the off-line model and compared to the output from the CCM2 (using the Tiedtke-scheme for convection). Both instantaneous and 1 day averages were calculated and the statistics for the updrafts mass fluxes (as indicator) are shown in Table 3.3. Updraft mass flux is a reasonable indicator of performance. The other variables are described in more detail below.

Table 3.3: Summary of Cases for Convection

CASE	Description	Instantaneous Correlations of PMFU
A	use archived T, q, read in $\dot{\eta}$	0.563
B	use archived T, advected q, read in $\dot{\eta}$	0.677
C	use advected T, q, read in $\dot{\eta}$	0.746
D	use archived T, q, calculate $\dot{\eta}$	0.561
E	use advected T, q, calculate $\dot{\eta}$	0.742
F	use advected T, q, read in $\dot{\eta}$, read in ω	0.748

There are several interesting results from this. First of all, using the advected moisture rather than the archived moisture improves the performance. Additionally, advecting temperature and using that instead of the archived temperature also improves the performance. This is consistent with the idea that the fields read in from the tape are conditionally stable, and need to be destabilized prior to convection.

But, changing how the vertical velocity is derived does not seem very important. Note that the

results from Cases C, E and F are quite similar as are Cases A and D. Thus, we decided to use Case E as our default case: that is, advect temperature and humidity, and calculate $\dot{\eta}$ in the model. (It turns out to be slightly faster to estimate ω than to read it in from the tapes).

The overall behavior of several important variables related to the convection scheme are shown in Table 3.4. The variables are PMFU (updraft mass flux), PMFD (downdraft mass flux), PRECC (convective precipitation), DEEPC (0 or 1 indicating whether deep convection is triggered in that grid box), MIDC (as in DEEPC but for mid-level convection), and SHALC (as in DEEPC but for shallow convection). Also shown for comparison is H_{pbl} as diagnosed from the non-local boundary layer scheme previously discussed. Shown in Table 3.4 for each variable are the correlations between off-line and on-line values at a given time step, the ratio of the standard deviation of the off-line model to the on-line model values, and the ratio of the mean off-line and on-line values. Also shown are the correlation of the one day averages from the off-line and on-line models.

Table 3.4: Tiedtke Convection Scheme

Variable Name	Correlation	Ratio of Standard Deviation (off/on)	Ratio of Mean (off/on)	1 Day Average Correlation
PMFU	0.742	1.03	1.15	0.839
PMFD	0.492	1.28	1.28	0.721
PRECC	0.627	1.04	1.15	0.805
DEEPC	0.724	1.07	1.17	0.855
MIDC	0.858	0.95	0.86	0.911
SHALC	0.770	1.03	1.14	0.871
H_{pbl}	0.954	0.898	0.898	0.953

Overall, the convection scheme seems to do adequately in recreating the convection in the on-line model when we look at one time step. The updraft is done more accurately than the downdraft. Of the types of convection, deep convection appears to be triggered the most differently while mid-level convection is doing the best. Convective precipitation has a moderately good correlation between the off-line and online models. Figures 3.1a and 3.1b show on-line convective precipitation and off-line convective precipitation at a particular time step. As indicated by the correlation, the model correctly diagnoses some convective events, but misses some and puts some in places not seen in the online model.

Once we average the fields for 1 day (4 time periods), we get much higher correlations, and now most of the correlations are above 0.8, which is considered strongly correlated.

3.4.2 Inverse Thermodynamic Convection

The inverse thermodynamic convection scheme is described in Chapter 2 in some detail, and is based on the idea that the convective mass fluxes are a heating term in the potential temperature budget. Thus, we can calculate what the convective mass fluxes must have been over the last period by calculating the residual in the other temperature tendency terms. Since this scheme performed well in the 1-dimensional simulations, we tried it in the 3-dimensional model. Unfortunately, it appears that numerical errors due to truncation, and time sampling are so large, that the convective mass fluxes seen in the online model had no correlation in the offline model. We tried several different numerical differencing schemes as well as virtual potential temperature and potential temperature, but were unable to obtain reasonable mass fluxes with either CCM2 archived winds or forecast center winds.

3.4.3 Pan Convection

Problems with the interhemispheric gradient in the simulations of CFC-11 using the truncated ECMWF winds (discussed in Chapter 5) caused me to add the ability to transport tracers using the NMC reanalysis winds, where truncation would be less of an issue. We first tried using the NMC reanalyses winds with the Tiedtke scheme, but were only getting half the precipitation seen in the NMC reanalysis archives, and there were some indications that there was not enough mid-latitude convection (as seen in the ECMWF with Tiedtke discussed later in this chapter). For these reasons, we decided to adopt the NMC reanalysis convective scheme to be used with the NMC data.

The NMC reanalysis model uses a moist convective scheme developed at NMC by Pan and Wu [1995]. The Pan scheme is a simplified Arakawa-Schubert [1974] scheme, following the work of Grell [1993] and Lord et al.[1982]. The closure for the scheme is that the convective available potential energy (CAPE) relaxes back to a reference profile (from Lord, et al. [1982]) during one time step. Only one type of cloud, or cloud top height is included in this implementation, and there is entrainment only below the cloud base, and detrainment at the cloud top. The cloud base is chosen as the level with the largest virtual static energy, and the height of the cloud is determined by buoyancy. Here, again, a modification was made to the scheme to insure that the convective mass fluxes out of a gridbox during one timestep could not exceed the mass in the gridbox. This scheme has the advantages of being based on a physically realistic theory (quasi-equilibrium), but the assumption that there is only one type of cloud is not realistic, nor is it realistic to assume that there is little entrainment or detrainment along the edges of the cloud (or equivalently that only air from the base and the cloud top mix [Emanuel, 1993]). However, these assumptions simplify the scheme in a manner to reduce the computational costs of the scheme, and have been shown to be consistent with some observations [Grell, 1993].

For the Pan scheme, no online CCM2 runs were available as they were for the Tiedtke scheme, so evaluation is made against precipitation, instead of comparing on-line versus off-line mass fluxes. The Pan scheme is also run in Case E from section 3.4.1 as the default case, since we would expect this scheme to behave similarly to the Tiedtke scheme.

3.4.4 Evaluation of Tiedtke and Pan Moist Convective Schemes

To verify that our convective mass fluxes are reasonable, we compare the off-line model's convective precipitation fields with the convective precipitation calculated by the forecast center on-line. ECMWF convective precipitation is not available, so we use the convective precipitation from the NMC reanalysis for the same time period. Figures 3.2 and 3.3 show the mean convective precipitation for the months of June, 1990 and January, 1991 from the model using NMC and ECMWF winds and from the NMC reanalysis.

For June, 1991, the correlation coefficient for the convective precipitation is 0.76 for ECMWF and 0.93 for NMC, which indicates moderately strong correlation. Similar values occur for the other 12 months. Notice that the NMC runs have a much stronger correlation. This is probably due to the fact that we are comparing different convective schemes when we do the correlation for ECMWF, but we also believe that there may be a systematic problem with the convective mass fluxes derived for the ECWMF runs. Figure 3.4 shows the zonal averaged precipitation for the ECMWF, NMC runs and for the NMC archived values for July, 1990. The convective precipitation calculated using the ECMWF data and the Tiedtke scheme is much too low in Southern Hemisphere mid-latitudes, and about half what it should be in the Northern Hemisphere mid-latitudes.

There are several reasons for the discrepancy between on-line and off-line predictions of convective precipitation. First is that the temperature and humidity fields have been truncated, which may reduce or increase the stability of the profile. There are also errors due to the calculation of the vertical velocity since convective precipitation will be highly sensitive to the vertical velocity. Additionally, the convective precipitation archived by the forecast centers represents a 6 hour average precipitation, thus the forecast model has "spun-up" from the analyses we use to calculate convective precipitation. The forecast model may have calculated a very different state at the end of 6 hours than what the initial values of the temperature, humidity and winds were (this initial state is what we have available from the forecast centers).

A comparison of the updraft mass flux indicates differences in the vertical structure of the convective mass fluxes between the ECMWF-Tiedtke simulation and the NMC-Pan simulation, as shown in Figure 3.5 for July, 1991. The mid-latitude convection is much deeper and stronger for the NMC-Pan simulation, consistent with the amount of precipitation.

3.5.0 Tracer Studies

Next, a simple bulk plume model was implemented to advect tracers using the mass fluxes calculated using the above methodologies. In order to test how well the tracer distributions can be simulated in the off-line model, a CCM2 run (with Tiedtke convection scheme, not the Hack) was made with 12 inert tracers over a 10 day run. Initially the tracers were concentrated at one point located at 6 latitudes extending from 75 N to 75 S at the date line at both 970 mb and 500mb (the same tracers as used in a previous study of time-sampling for off-line models). This tests the ability of the model to simulate very discontinuous tracer distributions over a wide range of latitudes.

The same tracer study is done for three different cases: 1), the off-line model deriving convection and diffusion; 2), with no convective mixing of the tracers in MATCH (but moist convective mix-

ing was allowed in the online model determining the winds); and 3) in a truly "off-line" mode, where the convection and diffusion are read in from the tapes, and only transport and mixing are done in the model, with no coefficients derived. We would expect that Case 3 should do the best job of recreating the on-line model transport, since the mixing parameters are the same. Case 2 should also do a reasonable job of recreating model transport, while Case 2 will test the importance of cumulus convective mixing in tracer transport.

Table 5 shows the average correlations and ratio of standard deviations overall all times and 12 tracers for the three cases.

Table 3.5: Tracer Simulation

CASE	Average Correlation	Average Ratio of Standard Deviation (off/on)
1) Derive Sub-grid scale transport	0.982	0.969
2) No moist convection	0.836	0.782
3)"Offline" (all meteorological variables read in)	0.995	0.958

Overall, the case run in the truly "off-line" mode did the best, as expected, since all the meteorological variables were read in instead of calculated in the off-line model. The case in which the convection and diffusion were derived in the off-line model did quite well as well. In the case of no convection, the average correlation is still above 0.8, but some of the tracers, especially those in the tropics had correlations below 0.5, and the ratio of standard deviations was also below 0.5.

Figure 3.6a shows the 500 mb tracer distributions for a tracer which was initially at 15 S 0 E, 970 mb after 9.75 days of integration, for the online run. Figures 6b and 6c show the same thing for CASES 1 and 2, respectively, with the off-line model. By comparing Figures 6a and 6b, we note that the off-line model is capable of capturing most of the large-scale and fine scale features of the tracer distribution. Figure 3.6c shows that by neglecting convection, we loose most of the fine-scale features, although we can still get the general large scale picture of the tracer distribution.

3.6.0 Summary

This chapter describes the development of the MATCH model which can derive reasonable boundary layer mixing and moist convective transports using NMC reanalysis or ECMWF forecast center winds. There is some possibility that mid-latitude moist convective transport with the ECMWF--Tiedtke combination are too small, but moist convection seemed well rederived when the NMC-Pan combination was used.

Finally, a simple analysis was conducted, demonstrating that offline transports of trace gases with

information only available every 6 hours seems adequate to simulate the transport in an on-line model at horizontal resolutions of T42 and vertical resolutions of 18 levels.

Note that this analysis has emphasized recreating the subgrid scale mixing that was seen in the forecast center winds. There is no attempt here to improve upon the forecast center winds, but merely to use these winds as our best available information about the dynamical state of the atmosphere at a particular time.

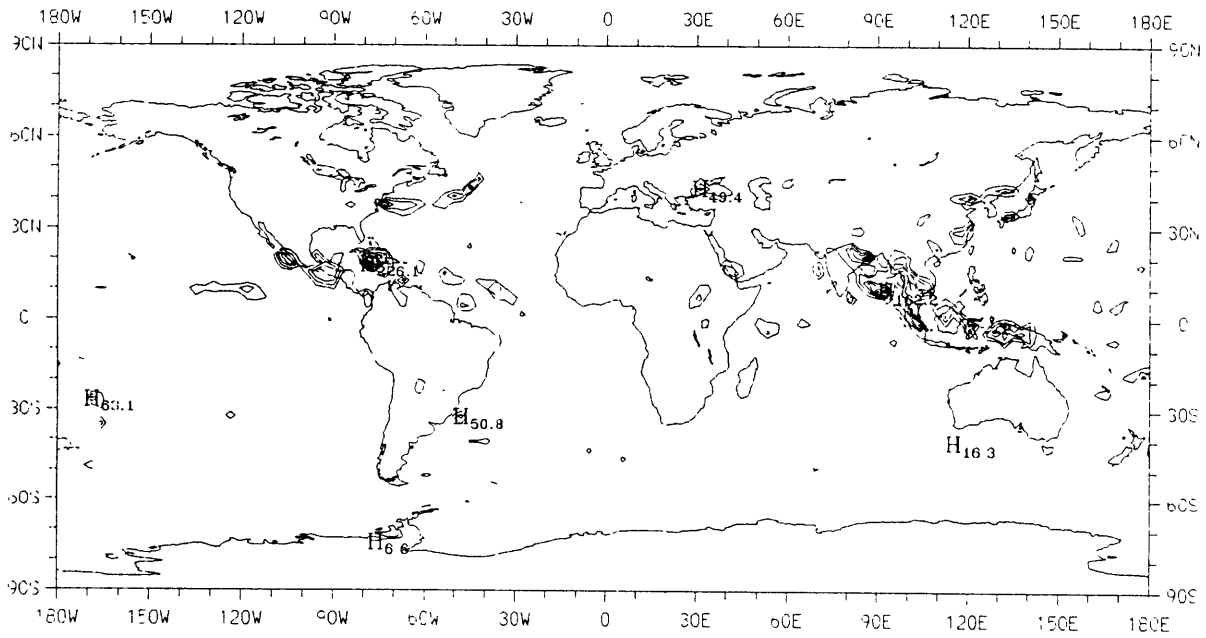

Figure 3.1a: Archived convective precipitation (mm/day) from the CCM2 on-line run with the Tiedtke moist convective scheme. Contour intervals are 20 mm/day.

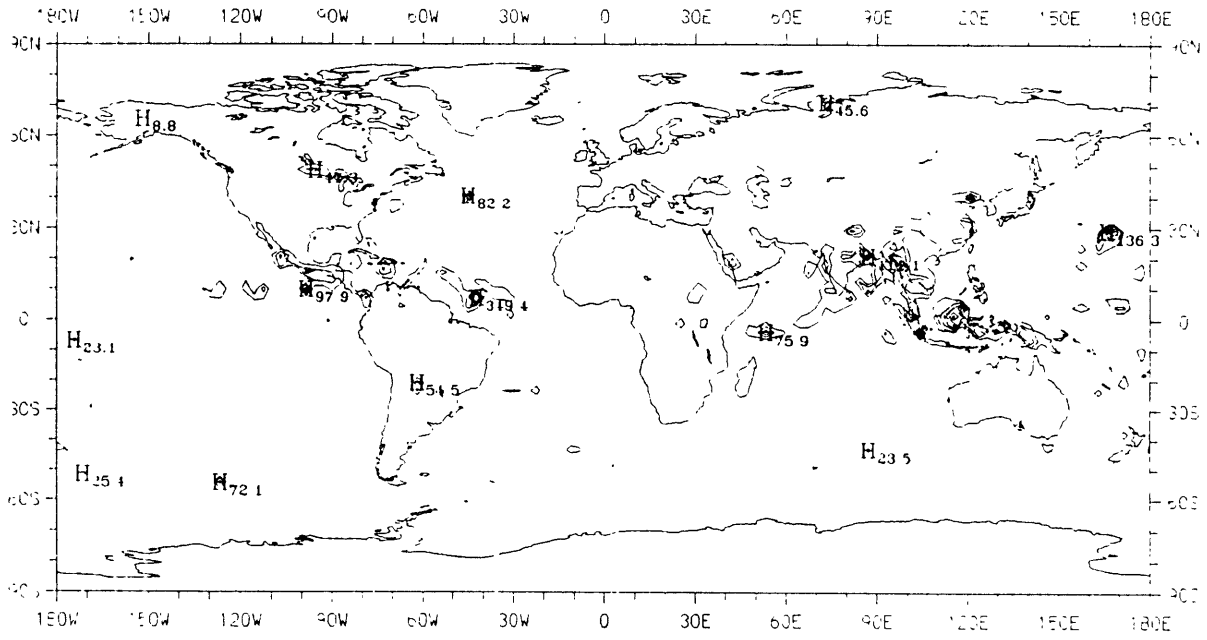

Figure 3.1b: Convective precipitation (mm/day) as derived in the off-line MATCH model using the Tiedtke scheme and CCM2 archived meteorological fields using Case E for the same time period as shown in Figure 3.1.a. Contour intervals are 20 mm/day

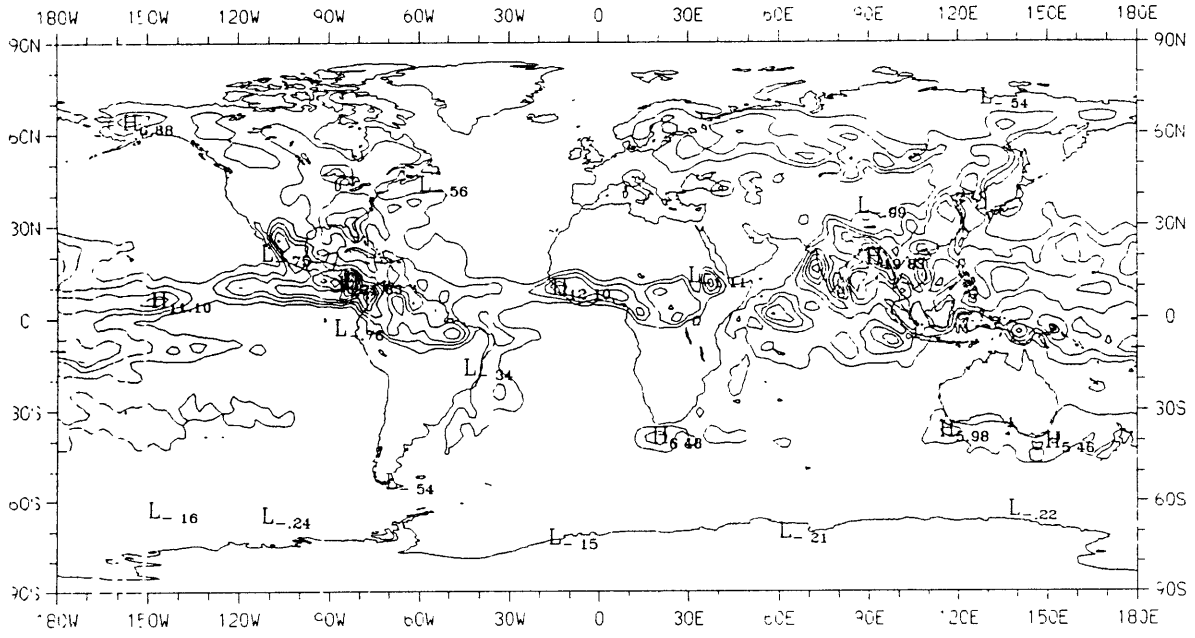

Figure 3.2a: Monthly averaged archived convective precipitation (mm/day)from the NMC reanalysis for July, 1990. Contour intervals are 2.5 mm/day.

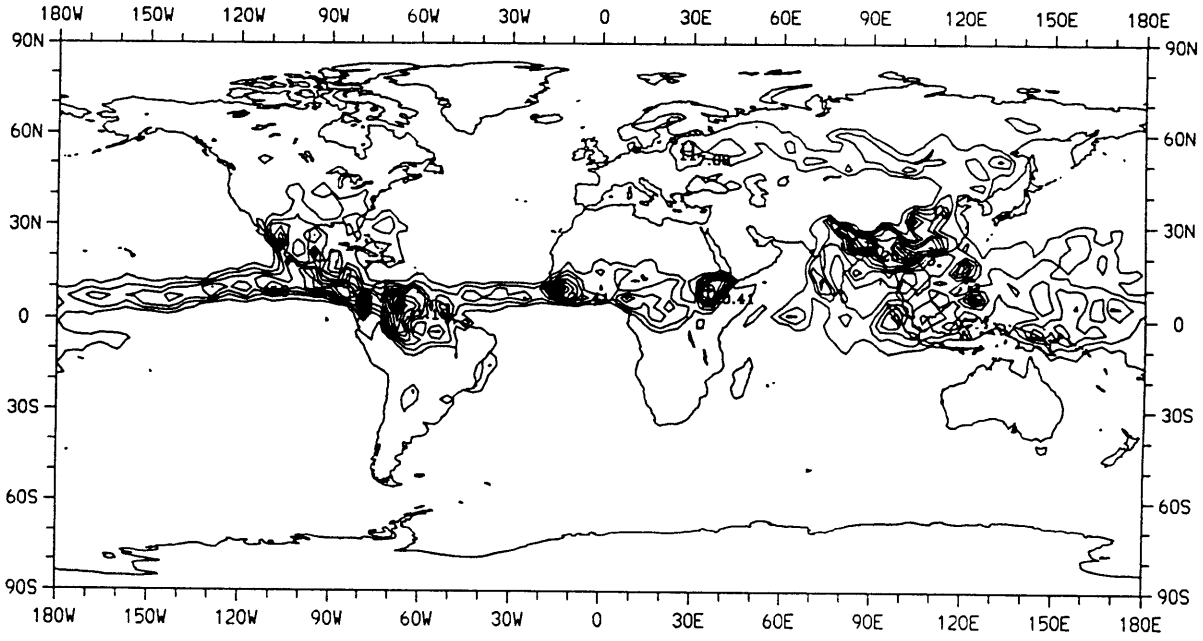

Figure 3.2b: Same as for Figure 3.2a, but derived off-line using the ECMWF analyses and the Tiedkte scheme in the MATCH model.

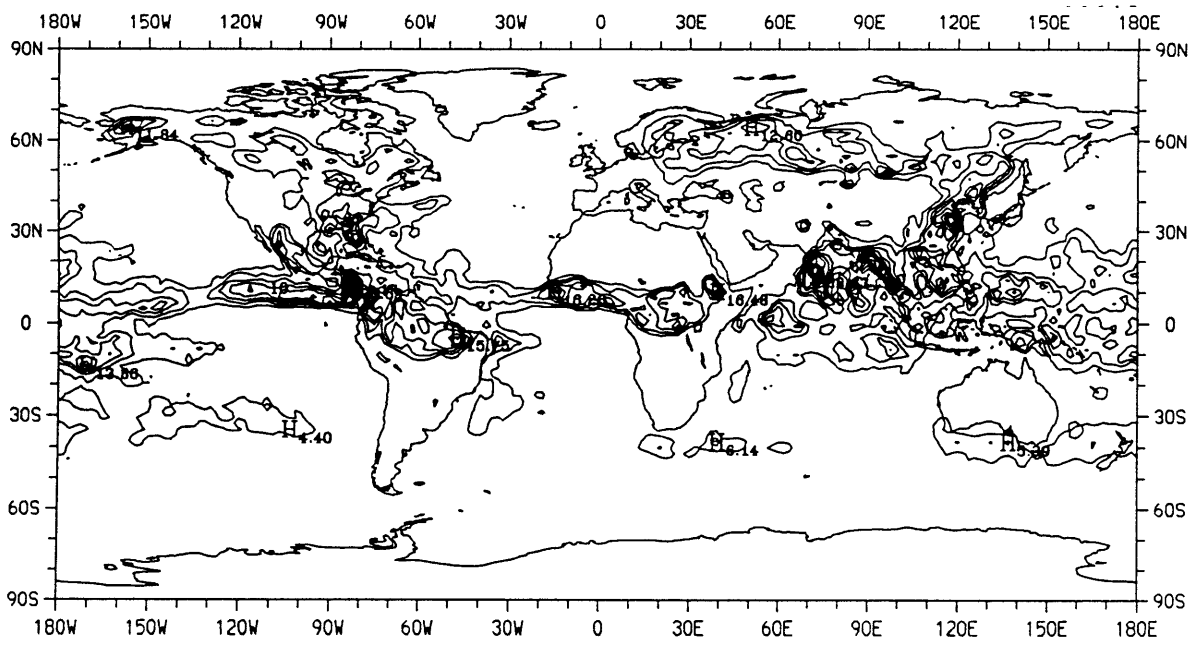

Figure 3.2c: Same as for Figure 3.2a, but derived off-line using the NMC reanalyses dataset and the Pan scheme in the MATCH model.

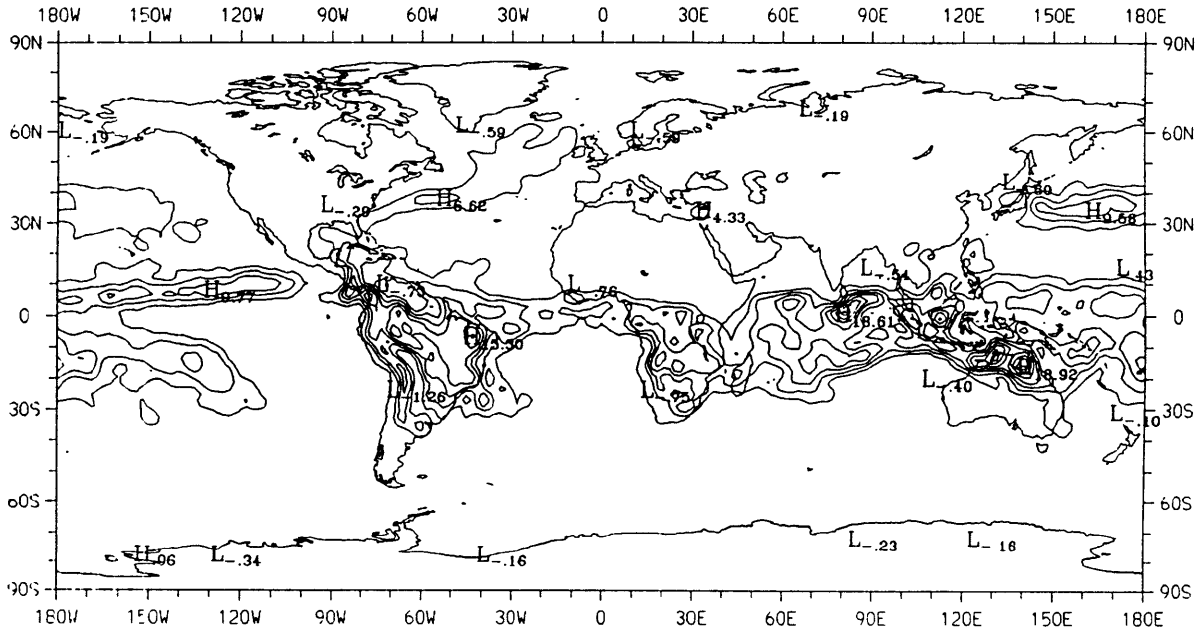

Figure 3.3a: Same as for Figure 3.2a, but for January, 1991.

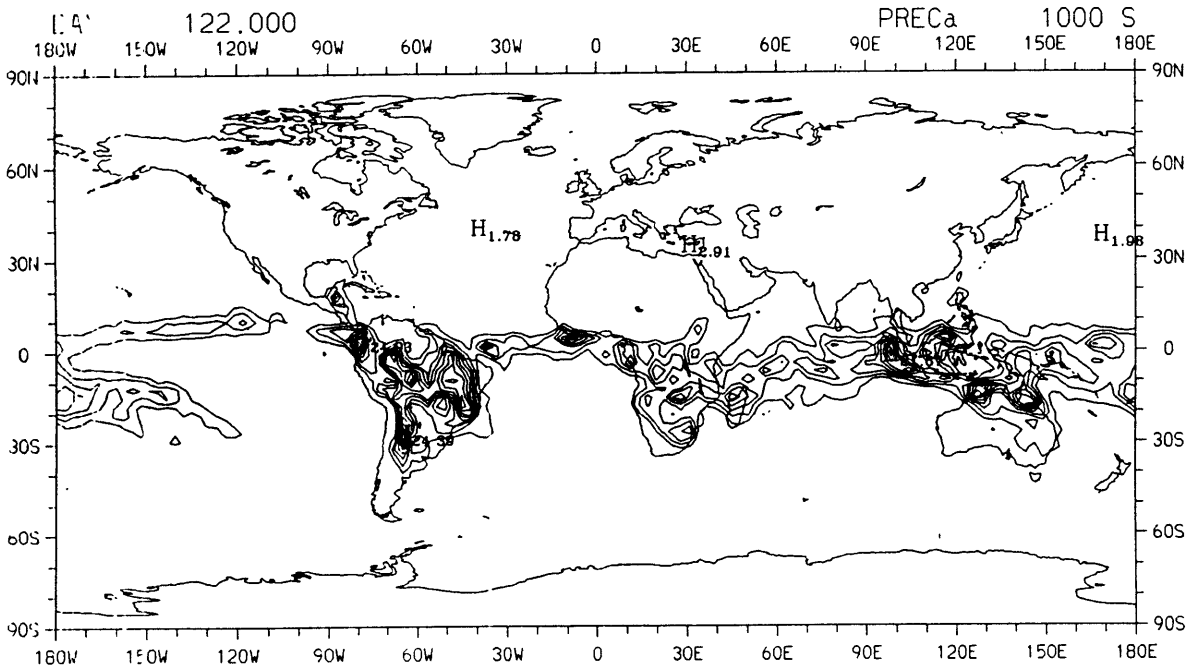

Figure 3.3b: Same as for Figure 3.2b, but for January, 1991.

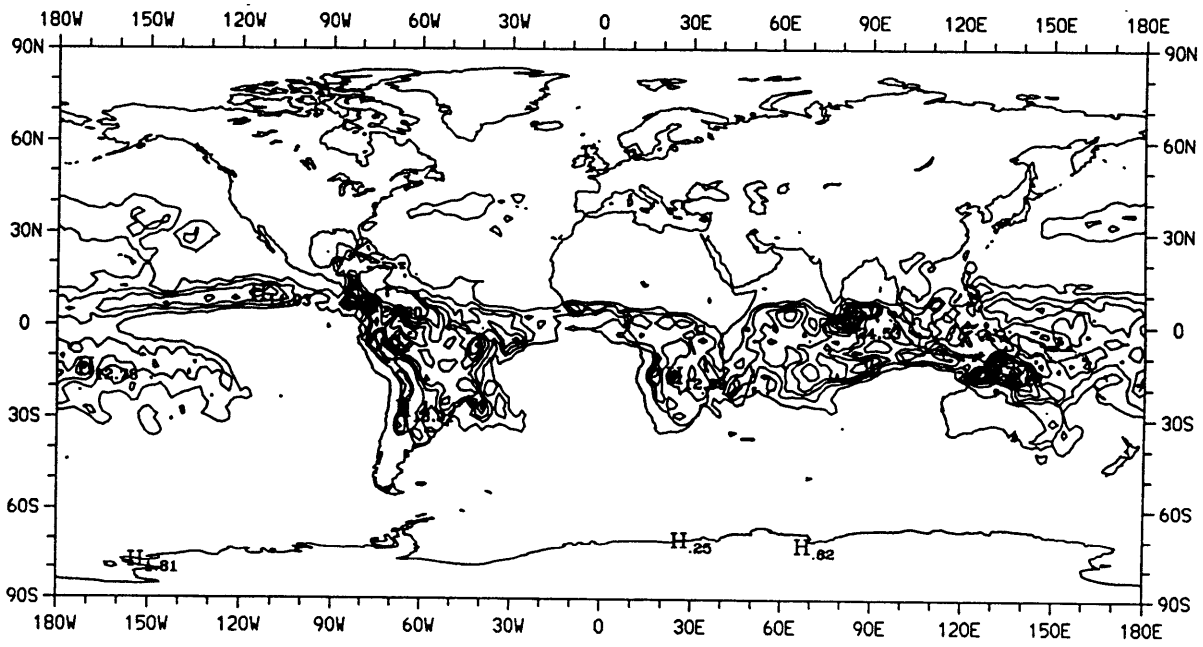

Figure 3.3c: Same as for Figure 3.3c, but for January, 1991.

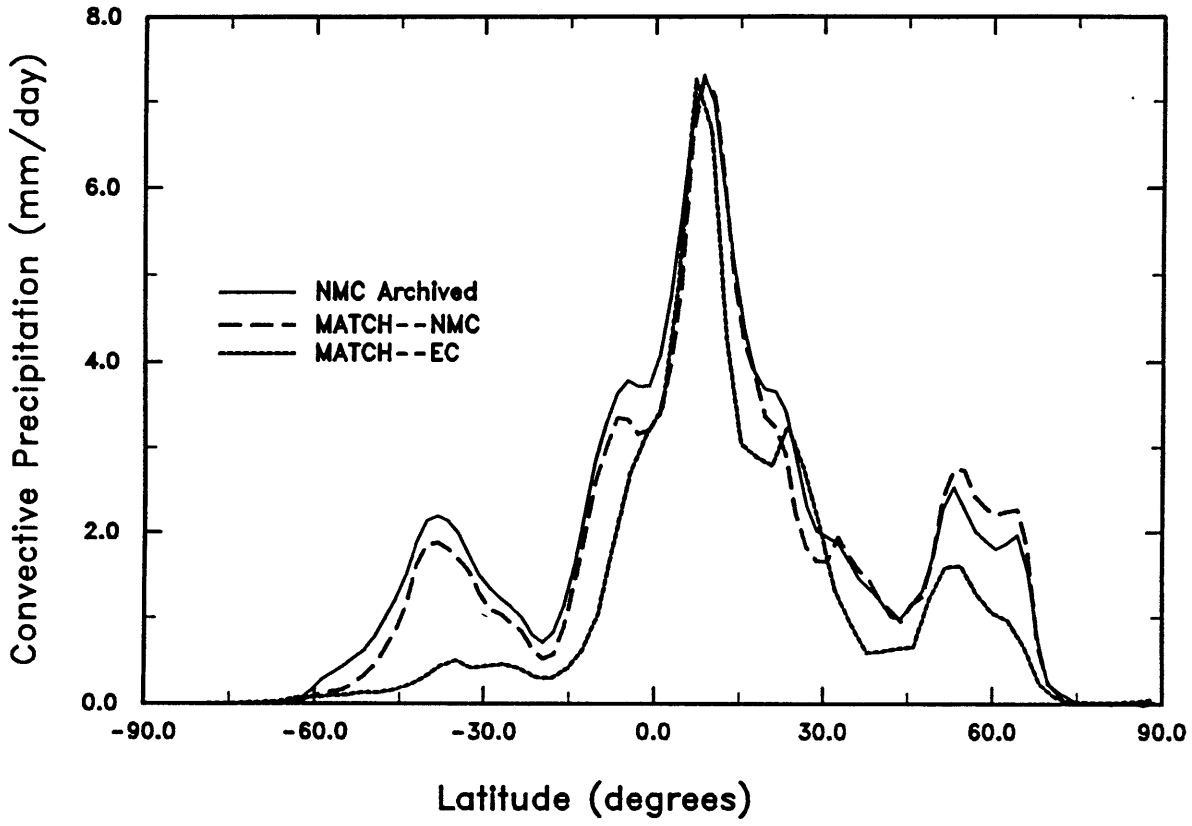

Figure 3.4: Zonally averaged convective precipitation (mm/day) for July, 1990 from the NMC reanalysis archive, the MATCH model using the NMC reanalysis winds and the Pan scheme, and the MATCH model using the ECMWF analysis winds and the Tiedtke scheme.

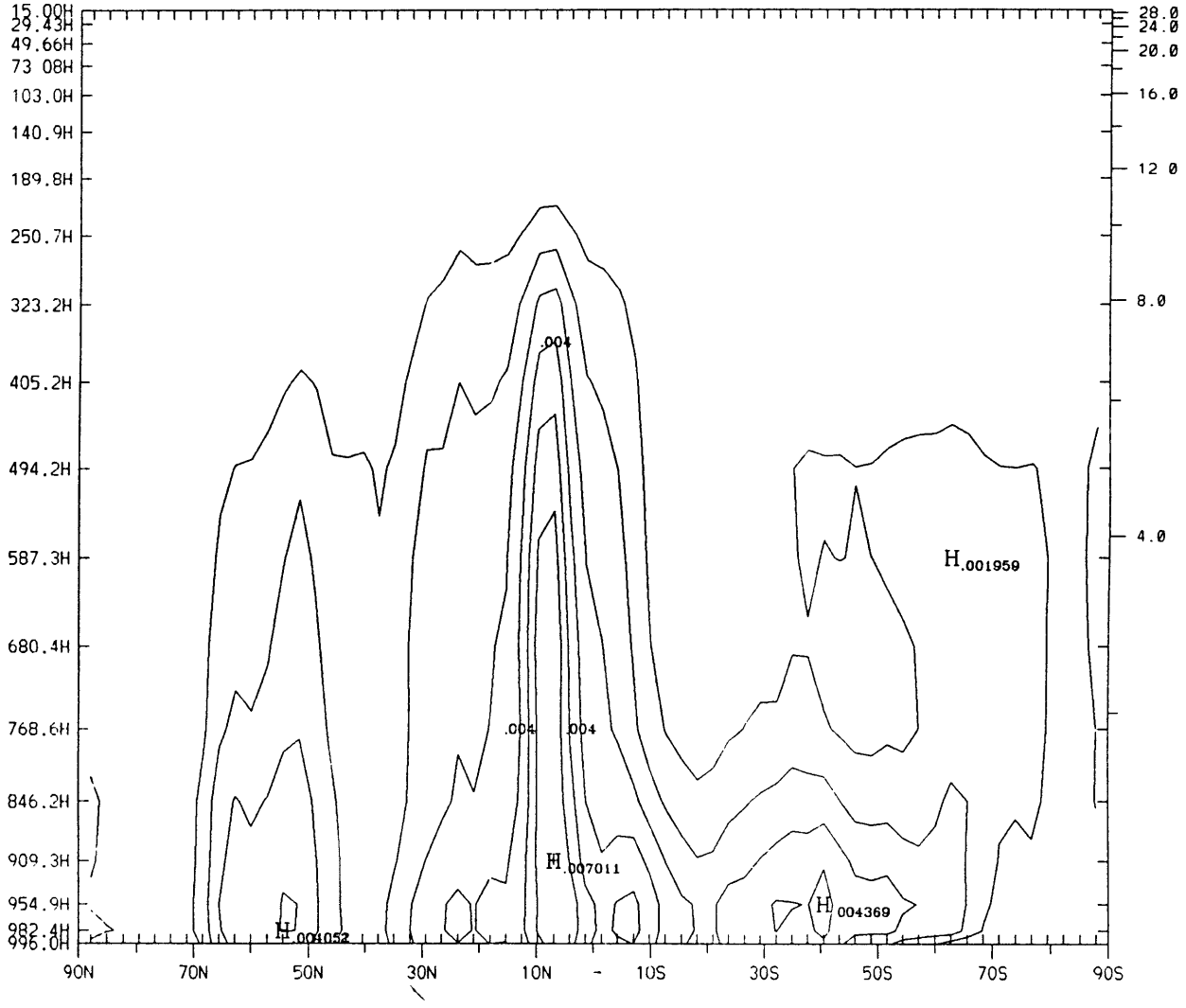

Figure 3.5a: Zonally and monthly averaged updraft mass fluxes (kg/m^2/sec) from the Tiedtke scheme using the ECMWF analyses in the MATCH model for July,1990. Contour intervals are 0.001 kg/m^2/sec.

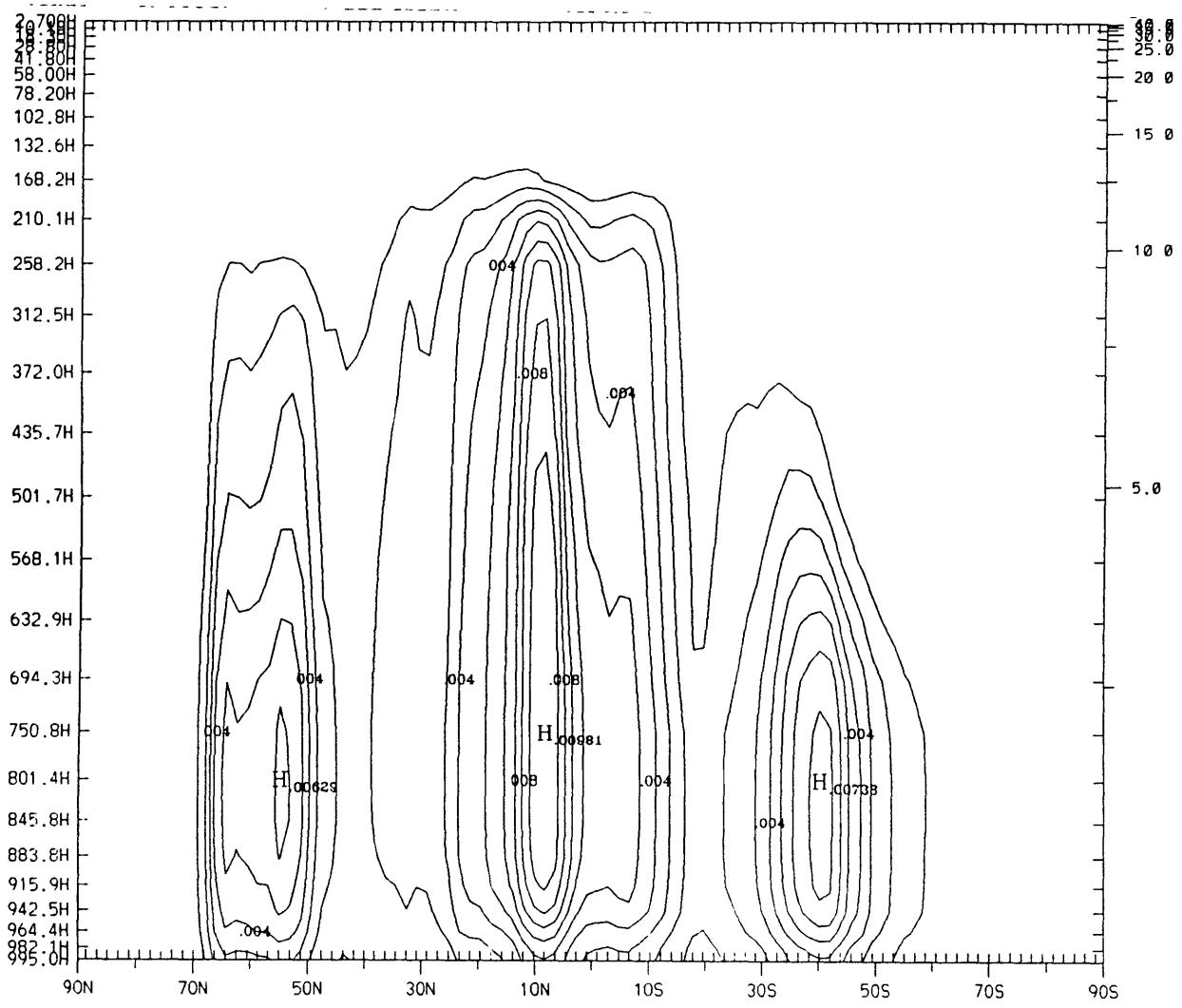

Figure 3.5b: Same as for Figure 3.5a except for the Pan scheme using the NMC reanalysis datasets in the MATCH model.

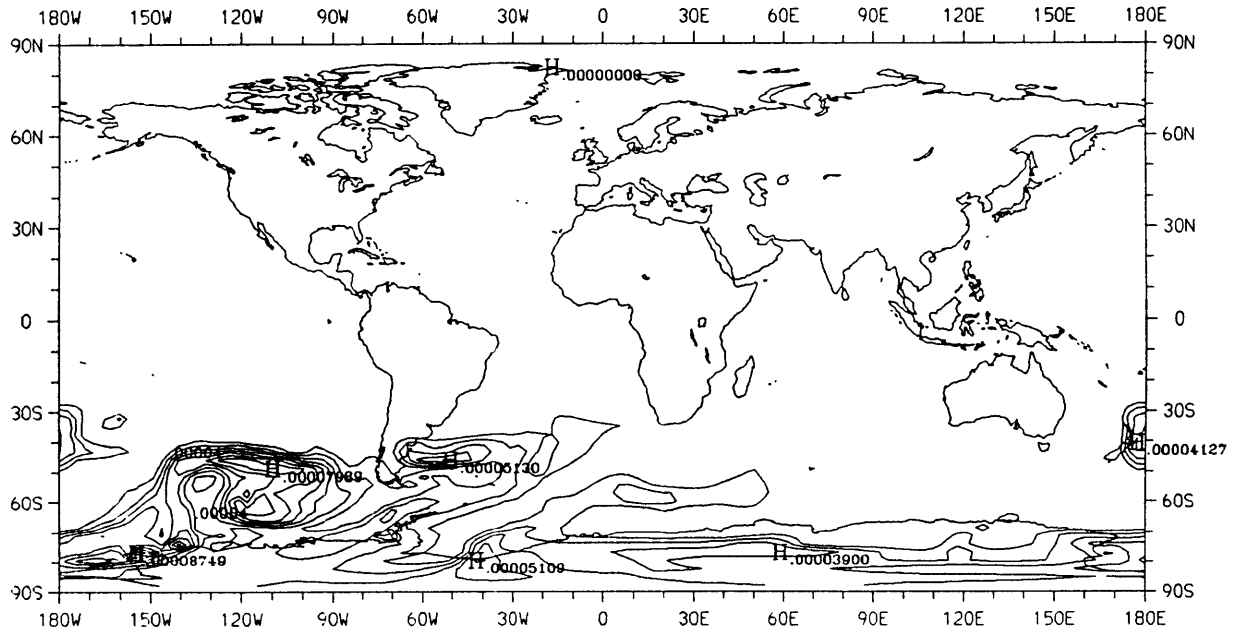

Figure 3.6a: Tracer distribution (kg/kg) after 9.75 days in the on-line CCM2 for a tracer released at a point at 15S, OE at 720 mb. Contour intervals are 0.00001 kg/kg.

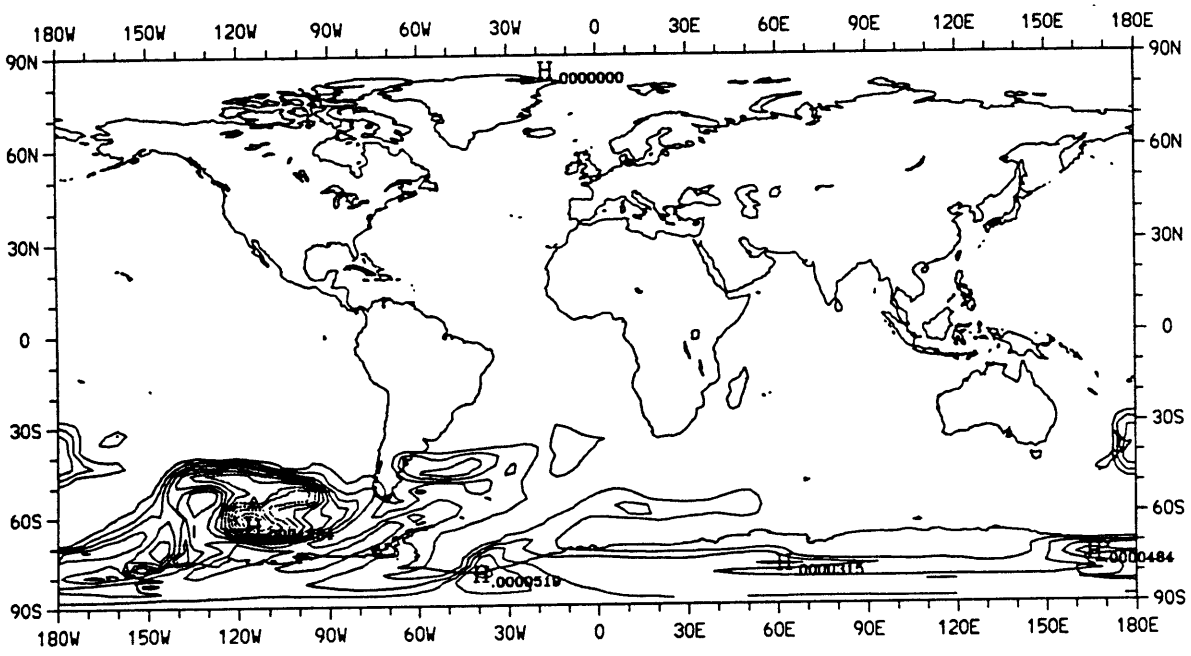

Figure 3.6b: Same as for Figure 3.6a, except for from the off-line MATCH model using the winds from the same simulation as shown in Figure 3.6a, and deriving the moist convective and boundary mixing in the off-line model.

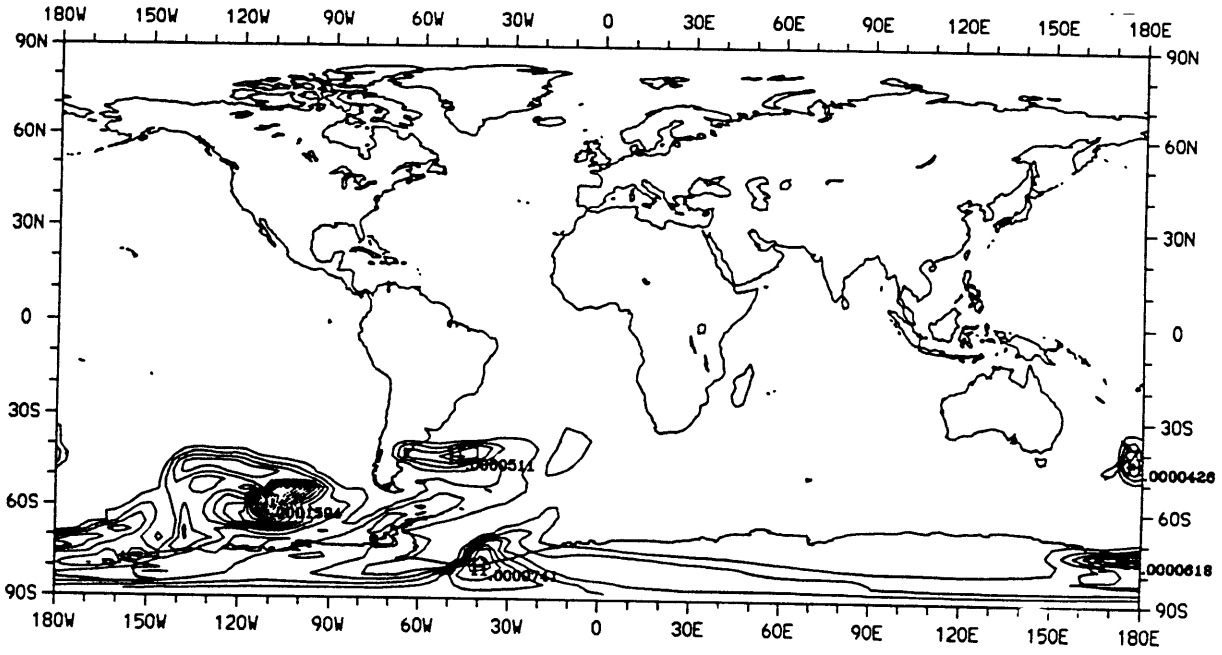

Figure 3.6c: Same as for Figure 3.6b, except that the moist convective mixing does not operate on the tracer distribution in the MATCH model.

Chapter 4:

A comparison of the transport characteristics of ECMWF and NMC winds in ^{222}Radon Simulations

4.1.0 Introduction

Chemical transport models (CTMs) are useful tools for studying the changes occurring in the atmospheric composition of radiatively and chemically active species. Traditionally, CTMs have used general circulation model (GCM) winds to transport trace gases. Winds from GCMs are often able to capture the climatology of tracer transport, but are unable to be compared to specific events. In addition, some applications of chemical transport models require an accuracy which GCMs may not be able to meet, e.g. inverse modeling of the sources of gases [Hartley and Prinn, 1993]. For this reason, we have developed an off-line CTM which is able to transport gases based on forecast center analyses. Forecast center analyses are a combination of the last forecast from the numerical weather prediction model and meteorological observations. As such, they represent our best knowledge of the state of the atmosphere.

However, using forecast center analyses has its disadvantages. These winds are created with the specific goal of making the best weather forecast possible, and thus are not optimized to transport trace gases. In addition, important sub-grid scale mixing parameters are not routinely archived at the forecast centers. We are therefore forced to develop parameterizations for boundary layer mixing and moist convective mixing in our off-line model. Issues surrounding the choice of a moist convective scheme were discussed in some detail in Chapter 2 of this thesis, in addition to Mahowald et al. [1995] and Rasch, Mahowald and Eaton [1996, manuscript in preparation].

This work uses the model described in Chapter 3 based on a semi-lagrangian transport scheme [Rasch and Williamson,1990]. Modifications have been made to the model in order that the forecast center winds can be used. The main modifications have to do with the moist convective scheme chosen to be implemented with the different forecast center winds.

The goal of this chapter is twofold: first, to demonstrate the ability of the MATCH model to simulate pollution events based on forecast center analyses; secondly, to examine the uncertainty in simulations of these events due to the chosen forecast center analysis. This is done by comparing the results of the MATCH model using both sets of winds, both to each other as well as to available observations.

^{222}Rn is a short-lived trace gas (e-folding time of 5.5 days) with natural sources in the continental crust. The sink is radioactive decay, while the source is from uranium decay in the crust. The source of ^{222}Rn is fairly well known, although its magnitude may vary between a factor of 2-4 in various regions. ^{222}Rn is used to evaluate the ability of CTMs to transport gases vertically as well as from continental to oceanic regions [e.g. Balkanski, et al, 1993; Allen et al, 1996]. Because of the uncer-

tainty in the ^{222}Rn source, comparisons at surface continental sites are not included for this study.

4.2.0 Description of Model

A new chemical transport model (MATCH) described in Chapter 3 which uses winds from the forecast centers is used in this study. The MATCH model and the use of off-line models has been described in a previous paper (Rasch, Mahowald and Eaton, 1996l, manuscript in preparation). This model has been designed to run "off-line" (meaning that most meteorological fields are read as archived data, rather than calculated) from either GCM output or from forecast center analyses. Because the routine analyses available from the forecast centers does not contain subgrid scale mixing information such as the boundary layer mixing and moist convective mixing, the off-line model can calculate these fields or it can read them in.

The MATCH model, as described in Chapter 3, contains the semi-lagrangian transport scheme developed by Rasch and Williamson [1990]. The non-local boundary layer scheme from the CCM2 [Holtslag and Boville, 1993] is used for the ECMWF, while the NMC run uses an updated version of this non-local scheme, which reduced the depth of the boundary layer to match observations better.

The version of MATCH used here also contains the Tiedtke moist convective scheme from the ECHAM3 model [Tiedtke, 1989], and the simplified Arakawa-Schubert [1973] scheme developed by NMC [Pan and Wu, 1995] based on work by Grell [1993]. The Tiedtke and Pan convection schemes were evaluated as described in Chapter 2. In addition, we chose to use a convection scheme consistent with that used at the forecast centers. Thus, the ECMWF model runs were conducted with the Tiedtke scheme, and the NMC runs were conducted with the Pan scheme. These schemes and their performance were discussed earlier in Chapter 3.

In this chapter, the MATCH model is used with meteorological driving fields from the ECMWF and the NMC reanalysis for the year from July, 1990 to June, 1991. The ECMWF upper air data is available at T106 horizontal resolution (equivalent to 1.1 by 1.1 degrees) and 19 vertical levels. Unfortunately, running the model at such high resolution is prohibitively expensive, so we chose to make the ECMWF model runs at a reduced resolution of T42 (equivalent to 2.8 by 2.8 degrees). Surface data from the same period is also available from ECMWF. The NMC reanalysis dataset is available at NCAR at T63 (equivalent to 1.8 x 1.8 degree resolution) with 28 levels. NMC reanalysis surface datasets are available for 1985 to the present, and are used for the same 1 year period.

4.2.1 Radon Sources

^{222}Rn is a good test of certain aspects of tracer transport since the sources of radon are reasonably well known and the sink is radioactive decay with an e-folding lifetime of 5.5 days. Radon has been used for previous studies of CTM transport ability (e.g. Jacob and Prather, 1990) and convective transport (e.g. Mahowald, et al., 1995, Feichter and Cruzten, 1991). The source of radon is the decay of uranium and its radioactive daughters in the earth's crust and the degassing from conti-

nental crust. The magnitude of the emissions has been estimated from observations to be close to 1.0 atom/cm^2/s from unfrozen soils [Jacob and Prather, 1990], although it varies depending on the geology and meteorology of a region.

Two different emission scenarios were used in the model development. The ECMWF scenario was conducted for verification of the model, and the most realistic emission scenario was used as described below. Later, the NMC scenario was conducted for the 1995 World Climate Research Programme (WCRP) Model Inter-comparison Workshop, which used a different emission scenario. Future work will entail using the same emission scenario for both the ECMWF and NMC simulations.

ECMWF simulation

Here, the emissions scenario developed by Jacob and Prather [1990] is used, where the emissions F from land at time t+1 are:

$$F(t+\Delta t) = F(t)\, e^{-\Delta\frac{t}{\tau}} + F_o\left(1 - k\frac{\Delta P}{\Delta t}\right)\left(1 - e^{-\frac{\Delta t}{\tau}}\right) \quad (4.1)$$

where Δt is the CTM time step $\frac{\Delta P}{\Delta t}$, is the surface pressure gradient, and k and τ are coefficients which characterize the response of the soil radon to surface pressure changes and are set to 1.1 hr/mb and 8 hr, respectively. F_0 is the baseline radon flux which is set to 1 atom/cm^2/sec when the soil is above freezing temperature and is 1/3 that value when the soil temperature is below freezing.

Over the oceans the emissions are two orders of magnitude smaller than that of frozen soil or 0.0033 atoms/cm^2/s.

The model is initialized with zero concentrations and allowed one month to spin up before a one-year simulation is conducted. In addition to the standard radon tracer, there are also different "flavored" radon atoms simulated in model so that the influence from each different continent can be calculated. In addition, a tracer which undergoes no convective transport was also simulated.

NMCsimulation

The model simulation using the NMC forecast center winds uses the emissions scenario from the 1995 World Climate Research Programme (WCRP) Model Inter-comparison Workshop. Here all land surfaces between 60 N and 60 S land between 60 N and 70 N over Greenland emit at 1 atom/cm^2/s, and other land surfaces and oceanic surfaces are not considered sources. Since emissions from oceans are 2 orders of magnitude smaller than from land, this approximation is considered reasonable. Here, the radon is "spun-up" for 3 months before the results are shown.

Because the two simulations used different emission scenarios, this will reduce the ability to compare the runs for differences due to meteorology or convection. The mass of radon in the NMC sim-

ulation averages 4.35 10^{-15} kg/ m^2 for either July or January, but is 3.41 10^{-15} in January and 4.41 10^{-15} kg/m^2 for July for the ECMWF run with the lower value in the Northern Hemisphere winter due to temperature modification. In this chapter, those specific results which are insensitive to these differences in emission scenarios are emphasized.

4.3.0 ^{222}Rn comparison to observational data

Two types of data are used to compare the model simulations with observations. Vertical profiles extracted from Liu, et al. [1974] for the western U.S. are used to compare model vertical transport with observed vertical transport. In addition, data taken at 6 remote sites (Bermuda, Mauna Loa, Cape Grim, Amsterdam Island, Kerguelen Island, and Crozet Island) are compared against model values.

Observations of ^{222}Rn have been at the Mauna Loa observatory for the period of interest in this study by Stewart Whittlestone from the Australian Nuclear Science and Technology Organization [Harris, et al., 1992]. These observations are made at the top of the Mauna Loa volcano (at approximately 680 mb). Only those observations which are considered to be in free tropospheric air are included in this study. The free tropospheric air data is obtained by excluding all data where the wind comes from a direction which might induce upsloping, and when the dew point is high enough to indicate boundary layer air origin (see MLOPEX description, Ridley and Robinson, 1992, Kasibhatla and Mahowald [1996, manuscript in preparation).

Measurements of ^{222}Rn are available for the July, 1990 to June, 1991 period at the Cape Grim, Tasmania station courtesy of Stewart Whittlestone [Harris, et al. 1992].

The three island stations in the South Indian Ocean (Amsterdam, Crozet and Kerguelen Islands) are operated by the Centre des Faibles Radioactivites (CFR) in France and managed by the French Polar Institute (IFRTP). The CFR has been involved for around 30 years in the measurement of Radon (220 and 222) at Antarctic and Subarctic stations. The measurement method is described in previous papers [Lambert, et al., 1970, Polian, et al., 1986, Heimann, et al., 1990, Ramonet, et al., 1996]. Data has been filtered for local effects by using the measured ^{212}Pb value. ^{212}Pb has a much shorter lifetime than radon, but has a similar source, so that if ^{212}Pb is measured in large amounts, this indicates local contamination. The value of ^{212}Pb which is used to indicate local contamination is different at the three sites and is 0.1, 0.2, and 0.4 pCi/m^3 at Amsterdam, Crozet and Kerguelen, respectively (G. Polian, CFR, 1995, personal communication)

^{222}Rn data has been collected at Tudor Hill, Bermuda by Richard Larson of the Environmental Measurements Laboratory in New York from July 1991 to the present [Hutter, et al., 1995]. Unfortunately, this time period does not overlap the year of meteorological data we have available from the ECMWF, so we can only compare this data to the model results in a climatological sense. For this, we use 1 year of observational data (July, 1991 to June, 1992). The observations are filtered at the Bermuda station by excluding data from the sector for air which blew over the island (Larson, personal communication, 1995).

4.3.1 Summertime convection over western U.S.

Because of its short lifetime, radon can be used as a test of the vertical transport characteristics of a model over continents. Here, the average of 16 profiles taken over the western U.S. is used to compare against the average summer profile in the model [Mahowald, et al., 1996, Liu, et al., 1974] as shown in Figure 2.8 from Chapter 2.

Figure 4.1 shows the modeled radon concentrations vs. observed radon concentrations. The model with ECMWF winds tends to overpredict the radon concentrations between 2 to 4 km substantially, which may be due to an overly-deep boundary layer. Between 5 and 7 km, the model under- predicts concentrations, but the concentrations are within one standard deviation of observed values. Above 10 km, observations show evidence of less radon than the model predicts, although not significantly different. The results with the NMC winds are also shown in Figure 4.1, and show largely the same behavior, but more exaggerated, with even less radon in the 5-7 km region, and radon concentrations overpredicted up to 14 km. The 3-dimensional model results show a column amount of radon which is approximately 25% more than the observed profile. This could be due to errors in the assumed emissions of radon (which are uncertain to 100%), or due to the small number of observed samples not being representative of the real atmosphere.

The reason that the NMC produces such a strong "C-shaped" profile is probably due to the moist convective scheme, which does not allow entrainment and detrainment along the edges of the cloud, but entrains only at cloud base and detrains only at cloud top. Overall the model does a moderate job of predicting the vertical profile of radon over the western USA, but the ECMWF winds and Tiedtke scheme seem to do a better job than the NMC winds with the Pan scheme.

The model was also run in a mode where the cumulus convection scheme was not allowed to operate. Figure 4.1 shows the result of this simulation. Without convection, the model overpredicts concentrations below 4 km and underpredicts concentrations between 6 and 9 km by a factor of approximately 6. The model simulation with the convective scheme performs substantially better than without a convection scheme.

There is not enough mixing from the boundary layer into the lower troposphere for the ECMWF--Tiedtke case, and this may well be related to the reduced convective precipitation predicted by the MATCH-ECMWF when compared with the NMC reanalysis data.

In Chapter 2, a comparison was made between 1-dimensional convective mixing results and the observed radon profiles. We can now compare the 1-dimensional results and the 3-dimensional results. Comparing Figure 2.8 and Figure 4.1 shows that the Pan scheme has a less strong "C-shaped" profile in the 3-dimensional simulations than in the 1-dimensional simulations. While with the Tiedtke scheme, the 3-dimensional model results show a similar profile as the 1-dimensional model results. For either scheme there is 60% of the radon mass in the 3-dimensional results over the western US, than in the 1-dimensional results, which is consistent with the reduced surface flux of radon in a more realistic world. Emissions from the ocean regions are two orders of magnitude

less than from land. The concentrations are less throughout the column in the 3-dimensional results than in the 1-dimensional results, but are more dissimilar in the upper troposphere, as expected, since these regions will be more heavily influence by the oceans upwind of the sampled region.

In Chapter 2, both the Pan and Tiedtke scheme compared well with the observations in the upper troposphere, although the Tiedtke scheme tended to have slightly too much radon in the upper troposphere. But in the 3-dimensional model simulations, the Tiedtke scheme compares better to the observations in the upper troposphere, while the Pan scheme seems to have too little radon in the upper troposphere. This highlights the difficulties of using 1-dimensional simulations to compare against observations. However, the differences between the 1-dimensional and 3-dimensional simulations seem systematic, since there is less radon in the 3-dimensional simulation, and the impact is seen more in the upper troposphere than the lower troposphere, as predicted in Chapter 2. Knowing the expected differences between 1-dimensional and 3-dimensional simulations can allow us to use 1-dimensional simulations to conduct sensitivities studies such as discussed in Chapter 2.

Later, in section 4.4.0, we will discuss the differences between the various model simulations of the vertical distribution of ^{222}Rn from a global point of view.

4.3.2 Mauna Loa

Figure 4.2 shows a comparison of four times daily model output and the twelve times daily observations (filtered) at the Mauna Loa observing station located at 680 mb on a volcano. The most important point to note is that the vertical scale on the observational plot is four times as large as for the model results. Clearly, the model underpredicts the concentrations, especially during the spring. This is seen more clearly in Figure 4.3, where the monthly mean concentrations for the MATCH-ECMWF and MATCH-NMC are compared against the observations.

In Figure 4.4, the modeled and observed concentrations for January of 1991 are shown. Both the ECMWF- and NMC-based model simulations are able to capture some of the important events as well as the seasonality of the events. However, the base-line and peak concentrations are too low by a factor of approximately 2 for these events, and by an even larger factor for the later spring months.

To test whether the model is able to capture specific events, we took the daily average of the modeled and observed concentrations and correlated them. The results of the correlations for all the stations examined here are shown in Table 4.1. The correlation between the ECMWF- and NMC-based model simulations is 0.78, which indicates a moderately strong correlation. This correlation probably represents the uncertainty we have in the calculation of a trajectory from the continents to the remote site. The correlation between the model results and the observations is 0.66 and 0.63 for the ECMWF and NMC simulations, respectively, indicating a moderate correlation. The models seem capable of simulating some of the synoptic scale events, but not all.

Table 4.1: Daily Correlations for ^{222}Rn

Location	EC-NMC	EC-Obs	NMC-Obs
Hawaii	0.7811	0.6591	0.6277
Cape Grim	0.8434	0.6770	0.7060
Crozet	0.7184	0.4566	0.4493
Kerguelen	0.7469	0.3977	0.4785
Amsterdam Island	0.7420	0.5864	0.6760
Bermuda	0.8054		

The ratio of observed concentrations to modeled concentrations is 3.6 and 2.8 for the ECMWF and NMC simulations, respectively. There is a clear discrepancy between the amount of radon reaching Mauna Loa in the models and in the real atmosphere.

Table 4.2: Ratio of Means at Observing Stations

Location	EC-NMC	EC-Obs	NMC-Obs
Hawaii	1.2668	3.5932	2.7641
Cape Grim	0.6852	0.6071	0.8383
Crozet	0.7098	0.4118	0.5858
Kerguelen	0.5651	0.4166	0.7416
Amsterdam Island	0.6479	0.4918	0.7628
Bermuda	1.2604		

For the ECMWF simulation, different "flavors" of radon were used, to identify the origin of the radon from the different continents. From this simulation we know that during the summer and fall, Mauna Loa is approximately equally influenced by North America and Asia, but during the winter and spring, the dominant influence from the continents is from Asia. The influence from the oceans is less important than from the continents.

There are at least three possible reasons why the model would underpredict the mean concentrations at Mauna Loa. First, the winds may be too weak or slightly north of Mauna Loa in the model. Note that although the ECMWF winds are constrained by the analysis procedure to be close to the observations, they may differ significantly from the real atmosphere in regions where there are sparse observations, and the Pacific Ocean is such a region. If the winds were simply too slow, we

can estimate how much faster they should be. The concentrations are 4 times too low and the half-life of radon is 3.8 days, while the distance to Asia is approximately 6400 km. In order to get the existing radon there in a time that will double its predicted concentrations, the radon would have to get to Mauna Loa within its half-life, so at a speed of 19 m/sec faster. It seems unlikely that the ECMWF and NMC winds are in error to that order.

The possibility that the winds are strong enough, but just located slightly too far north is more likely. Figure 4.5 shows the mean May vertical profile of radon in the model for the grid box at Mauna Loa, as well as the concentrations in the two gridboxes north of Mauna Loa (the gradients in the east-west direction are much smaller). Notice that the gridbox which should contain Mauna Loa has the lowest concentration, while by moving one grid box north and slightly higher than the 680 mb, the modeled concentrations go up by a factor of 2.5--not enough to agree with observations, but certainly in better agreement. Thus, the model may not be bringing the radon to exactly the correct latitude and height, but may be otherwise doing a reasonable job.

Secondly, the assumed emission rate of radon from Asia might be too small [Kasibhatla and Mahowald, 1996, manuscript in preparation]. There are very few observations in Asia, so it is difficult to assess how much error they may due to emission rate. There is some collaboration for this hypothesis--the modeled deposition of Pb-210 (a daughter species of ^{222}Rn) is much less than the observed deposition at sites in Japan in the WCRP intercomparison [Feichter, Law, Penner and Rasch, 1996,manuscript in preparation].

Thirdly, the observations at a particular location are not representative of the concentration in an entire gridbox at the exact location and height. The designers of the MLOPEX experiment have gone to considerable lengths to prove that their filtered observations actually represent free tropospheric air, not boundary layer air, and their arguments are convincing [Ridley and Robinson, 1992]. It is also possible, that the air originates slightly higher or lower than 680 mb, due to the wake effects of the island, which has not been excluded by their analyses. As seen in Figure 4.5, the vertical gradient in radon during some months may be significant, so this may affect the results. But the fact that there is a long time series available makes it more likely that the observations are representative of area near the site.

4.3.3 Cape Grim, Tasmania

Measurements of ^{222}Rn are available for the July, 1990 to June, 1991 period at the Cape Grim, Tasmania station made available by Stewart Whittlestone at the Australian Nuclear Science and Technology Organization [Harris, et al., 1992]

Figure 4.6 shows a comparison of the four times daily model results and the observations at Cape Grim. Overall, the models seem to be able to simulate the frequency and seasonality of the pollution events. In addition, as shown in Figure 4.7, the model simulations are able to capture much of the seasonal cycle seen at Cape Grim.

By comparing the daily average observed and modeled concentrations, we get a correlation coefficient of 0.70, which indicates moderate correlation, as shown in Table 4.1. An analysis of the two model runs shows a correlation coefficient of 0.84. This is consistent with the fact that Cape Grim is close to the region where most of the relevant sources of radon are (Australia), so that the trajectories are less uncertain than at the other remote sites considered here. Figure 4.8 shows the model results and observations for January, 1991, showing that the model is capable of capturing specific pollution events at this site.

An analysis of the "flavored" radon in the ECMWF simulation indicates that most of the influence at Tasmania comes from Australia, as expected. The model can predict the background concentrations at Tasmania to within 20%, but the peak values are overpredicted by a factor of 1.88 for the ECMWF data, and slightly less for the NMC simulations. Overpredicting the peak concentrations by a factor of 2 is within the uncertainties in the source, although it may also be due to problems in the boundary layer scheme or boundary layer venting in the model.

4.3.4 Amsterdam, Crozet and Kerguelen

Here, data from July, 1990 to June, 1991 are compared to model output for the three stations. The radon concentrations from the model simulations and observations for the year are shown in Figure 4.9a-c for Amsterdam, Crozet and Kerguelen, respectively. The model seems to be able to simulate many of the pollution events, and the seasonal cycle in these events. A comparison of the seasonal cycle is more easily seen in Figure 4.10a-c, where the monthly averages are shown for Amsterdam, Crozet and Kerguelen, respectively. The MATCH-ECMWF overpredicts concentrations at all three stations by a factor of approximately two, while the MATCH-NMC is within 25%. All three stations are influenced fairly evenly by Africa and South America in the model simulation using ECMWF winds.

The observational data and model results were averaged each day and correlated. The correlation coefficients were 0.60, 0.46, and 0.40 for Amsterdam, Crozet and Kerguelen, respectively, using MATCH-ECMWF, and 0.68,0.45 and 0.48 for Amsterdam, Crozet and Kerguelen, respectively, using MATCH-NMC thus indicating a moderately weak correlation for individual events (as shown in Table 4.1). The correlation between the MATCH-ECMWF and MATCH-NMC runs indicates moderate correlations of about 0.7 for all stations. Figures 4.11a-c show January, 1991 results for the observations and model, and suggest that the MATCH-NMC simulation does a better job. This is probably due to the differences in the sources for the two model runs, since the biggest difference is in the background concentrations. The differences in the source is the largest at high latitudes, where these islands are located. This suggests that the latitudinal distribution from the WCRP sources is despite its relative simplicity more realistic than that from the Prather and Jacob paper.

Since the meteorological observational data are very sparse in the Southern Hemisphere and the southern oceans, especially, it is not unexpected that the model transport would not do very well at these three stations. In addition, the stations are far from continents, so that uncertainties in the tra-

jectories will add further uncertainties to the modeled concentrations.

4.3.5 Bermuda

Figure 4.12 shows the concentrations from the model simulations for 1990-91 and from the observations for 1991-2. Specific pollution events cannot be captured, since the observations are not available for the year that was simulated. However, the frequency and size of the pollution events, as well as much of their seasonality seems to have been captured, with the exception of the month of June, where the model predicts too many pollution events.

Figure 4.13 shows the monthly mean concentrations from the model for 1990-91 and for the observations for 1991-2. The agreement is fairly good for MATCH-EC, except in May and June, where the model substantially overpredicts the concentrations, while the MATCH-NMC seems to overpredict the mean concentration. It is unclear whether this is due to a difference in the meteorology of the specific years compared here, or whether the model is incorrectly simulating the spring in the North Atlantic. In the model, the radon from Bermuda comes almost exclusively from North America.

The correlation coefficient calculated by comparing the model simulations was 0.8, and the mean concentrations were with 25%, so the model simulations using the different meteorology are similar.

4.4.0 Comparison of vertical structure of simulations

Previous studies have indicated substantial differences in the vertical structure of radon concentrations simulated by global chemical transport models [e.g. Jacob, et al., 1996]. It is often unclear whether this is due to interannual variability or systematic differences in vertical transport, because the models which were compared have often used different input meteorology. But one- dimensional studies have suggested that convection schemes can result in very different vertical profiles based on the same meteorology [see Chapter 2 and Mahowald, et al., 1995].

Here, we can compare the vertical transport predicted using the same year of meteorology, but different forecast center datasets and moist convection algorithms. This allows us to make some conclusions about uncertainties in tracer profiles due to the model. In considering again Figure 4.1, we can see that there are substantial differences in the concentrations predicted by the various versions of the MATCH model. And there are other regions where the moist convective scheme is of even greater importance than the western U.S. in determining the vertical transport, as seen in the June-July-August averaged vertical profile over tropical South America (down to 30 degrees S) as shown in Figure 4.14. There is a factor of 5-10 higher radon concentrations in the simulations with a moist convective scheme than without for the case of ECMWF winds between 9 and 14 km. (There was no simulation using the NMC winds and no convective transport of the trace gases.) In the same region, there is a difference of 40% between the concentrations predicted by MATCH-ECMWF and MATCH-NMC. So even with moist convective schemes, there can be substantial dif-

ferences in model predicted concentrations in the upper troposphere.

The differences in these profiles may be due to differences in the sources of radon used for the two simulations, but the net amount of radon in the atmosphere is the same and sources are very similar for all but the high latitudes during the winters.

Zonally and monthly averaged concentrations for the ECMWF, NMC and ECMWF-NOC (the ECMWF simulation with no moist convective mixing of the tracer) simulations are shown in Figure 4.15a, 15b, and 15c, respectively. There is substantially more radon mixed into the northern mid-latitudes in the NMC case than in the ECMWF case and also in the ECMWF case versus the EC-NOC case. In order to more quantitatively compare the cases, we interpolated the MATCH-NMC monthly averaged field for July, 1990 and January, 1991 onto the MATCH-ECMWF horizontal and vertical coordinate system, and compared the fields. Figure 4.16a shows the percent difference in concentrations between the ECMWF and the ECMWF-NOC case. Between 4 and 16 km high, and between 10 S and 70 N there is over a 30% difference in predicted radon concentrations between having a moist convective scheme and not having a moist convective scheme.

In addition, there can be a substantial difference in concentrations predicted by different meteorological fields using different moist convective schemes, as shown in Figure 4.16b.Between 8 and 14 km high and between 10S to 70N there is over a 40% difference in predicted concentrations. This suggests that the difference seen in Figure 4.14 is a systematic difference in vertical transport between the two simulations (ECMWF and NMC).

Since the differences between the NMC and ECMWF simulations are less than the differences between the ECMWF and EC-NOC simulations, it suggests that differences in the moist convective scheme are responsible for the differences in vertical transport.

4.5.0 Summary and Conclusions

The MATCH model is able to simulate large scale features of the observed ^{222}Rn distribution such as the mean vertical profile and the surface time series at some remote oceanic stations. However, underprediction of radon was significant at Hawaii indicating not enough ^{222}Rn was transported to the Mauna Loa site. This could be due to model error or error in the assumed emissions of ^{222}Rn in Asia. The simulations at Cape Grim and Mauna Loa indicate that the model is able to capture the timing if not the magnitude of many specific pollution events quite well. But simulations at Crozet, Amsterdam and Kerguelen Islands, were only able to capture the seasonal cycle of events, which is consistent with the fact that these sites are in areas where there is limited observations of the meteorology, and the trajectories from continental regions are quite long.

Comparisons of the two model simulations of radon using ECMWF and NMC winds indicate the uncertainties in models of this kind. The results indicate moderately strong correlations between model predictions at the surface. Because there were differences in the sources used for this source,

however, our conclusions have an added uncertainty. Mean concentrations at the surface in remote oceanic regions can differ by 40% in the two model runs, which could equally well be due to differences in transport or sources.

The results here indicate that the inclusion of a moist convective parameterization for mixing due to cumulus clouds is important to simulate the vertical distribution of trace gases. In addition, there is an indication that differences in moist convective schemes and meteorological winds can change the mean upper troposphere concentrations in large sections of the globe, especially the tropics by 40% (this difference should be insensitive to source differences)

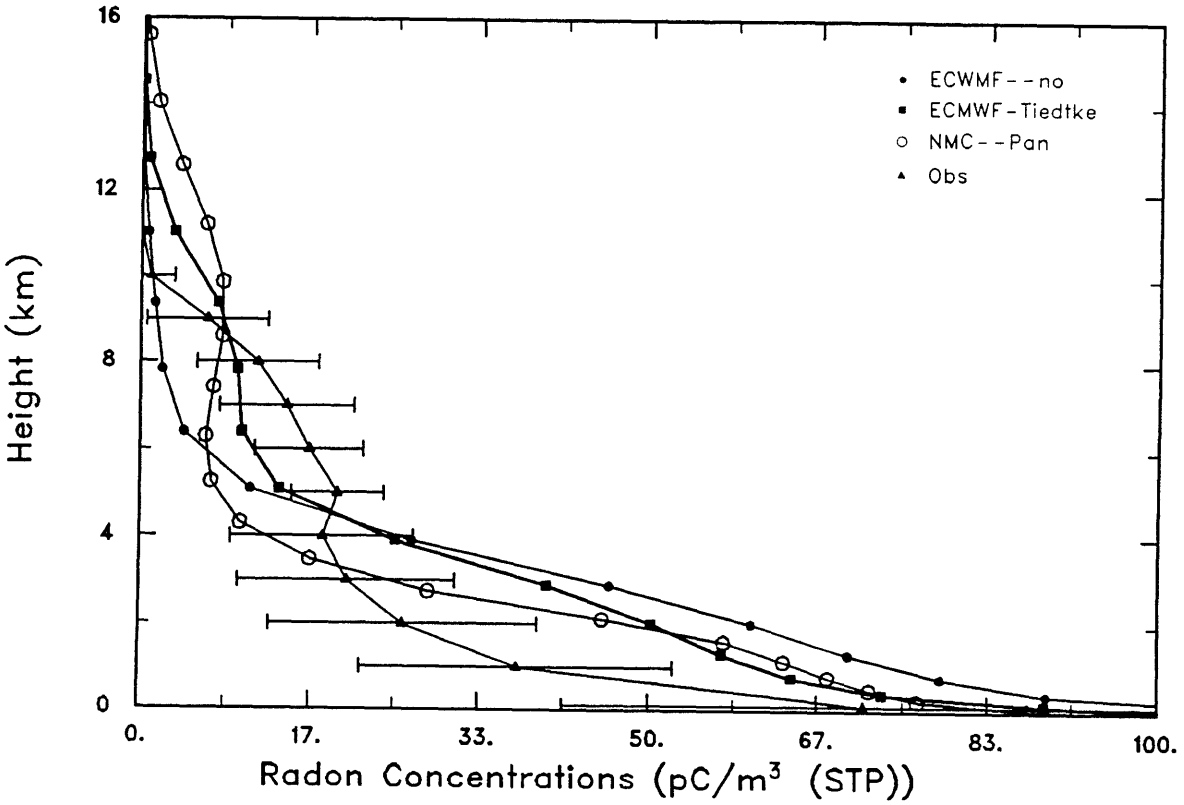

Figure 4.1: Vertical profile of 222Rn over the western USA. Observations taken from Liu, et al [1974] as described in Chapter 2. Model concentrations are summer averages over the western USA for the MATCH model using ECMWF winds with no convection and Tiedtke convection and using NMC reanalysis winds with Pan convection.

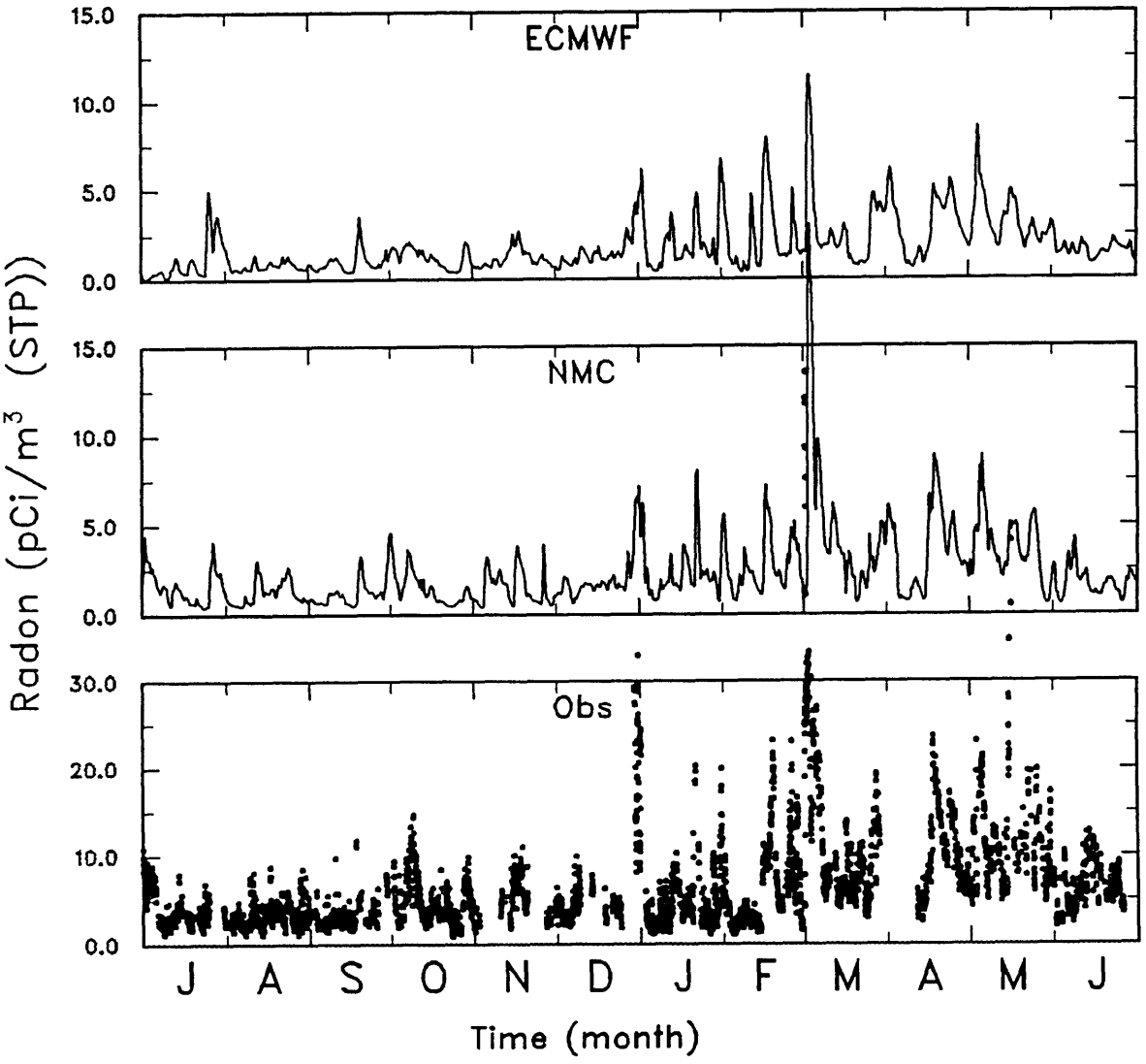

Figure 4.2: Radon concentrations (pCi/m^3 at STP) observed and modelled at the Mauna Loa site on Hawaii for July, 1990 to June, 1991. Observations courtesy of Stewart Whittlestone, and have been filtered to represent free tropospheric air, as described in the text. Modelled concentrations from the MATCH model using ECMWF and NMC winds. Note that the vertical scale on the observations is much larger than for the model results.

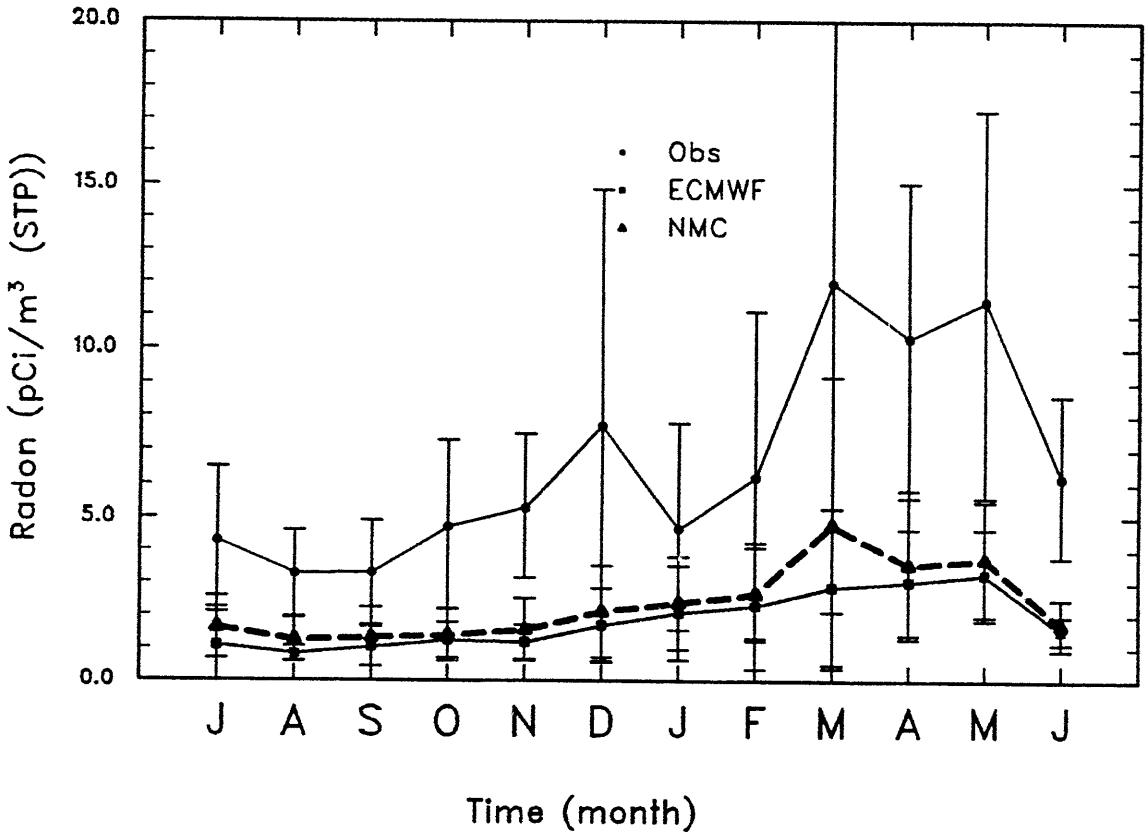

Figure 4.3: Monthly mean radon concentrations for the Hawaii observing station ε s described in Figure 4.2.

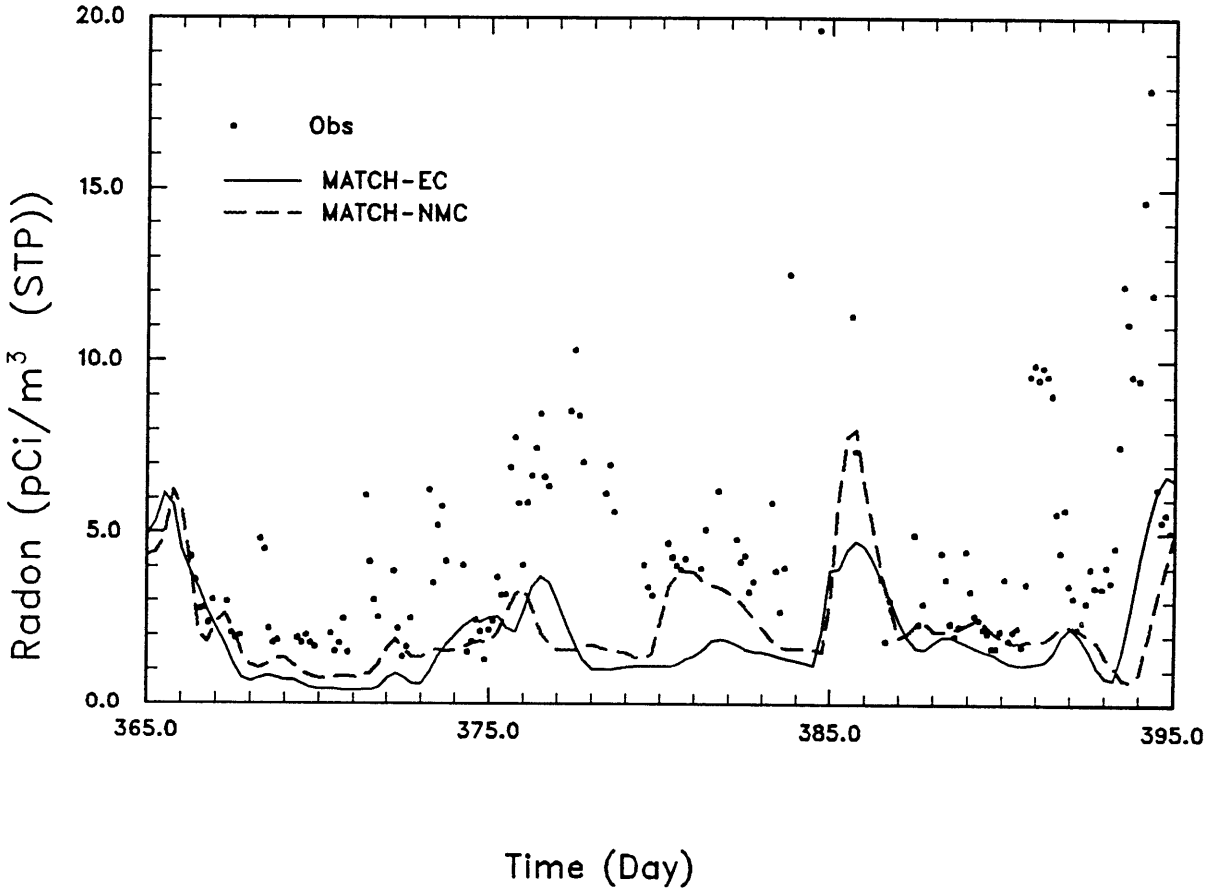

Figure 4.4: Radon concentrations at Hawaii for January 1 through January 30, 1991 from the observations and two model simulations, as described in Figure 4.2.

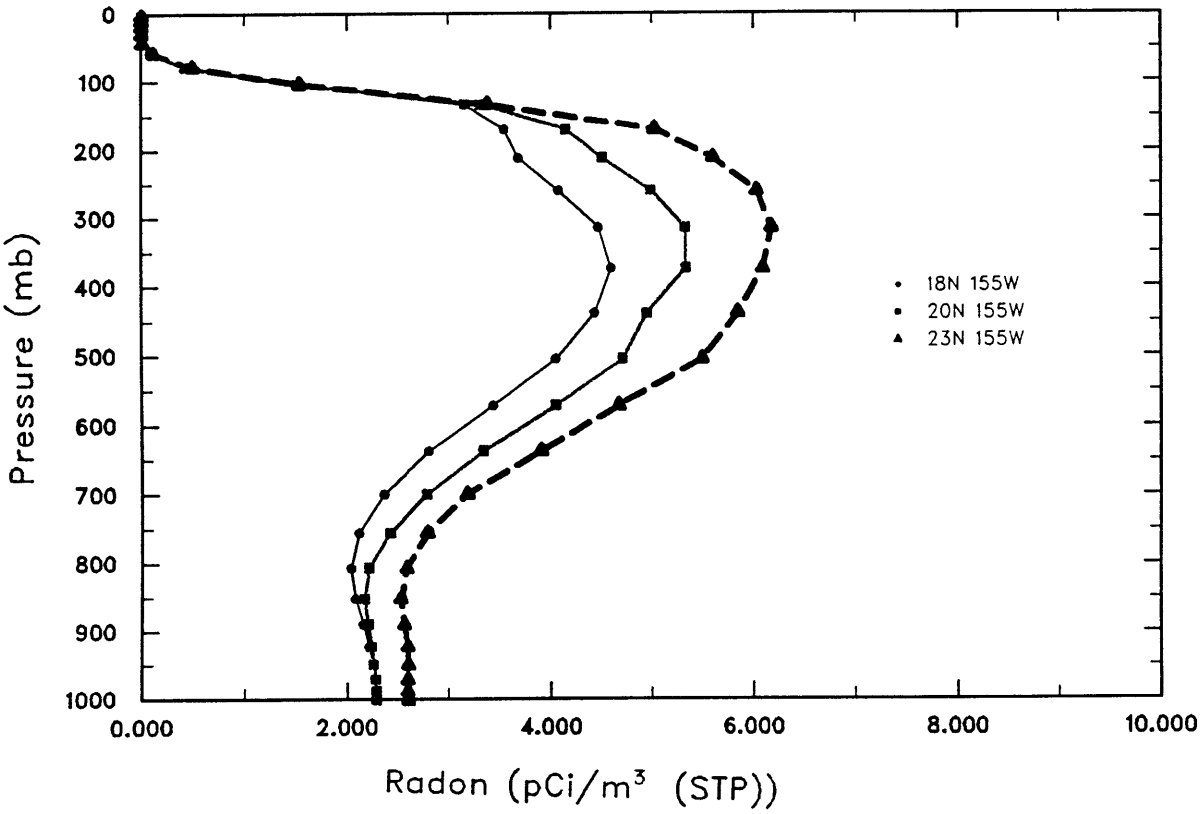

Figure 4.5: Vertical profiles of 222Rn in the MATCH-NMC simulation for latitudes close to the Mauna Loa Observatory, as listed in the legend. The Mauna Loa Observatory is located at 680 mb at 20N and 155E. Notice that the vertical and latitudinal gradients are large at this station.

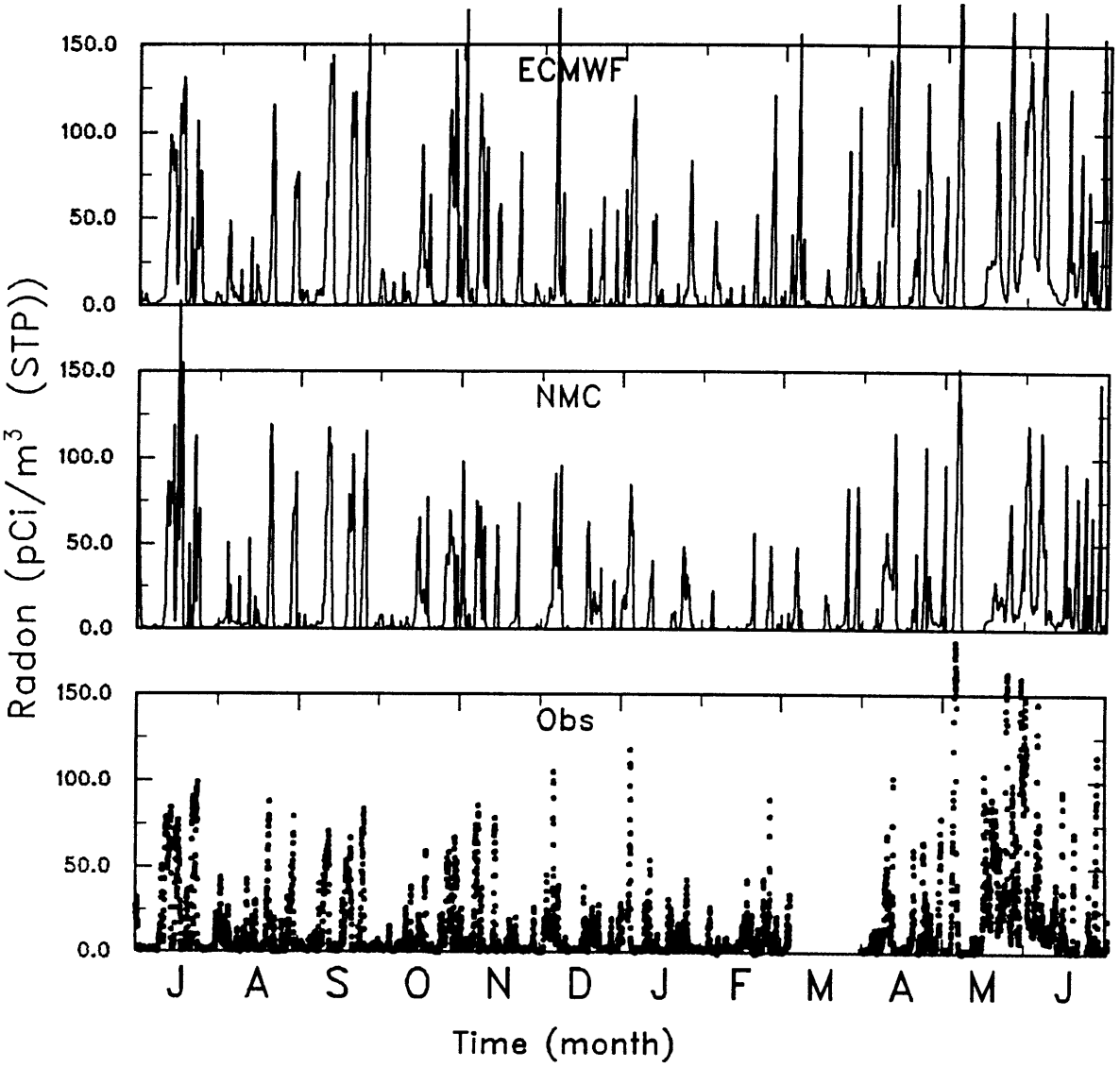

Figure 4.6: Radon concentrations (pCi/m^3 at STP) observed and modelled at the Cape Grim, Tasmania site for July, 1990 to June, 1991. Observations courtesy of Stewart Whittlestone. Modelled concentrations from the MATCH model using ECMWF and NMC winds.

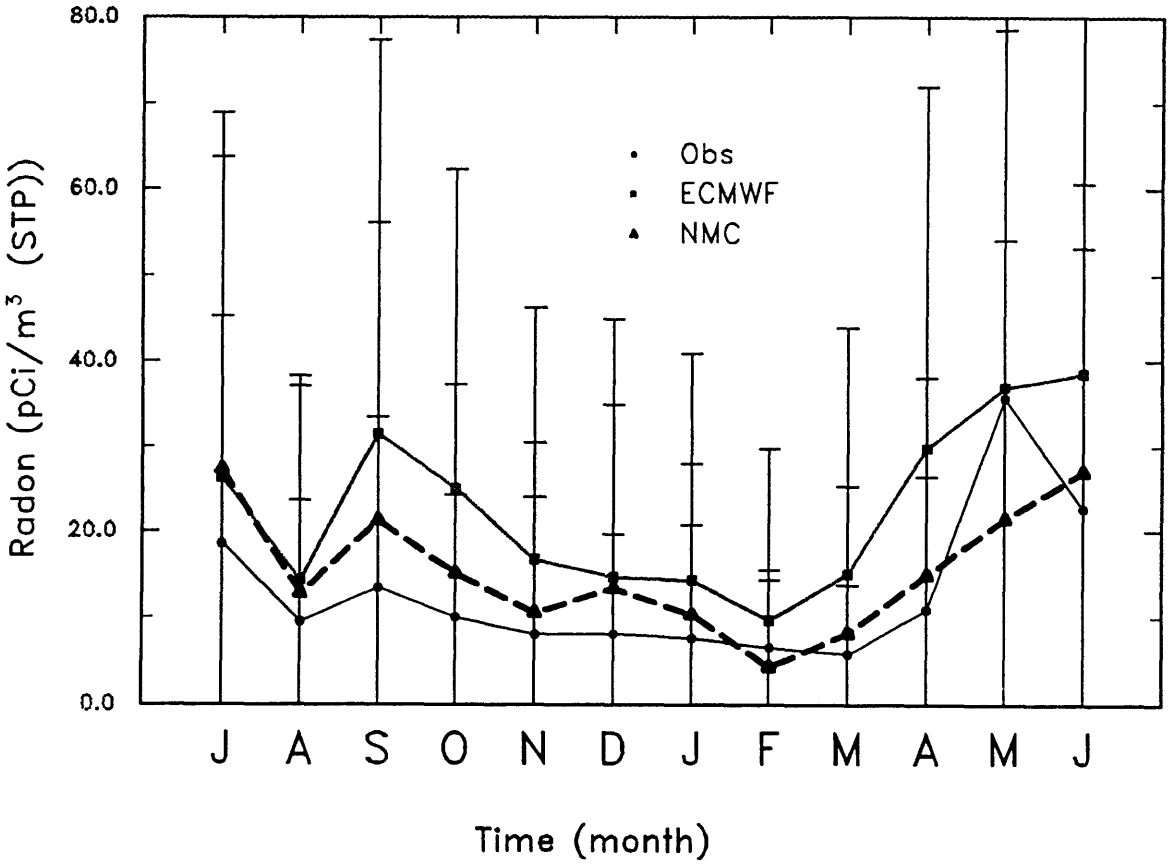

Figure 4.7: Monthly mean radon concentrations for the Cape Grim, Tasmania observing station as described in Figure 4.6.

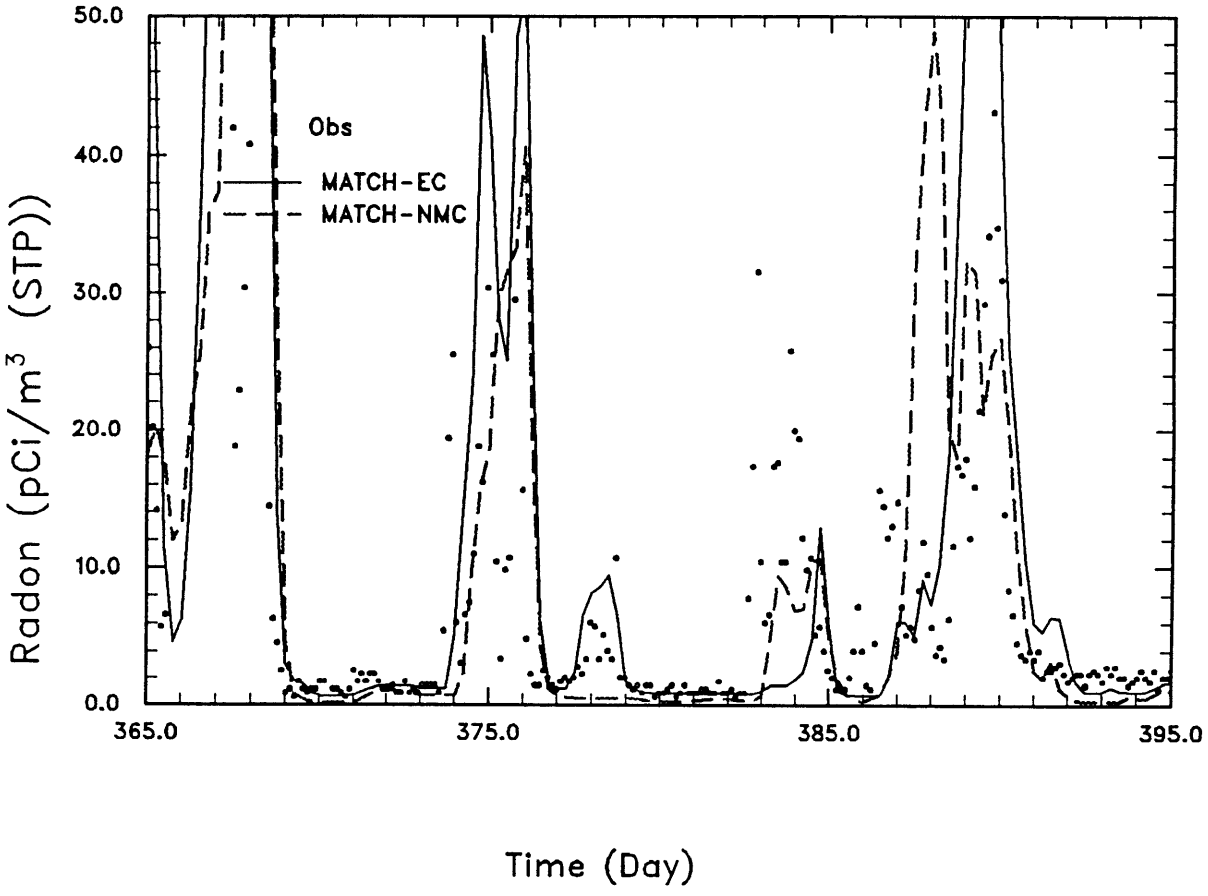

Figure 4.8: Radon concentrations at Cape Grim, Tasmania for January 1 through January 30,1991 from the observations and two model simulations, as described in Figure 4.6.

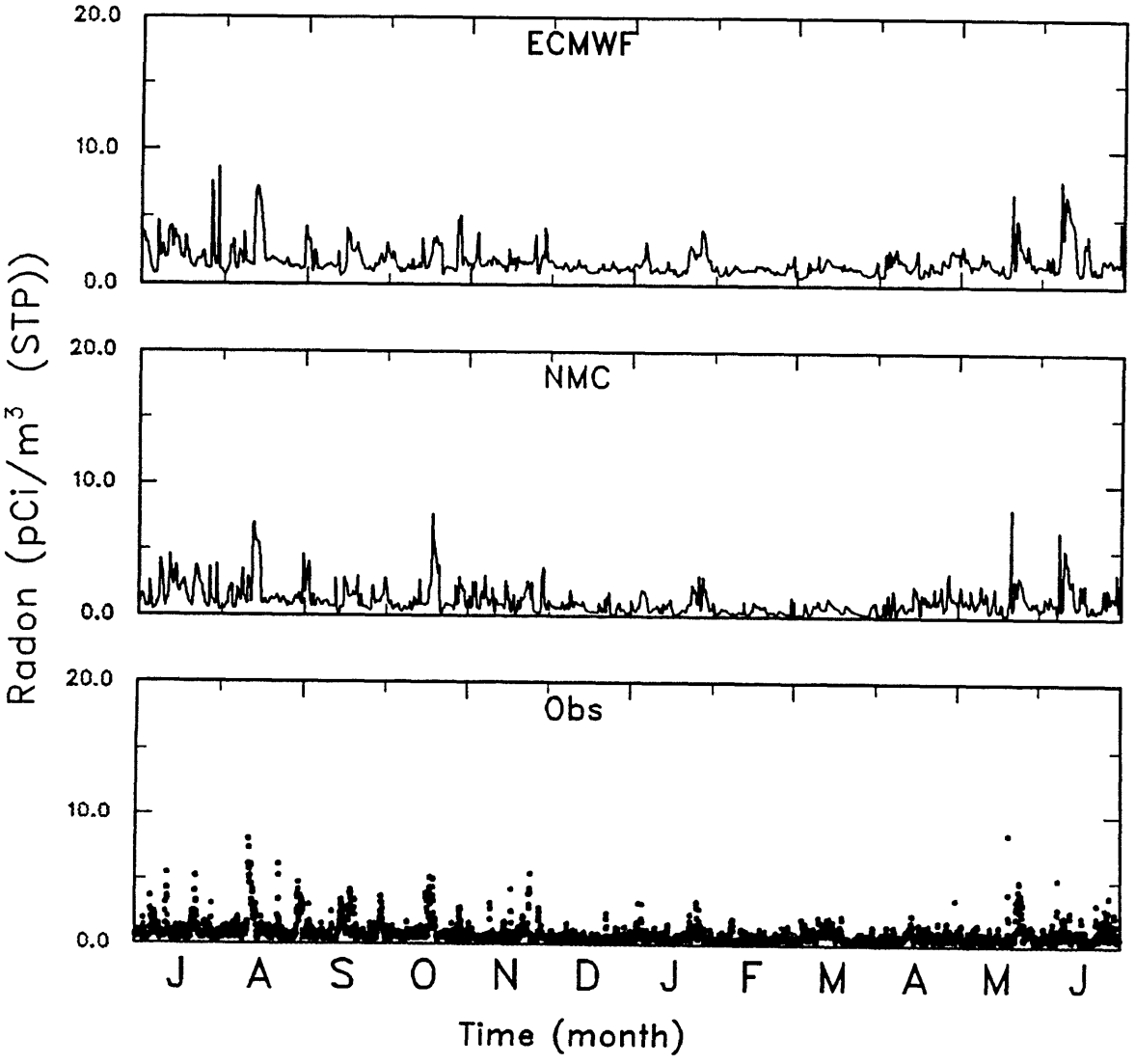

Figure 4.9a: Radon concentrations (pCi/m3 at STP) observed and modelled at the Amsterdam Island site in the South Indian Ocean for July, 1990 to June, 1991. Observations courtesy of Georges Polian. Modelled concentrations from the MATCH model using ECMWF and NMC winds.

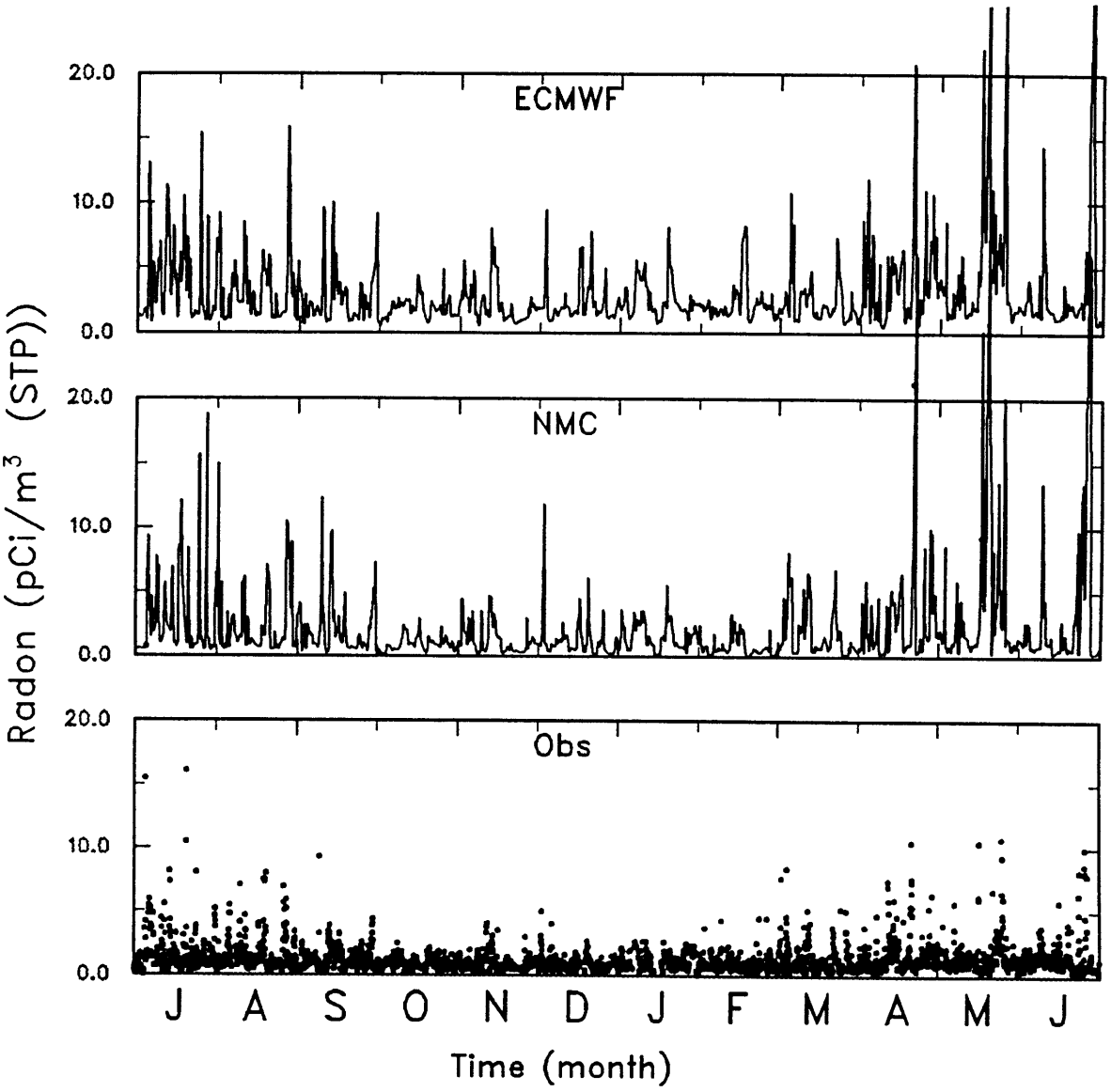

Figure 4.9b: Radon concentrations (pCi/m3 at STP) observed and modelled at the CrozetIsland site in the South Indian Ocean for July, 1990 to June, 1991. Observations courtesy of Georges Polian. Modelled concentrations from the MATCH model using ECMWF and NMC winds.

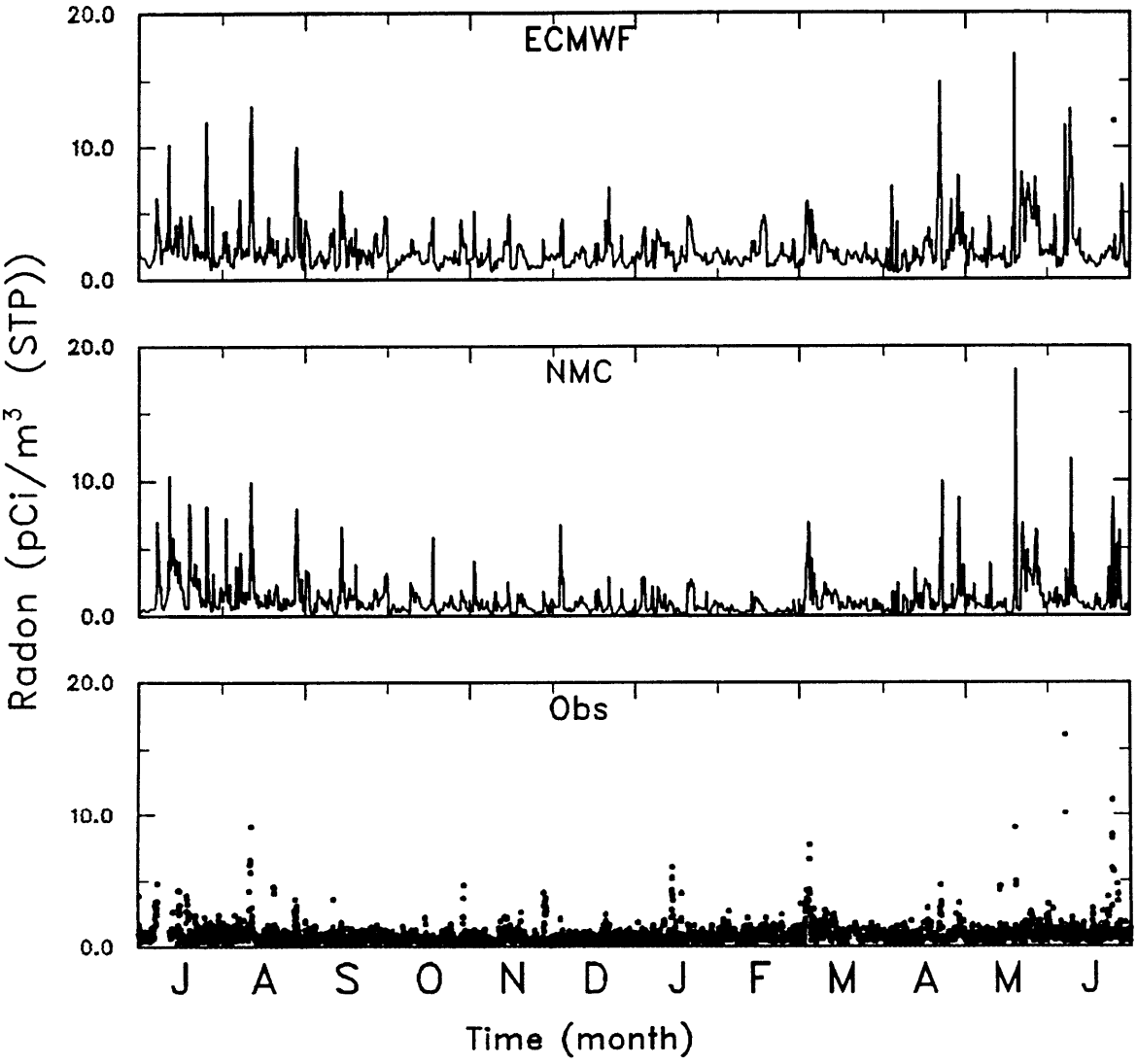

Figure 4.9c: Radon concentrations (pCi/m3 at STP) observed and modelled at the Kerguelen Island site in the South Indian Ocean for July, 1990 to June, 1991. Observations courtesy of Georges Polian. Modelled concentrations from the MATCH model using ECMWF and NMC winds

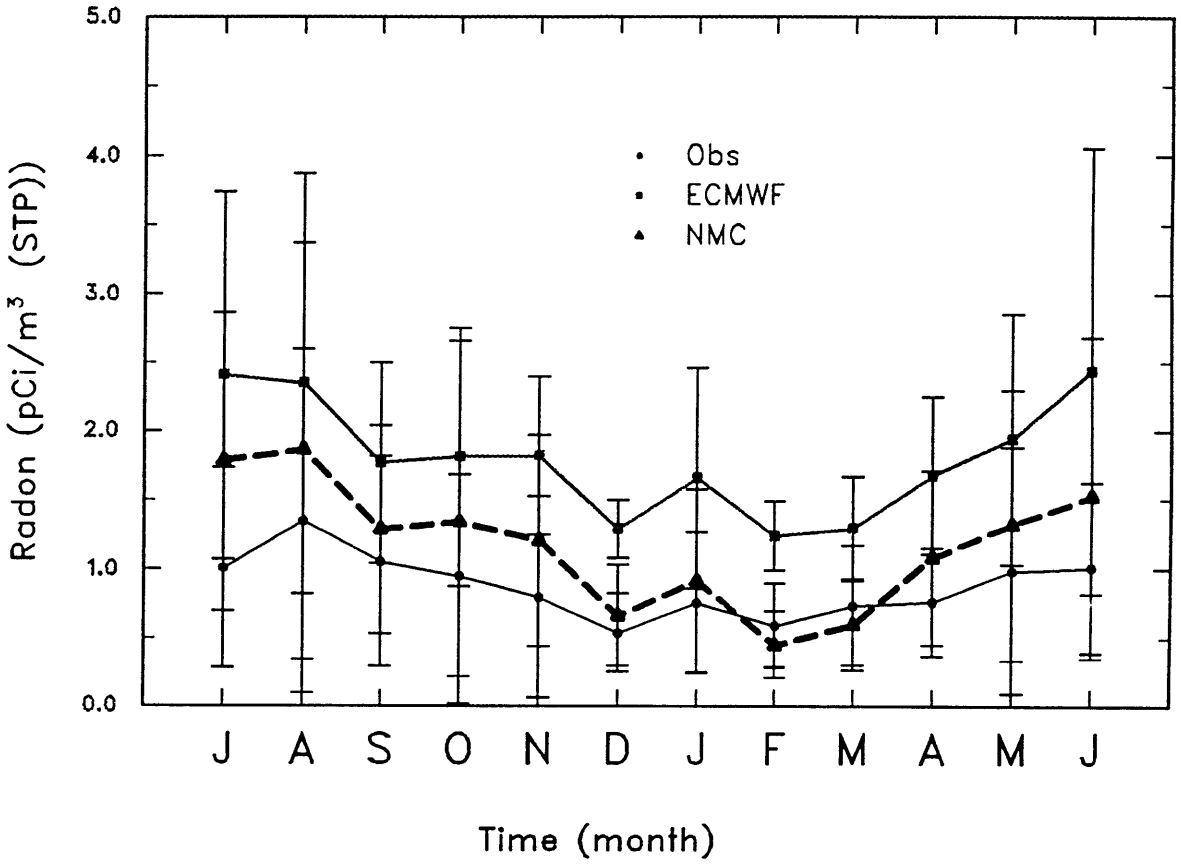

F.igure 4.10a: Monthly mean radon concentrations for the Amsterdam Island observing station as described in Figure 4.9a.

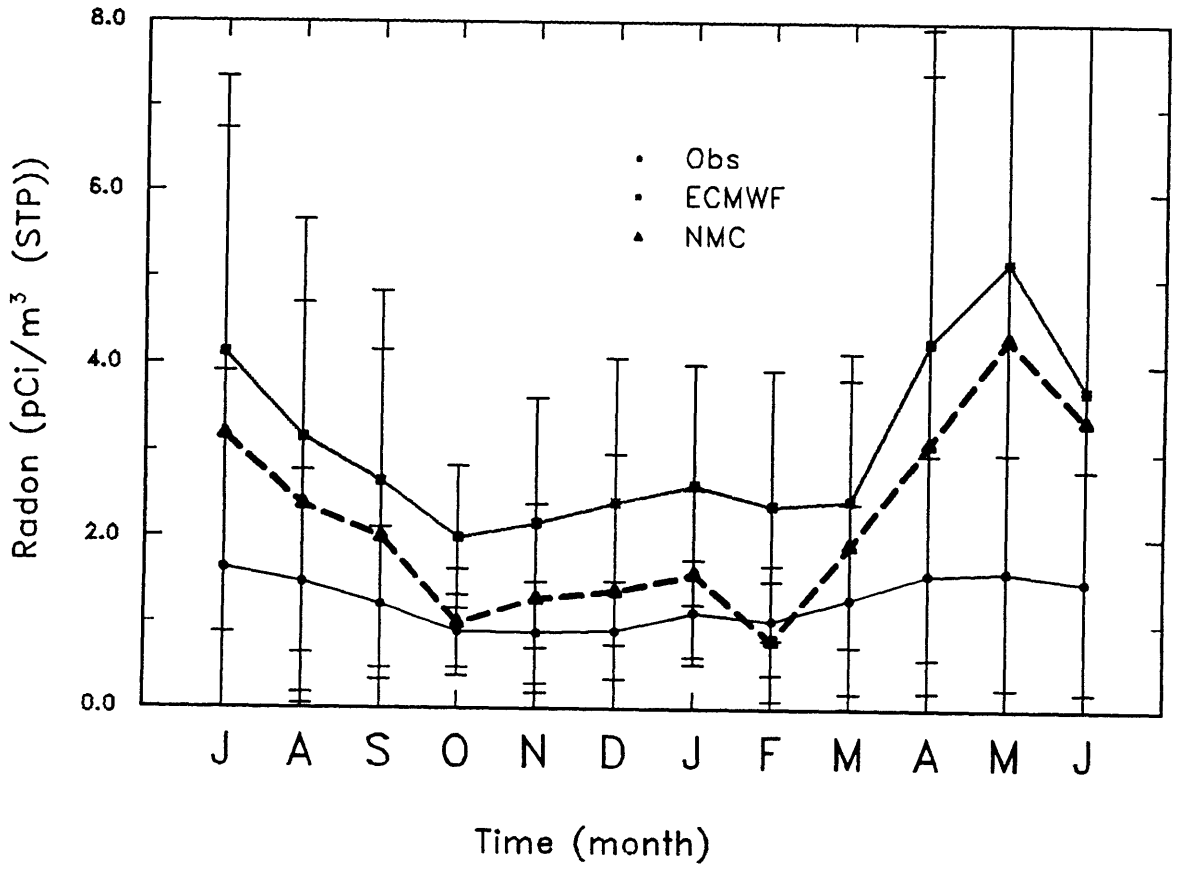

F.igure 4.10b: Monthly mean radon concentrations for the Crozet Island observing station as described in Figure 4.9b.

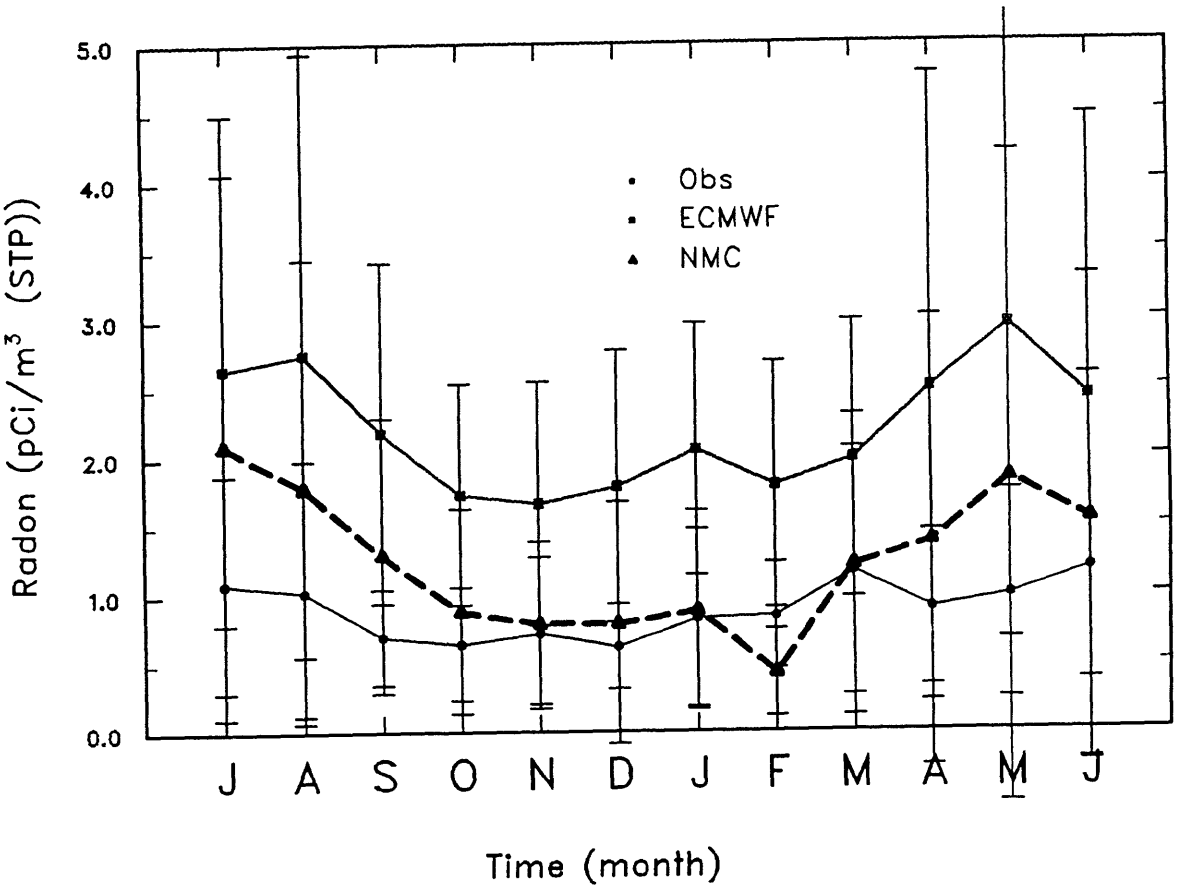

Figure 4.10c: Monthly mean radon concentrations for the Kerguelen Island observing station as described in Figure 4.9c.

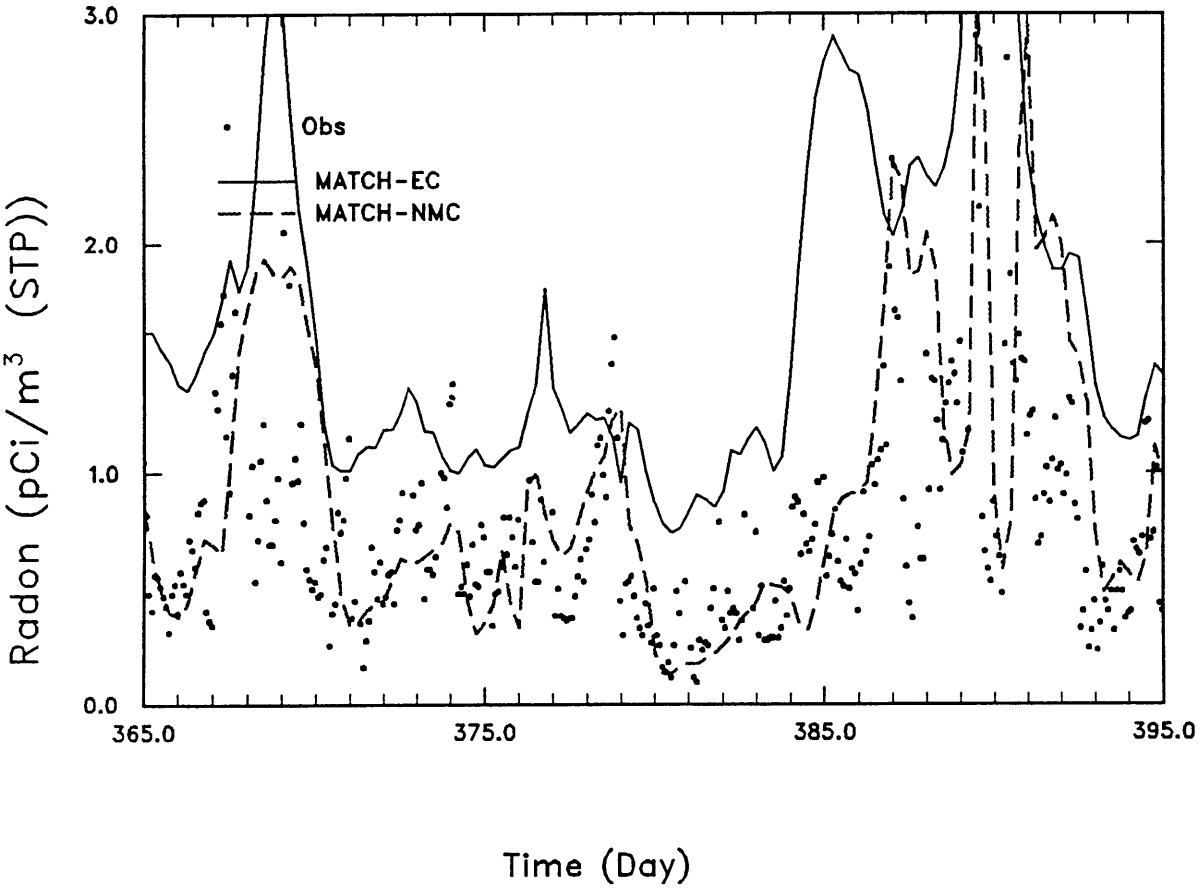

Figure 4.11a: Radon concentrations at Amsterdam Island for January 1 through January 30, 1991 from the observations and two model simulations, as described in Figure 4.9a.

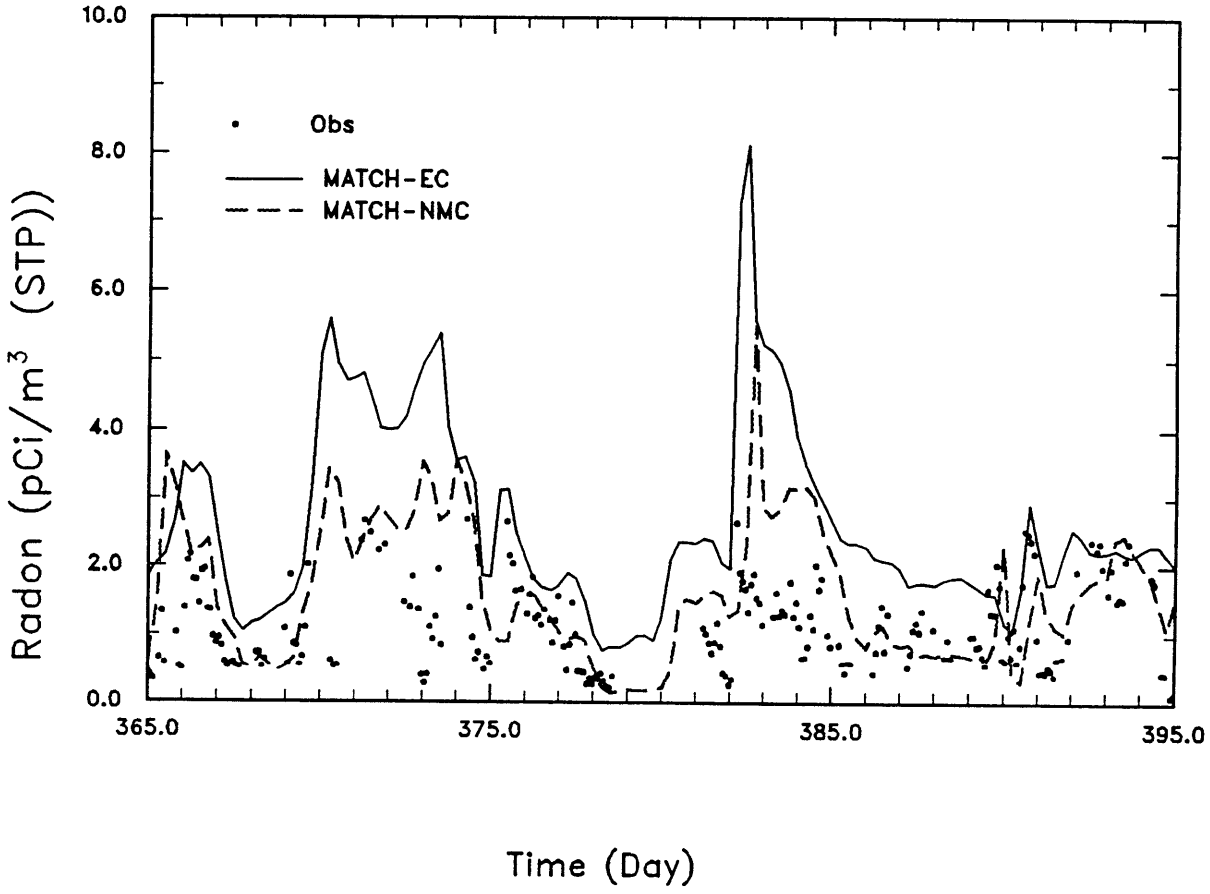

Figure 4.11b: Radon concentrations at Crozet Island for January 1 through January 30, 1991 from the observations and two model simulations, as described in Figure 4.9b.

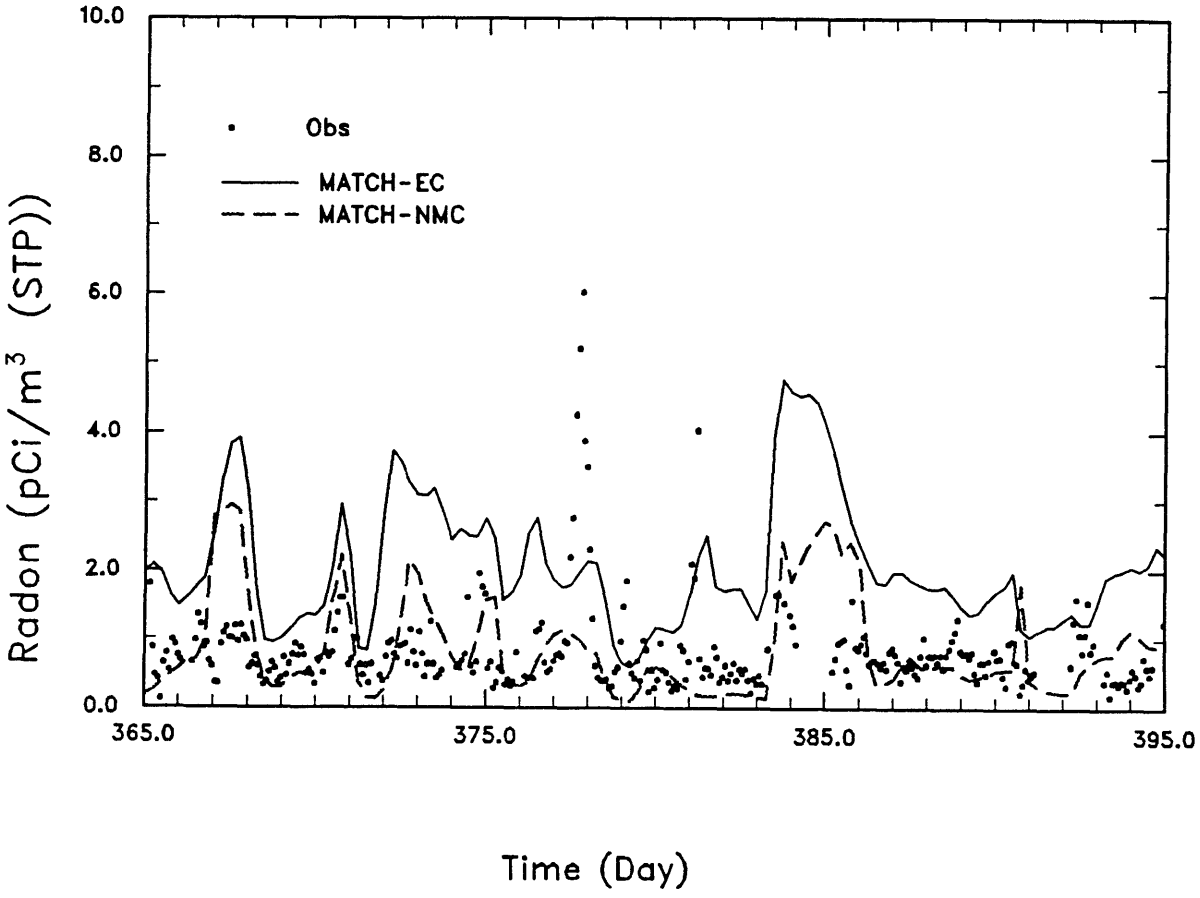

Figure 4.11c: Radon concentrations at Kerguelen Island for January 1 through January 30, 1991 from the observations and two model simulations, as described in Figure 4.9c.

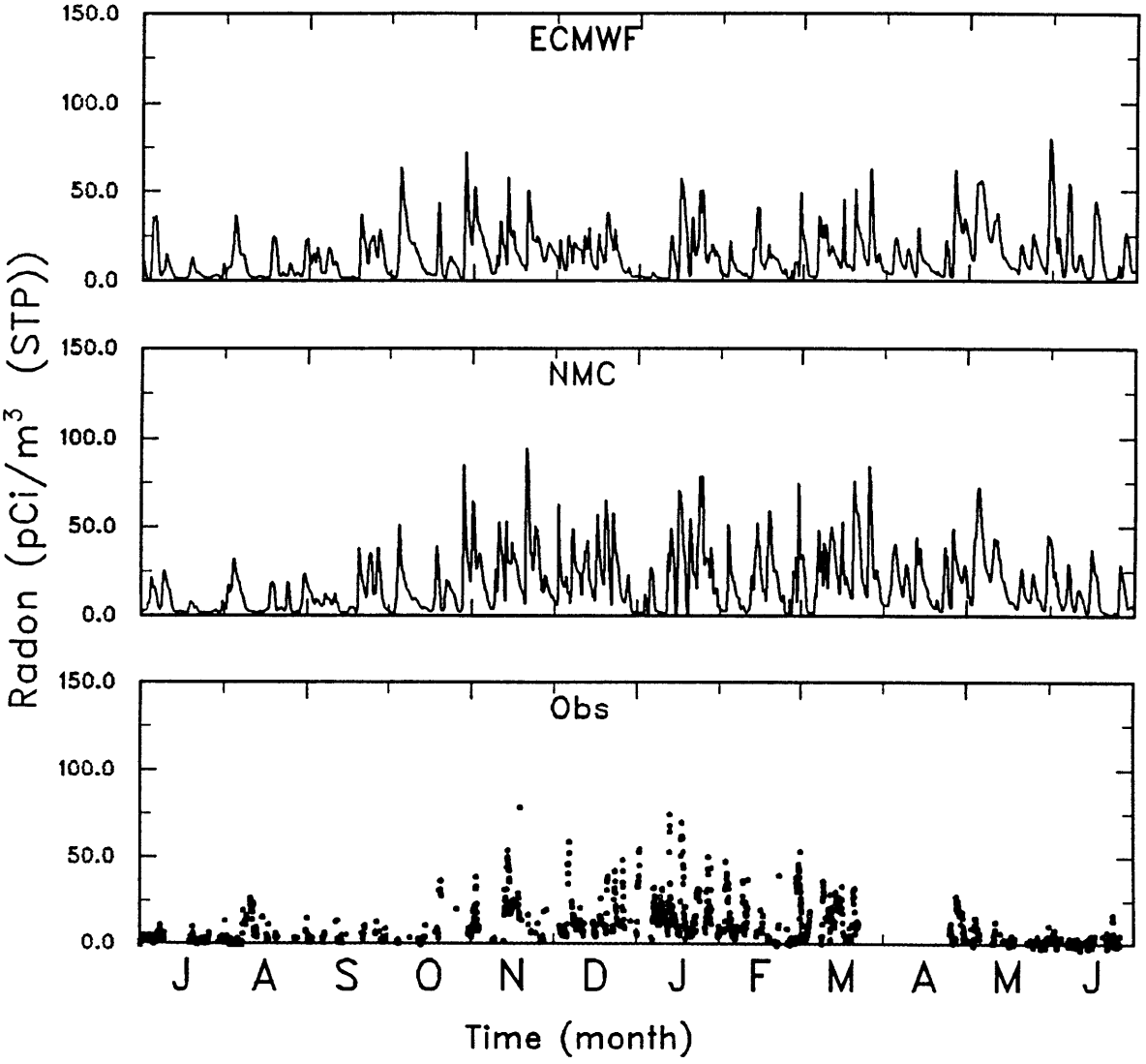

Figure 4.12: Radon concentrations (pCi/m3 at STP) observed and modelled at the Tudor Hill observing station in Bermuda for July, 1991 to June, 1992. Observations courtesy of Richard Larsen. Modelled concentrations from the MATCH model using ECMWF and NMC winds.

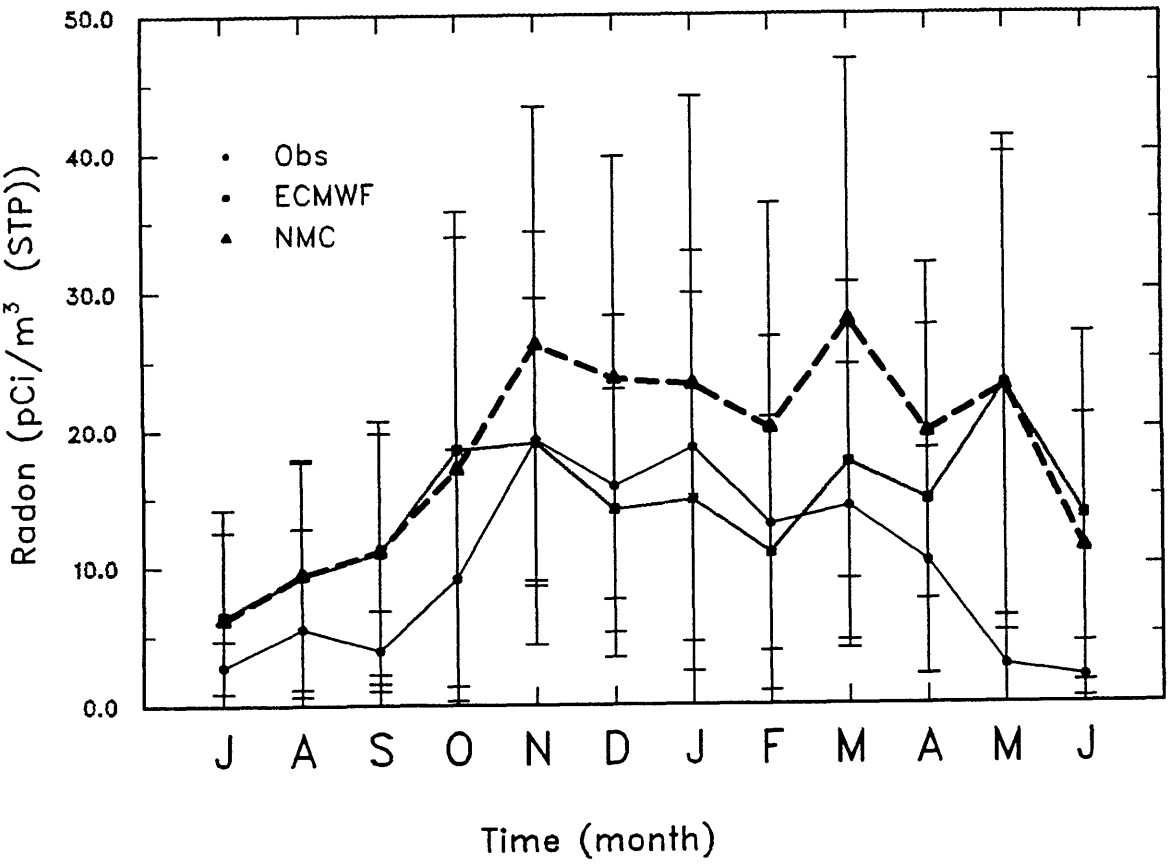

Figure 4.13 Monthly mean radon concentrations for the Bermuda observing station as described in Figure 4.12.

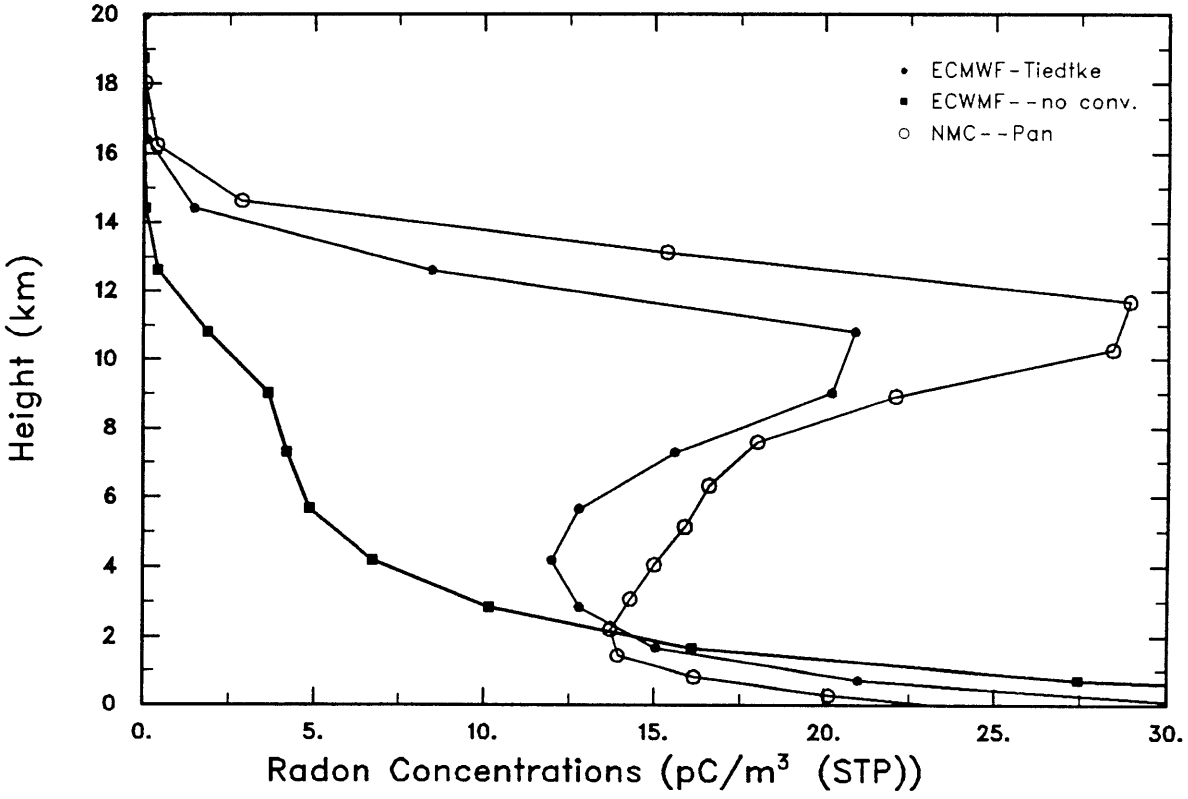

Figure 4.14: Three-month average (June, July and August) of modeled radon concentrations (pCi/m^3 at STP) over the tropical region of South America (north of 30S) for the MATCH-ECMWF, MATCH-NMC, and MATCH-ECNOC simulations (described in text).

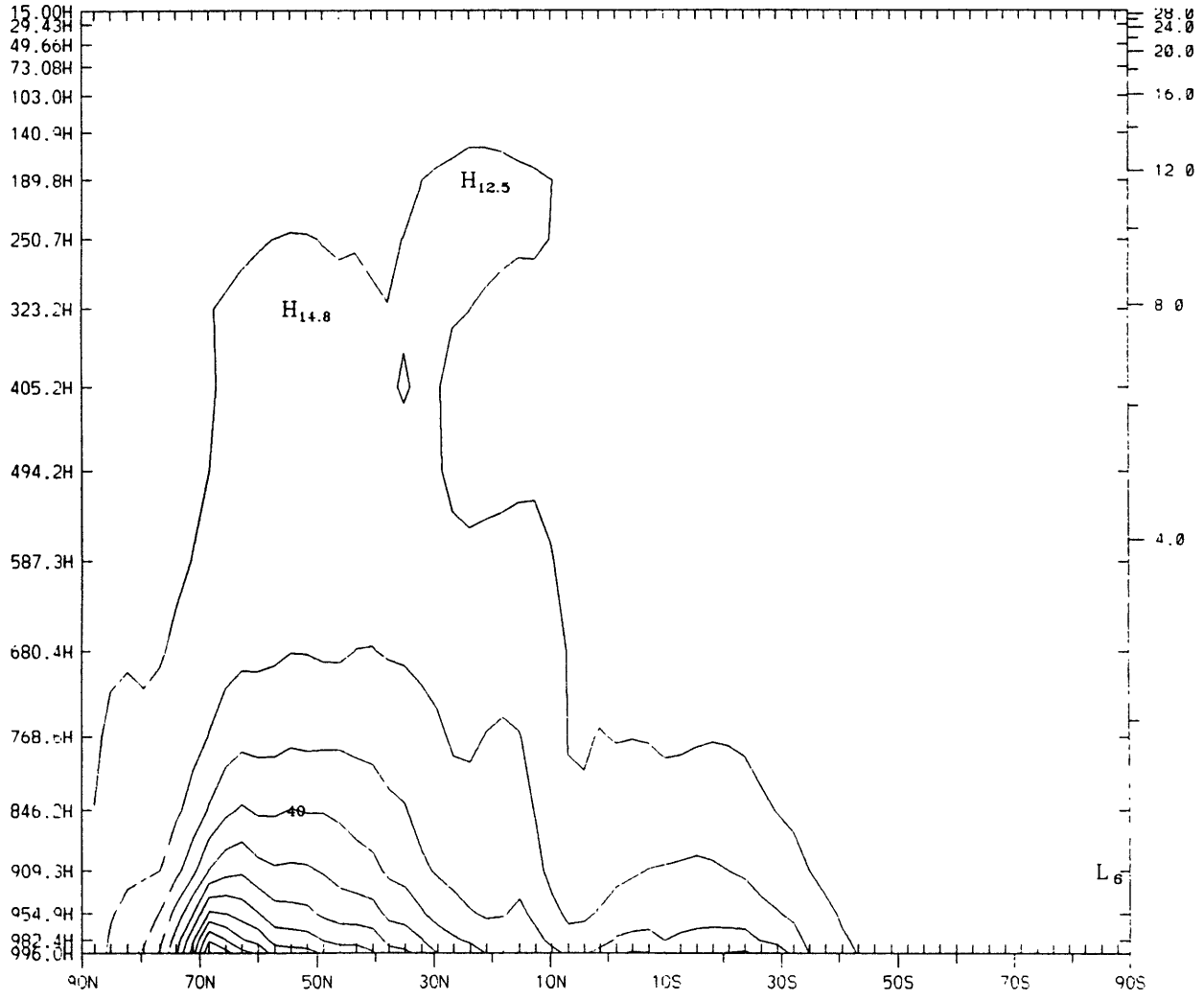

Figure 4.15a: Zonally averaged radon concentrations (pCi/m^3 at STP) from the MATCH-ECMWF simulations. Contour intervals are 10 pCi/m^3.

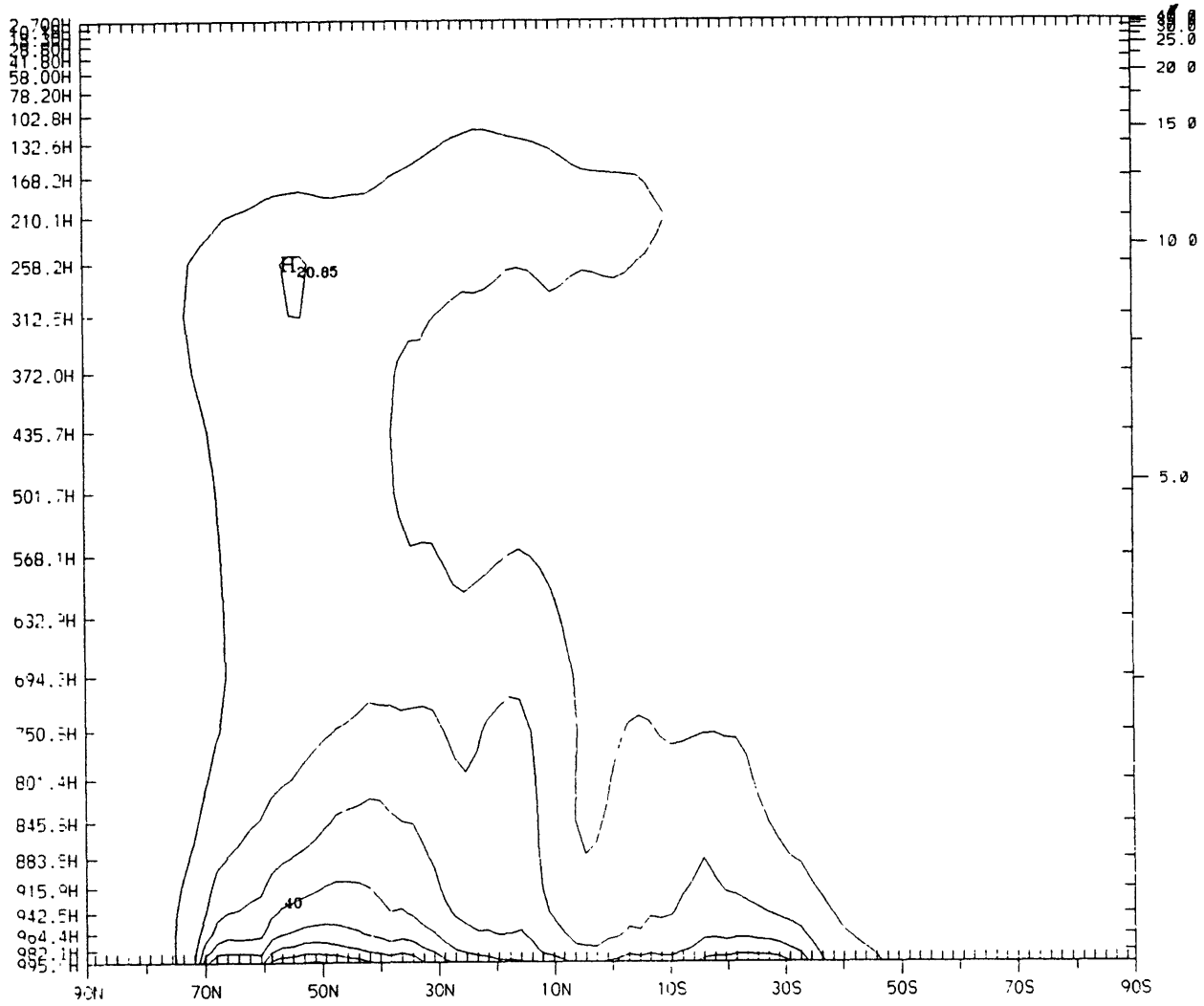

Figure 4.15b: Same as Figure 4.15a, except for the MATCH-NMC simulations.

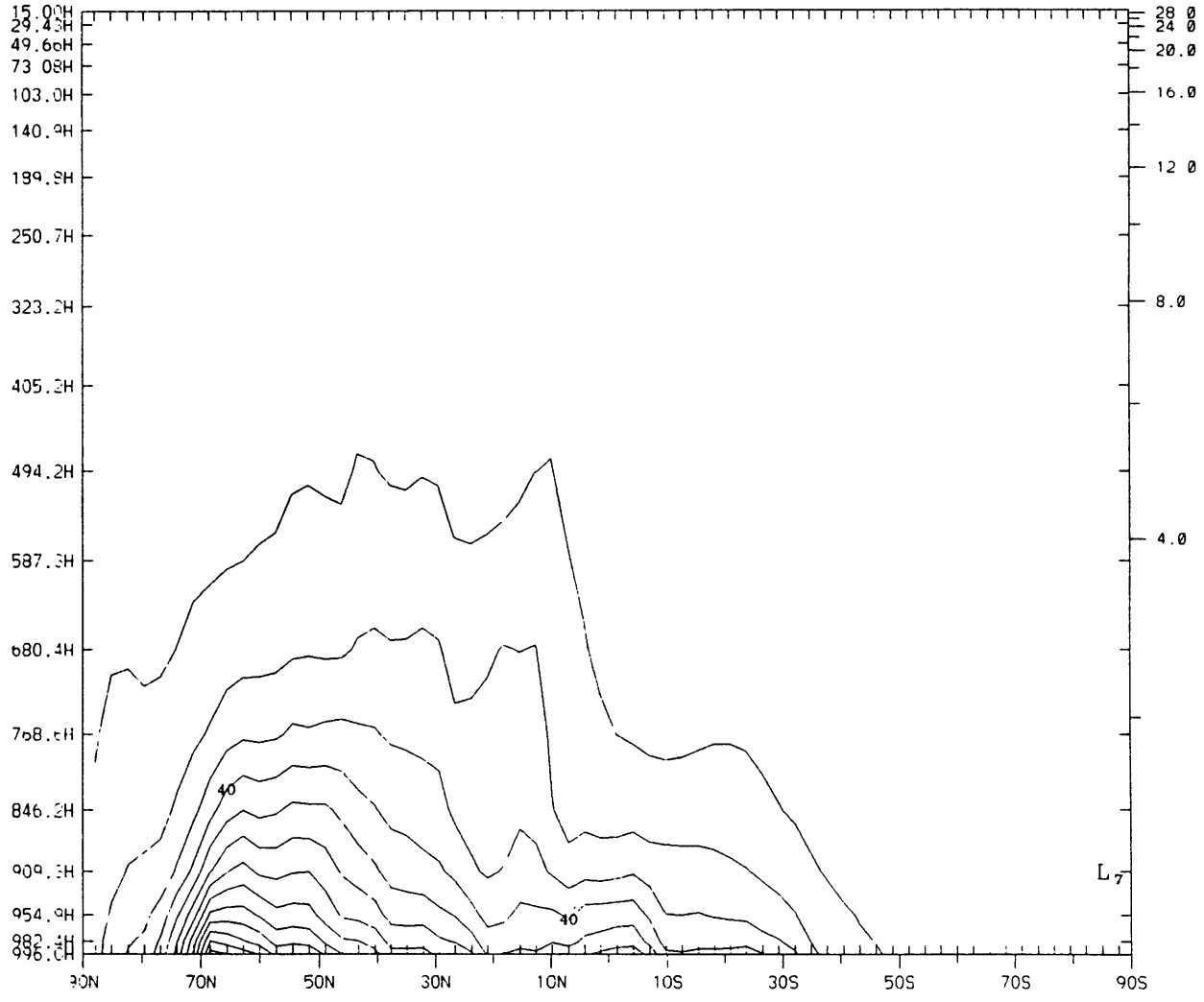

Figure 4.15c: Same as for Figure 4.15a, except for the MATCH-ECNOC simulation.

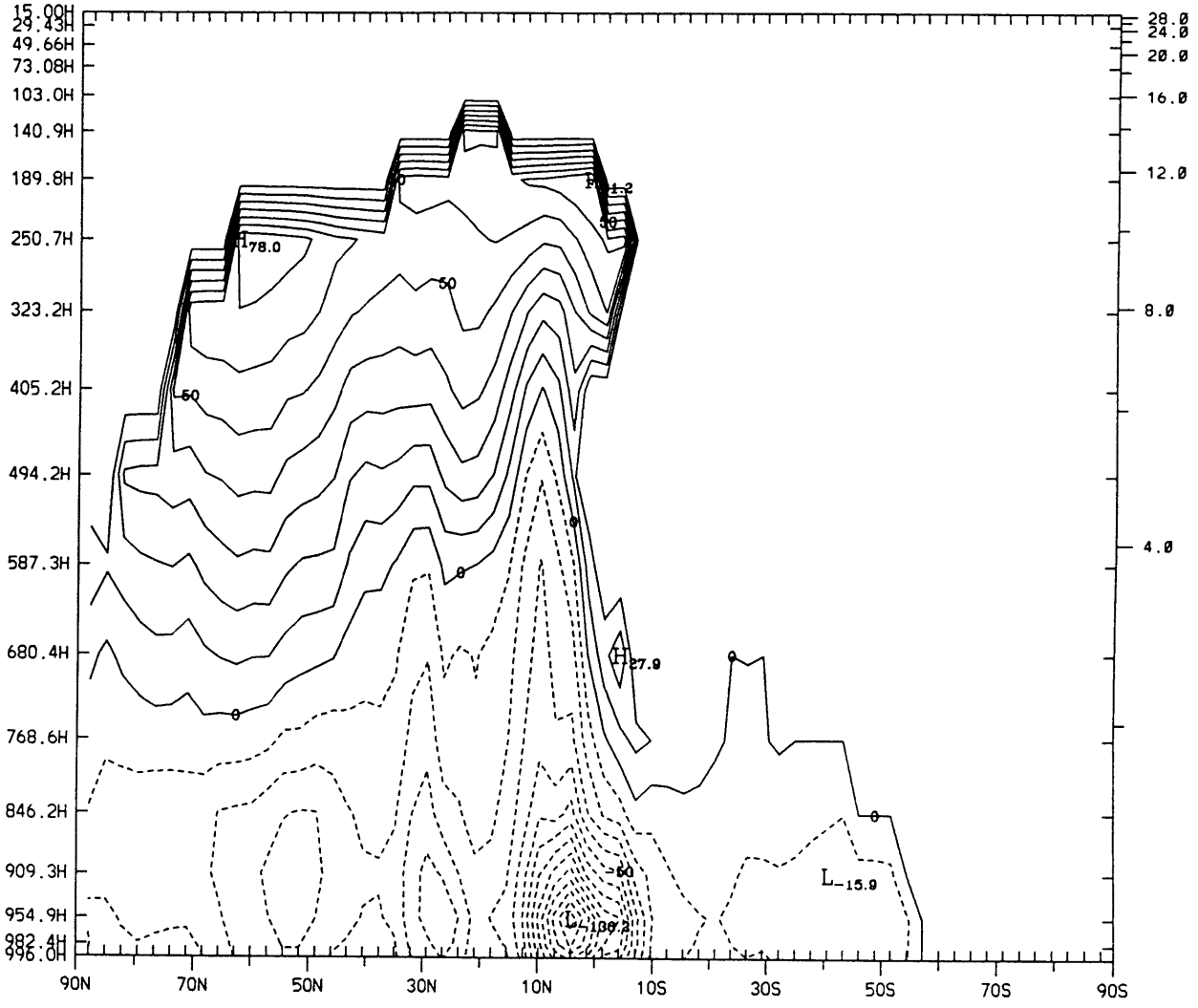

Figure 4.16a: Zonally averaged plot of the percent differences between the MATCH-ECMWF and MATCH-ECNOC simulations of radon concentrations. Percentages are only shown in areas where concentrations were above approximately 10 pCi/m^3.

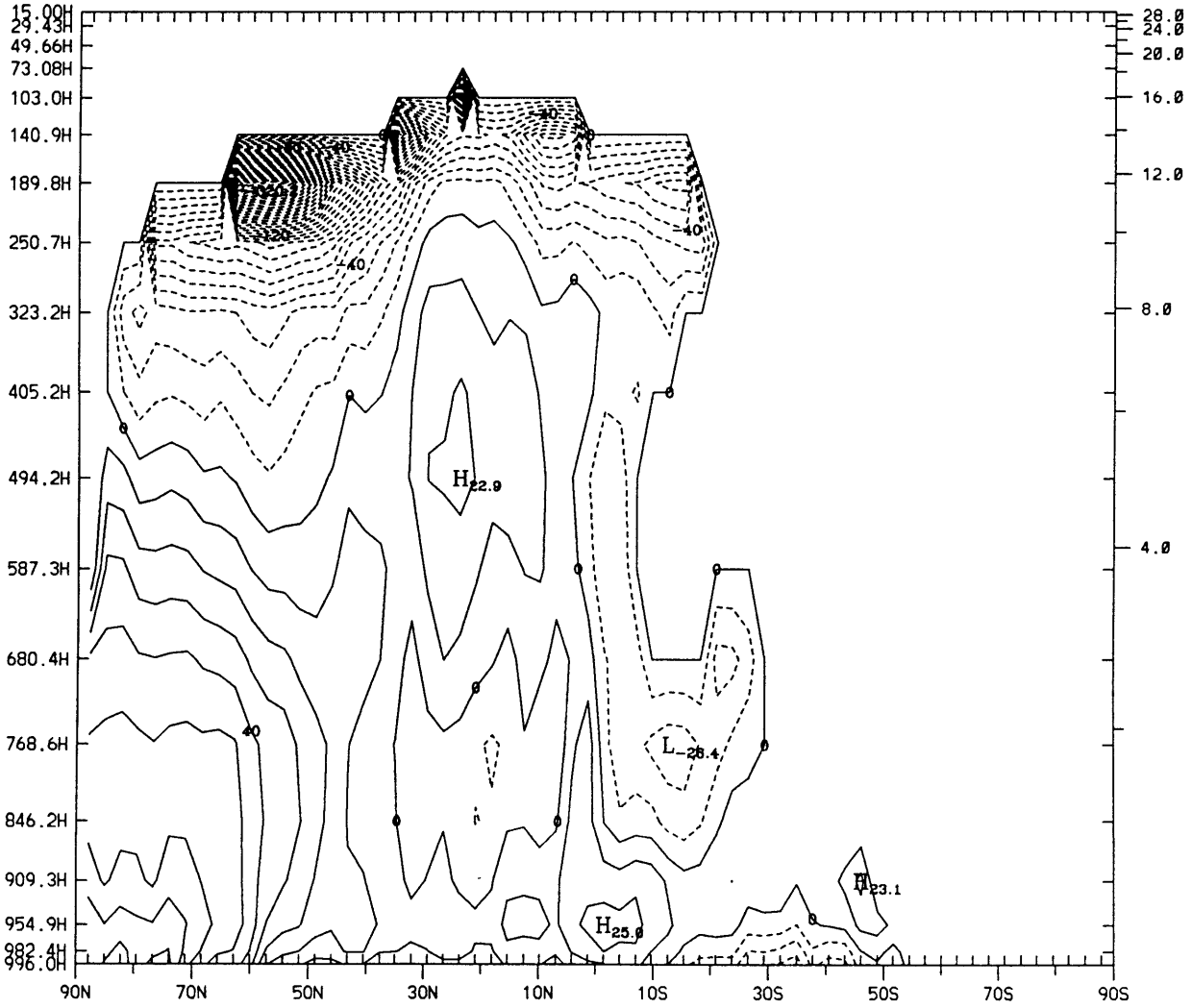

Figure 4.16b: Same as for Figure 4.16a, except the percent differences between MATCH-ECMWF and MATCH-NMC.

Chapter 5:

The simulation of CCl_3F using ECMWF and NMC winds in MATCH

5.1.0 Introduction

In this chapter we consider the ability of the model to simulate CCl_3F when we assume the sources are known. CCl_3F (CFC-11) is a freon with only anthropogenic sources, and a sink in the stratosphere due to photolysis, with a lifetime of 40-50 years.

The MATCH model is used for the simulations with both the ECMWF and NMC winds. This model can be driven by a GCM [Rasch, Mahowald and Eaton, 1996., manuscript in preparation] or forecast center winds (Chapter 3 and 4). A model driven by forecast center winds has the advantage that the concentrations in the model are representative of concentrations on a specific day, and can thus be more easily compared with observations.

The goals of this chapter are: 1) To demonstrate the ability of the model to simulate long-lived gas transport in synoptic scale events, 2) to demonstrate the ability of the model simulate large scale transport such as interhemispheric gradients and, 3) to compare the difference in the simulations using the ECMWF and NMC winds.

5.2.0 Model Description

The MATCH model is used for the simulations, as described in Chapter 3 and 4. The only modifications are to include the sources and sinks of CCl_3F and are noted below.

5.2.1 CCl_3F sources

CCl_3F does not occur naturally, but is an industrially produced compound. In previous years, the total emissions of CCl_3F were well known, since there were only a few companies producing CCl_3F, and they made available emissions estimates. However, since the Montreal Protocol, emissions from the reporting companies has decreased, while emissions from non-reporting companies have been increasing. Thus, there is increasing uncertainty in the emissions of CCl_3F.

The magnitude of annual emissions is taken from Cunnold, et al [1994], and is increasing until 1988, at which point the maximum emissions occur, and emissions begin decreasing. The total sales and consumption of CCl_3F is better known than the emissions, since for some uses of CCl_3F, there is a time delay before the gas is released to the atmosphere. Thus, there is some uncertainty in the total emissions, even from regions reporting their consumption. In addition, the emissions from non-reporting companies must be estimated. The annual estimated emissions for the 1988-91 period are shown in Table 5.1.

Table 5.1 Emissions of CCl_3F

Year	Emissions
1988	350
1989	305
1990	255
1991	223

To distribute the emissions globally, we use the estimated distribution of emissions from Hartley and Prinn [1993] for 1988 shown in Figure 5.1, although it is certain that the distribution of emissions has changed somewhat between 1988 and 1991. This regional distribution is derived from the reported country emission estimate. In order to distribute the emissions within countries, electricity usage is used as a proxy. Thus, the distribution of emissions within each region have uncertainty, even for the year 1988. Another emission estimate was made for the year 1986 by McCulloch, et al. [1994] based on a gross domestic product (GDP) proxy for emission and a comparison of these two emission estimates can provide some insight into the uncertainty in the source distributions. The two source distributions are divided on different criteria (geographic versus political), so there is some difficulty in comparing the two emission distributions. However, some tentative conclusions can be made.There were substantial differences in the two estimates, as shown in Table 5.2.

Table 5.2: Regional Emission Distributions

Region	Hartley and Prinn [1993]	McCulloch et al [1994]
North America	36%	28%
Europe	33%	43%
Asia	13%	13%
Japan and Korea	10%	9%
Other Source Regions (Central and South America, Africa, Australia)	8%	6%

The size of the North American source is much lower in the McCulloch estimate, while the European estimate is larger. In addition, the Southern Hemisphere source is smaller in the McCulloch estimate.

The emission distribution within each region (e.g. within the U.S.) will also be uncertain, and it is

difficult to assess how large these uncertainties are. These uncertainties could certainly bias our results if they result in too large or too small emissions from source regions close to an observing site. In addition, there are likely to be temporal trends in the emissions in each region which are different than the global trends because the Montreal Protocol regulates emissions from North America, Japan and Europe more than from other parts of the world. It is difficult to assess how these changes in emission estimates will affect the simulations.

.

5.2.2 CCl_3F sinks

CCl_3F is lost largely through photolysis in the stratosphere, although there is a small sink of CCl_3F into the soils [Khalil and Rasmussen, 1989]. This means that the lifetime of CCl_3F is a function of the stratospheric-tropospheric exchange time and the photolysis rates. The photolysis rates used for this study come from Hartley and Prinn [1994] and Golombek and Prinn [1986].

Photolysis rates are uncertain to at least 20-40 percent [Fraser, et al., 1994]. This is due to the uncertainty about the amount of ozone above a particular level, and since at the levels where the CCl_3F is sharply decreasing with height, the photolysis rates are increasing by several orders of magnitude, there may be substantial sensitivity to the lower stratospheric circulation and stratospheric-tropospheric exchange and to the photolysis rates chosen.

The lifetime of CCl_3F in the simulations is thought to be between 40-50 years, and so in the model simulations conducted here, the photolysis rates are tuned to give the correct lifetime. For the ECMWF simulation, this was achieved with the initial photolysis rates. However, the NMC simulation required that the photolysis rates be 40% of their Golombek and Prinn [1986] values in order that the lifetime of CCl_3F be between 40-50 years. This implies that the stratosphere-troposphere exchange time is much faster in the NMC simulations than the ECMWF simulations, and is perhaps too fast. This will be discussed more in Section 3.

5.2.3 CCl_3F initialization

Since the lifetime of CCl_3F is 40-50 years, our initial conditions are important, unless we want to run since the 1930's, when CFCs were first used. The long time scales result from two sources: 1) the stratospheric-tropospheric exchange (and the exchange time from the tropopause up to about 20 mb, where the destruction occurs at a faster rate) and subsequent loss mechanism in the stratosphere and 2) the interhemispheric transport time. In order to reduce the computational expenses, we begin with three different initial conditions, and consider our result to be insensitive to the initial conditions when the three initial conditions have converged to very similar solutions. Our three different initial conditions are:

Case 1: Low interhemispheric gradient and low vertical profile

Case 2: Low interhemispheric gradient and high vertical profile

Case 3: High interhemispheric gradient and high vertical profile

We used no interhemispheric gradient in this study for our low gradient, and a 40% interhemispheric gradient for our high gradient. Our low vertical profile means that the profile extends less into the stratosphere than our equilibrium value, while the high vertical profile extends higher than our equilibrium value.

Figures 2a and 2b show that the interhemispheric gradient is roughly in equilibrium after the two year spin-up period, for the ECMWF and NMC simulations, respectively. In Figures 5.2a and 5.2b the zonally averaged surface concentration divided by the global mean surface concentration for that simulation is shown. We have normalized the surface concentrations for ease of comparison, since the different years and cases will have different amounts of mass and thus surface concentration. Notice that the final surface concentrations are within 0.5% of each other.

Figures 5.3a and 5.3b show that the vertical profile of CCl_3F is in equilibrium after the spin-up for both the ECMWF and NMC simulations, respectively. Figures 5.3a and 5.3b show the initial globally averaged vertical profile, and the vertical profile after 2 years for three cases, again normalized by the mean surface concentration, for ease of comparison. Figures 5.4a and 5.4b also demonstrate that the lifetime of CCl_3F is independent of the initial conditions after two years of simulation for the ECMWF and NMC simulations, respectively.

These figures demonstrate that the interhemispheric and vertical gradients are independent of the initial conditions after a two year spin-up period. However, the absolute amount of mass in the atmosphere at the end of the two year period is still not constrained by these simulations. In order to constrain this, we match the global average concentrations at the 9 surface stations described in Section 3 from both model simulations and observations.

5.3.0 Comparison with observations

Using our a priori best estimate of the sources of CCl_3F we conduct a simulation of July, 1990 to June, 1991 using both the ECMWF and NMC meteorological data. The results of these simulations are compared to observations at 9 surface observing stations and available vertical profiles.

The CCl_3F data we use are from the ALE./GAGE/AGAGE [Cunnold, et al., 1994] and the CMDL [J. Elkins, personal communication, 1995] networks. The ALE/GAGE/AGAGE network has available several times daily observations from an *in situ* gas-chromatograph at Ireland, Barbados, and Cape Grim for this time period. The CMDL network has flask data (which is used for monthly means at Alert, Canada; Barrow, Alaska; Niwot Ridge, Colorado; Mauna Loa, Hawaii; Samoa; and the South Pole. The CMDL network also has *in situ* high frequency observations available at all the above stations except Alert for the time period used here.

The latitude and longitude of each site is shown in Table 5.3

Table 5.3: CCl_3F Station Locations.

Observing Station	Network	Latitude	Longitude
Alert, Canada	CMDL	82.5 N	62.3 W
Barrow, Alaska	CMDL	71.3 N	156.3 W
Mace Head, Ireland	ALE/GAGE	53.3 N	9.9 W
Niwot Ridge, Colorado	CMDL	40.1 N	105.4 W
Mauna Loa, Hawaii	CMDL	19.5 N	155.4 W
Barbados	ALE/GAGE	13.2 N	59.5 W
Samoa	CMDL (ALE/ GAGE)	14.3 S	170.5 W
Cape Grim, Tasmania	ALE/GAGE (CMDL)	40.7 S	144.78 E
South Pole	CMDL	89.9 S	24.8 W

In addition, the network to which each belongs is indicated. At some sites, there is information from both networks, but this duplicate information is available only for a limited number of months, or only as monthly averaged, so that information from one network is used more predominantly at Samoa and Tasmania in this analysis. The location of the sites is also shown in Figure 5.1.

The absolute calibration from the two networks is not the same, so that there is a 2.7% difference based on preliminary intercomparisons between ALE/GAGE/AGAGE and CMDL [P. Fraser, personal communication, 1994] and a similar difference is found by ratioing the reported values at Samoa. For this study, the ALE/GAGE measurements are multiplied by 1.027 for comparison against the CMDL and model result. It is somewhat arbitrary how we choose to correct for this difference in absolute calibration (i.e. which network calibration is correct), and we therefore do it in a way that allows the model results to match the observations as well as possible.

5.3.1 Interhemispheric transport

CCl_3F is a good trace gas for testing the ability of a CTM to simulate the interhemispheric exchange, since its sources are largely in the Northern Hemisphere [Golombek and Prinn, 1986; Prather, et al.,1987]. It is unclear exactly what processes dominate the interhemispheric transport, but recent studies suggest that mixing in convective regions may be responsible [Hartley and Black, 1995] or transport across westerly ducts in the upper troposphere [Webster and Holton, 1982].

Using the method of Prather et al. [1987], we calculate the flux between hemispheres over a year and divide that into the mean gradient between the hemispheres. This gives us an exchange time

for interhemispheric transport of CCl_3F. Observations and a 2-dimensional model suggest the exchange time should be approximately 11 months [Cunnold, et al., 1994]. The MATCH model simulates interhemispheric exchange times of 9 months and 7 months for the ECMWF and NMC simulations, respectively, suggesting somewhat too fast exchange between the hemispheres.

However, comparison of mean concentrations between the model and observations indicate that the interhemispheric gradient may be too large in the model, as shown in Figures 5.5a and 5.5b for the ECMWF and NMC simulations, respectively. These figures show the mean July, 1990 concentrations at each of the 9 stations from the observations and model results. In Figure 5.4a, it is clear that the ECMWF simulation gives an interhemispheric gradient which too large--19 ppt (parts per trillion) instead of the observed 15 ppt. Figure 5.4b indicates that NMC simulations result in an interhemispheric gradient of 16 ppt--much closer to the observed value. These results suggest too slow exchange between the hemispheres.

The result that the interhemispheric gradient is too large in the model is not unique to this model, but is observed in previous studies of CCl_3F in the CCM2 model [Hartley, et al., 1994], and the NASA/GISS model in which diffusion was added to increase the mixing rate between hemispheres [Prather, et al., 1987].

It is unclear from this analysis why the exchange time is too fast, while the interhemispheric gradient is too large in the model simulations. This might indicate that the Prather et al. [1987] method of calculating interhemispheric transport times is not always a good indicator of a model with a reasonable simulation of the interhemispheric gradient. Another explanation might be that the two-dimensional model results of mixing time are not useful for a 3-dimensional model result. This issue will be addressed again in section 6.3.2.

5.3.2 Vertical profile

Next we compare the simulations with the observed vertical profiles. Unfortunately, for the period, we are considering there are a limited number of vertical profiles. It is also unclear how characteristic a single profile should be of the atmosphere, but since it has a long lifetime, CCl_3F should be reasonably well mixed in the longitudinal direction at each latitude and height.

For the tropics, there were some profiles made during March of 1978 and 1979 over Brazil by Goldan, et al. [1980], but there are no more recent profiles for comparison. A comparison of the observations with the monthly and zonally averaged concentrations at 5 S for March, 1991 are shown for the MATCH-EC and MATCH-NMC simulations in Figure 5.6. Since there is more CCl_3F in the atmosphere in 1991 than in 1979, we would estimate that the entire profile would shift to the right by 1991, but that the shape of the profile would remain roughly the same. There would in fact be some changes in the vertical profile with time, since CCl_3F is not in equilibrium in the atmosphere, but those changes should be minor compared to the 2 order of magnitude change in the concentration of CCl_3F as we go from 15 km to 30 km in the atmosphere. Figure 5.6 suggests

that the two model simulated vertical profiles of CCl_3F in the tropics are reasonable.

Figure 5.7a and 5.7b show similar vertical profiles, but for the northern mid-latitudes and northern high latitudes. The observations are taken from Fraser, et al [1994] and use observations made by KFA-Julich in 1990 [Schmidt, et al., 1986, 1989,1991]. The observations show a much faster reduction of the concentrations of CCl_3F with altitude than simulated by either version of the MATCH model. Concentrations of order 0.01 ppt are observed at a height of 28 km at 44N, but the model is simulating concentrations 2 orders of magnitude higher at this altitude and latitude.

Although concentrations of both the MATCH-EC and MATCH-NMC simulations tend to show too high of concentrations, the NMC simulations seems to exaggerate the problem. This is consistent with the increased vertical exchange into the stratosphere suggested in section 2.3.

Why the model seems unable to capture the northern mid-latitude and high latitude vertical profile is unclear. This could be due to insufficient model resolution at the tropopause and in the stratosphere, even though the NMC simulations have several levels at the tropopause and in the stratosphere. In addition, it may be that the model has too much mixing along pressure surfaces (or along isentropes), which would tend to reduce the horizontal gradients between the tropics and the mid-latitudes. Other simulations with the model indicate that too much ozone is being brought into the troposphere from the stratosphere with the NMC winds [Lawrence, MPI-Mainz, 1995, personal communication]. This would be consistent with too much vertical mixing near the tropopause in the model, mixing high ozone air downward, and high CCl_3F air upward.

5.3.3 Time series at surface sites

The sites described in section 3.0 are used to consider the ability of the model to simulate the pollution events, frequency of pollution events and seasonal cycle at the observing stations. Although, strictly speaking we only have one year of model results, and thus a seasonal cycle is not very well determined, we will refer to changes in the concentrations during the year which are seen above the mean trends as a seasonal cycle in the concentrations. Although there are uncertainties in the distribution of CCl_3F, for the most part, we will consider differences in the simulations to be the fault of the model's transport characteristics.

Alert, Canada

Figure 5.8 shows the monthly averaged concentrations from the CMDL flask network and the two model simulations for the Alert station. The model simulations seem to be able to simulate the observations, except during May, 1991. No high frequency observations are available for this station.

Barrow, Alaska

The monthly averaged concentrations from the CMDL flask network and *in situ* network and the model simulations are shown in Figure 5.9. Both model simulations seem able to capture the seasonal cycle seen in the observations, but slightly overpredict the concentrations. We can gain some insight into the uncertainties in the observations by comparing the values from the flask and the *in situ* CMDL networks, which can show differences of 2 ppt in the monthly mean values. Figure 5.10 shows the model results and the high frequency observational data for Barrow. The ECMWF and NMC simulations show similar pollution events. This is seen more clearly for January of 1991 in Figure 5.11. It appears that the models are capturing some of the pollution events that are seen in the observations, but perhaps not all, and not unambiguously.

The daily averaged concentrations from both the model and observations are calculated, and these values are correlated and shown in Table 5.4, along with the results at the other stations.

Table 5.4: Correlations at Surface Stations

Site	Correlation NMC to EC	Correlation EC to Obs.	Correlation NMC to Obs.
Barrow	0.83	0.69	0.80
Ireland	0.82	0.80	0.86
Colorado	0.58	0.48	0.50
Hawaii	0.58	0.66	0.33
Barbados	0.75	0.25	0.25
Samoa	0.91	0.90	0.86
Tasmania	0.82	0.66	0.64
South Pole	0.89	0.89	0.85

The model simulations and observations are moderately strongly correlated for both the EC and NMC simulations with values for the correlation coefficients of 0.69 and 0.80, respectively. The two model simulations are also well correlated, with a coefficient of 0.83. Both versions of the model seem to do a good job of simulating observations at Barrow.

Mace Head, Ireland

The monthly averaged concentrations from the ALE/GAGE site at Ireland is compared to model simulations in Figure 5.12, indicating that the model simulations are able to capture some of the seasonal cycle, although the winter minimum is not well captured, but the models over-predict the observed concentrations. Figure 5.13 shows the model output and observations without averaging. One can see that the model is capturing some of the pollution events at the site, and this can be seen

more clearly for January 1991 in Figure 5.14.

The daily averaged values are correlated and shown in Table 5.4, and indicate strong correlations between model simulations and output (0.80 and 0.86 for ECMWF and NMC, respectively) and between the model simulations (0.82). Both model versions seem to do a good job of simulating the observations at the Ireland site, although modeled concentrations are slightly high.

Niwot Ridge, Colorado

Monthly averaged concentrations at the CMDL station at Niwot Ridge is compared against monthly averaged model concentrations in Figure 5.15. Again, the models overpredict concentrations, but seem to do a reasonable job in the seasonal cycle. Once again, this Figure 5.gives some insight into the magnitude of the uncertainty in the concentrations, since values are available from both the flask and *in situ* CMDL networks, again showing differences of up to 2 ppt. Figure 5.16 shows the unaveraged data. There are differences in the number of events seen in the ECMWF and NMC model simulations, and the data seem to indicate more strong events, as seen in the NMC simulations. A closer look at January, 1991 shows that there seems to be some correspondence between the observations and model during some periods, but not all, as seen in Figure 5.17.

The correlation coefficients for the daily averaged values are 0.48, 0.50 and 0.58 for the correlation between the ECMWF and observations, and NMC and observations and the NMC and ECMWF simulations, indicating moderate to poor correlations, as seen in Table 5.4. Niwot Ridge is a difficult geographical location to model correctly, since it is located between major sources of CCl_3F in mountainous terrain, so it is not expected that the models would do a very good job here. Considering the difficulties, Niwot Ridge seems adequately modelled, in that the observed lack of a seasonal cycle is captured in the model simulations. Mean predicted concentrations are a little high at this site.

Mauna Loa, Hawaii

Figure 5.18 shows the monthly averaged model and observations (from CMDL) at the Mauna Loa Observatory in Hawaii. Both models tend to underpredict concentrations at this site, especially during the months of March through May. There is some disparity in the events and seasonal cycle in the models and observations, as seen in Figure 5.19, which shows the observations and model results for the year. Figure 5.20 shows the results just for January, 1991, and demonstrates that the model can capture some events rather well, as seen on the 20th of January.

The correlation coefficients for the daily averaged values are 0.66, 0.33 and 0.58 (as shown in Table 5.4) or the ECMWF and observations, NMC and observations, and the ECMWF and NMC simulations, which indicate moderate to poor correlations, except for the NMC and observations, which is a low correlation. The model seems to do an adequate job of modeling some of the events at this site, but the modeled concentrations are too low, and the seasonal cycle is not well captured by either model simulation.

Barbados

The monthly averaged concentrations at Barbados are shown in Figure 5.21, indicating that the ECMWF simulation is unable to reproduce the seasonal cycle, and tends to overpredict concentrations. The NMC simulation is much more similar to the observed concentrations. This can also be seen in Figure 5.22, which shows the unaveraged concentrations. Figure 5.23 shows a closer view of January, 1991, and seems to indicate much scatter in the data, and few significant events seen in the observations for this period.

The correlations between the model simulations and observations indicate no correlation (0.25), but the two model results are moderately strongly correlated (0.75) as shown in Table 5.4. Barbados seems to be a difficult station to capture--the MATCH-EC simulation seems far off the observed concentrations. This may be due to inaccurate winds (the movement of the intratropical convergence zone would dominant changes in concentration here) or to the emissions scenario. The MATCH-NMC simulation seems to a slightly better job, but the correlations in daily averaged values are similarly low for the NMC simulation.

Samoa

The monthly mean observed and model concentrations are shown in Figure 5.24 for Samoa. The models seem to capture the seasonal cycle well, but tend to underpredict the concentrations, especially the ECMWF simulations. This is consistent with the overprediction of the interhemispheric gradient seen in Figure 5.6a. Figure 5.24 allows a comparison between all three observational networks, and demonstrates some disparities in concentrations of order 4 ppt, in addition to differences in seasonal cycle at the site. Figure 5.25 shows the unaveraged data for the models and observations and seems to indicate less correspondence between the model simulations than seen at most of the other stations. In addition, there are no pollution events clearly visible, consistent with the location of Samoa, which is far from most of the sources. Figure 5.26 shows just January, 1991 and also shows no unambiguous pollution events.

The daily averaged values are well correlated between both model simulations and the observations and between model simulations, with correlation coefficients between 0.86 and 0.90, as seen in Table 5.4. Although the models had a difficult time at both the Hawaii and Barbados stations, the model seems to do better at Samoa. The largest errors in the wind fields might be expected in the tropics or the southern hemisphere, so it is not surprising that the model might do a poor job of simulating the tropical stations, but the model seems to simulate Samoa rather well.

Cape Grim, Tasmania

Figure 5.27 shows the monthly mean concentrations at the Cape Grim, Tasmania station. The two model simulations have similar seasonal cycles, while the observations deviate during April May and June. The NMC simulation has more similar annual mean concentration (consistent with the interhemispheric gradient discussion above). Figure 5.28 shows the unaveraged concentrations, showing the size and frequency of the pollution events. The number and size of pollution events

seen in the model simulations are much larger than in the observations. However, during January, 1991, the observations and model results seem to agree that there is only one pollution event large enough to be seen in the scatter of the observations, as shown in Figure 5.29.

The daily averaged correlations are 0.65 for ECMWF and NMC, and 0.82 between the two model simulations, as seen in Table 5.1. Since winds in the southern hemisphere and tropics are the least well-defined by the meteorological observations (although Australia is well sampled), it is not surprising that the southern hemisphere sites are not well simulated by the model. One would expect to get the pollution events correct, however at Cape Grim, since it is so close to Australia, and the Radon-222 simulations (in Chapter 4) showed good correspondence. So the model does seem to do a reasonable job simulating the Tasmanian site, but doesn't seem to capture the pollution events as well with CCl_3F as it did with Radon-222. The model does a better job with the NMC winds than with the ECMWF winds in capturing the mean concentration, as seen in Figures 6a and 6b.

South Pole

Monthly mean concentrations at the south pole observing station are shown in Figure 5.30. There is very little seasonal cycle in the observations or model simulations. Again the interhemispheric gradient problem in the ECMWF simulation is seen as the model underpredicts the concentrations significantly. Figure 5.31 shows the unaveraged data, which shows some rapid variations in the model results, which are not seen in the observations. This is seen clearly in Figure 5.32, which shows just the month of January, 1991.

Correlations between daily averaged values show strong correlations (0.85-0.88) between the models and observations, as seen in Table 5.4. The model with the NMC winds seems able to capture the observations at the South Pole site, but the ECMWF simulation was less able to simulate the mean concentration and the trend in the data.

5.4.0 Summary and conclusions

The MATCH model was used to simulate CCl_3F with both ECMWF and NMC winds. A comparison of model results with observations at 9 sites indicates the MATCH-NMC model is capable of simulating the interhemispheric gradient with reasonable success. However, the MATCH-EC model had too an large interhemispheric gradient.

Both versions of the model seemed to do a reasonable job simulating the vertical gradient in the tropics between the troposphere and stratosphere, but maintain concentrations that are too large in the lower stratosphere in the northern mid-latitudes and high-latitudes. It is unclear why the model is unable to capture the vertical profile, but this may be related to several factors: the most likely being too much mixing in the mid-latitudes and high latitudes near the tropopause. The cause of this mixing overprediction is unknown.

The CCl_3F simulations seem to indicate that the MATCH model is capable of simulating the seasonal cycle at many of the stations with both the ECMWF and NMC winds. At Barbados and Hawaii, the model seemed to have the hardest time capturing the seasonal cycle. In addition, the model seems to be able to capture pollution events at many of the stations rather well.

Although the model does a good job simulating the atmosphere, there are discrepancies between observations and the model. Realize that problems in simulating the observations using this chemical transport model may be problems that are inherent to CTMs. We cannot blame all of the discrepancies seen here on the analyzed observed winds, since we are using two different versions of analyzed observed winds that are as good as they can be. Some problems seen here may be related to emissions inventory, or problems in model implementation (e.g. moist convective mixing, boundary layer mixing), which can be improved. But the discrepancies seen in this study may also be due to problems with the way CTMs are constructed--it may well be that comparing CTM output to individual sites is not a good way to test a CTM, since a grid box is 200 km by 200 km, and the observing sites may be strongly affected by local meteorological effects. In addition, there are limits to how good trajectory calculations are, and when we compare pollution events, we are expecting the model to have correctly calculated a trajectory for several days. Also, boundary layers are difficult to simulate well, and most observations are made in boundary layers.

It is not clear how to determine which of the above reasons for the discrepancies dominants. The first step to determining the reasons might be to try to improve portions of the model which we suspect are poorly treated. We would suggest that the boundary layer mixing and the moist convective mixing are perhaps the most important pieces of the transport model that could be improved. Most of the observations are made in the bottom of the boundary layer, and improving the determination of the concentration at the height of the observations might improve the simulations. In this study, it was assumed that the bottom layer is well mixed, but this is probably not true close to the emission regions. In addition, Chapter 3 and 4 indicated that there are known problems with the implementation of both of the moist convective schemes used in this study. Improving the moist convective parameterization might improve the simulations. In addition, a sensitivity study of the emission inventory might shed some light on how sensitive the concentrations of CCl_3F are to the assumed emission distribution. If these steps do not improve the simulations of the observations, this might suggest that we are approaching the limit of the ability of a global CTM with grid sizes of order 200 km to adequately simulate observations taken at a single point, where microscale and mesoscale effects may be important.

In conclusion, using a chemical transport model based on observing winds seems to be an approach which improves the performance of the chemical transport models. The model seems able to capture the interhemispheric gradient (with NMC winds), the seasonal cycle at many stations, and many of the specific pollution events. There are problems with the model, especially in the vertical gradient of the CCl_3F in the lower stratosphere, and in the seasonal cycle at some stations.

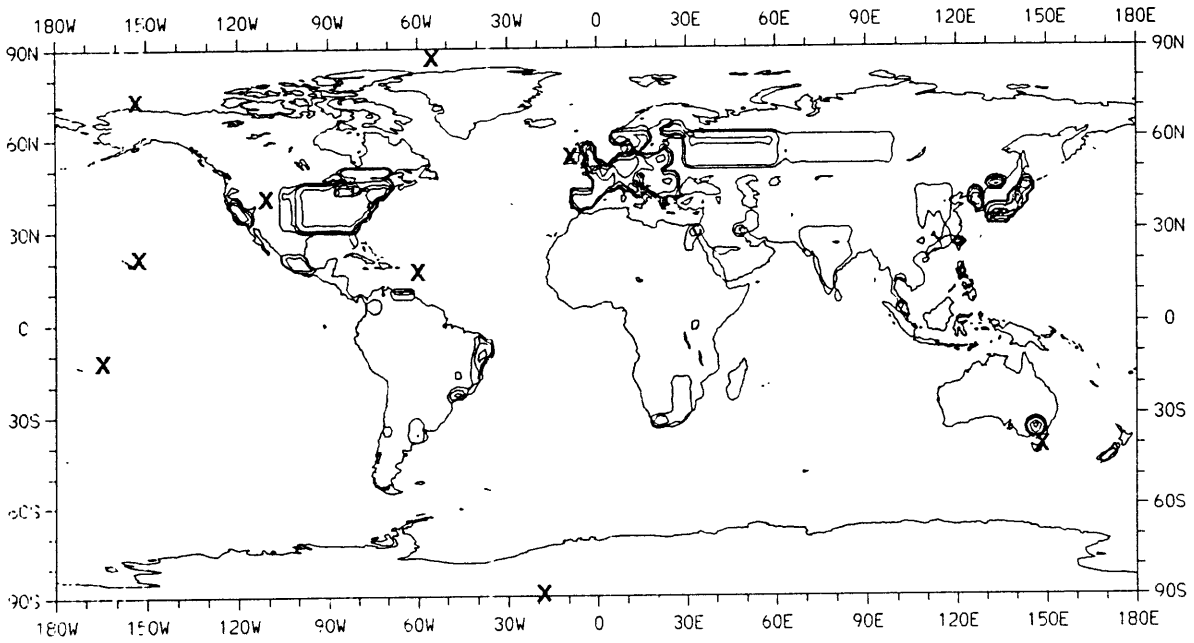

Figure 5.1: Distributions of CCl_3F emissions globally [Hartley and Prinn, 1993] as well as the location of the observing sites used in this study.

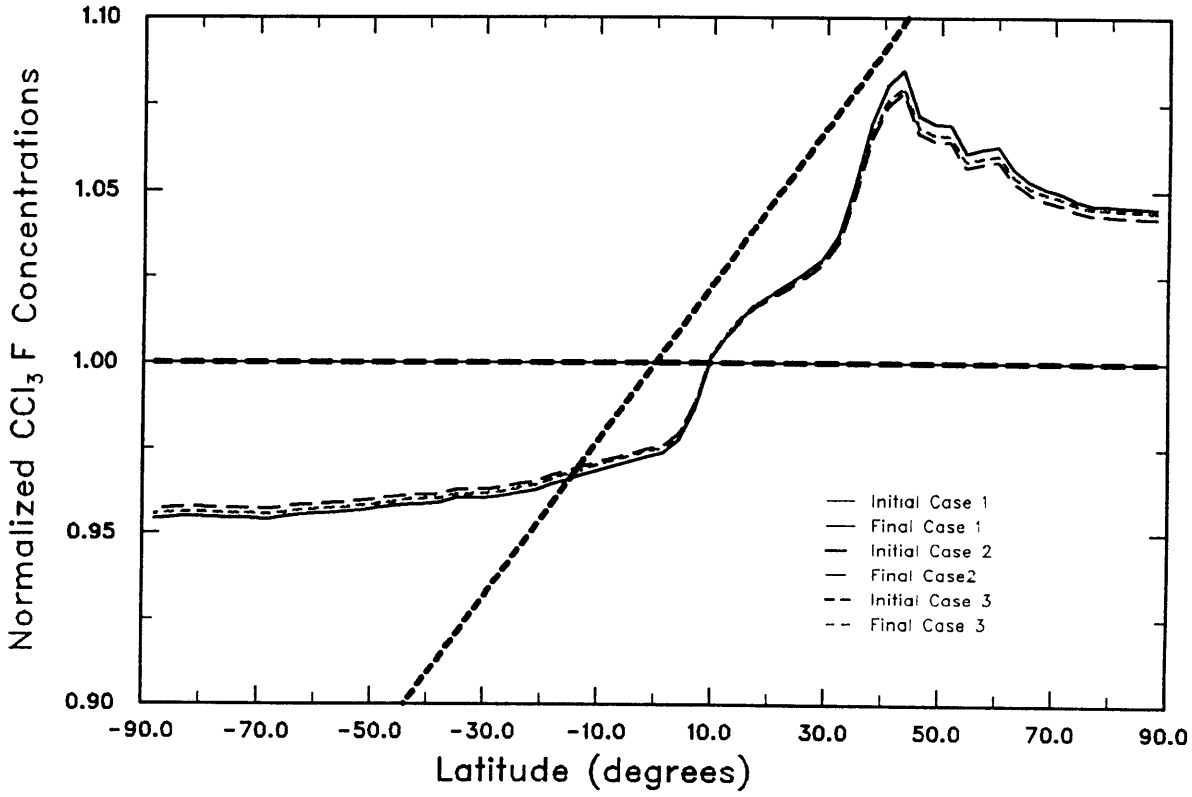

Figure 5.2a: Zonally averaged normalized surface concentration of CCl_3F for the three initial conditions described in the text for the MATCH-ECMWF simulation as a function of latitude. The initial distribution, as well as the monthly averaged distribution after 2 years of "spin-up" are shown. The concentrations have been normalized by the mean concentration for that month, for ease of comparison, since the CCl_3F has accumulated in time.

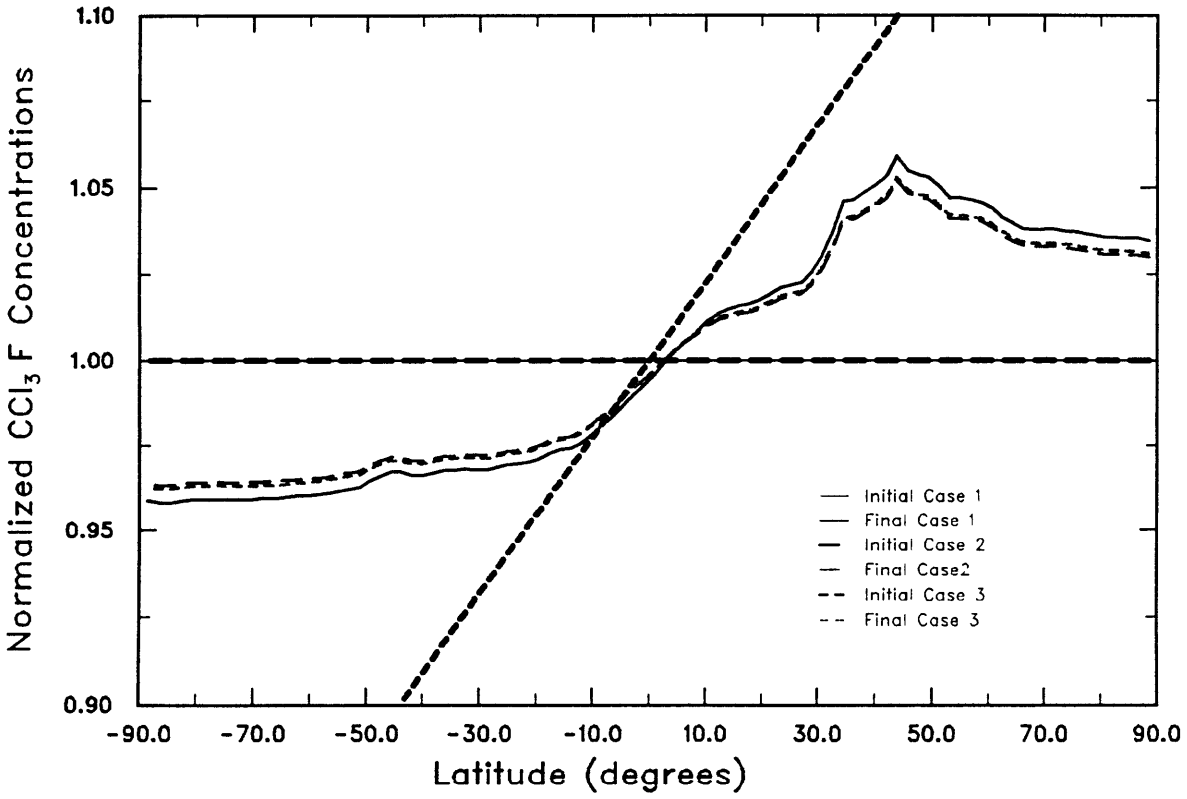

Figure 5.2b: Same as Figure 5.2a, but for the MATCH-NMC simulation.

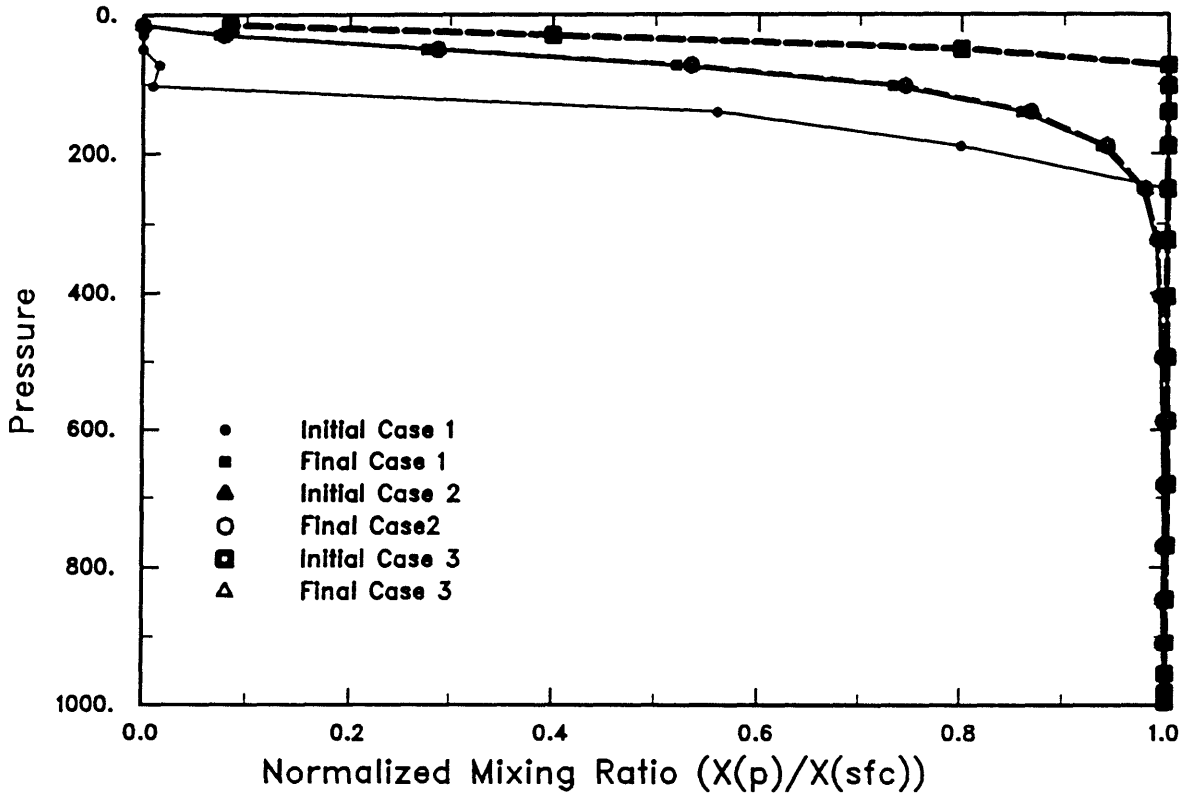

Figure 5.3a: Globally averaged vertical profile of CCl3F for the three initial conditions described in the text for the MATCH-ECMWF simulation. The initial profile, as well as the monthly mean profile after 2 years of "spin-up" are shown. The concentrations have been normalized by the mean surface concentration for ease of comparison.

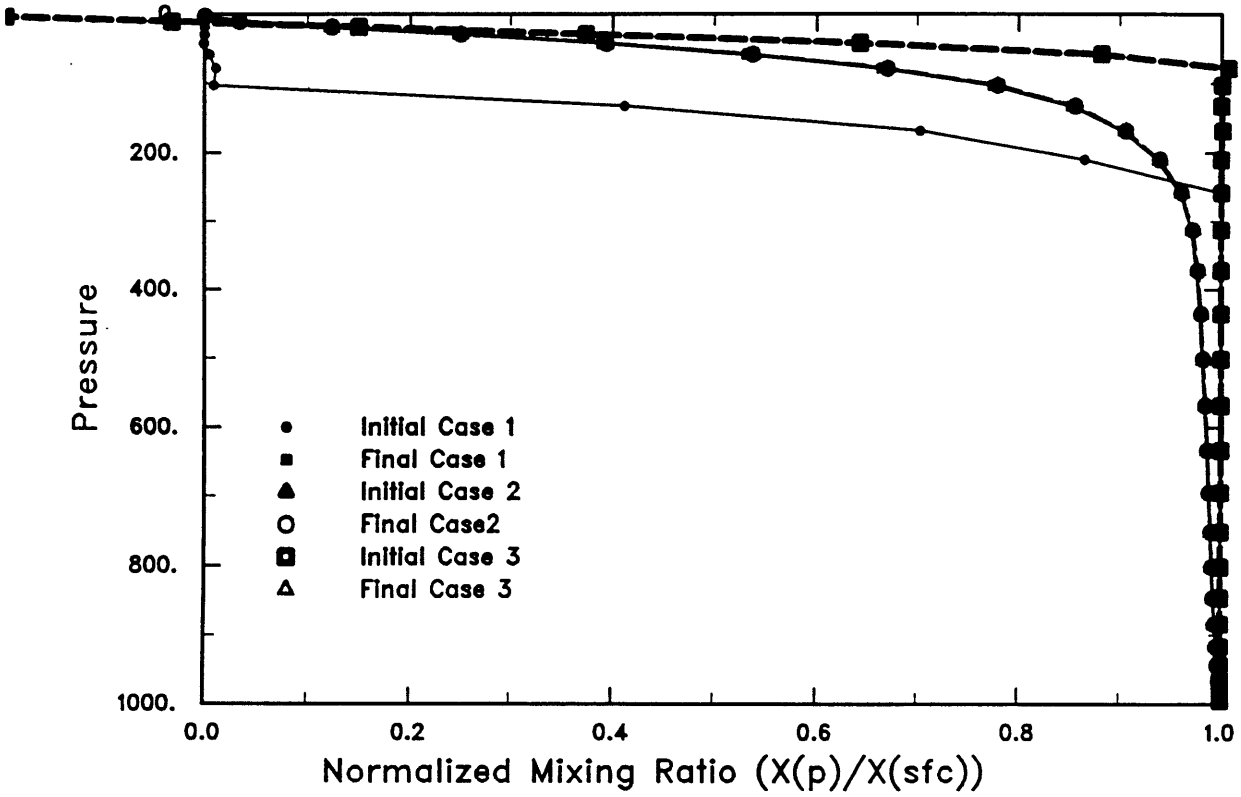

Figure 5.3b: Same as Figure 5.3a, but for the MATCH-NMC simulation.

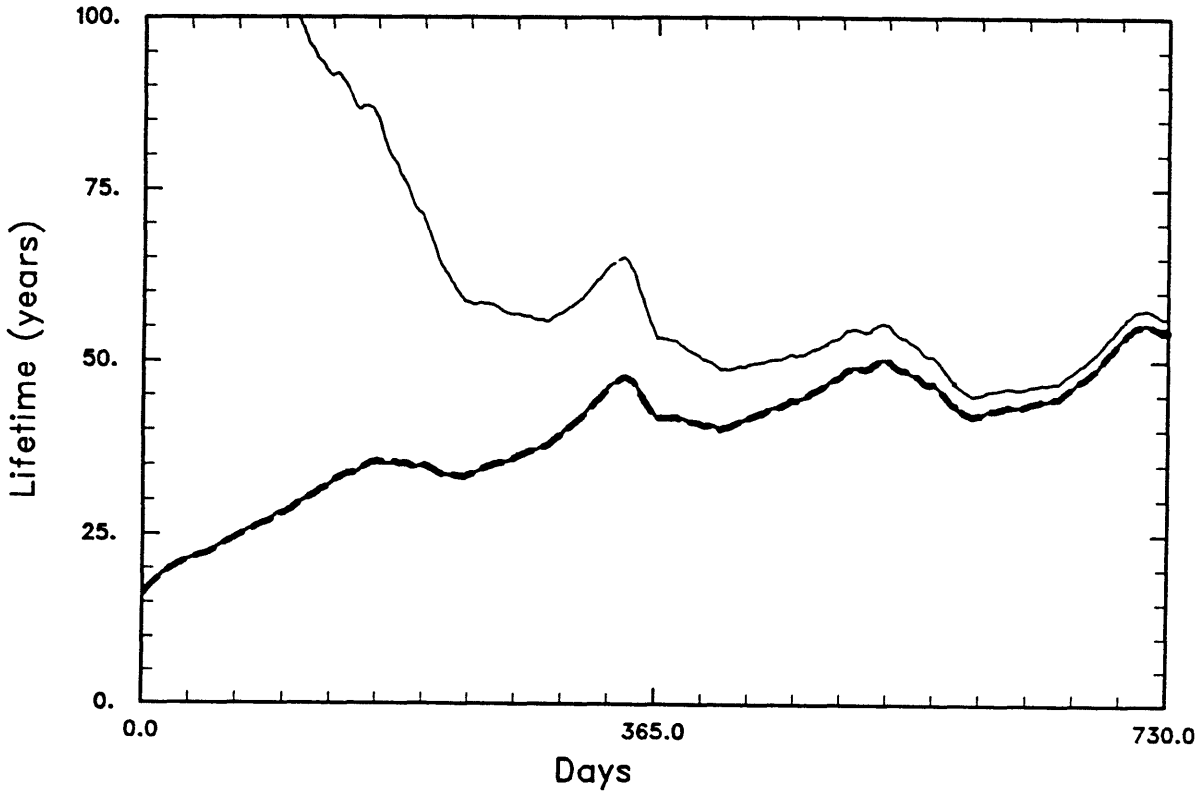

Figure 5.4a: Model calculated lifetime (years) for the MATCH-ECMWF simulation for the two year spin up period for the three initial conditions described in the text. Lifetime is calculated as the mass in the model atmosphere divided by the loss due to photolysis in the model.

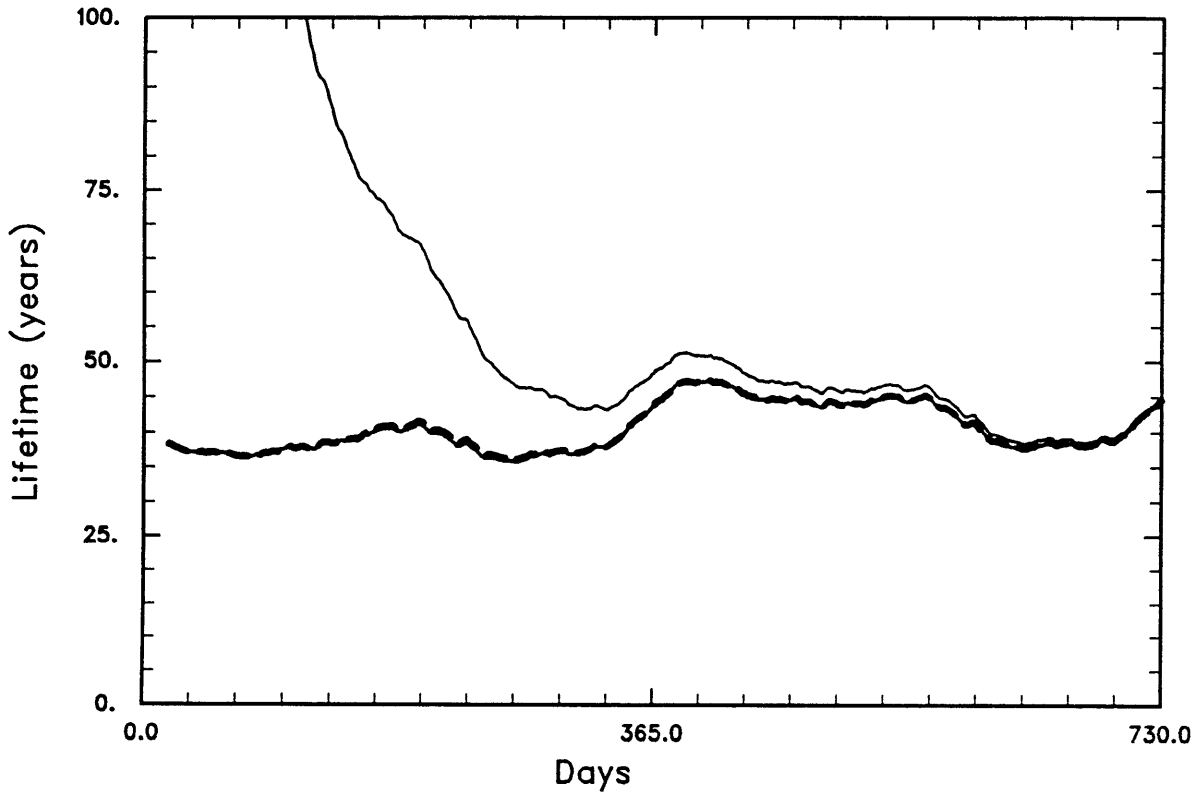

Figure 5.4b: Same as Figure 5.4a, but for the MATCH-NMC simulation.

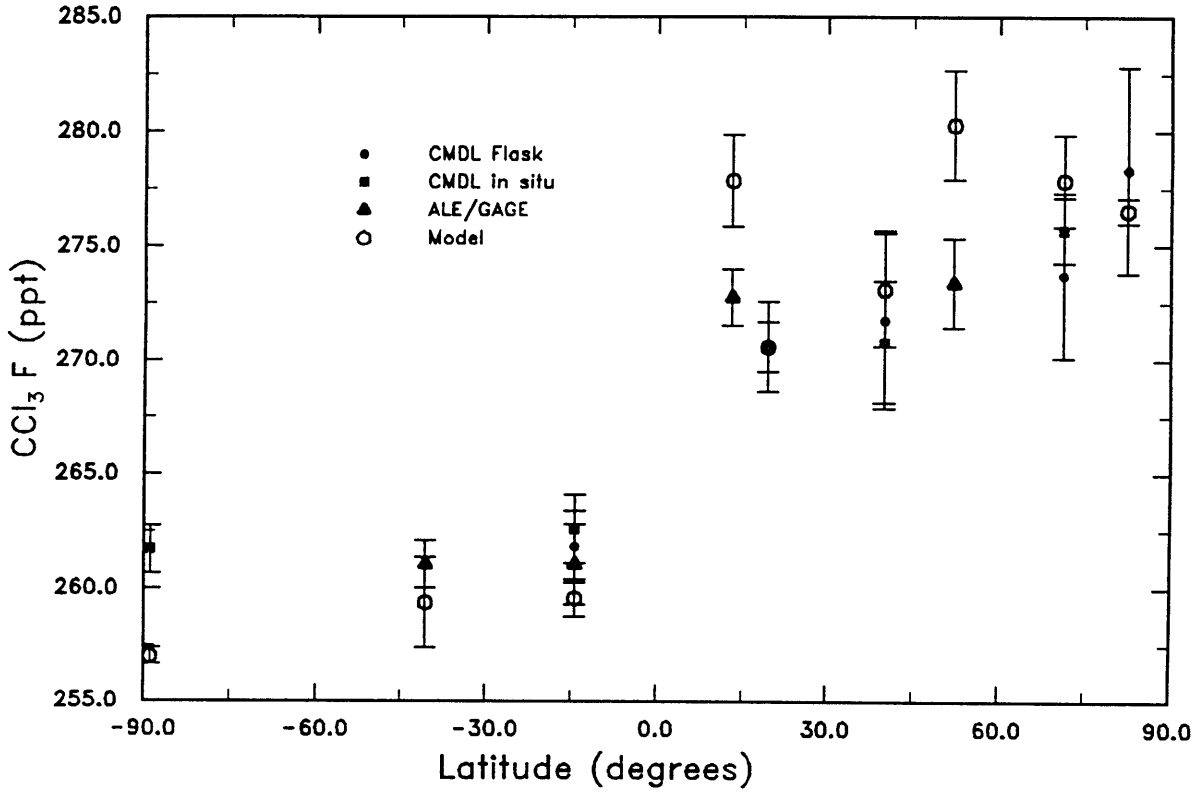

Figure 5.5a: Monthly averaged CCl_3F concentrations as a function of latitude at the 9 stations for July, 1991 from the MATCH-ECMWF model simulations as well as the from observations.

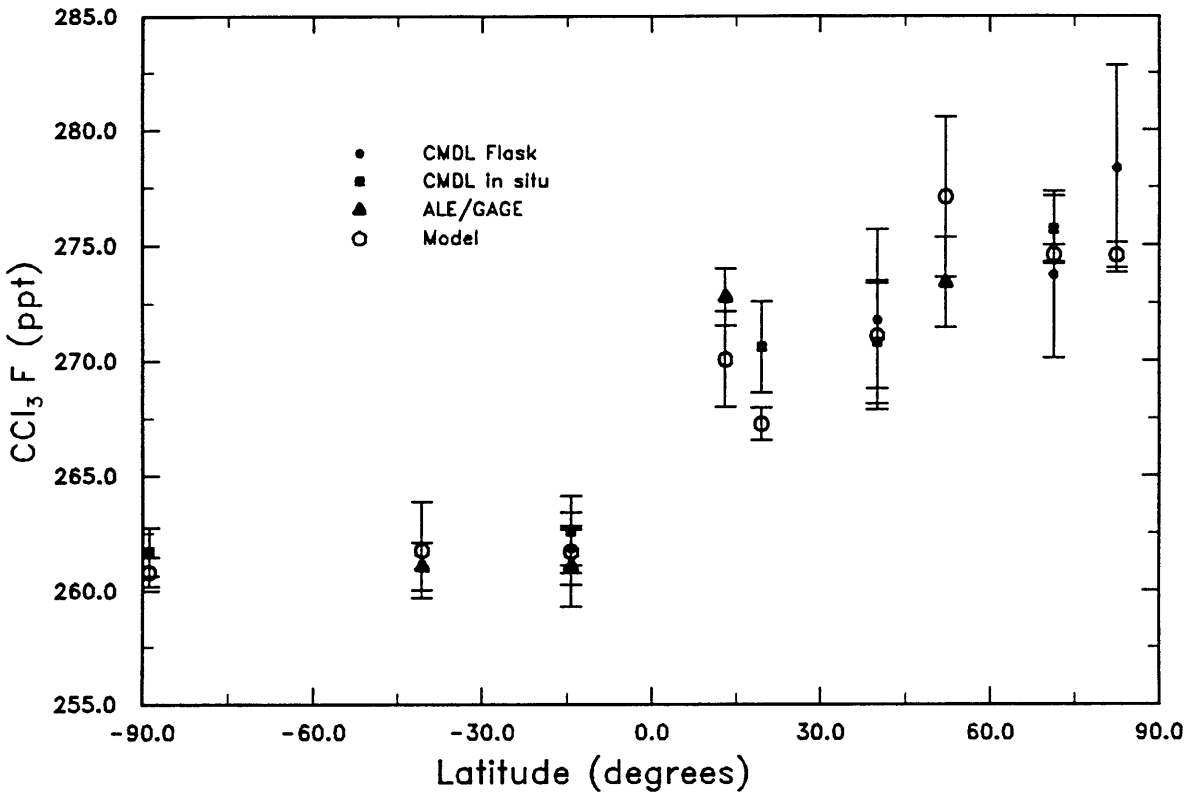

Figure 5.5b: Same as Figure 5.5a, but for the MATCH-NMC simulation.

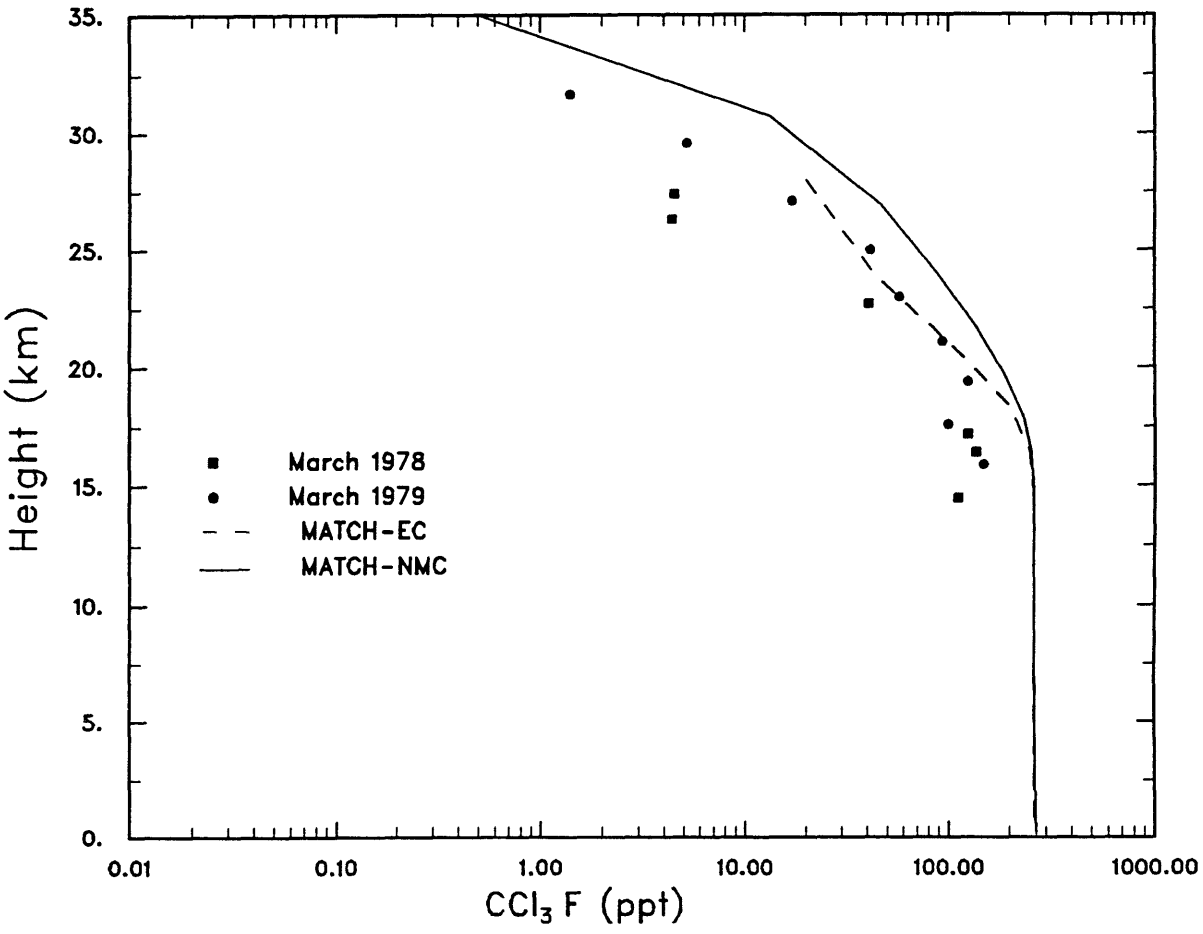

Figure 5.6: Vertical profile of CCl_3F for the tropics. Observations are taken from Goldan, et al., [1980] and were made over Brazil at 5 S in March of 1978 and 1979. Monthly averaged concentrations from the MATCH-ECMWF and NMC simulations are shown for March, 1991 and calculated from an zonal average from 0 N to 10 S.

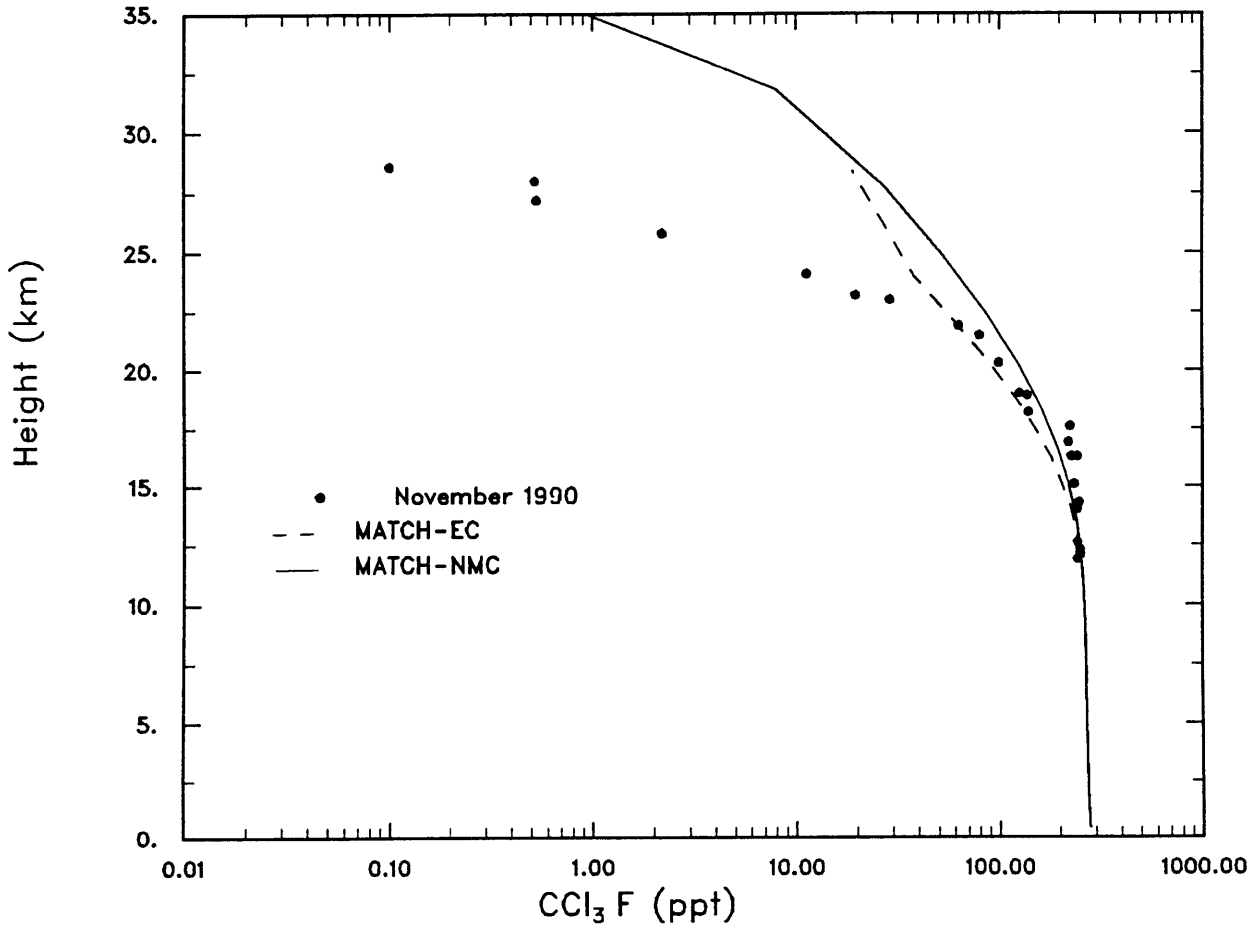

Figure 5.7a: Vertical profile of CCl_3F for the northern midlatitudes. Observations are taken from Fraser, et al, [1994] and were made by KFA-Julich [Schmidt, et al., 1991] during November, 1990 at 44 N. Monthly averaged concentrations from the MATCH-ECMWF and NMC simulations are shown for November, 1990 and calculated from zonal average from 40 to 48 N.

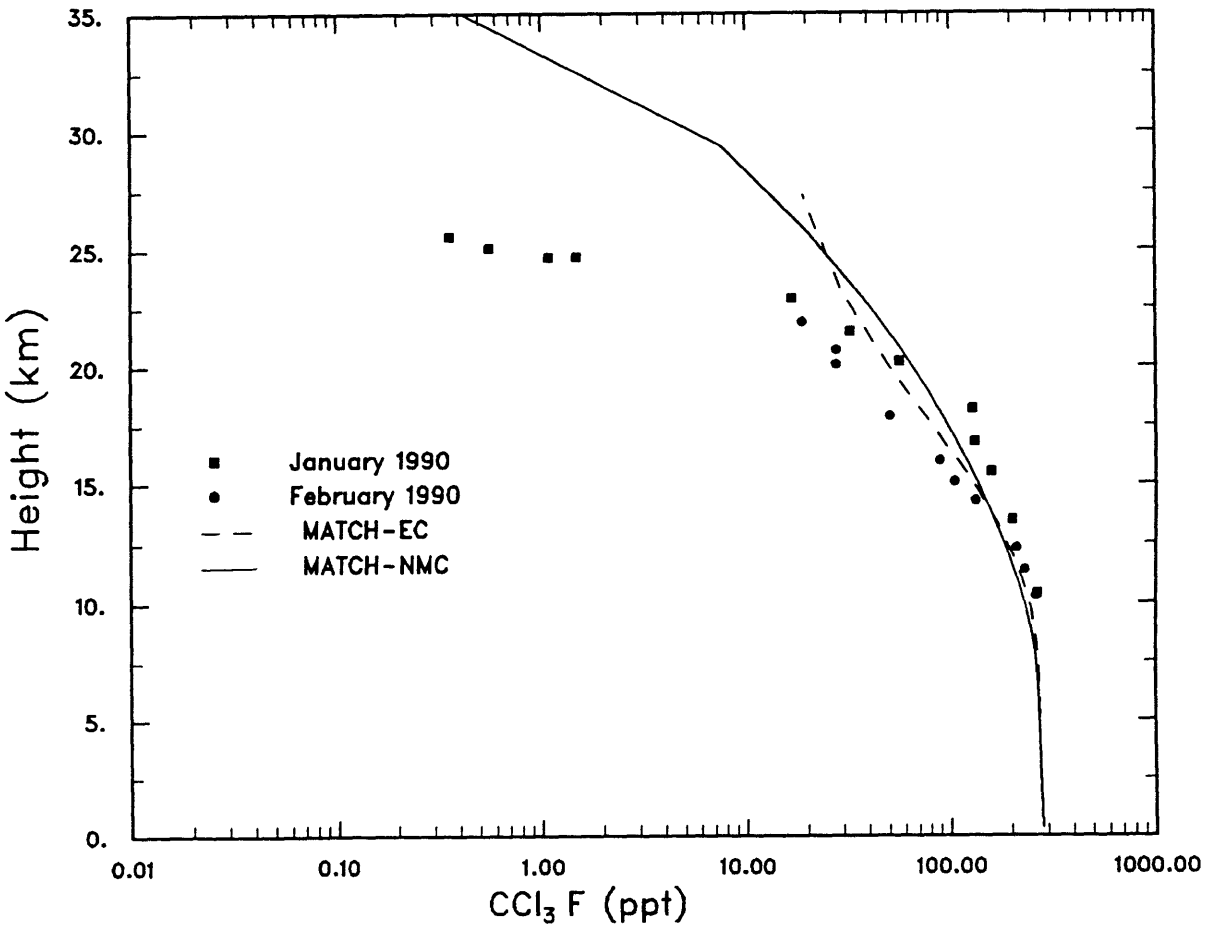

Figure 5.7b: Same as for Figure 5.7a. but for the northern high latitudes. Observations are taken from Fraser, et al, [1994] and were made by KFA-Julich [Schmidt, et al., 1991] during January and February, 1990 at 68N. Monthly averaged concentrations from the MATCH-ECMWF and NMC simulations are shown for January and February, 1991 and calculated from zonal average from 64 to 72 N.

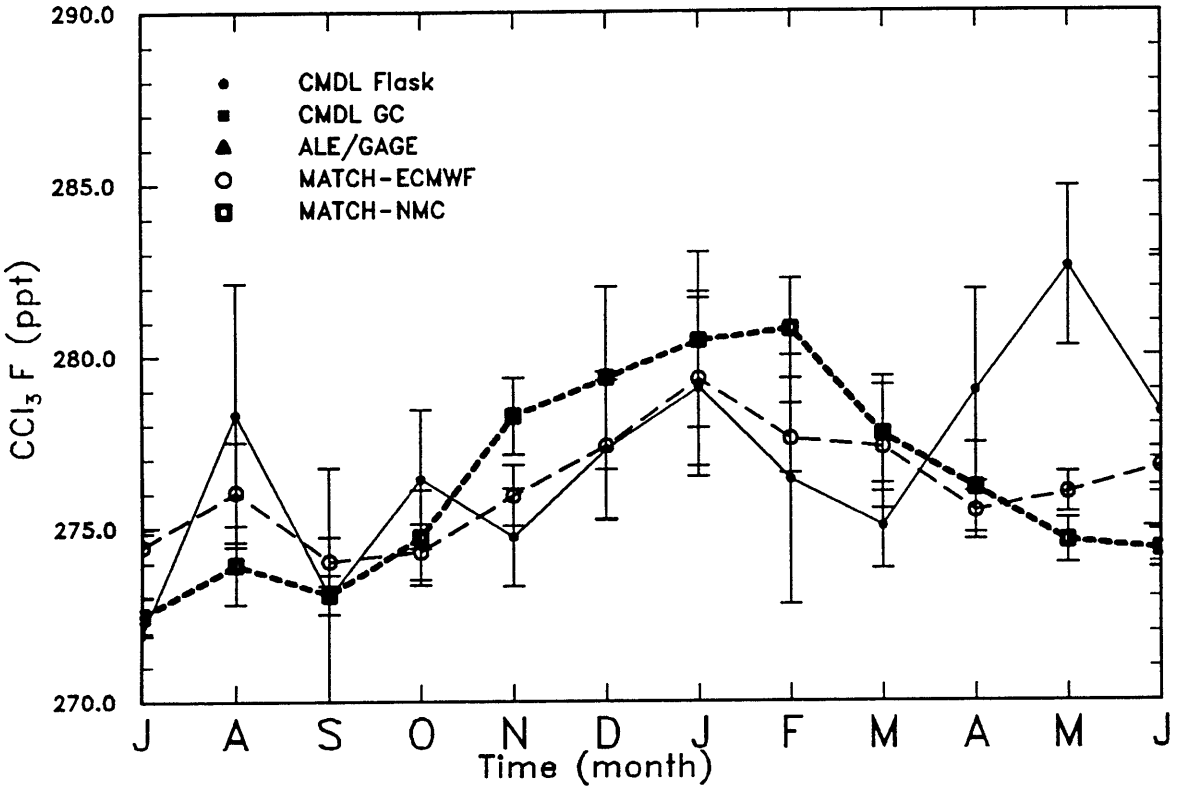

Figure 5.8: Monthly mean CCl_3F concentrations (ppt) at the Alert, Canada observing station for the MATCH-ECMWF and MATCH-NMC model simulations, as well as observations from the CMDL flask network [Elkins, et al., 1993] for July, 1990 to June, 1991.

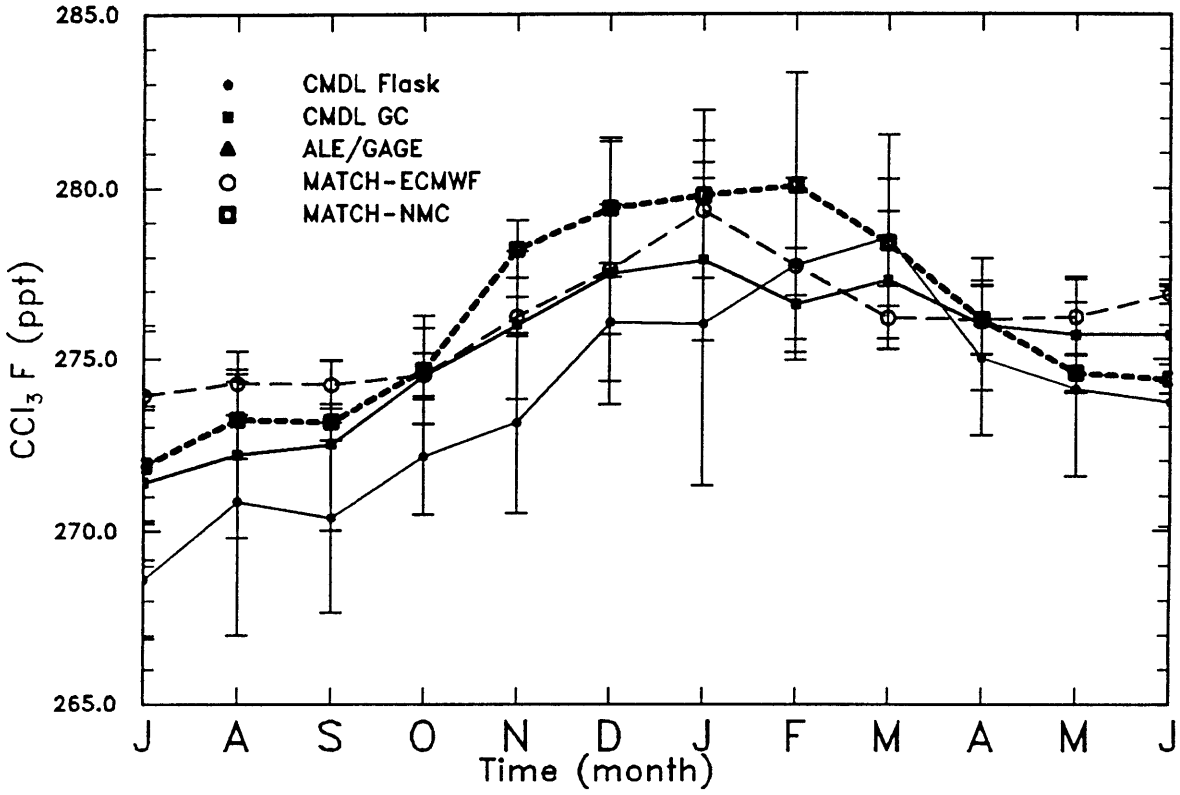

Figure. 5.9. Monthly mean CCl_3F concentrations (ppt) at the Barrow, Alaska observing station for the MATCH-ECMWF and MATCH-NMC model simulations, as well as observations from the CMDL flask and *in situ* network [Elkins, et al., 1993] for July, 1990 to June, 1991.

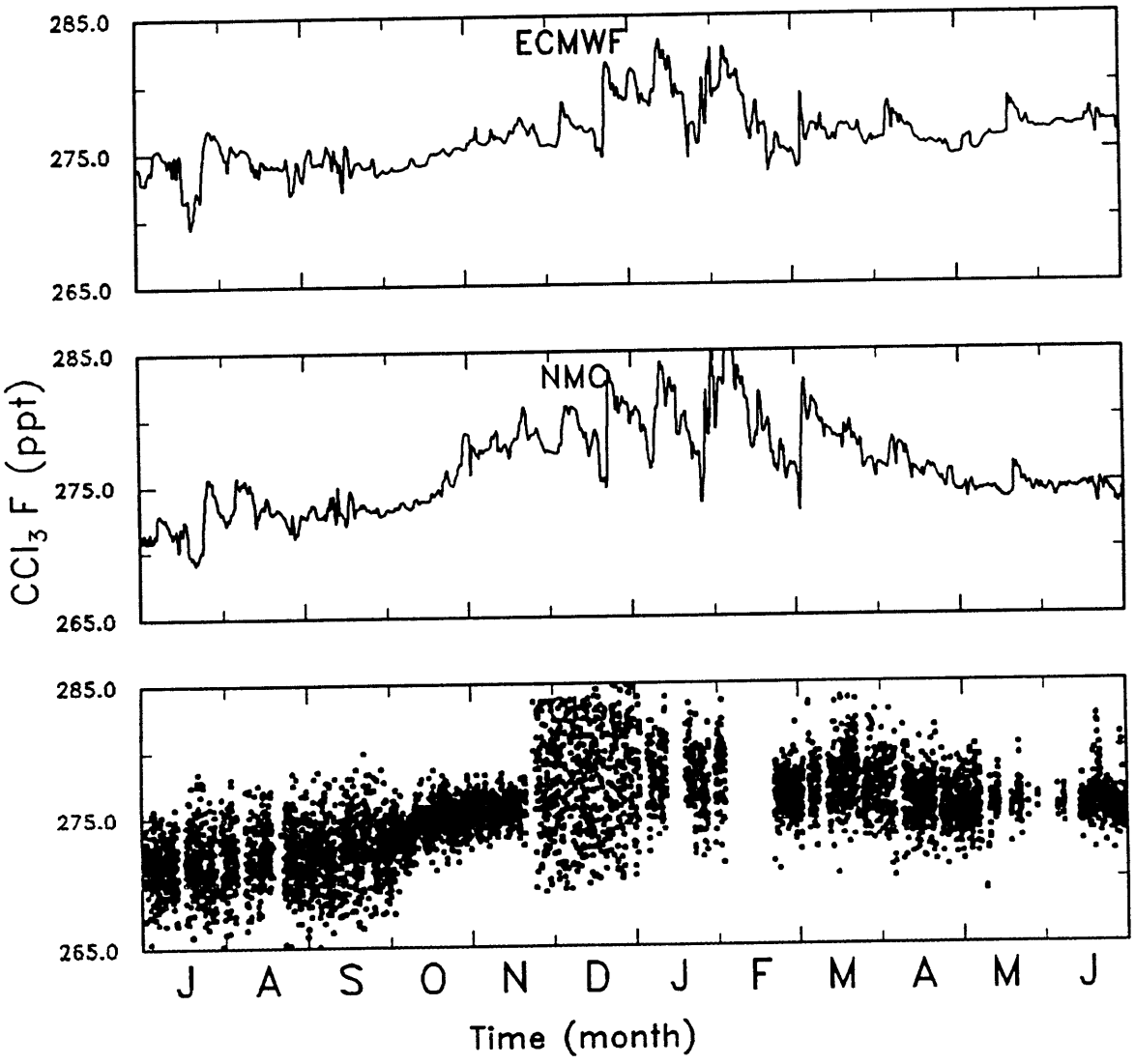

Figure 5.10: CCl_3F concentrations (ppt) at the Barrow, Alaska observing station for the MATCH-ECMWF and MATCH-NMC model simulations, as well as observations from the CMDL *in situ* network [Elkins, et al., 1993] for July, 1990 to June, 1991.

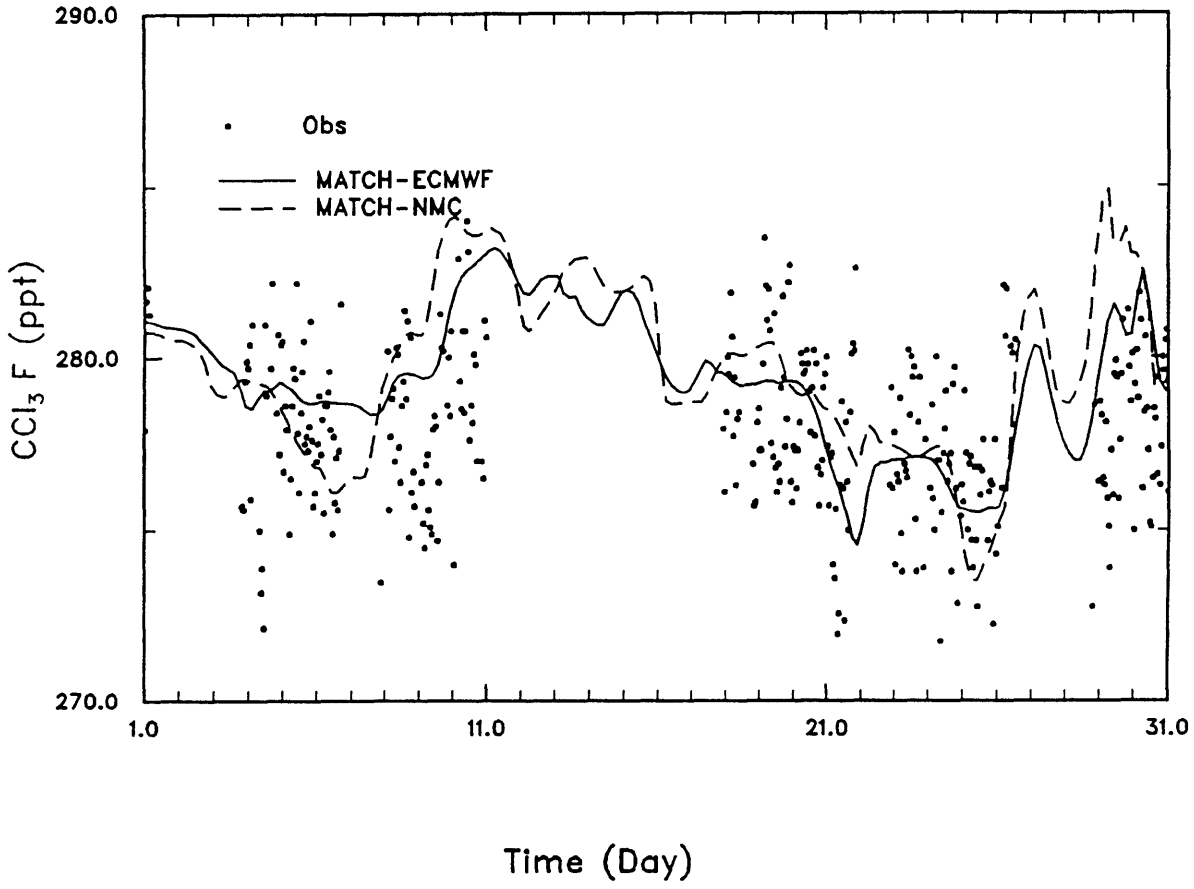

Figure 5.11: Same as Figure 5.10, except for January, 1991.

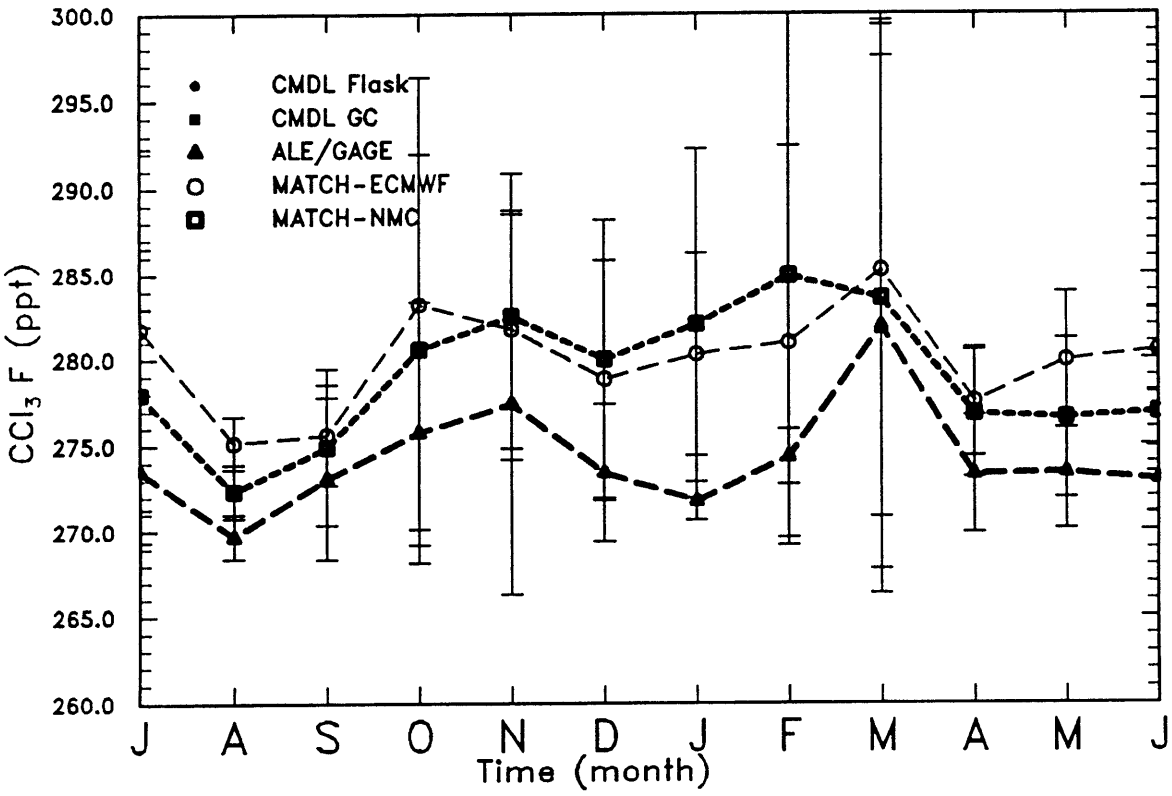

Figure 5.12: Monthly mean CCl_3F concentrations (ppt) at the Mace Head, Ireland observing station for the MATCH-ECMWF and MATCH-NMC model simulations, as well as observations from the ALE/GAGE *in situ* network [Cunnold, et al., 1994] for July, 1990 to June, 1991.

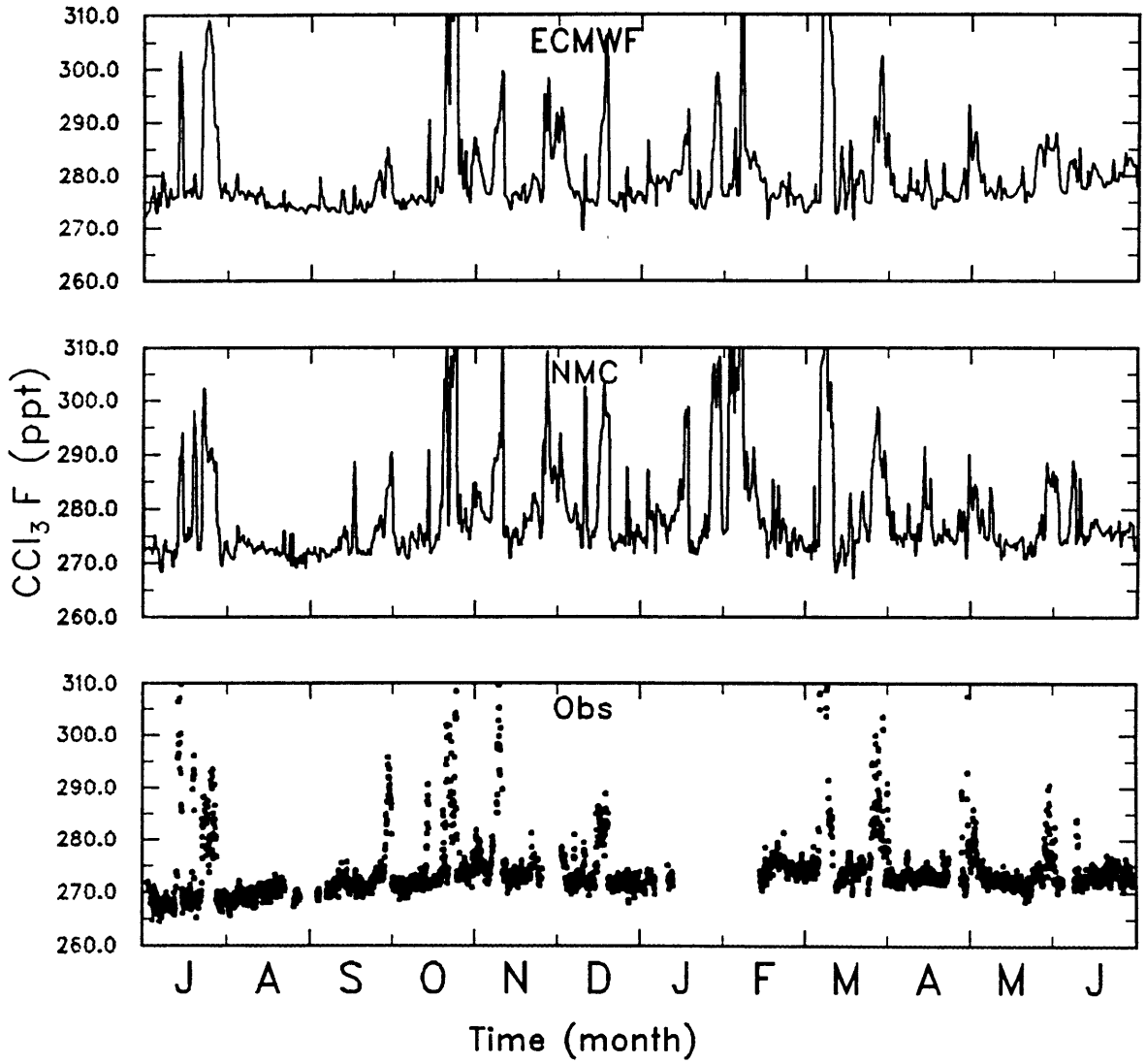

Figure 5.13: CCl_3F concentrations (ppt) at the Mace Head, Ireland observing station for the MATCH-ECMWF and MATCH-NMC model simulations, as well as observations from the ALE/GAGE *in situ* network [Cunnold, et al., 1994] for July, 1990 to June, 1991.

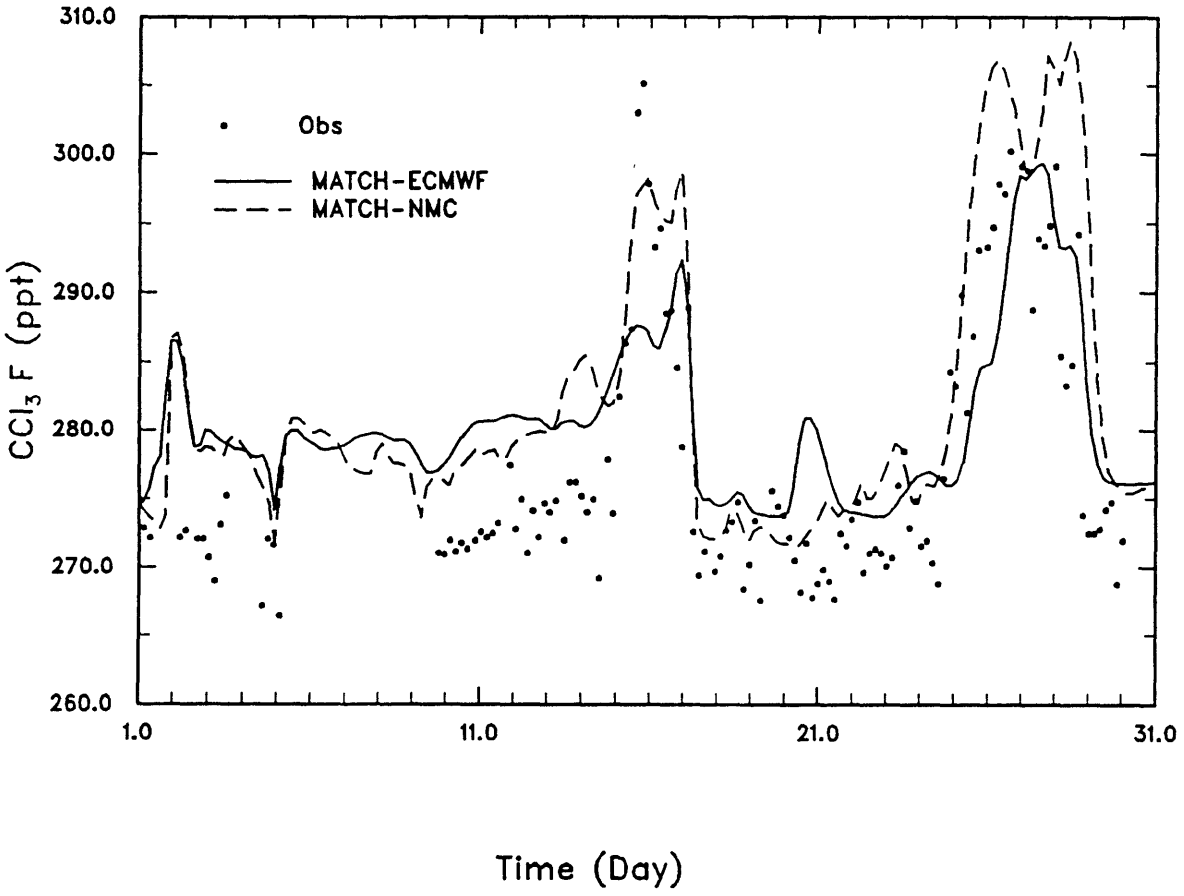

Figure 5.14: Same as Figure 5.13, except for January, 1991.

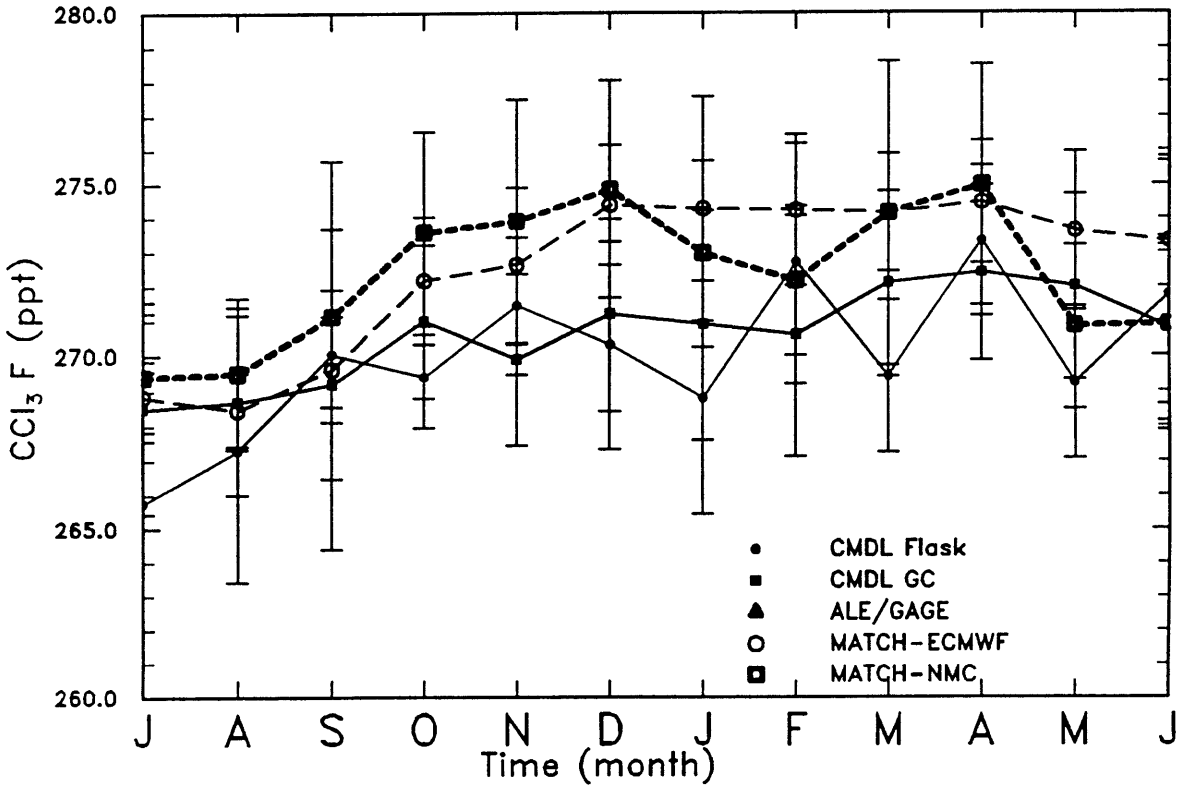

Figure. 5.15. Monthly mean CCl_3F concentrations (ppt) at the Niwot Ridge, Colorado observing station for the MATCH-ECMWF and MATCH-NMC model simulations, as well as observations from the CMDL flask and *in situ* network [Elkins, et al., 1993] for July, 1990 to June, 1991.

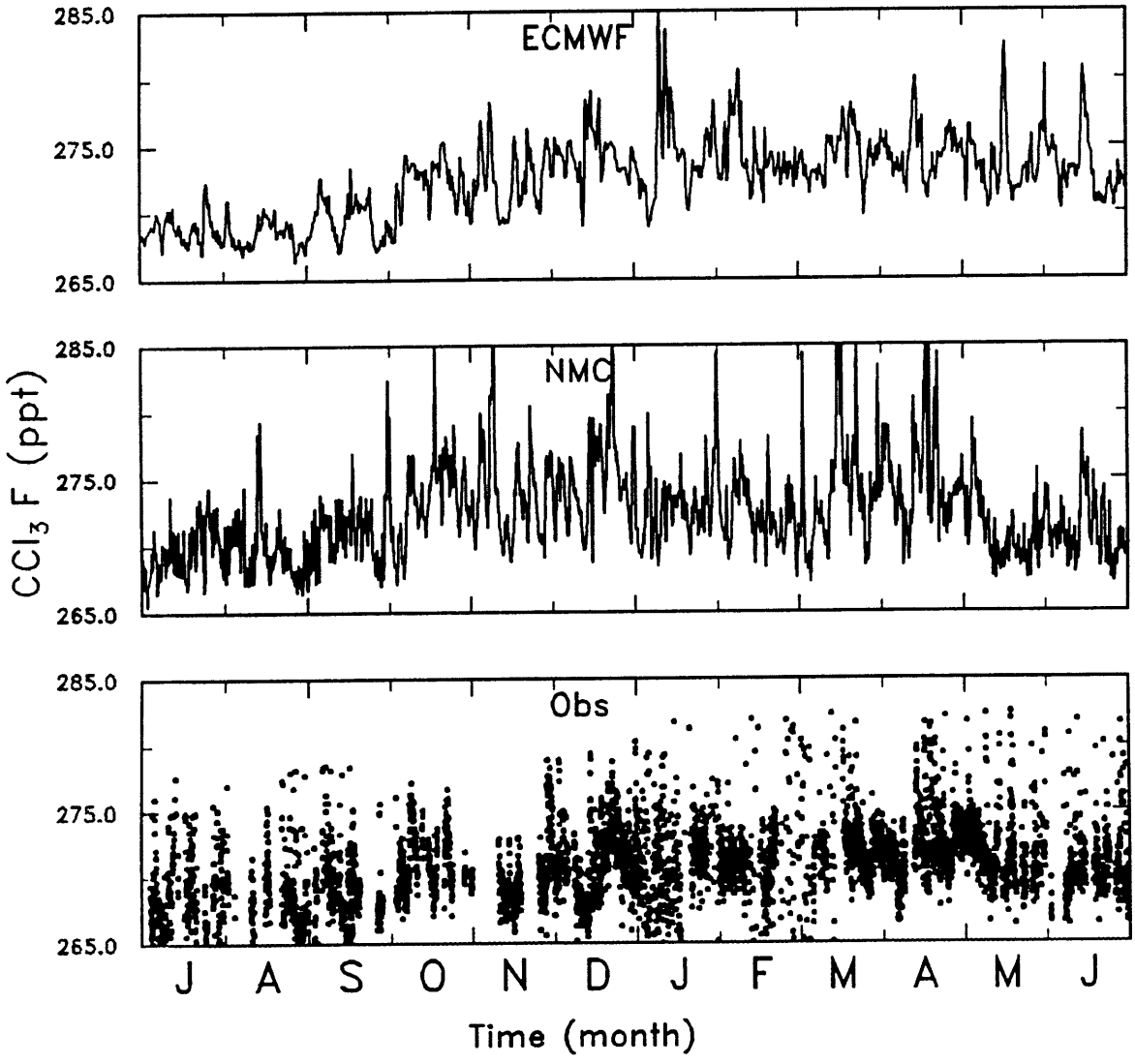

Figure 5.16: CCl_3F concentrations (ppt) at the Niwot Ridge, Colorado observing station for the MATCH-ECMWF and MATCH-NMC model simulations, as well as observations from the CMDL *in situ* network [Elkins, et al., 1993] for July, 1990 to June, 1991.

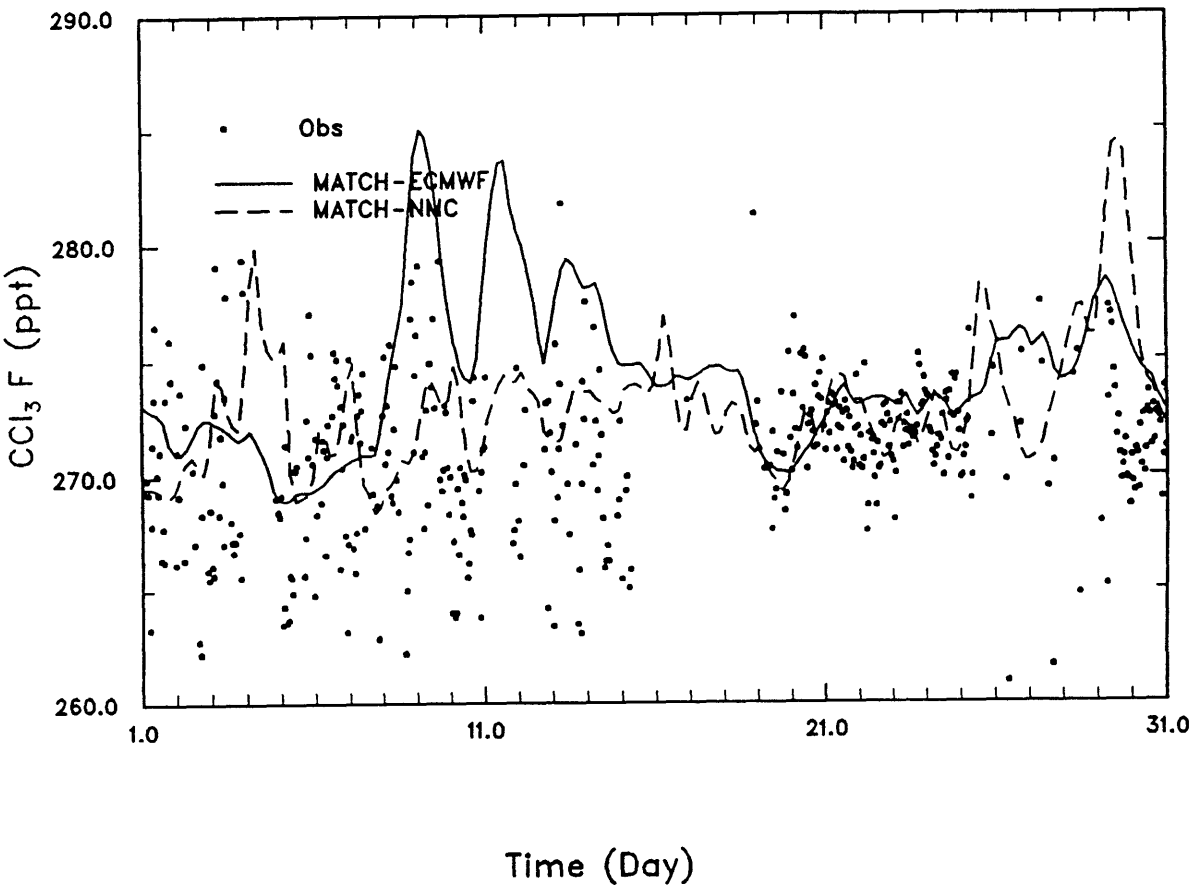

Figure 5.17: Same as Figure 5.16, except for January, 1991.

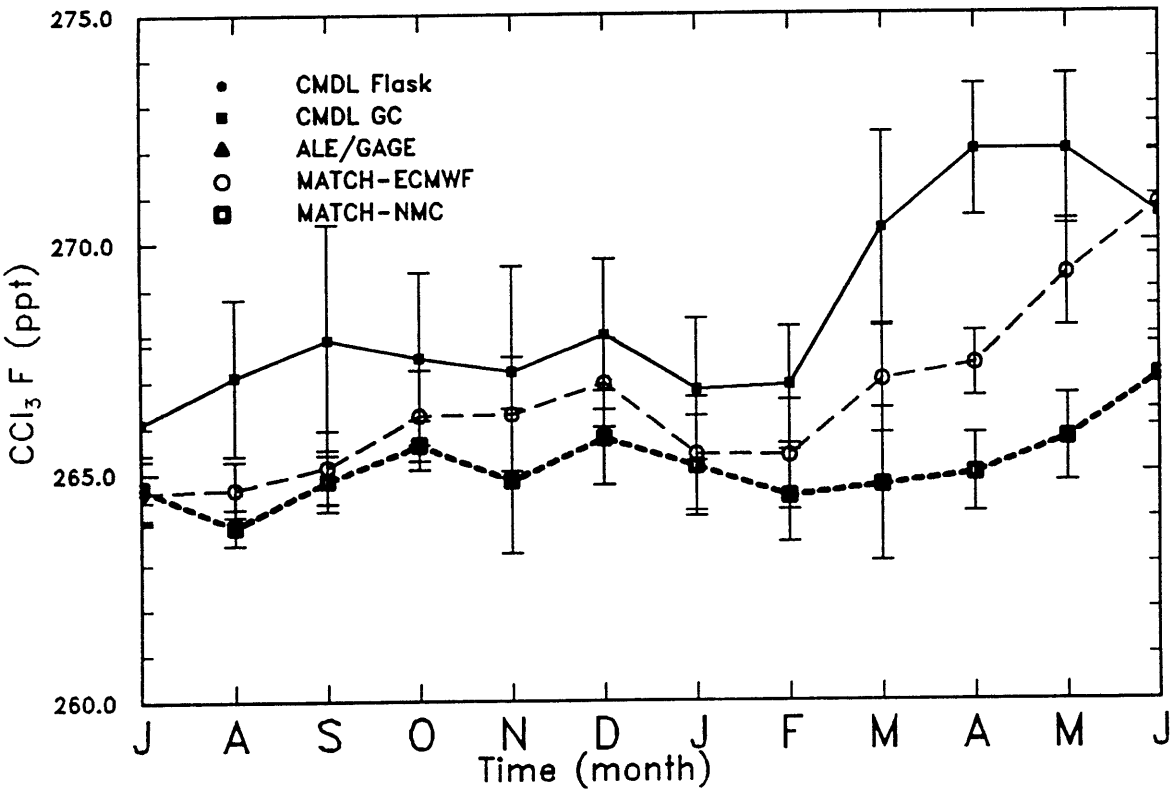

Figure. 5.18. Monthly mean CCl_3F concentrations (ppt) at the Mauna Loa, Hawaii observing station for the MATCH-ECMWF and MATCH-NMC model simulations, as well as observations from the CMDL *in situ* network [Elkins, et al., 1993] for July, 1990 to June, 1991.

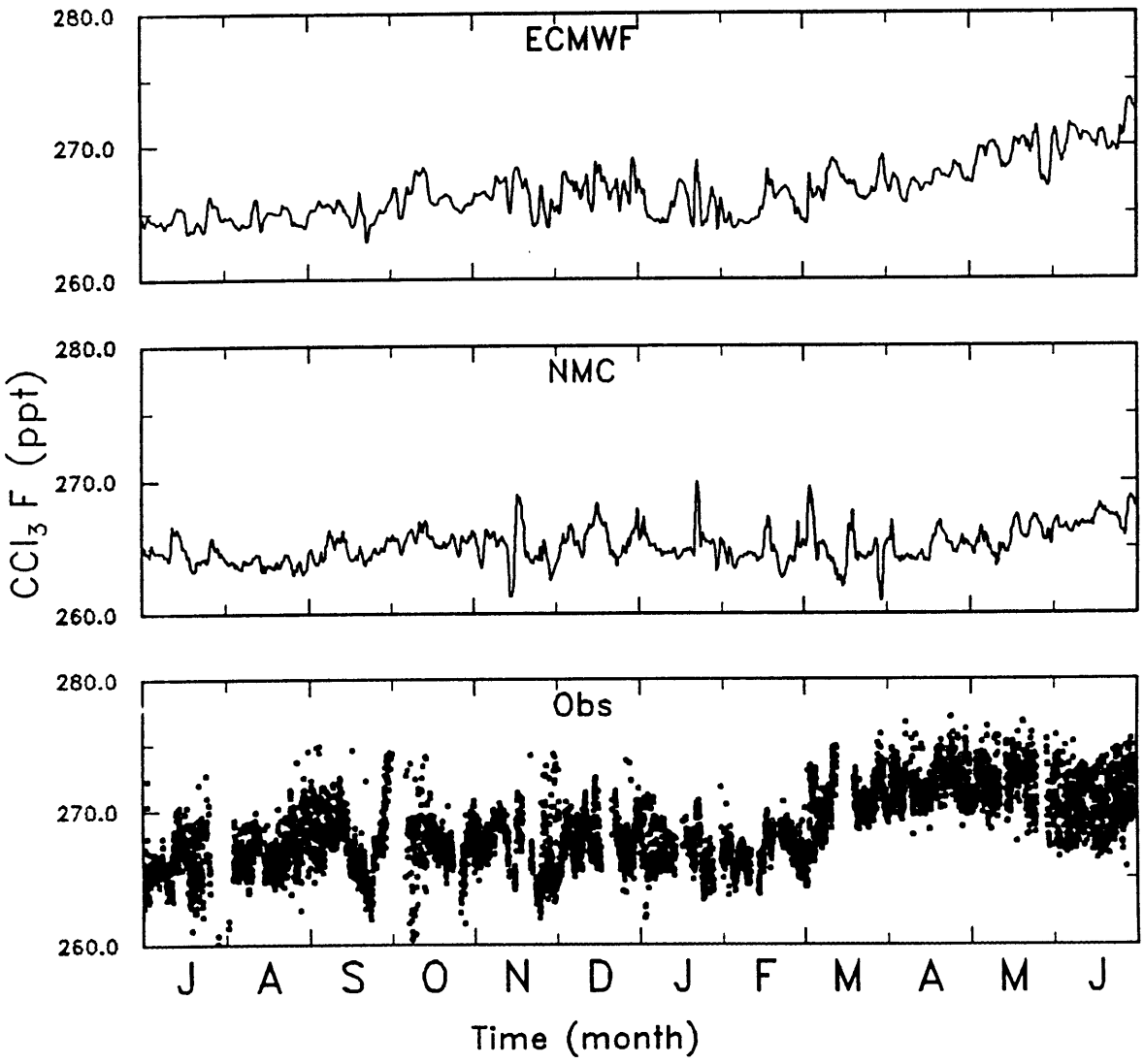

Figure 5.19: CCl_3F concentrations (ppt) at the Mauna Loa, Hawaii observing station for the MATCH-ECMWF and MATCH-NMC model simulations, as well as observations from the CMDL *in situ* network [Elkins, et al., 1993] for July, 1990 to June, 1991.

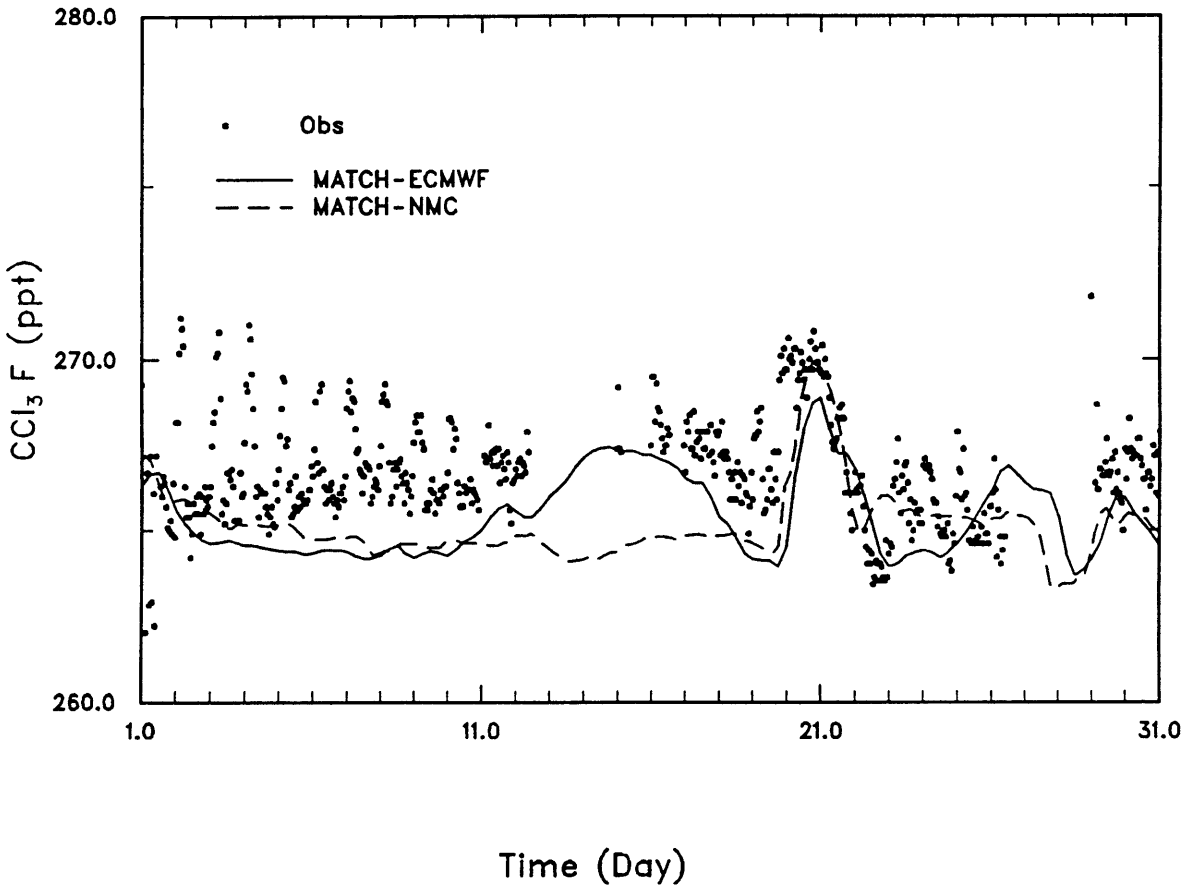

Figure 5.20: Same as Figure 5.16, except for January, 1991.

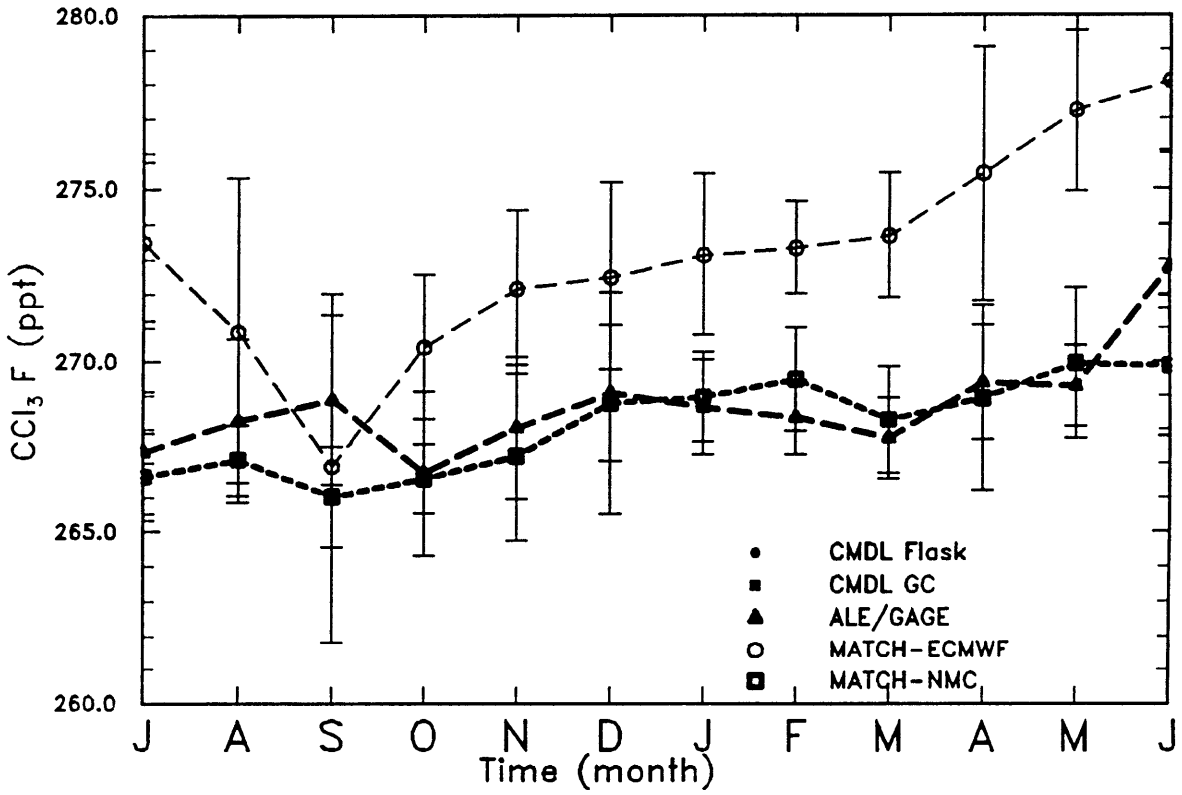

Figure 5.21: Monthly mean CCl_3F concentrations (ppt) at the Barbados observing station for the MATCH-ECMWF and MATCH-NMC model simulations, as well as observations from the ALE/GAGE *in situ* network [Cunnold, et al., 1994] for July, 1990 to June, 1991.

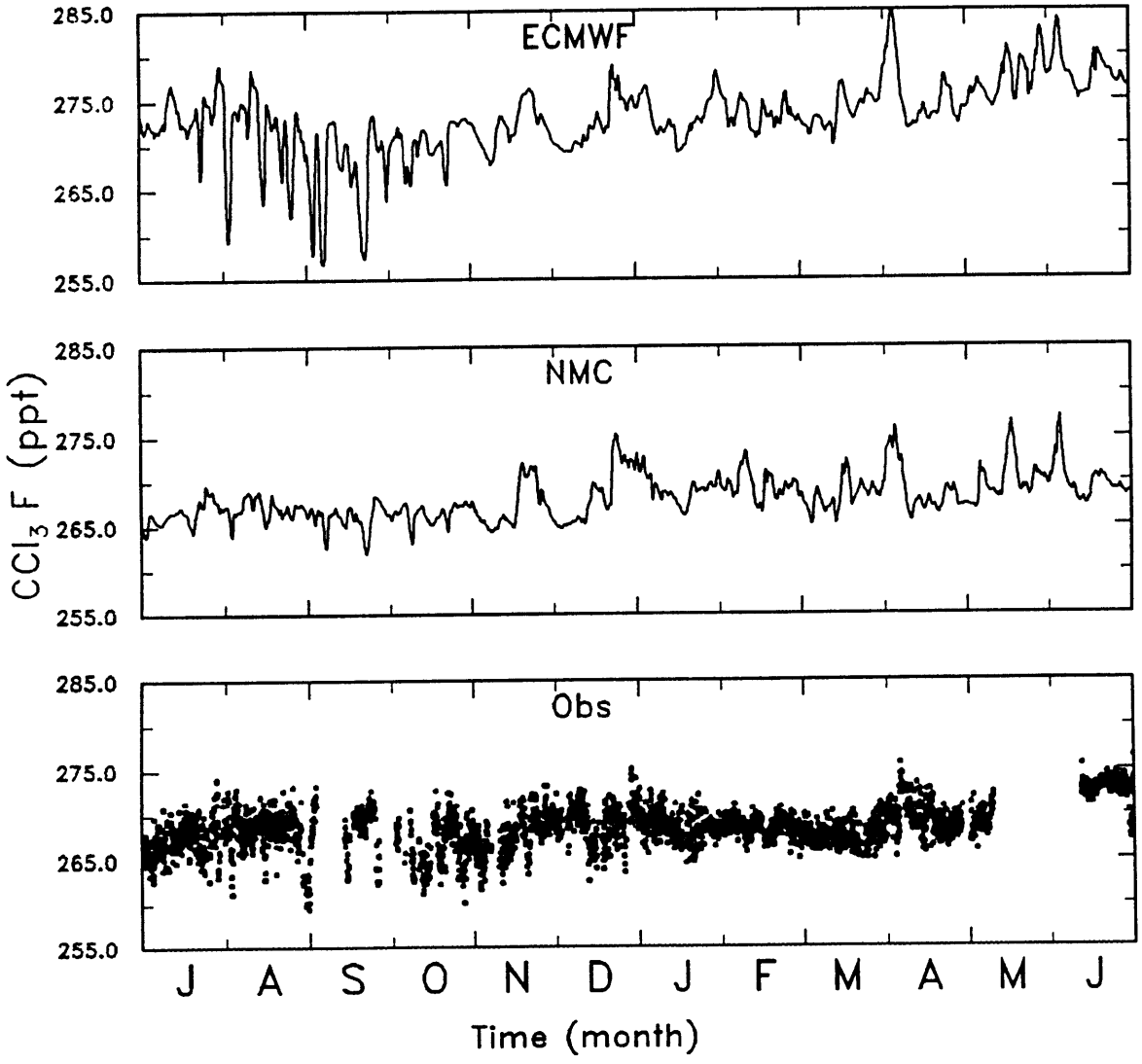

Figure 5.22: CCl_3F concentrations (ppt) at the Barbados observing station for the MATCH-ECMWF and MATCH-NMC model simulations, as well as observations from the ALE/GAGE *in situ* network [Cunnold, et al., 1994] for July, 1990 to June, 1991.

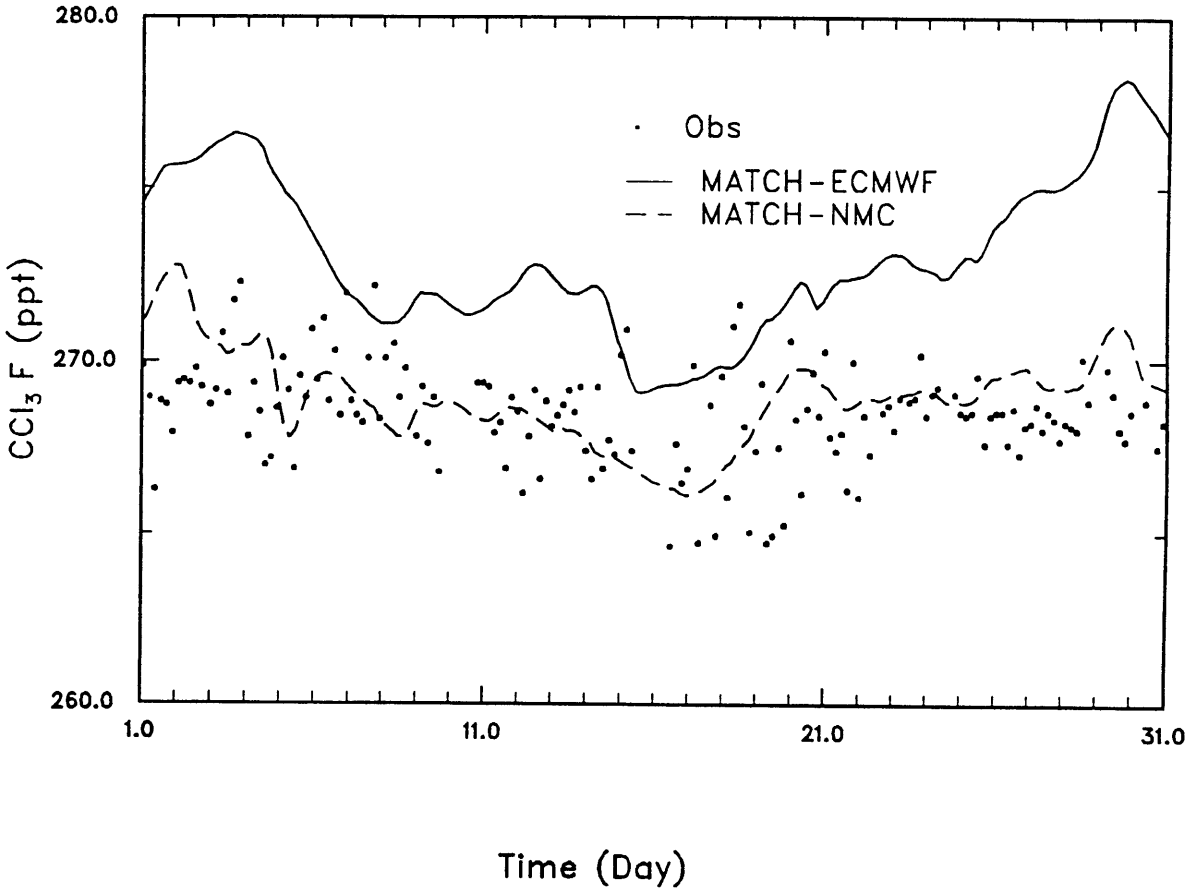

Figure 5.23: Same as Figure 5.22, except for January, 1991.

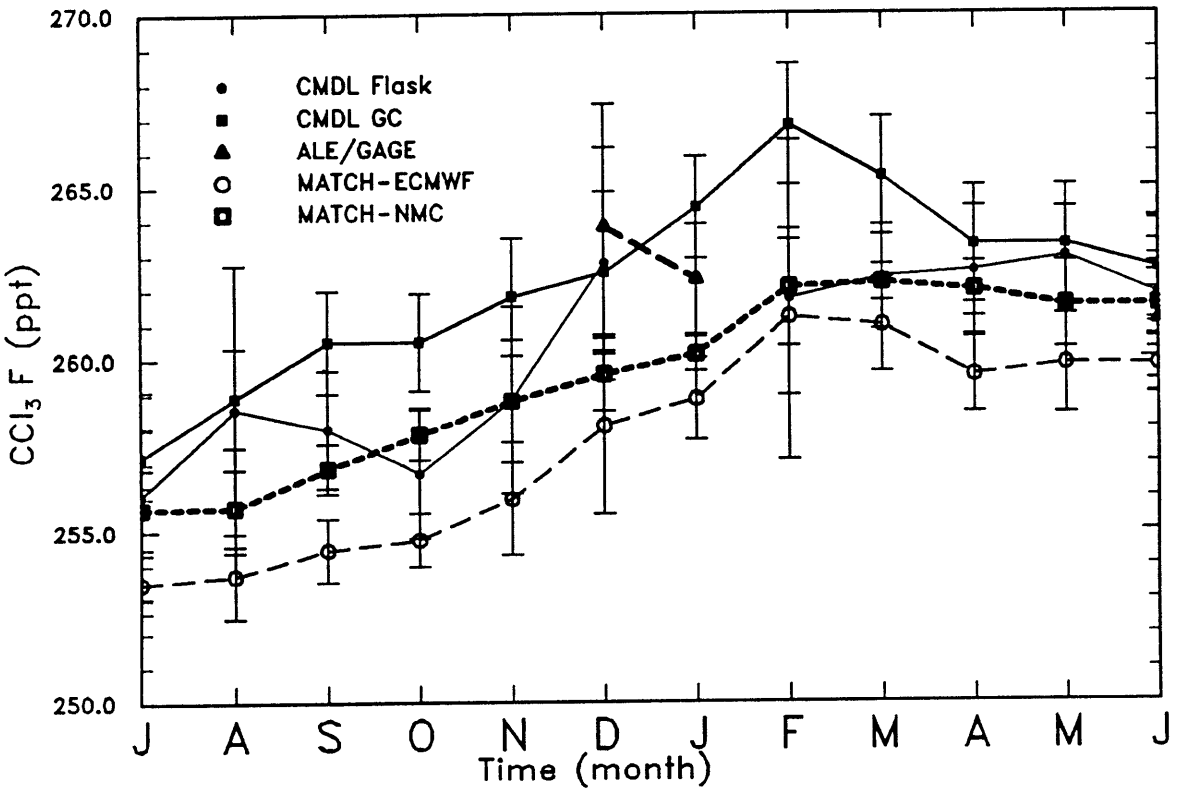

Figure 5.24: Monthly mean CCl_3F concentrations (ppt) at the Samoa observing station for the MATCH-ECMWF and MATCH-NMC model simulations, as well as observations from the ALE/ GAGE *in situ* network [Cunnold, et al., 1994] and the CMDL flask and *in situ* network [Elkins, et al., 1993] for July, 1990 to June, 1991.

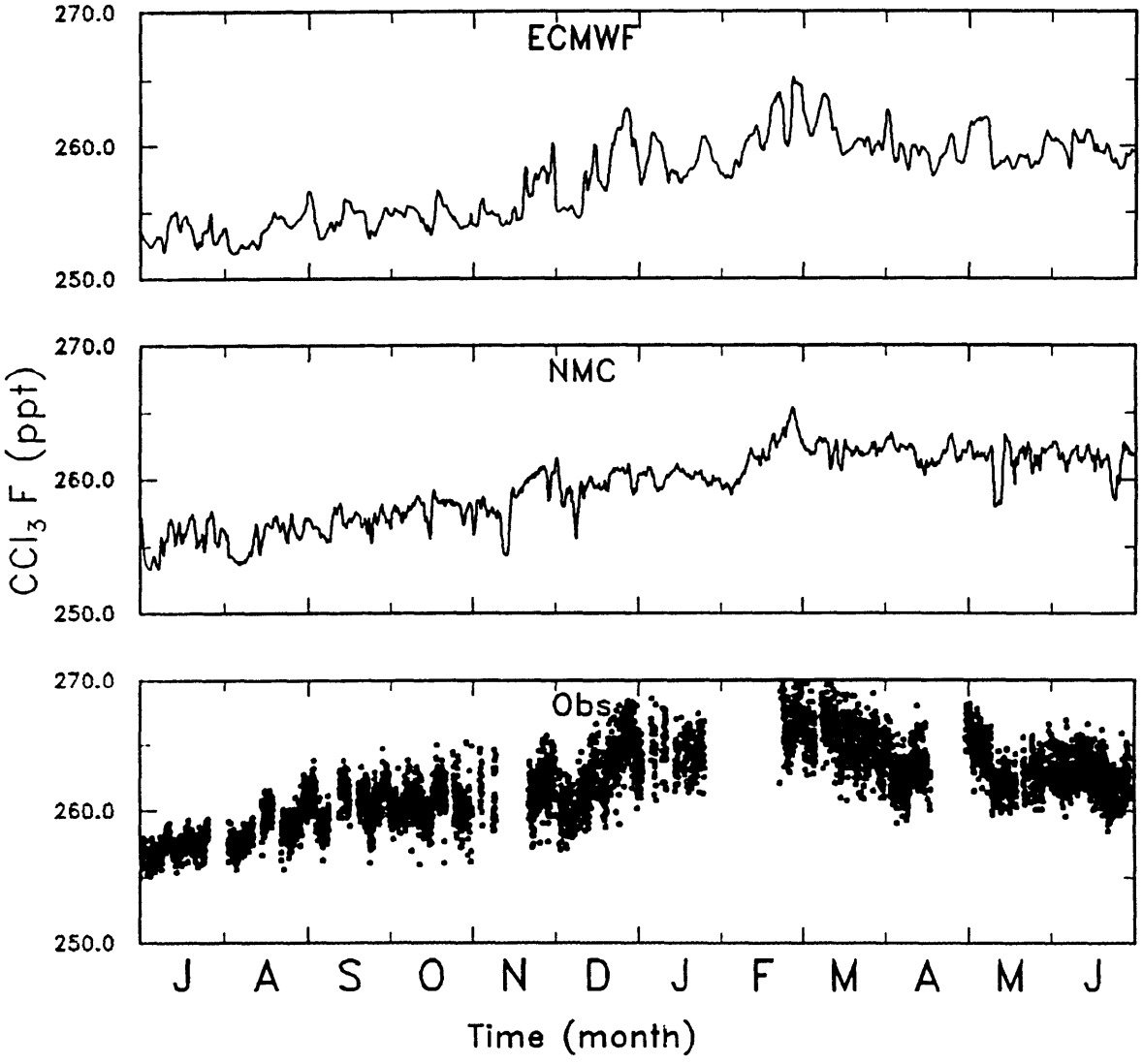

Figure 5.25: CCl_3F concentrations (ppt) at the Samoa observing station for the MATCH-ECMWF and MATCH-NMC model simulations, as well as observations from the CMDL *in situ* network [Elkins, et al., 1993] for July, 1990 to June, 1991.

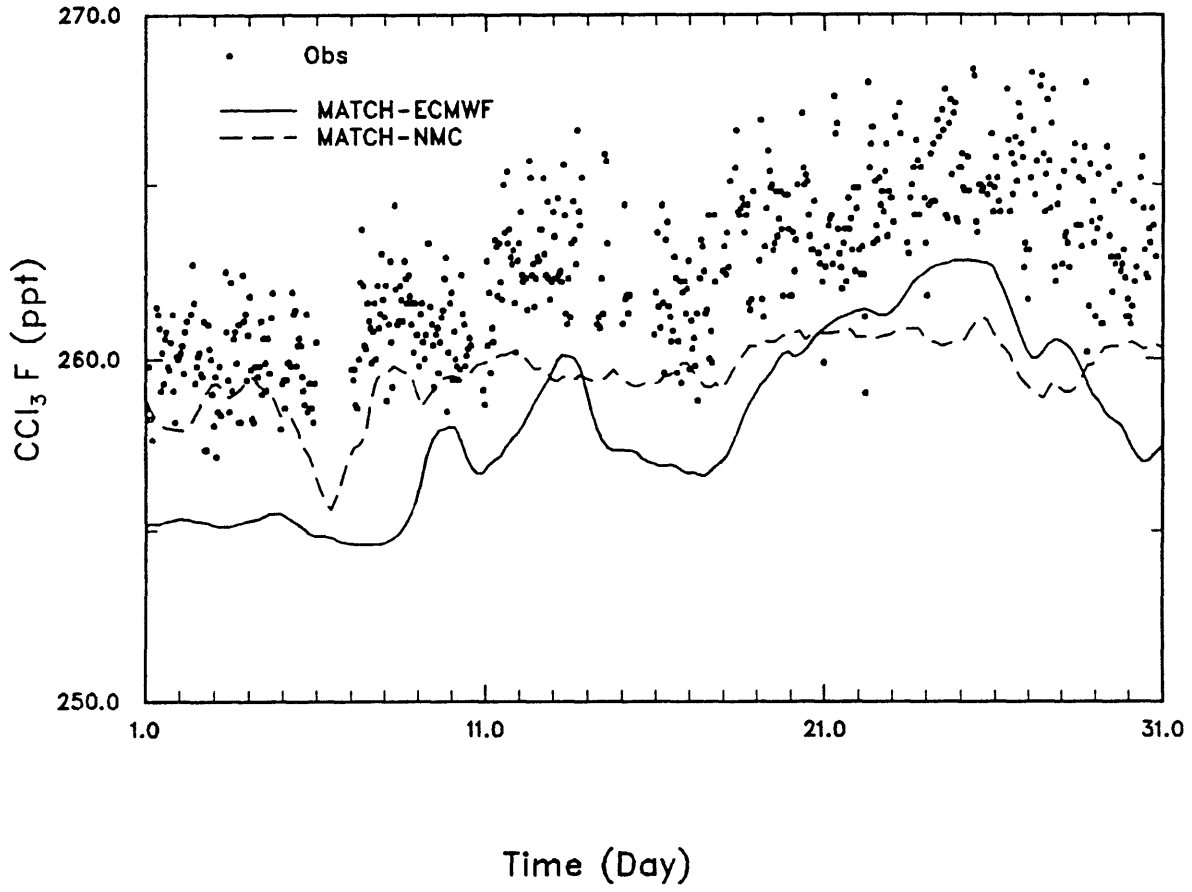

Figure 5.26: Same as Figure 5.25, except for December, 1990.

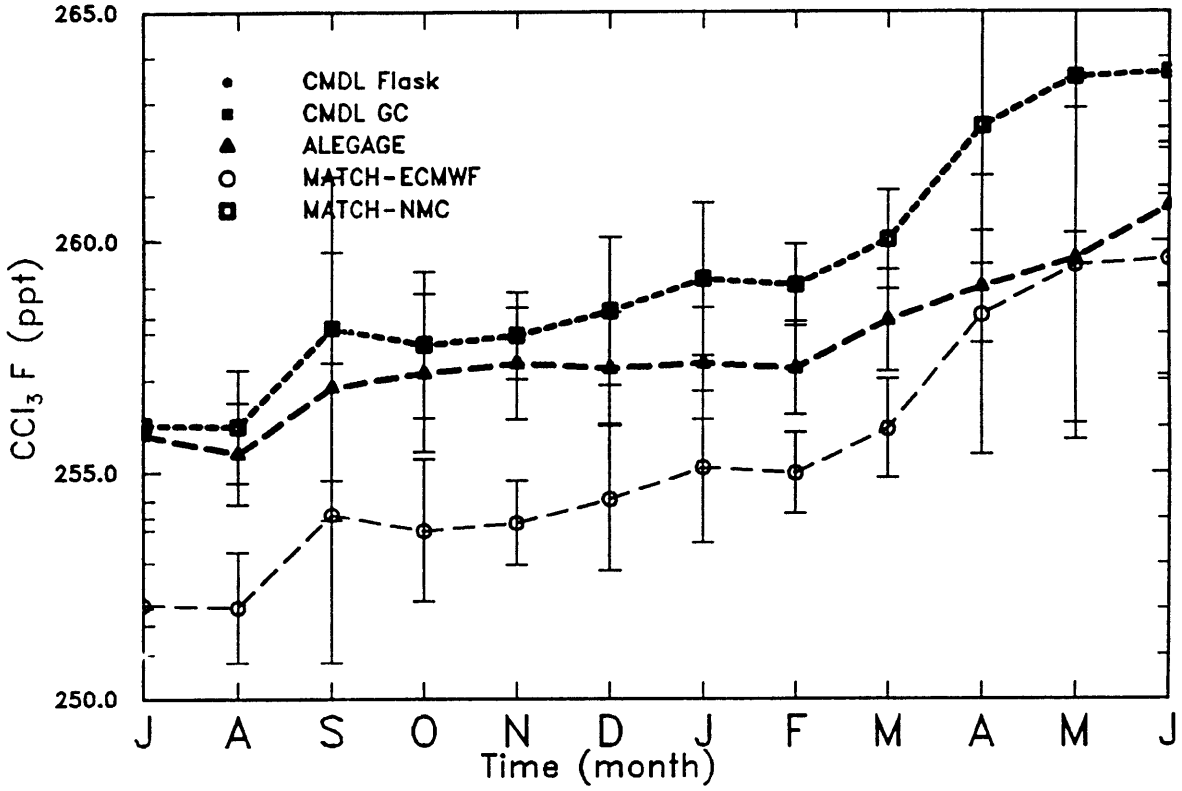

Figure 5.27: Monthly mean CCl_3F concentrations (ppt) at the Cape Grim, Tasmania observing station for the MATCH-ECMWF and MATCH-NMC model simulations, as well as observations from the ALE/GAGE *in situ* network [Cunnold, et al., 1994] for July, 1990 to June, 1991.

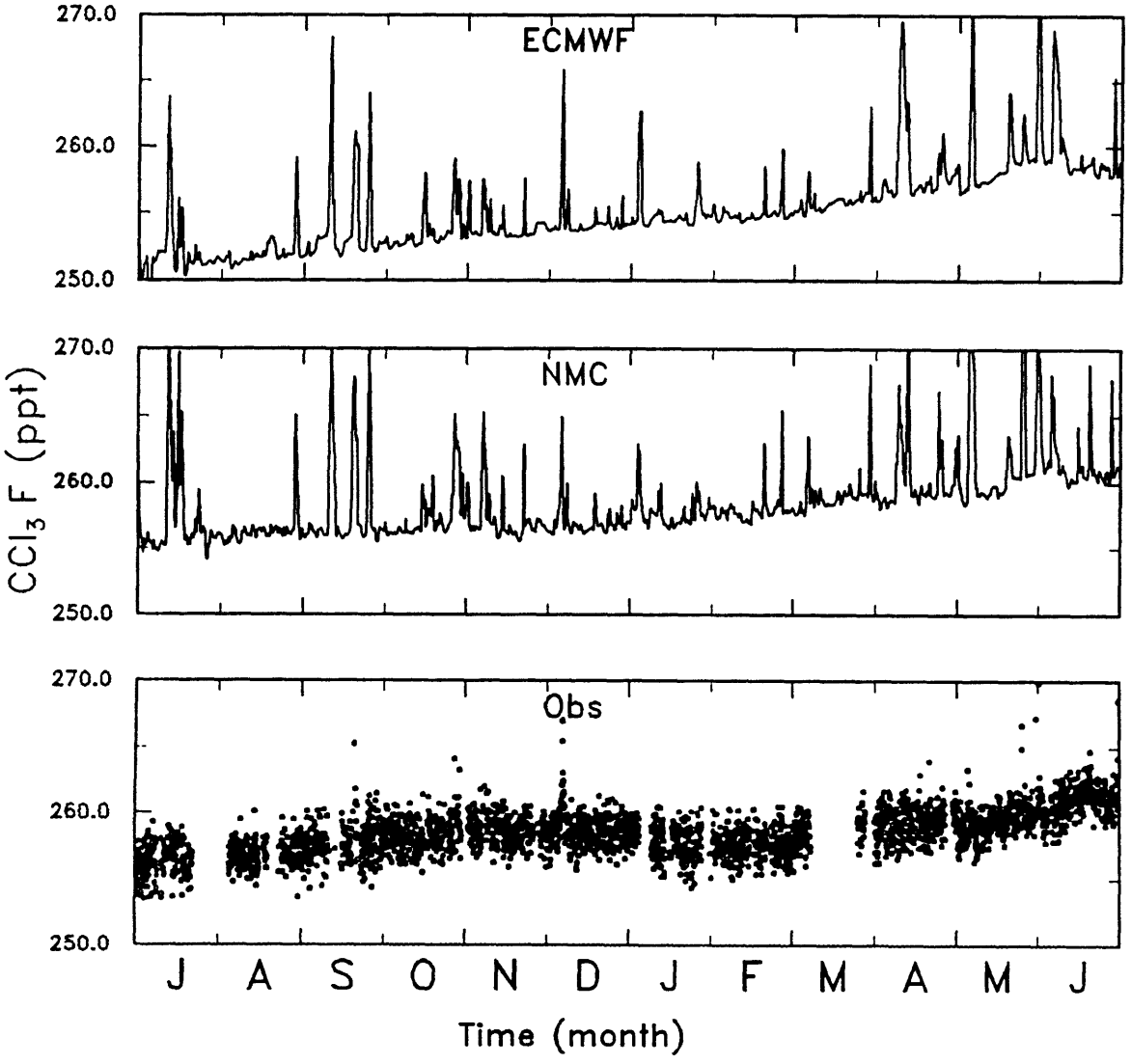

Figure 5.28: CCl_3F concentrations (ppt) at the Cape Grim, Tasmania observing station for the MATCH-ECMWF and MATCH-NMC model simulations, as well as observations from the ALE/ GAGE *in situ* network [Cunnold, et al., 1994] for July, 1990 to June, 1991.

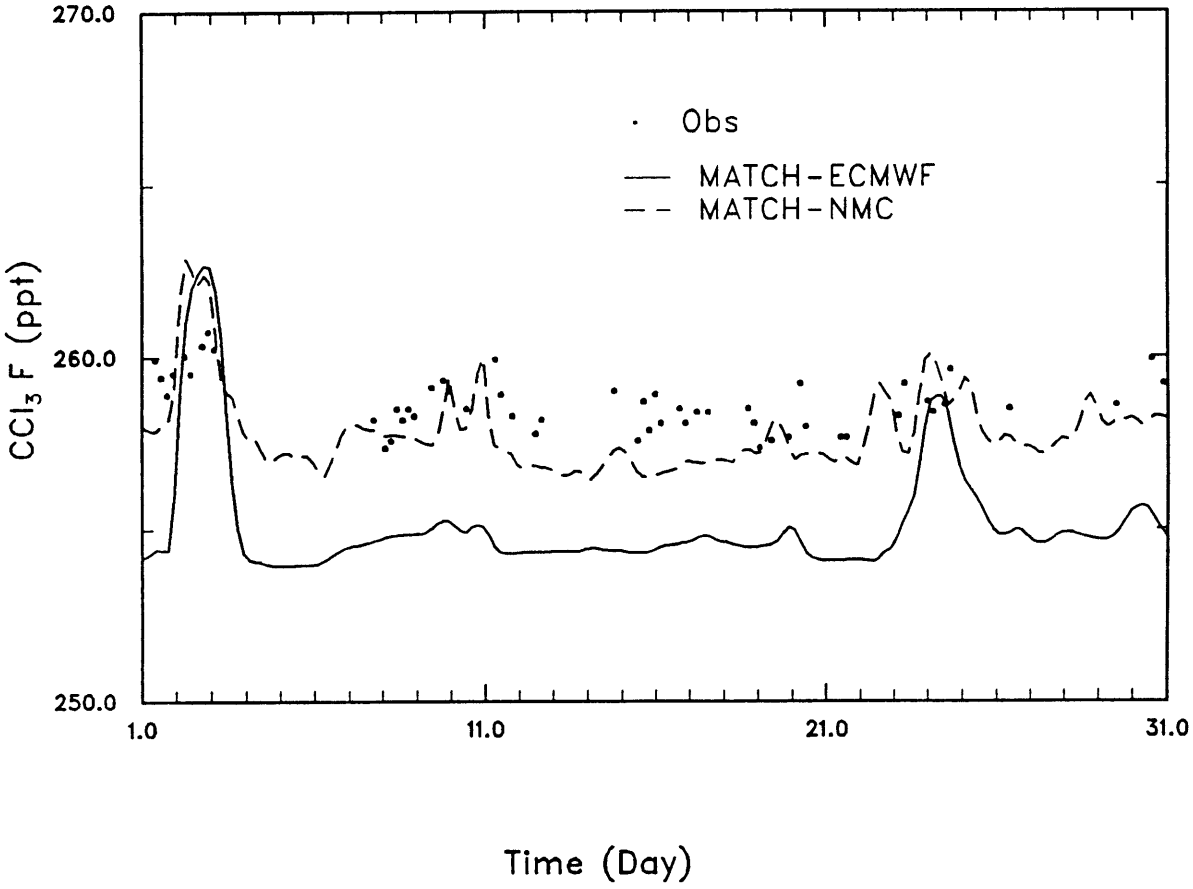

Figure 5.29: Same as Figure 5.28, except for January, 1991.

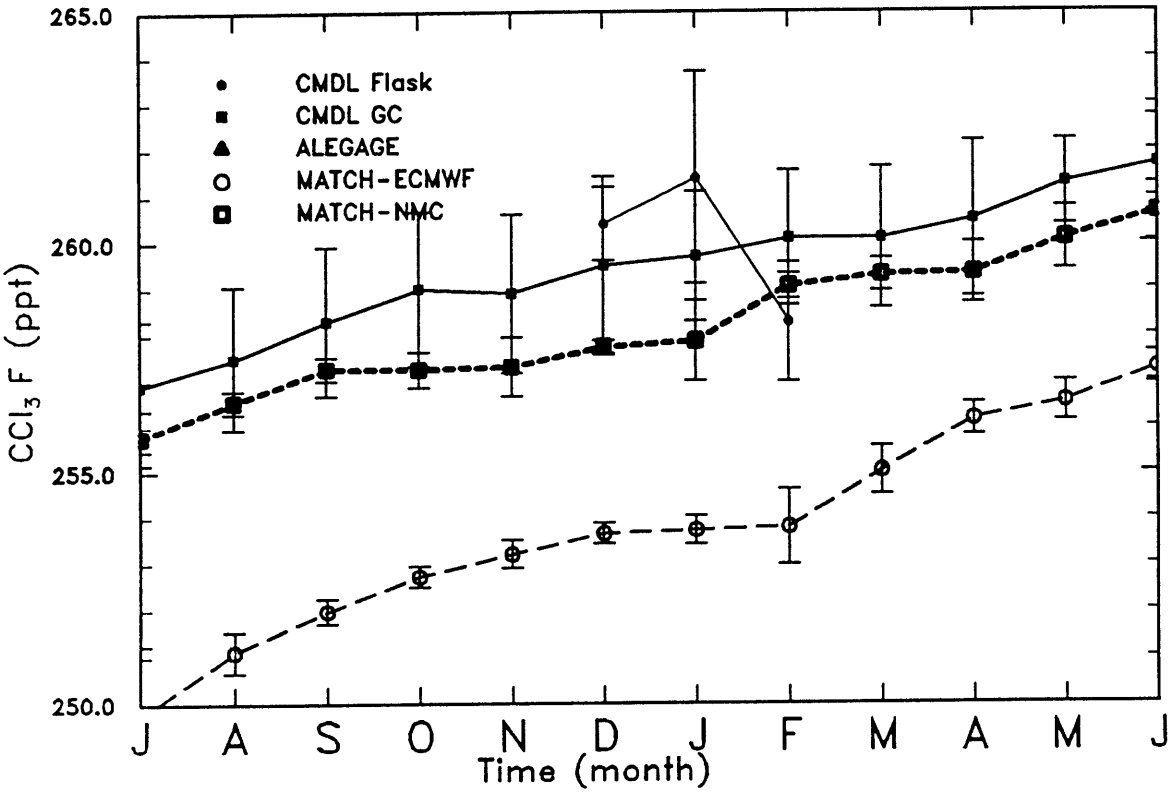

Figure 5.30: Monthly mean CCl_3F concentrations (ppt) at the South Pole observing station for the MATCH-ECMWF and MATCH-NMC model simulations, as well as observations from the CMDL *in situ* network [Elkins, et al., 1993] for July, 1990 to June, 1991.

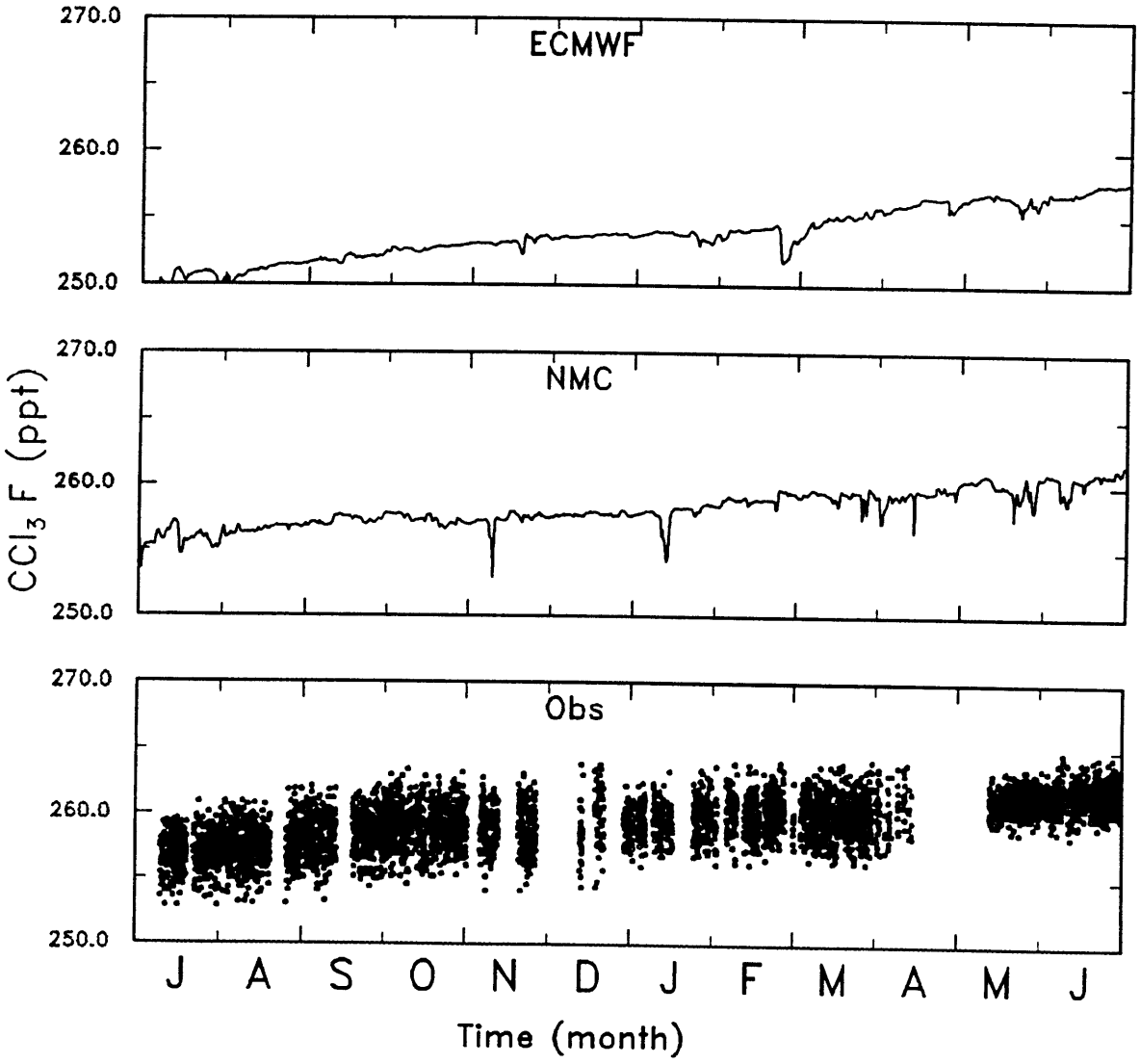

Figure 5.31: CCl_3F concentrations (ppt) at the South Pole observing station for the MATCH-ECMWF and MATCH-NMC model simulations, as well as observations from the CMDL *in situ* network [Elkins, et al., 1993] for July, 1990 to June, 1991.

Chapter 6:
Deducing the Sources of CCl_3F using an Inverse Method

6.1.0 Introduction

There are large uncertainties in the source and sink estimates of many important naturally occurring long-lived gases, such as carbon dioxide and methane. In addition, there is the possibility that the Montreal Protocol restrictions on the use of chlorofluorocarbons may not be followed by all countries. Thus, having a methodology which could use existing observational networks and chemical transport models to estimate the emissions of trace gases at the regional scale would be very beneficial. Simple trial and error approaches have been used to estimate sources and sinks of carbon dioxide [Tans, et al., 1989] and methane [Fung, et al., 1990] using observations and transport models. Potentially far superior, there are optimal estimation schemes which minimize certain "objective" or "cost" functions (e.g.the difference between model and observed concentrations or the variances in the estimates of emissions), which are a type of inverse method. They are powerful tools with a large literature surrounding them [e.g. Gelb, 1988]. These have recently been used in chemical transport models to deduce the sources of CCl_3F [Hartley and Prinn, 1993] and methane [Heimann, et al., 1995], but, due in large part to inadequacies in the transport model, with limited success.

There is some question as to whether the inverse modeling of sources will produce emission fields that are reasonable. The atmosphere is diffusive, so that the emissions from a particular region mix with emissions from other regions, reducing the ability of an inverse method to deduce the correct regional emissions [Enting and Newsam, 1990]. This raises the possibility of several solutions being equally likely [Fung, et al., 1990] In addition, there are errors in the transport models, which will cause the emission estimates to be incorrect. This chapter seeks to address whether inverse modeling of sources can produce reasonable results.

In order to address the ability of inverse methods to correctly estimate the sources of long-lived gases, CCl_3F is an ideal test case, since the global surface sources of CCl_3F are relatively well-known (as discussed in Chapter 5). The ability of the combination of the inverse method (here defined as the combination of an optimal estimation scheme, the transport model and the observational network) to produce useful estimates of emissions is dependent on three factors: the accuracy of the transport in the chemical transport model, the validity of the optimal estimation scheme, and lastly the location, size and accuracy of the observing network. Here the MATCH simulation of CCl_3F using the NMC reanalysis winds, described in Chapter 5, is used to explore this question.

The method used here is a recursive weighted least squares. A recursive weighted least squares is a simple form of a Kalman filter where the state vector (or the variable to be estimated) is constant in time instead of time varying as in a Kalman filter. The estimates which result from applying a recursive weighted least squares iteratively using data from many time samples are the same as those resulting from a weighted least squares using all the data. There is substantial literature discussing recursive weighted least squares, Kalman filters and weighted least squares [Strang, 1988; Gelb, 1988].

6.2.0 Description of Inverse Method

This section will describe the methodology used for this study. The basic inverse method used is a recursive weighted least squares. The next section will relate this method to the standard inverse method terminology and error analysis.

The goal of the inverse method is to estimate emissions e from a particular region which minimizes the difference between the observed and model concentrations at the observing sites. This is made easier by the fact that the modelled concentrations at a site are very nearly linear with emissions so that the Taylor expansion:

$$\chi_a(t) = \chi_a(t) + \Delta e \frac{\partial \chi_a}{\partial e} \quad (6.1)$$

where $\chi_a(t)$ is the model concentration at site a at time t, Δe is a change in emissions at an emission region, while $\frac{\partial \chi}{\partial e}$ is the response in concentration at site a for a unit change in emissions e. Equation 6.1 is approximately valid over the entire space of possible emissions. The reason for this linearity is that the transport is largely linear (with the exception of non-linearities due to the semi-lagrangian transport scheme's fixer and the diffusion) and the sink of CCl_3F is linear with concentration. A doubling of emissions from a particular emission region will double the impact of that emission region on a particular site's concentration. Thus, we can modify the emissions from each region, until the optimal fit between the observed and modeled concentrations is obtained, using the inverse method.

In this study we divide the emissions into 5 different regions, similar to Hartley and Prinn [1993]: North America, Europe, Asia (not including Japan and Korea), Japan and Korea, and Southern Hemisphere (which includes all other emission regions, which mostly lie in the southern hemisphere). From each of these emission regions, using the best estimate of CCl_3F emissions we have, we deduce the impact on each of the observing sites using the MATCH model and either ECMWF or NMC winds. The distribution in each region is as described in Chapter 5 and the regions are shown in Figure 6.1.

We also need information about the initial state of the atmosphere in June, 1990 and its impact at the stations as a function of time. This initial state is subject to transport and the photolysis loss mechanisms, but there is no surface flux of CCl_3F in this simulation. Thus we have the impact of each emission region on the observing site $\frac{\partial}{\partial e^i}\chi_a(t)$, as well as the contribution of the initial distribution on each observing site $\chi_a^{initiadistribution}(t)$, which changes with time as the winds advect the initial distribution, and the CCl_3F is lost through photolysis. So to calculate the modeled concentrations at a site we use the following equation:

$$\chi_a^{model}(t) = \chi_a^{initialcdistribution}(t) + \sum e^i(t) \frac{\partial}{\partial e^i} \chi_a(t) \qquad (6.2)$$

where $e^i(t)$ from each source region i is the guess at time t. For this problem, only the magnitude of emissions is deduced, and the temporal distribution is given in Chapter 5, and is a steady decrease in the emissions over this period. To calculate $\frac{\partial}{\partial e^i}\chi_a(t)$, the best estimate for emissions for each source region was used as the surface flux in the transport model. Then, the concentrations at the observing stations was extracted from the transport model, and these concentrations were divided by the emissions from each region for the first month. Since emissions are decreasing with time, we are thus calculating a magnitude of the emissions from each region which is constant with time, and the spatial and temporal resolution of the emissions from each region have already been specified.

The summation in equation 6.2 occurs over all emission regions. This method has the advantage that previous bad estimates of the emissions do not affect current model concentrations at the sites. It has the disadvantage that this method can only be used for systems where the temporal tendencies at each emission region are reasonably well known.

Our objective in this study is to minimize the difference between the observed and modeled concentrations at 8 observing stations (described in Chapter 5, except that Alert is excluded, since there is only monthly averaged data at this station) at all times we have data. This translates into having an objective function, J, such as:

$$J = \sum_{time} \sum_{stations} \left(\frac{(\chi_a^{obs}(t) - \chi_a^{model}(t))}{\sigma^2{}_a(t)} \right)^2 \qquad (6.3)$$

Where $\chi_a^{obs}(t)$ is the concentration at station a that is measured, σ_a is the error estimate in the measurement (and the model result, as discussed in the next section) and J is the objective function which we are trying to minimize. In equation 6.3, we weight the different stations or times, depending on how accurate our measurements are at different times. In this study the time is usually every day, since we have available daily averaged concentrations from the observational and model simulations for most days. In addition, there will be some discussion of monthly averaged values.

We want this objective function to be minimized as we progress through time, using each new observation and model value to refine our best guess of the emissions. This translates into the following equation:

$$e^i(t+1) = e^i(t) + G(t)\,[\chi_a^{obs}(t) - \chi_a^{model}(t)] \qquad (6.4)$$

where G is so far undefined, but tells the inverse method how much to modify the emissions so as to translate differences in the observations and modeled concentrations at station a into modifications to the emissions.

This can also be defined in matrix form, so that **e** is a vector of emissions from each of the i source regions, the **x** are vectors of the observed and modeled concentrations (the χ above) at each station a, and **G** is a matrix relating the difference in observations at each observing station to an improvement in the estimate of **e**.

We chose **G** such that our objective function is minimized. This results in the following definition of **G**, which is referred to as the Gain matrix [details in Hartley, 1993; Gelb, 1983]:

$$\mathbf{G}(t) = \mathbf{C}(t)\,\mathbf{P}^T(t)\,[\mathbf{P}(t)\,\mathbf{C}(t)\,\mathbf{P}^T(t) + \mathbf{N}(t)]^{-1} \qquad (6.5)$$

where **C**(t) is the covariance matrix, or the uncertainty in the emission estimate, **P**(t) is the partial derivative matrix $\frac{\partial}{\partial E^i}\chi_a(t)$ and **N**(t) is the noise covariance matrix (whose diagonal elements are the variances of the observations).

This method also gives an estimate of the covariance matrix, whose diagonal elements are the variances in the emissions **C**(t). Given an initial (a *priori*) estimate of **C**, we can follow the uncertainty in time using the following formula, which again results from minimizing the objective function

$$\mathbf{C}(t+1) = \mathbf{C}(t) - \mathbf{G}(t)\,\mathbf{P}(t)\,\mathbf{C}(t) \qquad (6.6)$$

Thus, the inverse method (the recursive weighted least squares) described here follows the following steps:

1. Make an initial estimate of the emissions (e(0)) for each region and the uncertainty (**C**(o)) in the emissions.

Repeat over:

2. Calculate the concentrations at each of the observing stations using the current best estimate of emissions from each region.

3. Compare the model and observed concentrations

4. Update the emissions and uncertainties for each regions, following equations 6.4 and 6.6. Go to Step 2

This results in an estimate of the magnitude of emissions for each region. We can see the time evolution of this emission estimate, although the emission estimate does not represent a time dependent variable, but a constant quantity describing the magnitude of emissions from each region. This methodology is equivalent to using a weighted least squares on all the data at once, but in this approach we can watch the evolution of the solution and the uncertainty and we do not have to solve a system of 2920 (365 times 8) equations at one time. Time in the inverse method is somewhat arbitrary, since the method is equivalent to a weighted least squares: we could have done the calculation with the time variable reversed and obtained the same result. Daily averaged

data was chosen for this study, since it allowed an averaging of the observations and model results to a time scale the transport model could reasonably be expected to simulate well, as well as still including large pollution events.

This optimal estimation method assumes that the transport model used is perfect. Unfortunately, the model is not perfect, as described in Chapters 4 and 5. Thus, the following section will look at the effects of an imperfect model on the emission estimates which results from the inverse method.

6.2.1 Error and Uncertainty Analysis

The previous section described the methodology for readers unfamiliar with inverse methods. Here the discussion continues, but more rigorously defines the errors involved in the inverse method.

We could refer to the approach used here (recursive weighted least squares) as a special case of a Kalman filter approach (since the state vector is constant with time). In that terminology, we have a state space vector of emissions from each of the source regions **e**, which is the magnitude of the emissions from each region, where the emissions have a specified temporal and spatial distribution. Although this magnitude of the emissions is a constant factor, unchanging with time, our estimate of the **e** vector does change with additional data. In Kalman filter terminology, the model for the state space vector is just that the **e** vector is constant with time or

$$\mathbf{e}(t+1) = \mathbf{e}(t) \quad (6.7)$$

The version of the Kalman filter used here assumes that this model of the state space vector is perfect, which is not necessarily true in our case. The magnitude of the emissions may not be correctly specified for each source region by the temporal changes in global emissions estimated from the chemical manufacturing companies. Errors in this term may be important, and it is difficult to assess the magnitude of these errors. Using the differences between the Hartley and Prinn [1993] and McCulloch et al [1994] European regional distributions (Table 5.2) as an estimate of uncertainties in the emissions estimates, we would calculate that the largest errors for regional emissions would be 25%. Since we have no better information, we will use this error estimate for the *a priori* errors in the size of the emissions, as well as for the errors in the temporal distribution. Since we can't include the errors due to the imperfection of our state space model (6.6) in that equation, we will include them in the errors due to observations, discussed next.

In addition to equation 6.6, we also have observational data which we will use to improve our estimates of the emissions at many different times:

$$\mathbf{x}_{obs}(t) - \mathbf{x}_{initiadistriubtion}(t) = \mathbf{P}(t)\mathbf{E}(t) + \mathbf{n} \quad (6.8)$$

$$\mathbf{n} = \mathbf{n}_{obs} + \mathbf{n}_{model} + \mathbf{n}_{emissions} + \mathbf{n}_{initialstate} \quad (6.9)$$

where $\mathbf{x}_{obs}(t)$ is the vector of the observed concentrations, $_{nitialdistribution}$ (is the vector of the impact at this station of the initial distribution of the atmosphere as it evolves in time, **n** is the total error, $\mathbf{n}_{obs}$ is the error in the measurement of the observation, $\mathbf{n}_{model}$ is the error due the model transport, $\mathbf{n}_{emission}$ is the error due to the uncertainty in the temporal and spatial distribution of the emission estimate, and $\mathbf{n}_{initialstate}$ is the errors due to errors in the initial state for the model. We try to minimize **n** and thus bring the observed and modeled concentrations as close to each other as possible. Equation 6.8 is thus used repeatedly for each time sample available, in effect, when we use Equation 6.5 and 6.6 to iterate through time.

As discussed in section 6.2.0, the errors in the "observations", which now include other errors in the problem, are used to determine the uncertainty of the emissions estimate (or more formally, the covariance of the state space vector). Thus it is important to assign reasonable values to the expectation value of the errors in equation 6.7. One difficulty is that the errors in equation 6.7 should not be biased errors, while our errors are biased. This cannot be avoided, but does suggest that this error analysis will only give an rough estimate of the errors.

The errors due to the measurement of the observation are probably the most straightforward to calculate. For this estimate, we will use the average of several values, so we can take the standard deviation, and determine the precision of the concentration estimate (σ_{meas}). In addition, there is some uncertainty in the absolute calibration of the system. There is a difference of 2.7% in inter-comparisons between the CMDL and ALE/GAGE network [Prinn, 1996, personal communication], as noted in Chapter 5 due to absolute calibration, which has been corrected. But this may indicate the size of the absolute calibration errors. Of course, this is not a precision error, but an accuracy error, and it would move all the concentrations up or downward with it. Since the initial state in the model was calibrated to the mean concentrations at the observing sites for June, 1990 (as described in Chapter 5), errors in absolute calibration will only affect the difference between the observed concentrations and the initial state. On average the difference in concentration between the observed values and the model predicted initial state is 15 ppt, so the absolute calibration error would be (15*0.027) 0.4 ppt, which is much smaller than precision errors. We can also estimate the error in the observations for the months when there is two sets of observational data, as shown in Chapter 5. We estimate that these errors are approximately 2 ppt.

Estimating the expectation value of the next three terms in equation 6.9 is more difficult. Fortunately, we have an estimate of the sum of the three terms from Chapter 5. Basically, the difference between the model predicted values and the observed values at the stations discussed in Chapter 5 can give us a rough estimate of the combined errors in the emission scenario, the transport model and the initial distributions. The difference between the annual mean model concentration and observed concentration are between -3.5 and 4. ppt, as shown in Table 6.1. These errors are not white noise, but are biases. In order to roughly compensate for the fact that they are not white noise, we will use an error estimate of 5 ppt for the noise due to the combination of the model transport, initial distribution and emission estimate.

Table 6.1: Model Errors at Observing Sites

Observing Site	Annual Mean Difference in Concentration (ppt)
Barrow	-0.5
Ireland	-4.0
Niwot	-1.5
Hawaii	3.5
Barbados	0.5
Samoa	1.5
Tasmania	0.0
South Pole	1.0

Note that it would be preferable to remove the bias errors shown in Table 6.1 from the concentrations at these sites, leaving a non-biased error. We will explore what happens when we remove these biases from the sites in section 6.4.0, but for a problem where the emissions are assumed to be unknown, we would not be able to remove these biases, so we will leave them in this problem. But note that they dominate the errors, and so removal of these bias errors could improve the estimate substantially. Without these biases, the errors in the model appear to be approximately 2ppt (from examining the monthly mean plots in Chapter 5).

The inverse method used here also assumes that the errors in the measurements and the model predictions are uncorrelated in time. When we use daily averaged values, this is untrue--concentrations are often correlated for a week or so in both the model and the observations, so if the transport model is in error, it will be so for longer than one day. This is called the colored noise problem. A simple way to compensate for this is just to reduce the number of degrees of freedom in the estimation of uncertainty calculation. This is done by increasing the noise by a factor equal to the number of days which we believe are autocorrelated, since the variance is the expectation in the noise divided by the number of independent samples as shown in the following equation:

$$\frac{\langle n^2 \rangle}{N} = \sigma_n^2 \quad (6.10)$$

A reasonable assumption for this study is that the errors in the concentrations are uncorrelated after 10 days. This will increase the noise variance by a factor of 10. For monthly averages, we assume that the errors are uncorrelated, although due to seasonal variations in circulation they may even be correlated month to month. A more thorough discussion of error correlation is given in Cunnold, et al. [1983], but for our purposes here, a simple approach is used.

The errors defined in this section are added to the diagonals of the noise matrix N defined in section 6.2.0. The total variance for a daily observation is therefore approximately:

$$\langle n_{tot}^2 \rangle = 10 \cdot ((2ppt)^2 + (5ppt)^2 + \sigma_{meas}^2) \quad (6.11)$$

Notice that the errors are roughly constant in time, but that the signal (the partial derivative matrix) grows with time as emissions from each source region accumulate in the model atmosphere, so that the signal to noise ratio would be expected to grow with time.

The above assumptions regarding *a priori* errors in the system are very important and will be summarized below:

1. The initial emission estimate is good to within 25%
2. Errors in model transport, emission regions and emission temporal scale, as well as errors in the initial values are 5 ppt. If we assume that the errors are due to transport problems, and remove the known bias (seen in Chapter 5 and in Table 6.1), the errors are 2 ppt.
3. Errors in the precision of the observations are 2 ppt, and the accuracy of the measurements is calculated from the standard deviations (often as large as 2 ppt).
4. The errors in the calculation of the difference between the observed concentration and the initial state of the model is assumed to be autocorrelated (colored noise instead of white noise).The variance of the noise is assumed to become uncorrelated after 10 days. The autocorrelation of the data is compensated for by simply increasing the variance in the noise by a factor of 10.

6.2.2 Singular Value Decomposition Analysis

Although we will use the recursive weighted least squares method (or a simple form of the Kalman filter) in a manner which will suggest time-stepping, the method is actually equivalent to a weighted least squares. This allows us to use the singular value decomposition (SVD) to obtain information about what observing sites are most important in the inverse method and how well we can resolve the different source regions.

In equation 6.8, we are trying to solve for **e**. In simple terms, we would invert the **P** matrix, multiply by $\mathbf{x}_{obs}$, and we would get an estimate of **e**. Using SVD, we can also gain an understanding of which observing sites are most important and what sources we are best able to resolve.

The matrix **P** (the partial derivative matrix) can be decomposed into three matrices (For more detail see e.g. Press, et al [1986]):

$$\mathbf{P} = \mathbf{U} \cdot \mathbf{S} \cdot \mathbf{V}^T \quad (6.11)$$

Since **P** is a matrix o by s, where s is the number of source regions (5) and o is the number of observational sites (8), **U** is a o by s matrix consisting of column-orthogonal vectors (there are o-s additional vectors in an overdetermined system, which represent data which is part of the residual of the solution), **S** is a diagonal matrix of s by s, and **V** is a matrix also of size s by s but with column orthogonal vectors. The state vector **e** is found by:

$$\mathbf{e} = \mathbf{V} \cdot \mathbf{S} \cdot (\mathbf{U}^T \cdot \mathbf{x}_{obs}) \quad (6.12)$$

In addition to being a method of solving least squares problems, **U**, **V** and **S** provide information about the system.

The diagonals of **S** are the singular values of the problem, which are related to the orthogonal vectors in **U** and **V**. The larger the singular value, the more information in the system is related to the orthogonal vectors associated with the singular value. The smaller singular values contain less information, and the related orthogonal vectors contain less information.

For our system, we have many different **P** matrices--one for every time-step considered in the inversion (note that the time-steps in the inversion are different than in the transport model). Thus we have 365 for the daily averaged inversion. For this analysis, we will use a few different methods to estimate the information in the many different inversions. We will consider an "averaged" P matrix and several daily averaged **P** matrices.

Appendix 6.1 shows an averaged **P** matrix. The partial derivatives are increasing with time at an approximately linear rate, if we ignore seasonal differences in transport. So in order to find the average influence at each station, we average the partial derivatives with a weighting that decreases in time. (Note that the answer does not change substantially when a different averaging procedure is used.)

The singular values λ of the matrix **P** in Appendix 6.1 are shown in Table 6.2. Following Plumb and Zheng [1996], an estimate of the error (s_m) in the last mode (and the hardest to distinguish) is:

$$s_m = \frac{\sigma_{tot}}{\Delta\sqrt{5}}\left(\frac{\lambda_1}{\lambda_m}\right) \quad (6.13)$$

where Δ is the mean difference between the observation and the model initial distributions and σ_{tot} is the total noise from the last section. In our analysis, the first mode is not the interhemispheric gradient, as in Plumb and Zhang [1996], but the mean difference in concentration between the observations and the initial state predicted in the model (as discussed above), so we use 15 ppt for Δ. Here we divide by the square root of 5 since that is the number of degrees of freedom in the calculation of the mean concentration. In the last section, the error analysis indicated an error of 5.7 ppt (if we assume the standard deviation is the measurements is 2ppt), this implies a relative error of 15% for the first mode, growing as shown in Table 6.2 using equation 6.13. This indicates that by the time we get to the last mode, there is little or no information in this mode.

Table 6.2: Singular Values and Relative Error

Mode	Singular Value	Relative Error
1	0.11	0.15
2	0.067	0.25
3	0.038	0.43
4	0.020	0.83
5	0.002	8.3

The largest errors come from the model errors deduced from Chapter 5, as noted previously. If we could remove these errors, the magnitude of the errors would be approximately 3.4 ppt instead of 5.7 ppt, reducing the errors in Table 6.2. The error in the first mode would be 10%, and the largest error would be 570%, still too large to expect to distinguish the last mode. The errors are still quite large in the second to the fourth mode. Note that in our problem, we will have these errors at 365 times, and the overall error in our final estimate will be smaller than the error at any one time sample.

Next we need to consider what the orthogonal vectors for each mode represent. In Table 6.3 and Table 6.4, there is a listing of the **U** and **V** vectors, respectively. First note that there are 8 **U** vectors representing the weighting of the observing sites, and only 5 singular values and **V** vectors. The last three **U** vectors represent sites or combination of sites that are not, on averaged, reflected in the solution, but instead in the residuals of the solution, since the system is overdetermined.

Table 6.3: U Singular vectors

	Mode 1	Mode 2	Mode 3	Mode 4	Mode 5	Mode 6	Mode 7	Mode 8
Barrow	0.3900	-0.0650	-0.0879	0.6929	0.0222	0.2712	-0.5302	-0.0249
Ireland	0.6098	-0.1362	-0.6236	-0.3752	-0.2178	0.1228	0.1313	0.0145
Niwot	0.5155	-0.0512	0.7633	-0.3198	-0.1114	0.1681	-0.0777	0.0019
Hawaii	0.2549	0.0286	0.1310	0.5130	-0.3527	-0.3256	0.6495	0.0396
Barbados	0.3536	-0.0060	-0.0159	-0.0238	0.6821	-0.6355	-0.0628	-0.0316
Samoa	0.0776	0.1830	0.0013	0.0960	0.5538	0.5937	0.4967	-0.2130
Tasmania	0.1123	0.9407	-0.0562	-0.0611	-0.1616	-0.0917	-0.1476	-0.1983
South Pole	0.0417	0.2353	-0.0117	0.0110	0.1313	0.1107	0.0354	0.9549

Table 6.4: V Singular vectors

Source	Mode 1	Mode 2	Mode 3	Mode 4	Mode 5
North America	0.6132	-0.0875	0.6430	-0.4500	0.0156
Europe	0.5954	-0.1293	-0.7547	-0.2426	-0.0214
Asia	0.2952	-0.0146	0.0501	0.5049	0.8095
Japan/Korea	0.3983	-0.0428	0.1148	0.6946	-0.5864
Southern Hemisphere	0.1540	0.9867	-0.0361	-0.0341	0.0149

The first mode of U represents a mean of the stations, especially the northern hemisphere stations, where the impacts from the emission regions are higher. In V, the first mode represents a mean source from the 5 sources, especially the Northern Hemisphere source.The second mode is the Tasmania station and it largely determines the Southern Hemisphere source region. The third mode is the difference between the Ireland and the Niwot station and distinguishes the European source region from the North American source region. The fourth mode uses data from the Barrow, Ireland, Niwot, and Hawaii stations to distinguish between the North American, Asian and Japan/Korean source regions. The fifth mode uses the Barbados, Samoa and Hawaii sites to distinguish between the Asian and Japan/Korean source regions. Note that errors grow with the modes, as described in Table 6.2, so that it is difficult to distinguish between the Asian and the

Japan/Korean source regions.

The last three vectors of the U matrix represent errors in the differences between the model and observed concentrations. The sixth mode contains information from the Barbados, Samoa, and Hawaii stations, the seventh contains information from the Samoa, Barrow and Hawaii stations, and the eighth mode is dominated by the South Pole station. Thus, the stations which are used less by the inversion process are the Southern Hemisphere observing sites (except for Cape Grim, Tasmania). This seems reasonable--if the model wants to deduce four Northern Hemisphere source regions, then information from all the Northern Hemisphere observing sites should be more valuable than information from the Southern Hemisphere, and the problem is overdetermined, so some information must be weighted less.

The resolution of the data, or basically the weighting that the inversion gives to a certain site is obtained by using the first five vectors of the U matrix and calculating $\mathbf{U}^*\mathbf{U}^T$. This results in conclusions similar to those made above--that the South Pole station does not weigh heavily in the inversion, and the Samoa and Hawaii stations weigh less than the other stations.

A similar analysis can be done to each of the 365 observational and model times where there is data, which is prohibitively difficult to conduct. However, a few days were analyzed. Several of the days gave results similar to the average partial derivative already analyzed. On other days, however, the source strength of one particular source region appeared as the first vector, largely determined by one station. For example, this occurred at Niwot for the North American source region, at Ireland for the European source region, and at Tasmania for the Southern Hemisphere source region. Physically, we would expect that these days represent meteorological conditions where the wind has blown directly from a source region to a station. There were also some days when the Barbados, Samoa and South Pole station were considered to have contained significant information by the SVD analysis. Thus, although on the average these stations were not as important as the other stations, for individual days they provided information.

6.3.0 Sensitivity of Inverse Method

The inverse method described in section 6.2.0 is a recursive weighted least squares, which is a form of the Kalman filter used when the values to be estimated are time-unvarying. It is also equivalent to a weighted least squares. Here we test some of the characteristics of the inverse method in combination with the transport in the model in order to assess the ability of the combination of the inverse method and the transport model (the inverse modeling) to deduce emissions from the regions described here.

These tests will all use output from the MATCH-NMC model runs described in Chapter 5, but with the regions described in section 6.2.0. These tests will use the forward model run (described in Chapter 5) as the observations. This is done so that we can assume that the transport model is perfect, and access the impacts of different types of imperfection in the transport model. We will refer to the cases where the MATCH model output is used as the observations in the inverse method as "pseudodata" cases [Hartley and Prinn, 1993].

In using the inverse method, we will make an initial estimate of the emissions from the different regions. Because we are testing the system to determine whether unknown sources could be correctly discerned, we will use an initial estimate of the emissions which is very different from our best estimate and see whether the inverse method converges to a solution which is similar to the best estimate. The inverse method is sensitive to this initial guess, as discussed later.

6.3.1 Pseudodata Case

The first test to ensure that the inverse modeling will work uses the above "pseudodata" so that the transport model is perfect. Since the methodology used here is a recursive weighted least squares, and the problem is linear, we would expect that this case will work.

Figure 6. 2 shows the time evolution of the solution for the "pseudodata" case. For each of the five regions, the figure shows the time evolution of the emissions estimate, as the inverse method time-steps through the observations and model results at each site. Time here, is not the same as in the transport model, but merely shows the addition of information at each observing station for the 365 days of the analysis. Note that although the original estimate of the emissions is incorrect (all emissions were from the Southern Hemisphere source region), the estimate of emissions converges to the correct value, which is the value used in the forward simulation to derive the "pseudodata" observations. The figure also shows that the emissions from some regions are better resolved by the inverse method than others. For example, the North American and European sources are well resolved, while the Asian and Japan and Korean sources are less well resolved, as seen in the larger uncertainties in the emission estimates.

This step shows that the inverse method in combination with a perfect transport model and the 8 observing stations is capable to determining emissions accurately, even with a very poor *a priori* estimate of the emissions.

6.3.2 Sensitivity to Errors at the Observing Stations

Unfortunately, our transport model is not perfect, as seen in Chapters 4 and 5. This section seeks to address how sensitive the emission estimates are to errors in the model transport which lead to errors in the concentration estimates at the stations. This information is also obtainable, but in an average sense from the SVD analysis conducted in Section 6.2.2. Here we assume that the errors seen in Chapter 5 are entirely due to transport in the models and not bad *a priori* emission estimates in order to gain an estimate of how the errors in the transport model will affect the emission estimates.

This analysis also gives us an estimate of how sensitive the emissions estimates are to realistic differences in concentrations at the observing sites. If the differences between the observed and modeled concentrations are due to the emission estimate we used in Chapter 5, we can then ask how much would the emission estimates have to change in order to reduce the error.

In order to study this, the pseudodata case was run, but at each station in succession, a mean bias was introduced. A unit mean bias was introduced at one station at a time, and the resulting impact at each emission region are shown in Table 6.5.

Table 6.5: Percent Emission Sensitivities to 1ppt Model Error

Observing Site	North America	Europe	Asia	Japan/Korea	Southern Hemisphere
Barrow	6.0	0.5	-34.7	-2.2	4.2
Ireland	-2.6	-6.0	19.1	-1.1	0.6
Niwot	-13.7	2.8	17.4	8.1	0.8
Hawaii	6.0	2.1	2.0	-41.3	-0.007
Barbados	-2.7	-0.9	4.2	-2.2	-0.3
Samoa	1.0	0.7	-8.4	0.8	-6.6
Tasmania	0.08	-0.07	-1.1	5.0	-19.9
South Pole	0.2	0.2	-3.7	4.0	-9.8

Some of the source regions are highly sensitive to model errors: for example Asia is sensitive to errors at Barrow, or Japan/Korea to errors at Hawaii, with sensitivities of 35 and 41 percent, respectively. This is consistent with the SVD analysis in Section 6.2.2, where we saw that the source strength of these two regions are very sensitive to errors in the measurements or transport model. The change in estimated source strength in the North American and Southern Hemisphere source regions are 14% and 20% for a 1 ppt error at the Niwot and Tasmania stations, respectively. The change is only 6% in the European source region to a 1 ppt error at Ireland. It is unclear why the North American and Southern Hemisphere source regions are so much more sensitive than the European source region to errors at the closest site. The average value of the partial derivatives for these cases are quite similar. Presumably, the North American and Southern Hemisphere source regions are less well constrained by other observing sites than the European source region.

In this section, we can gain a sense of the propagation of errors in the whole system of 365 equations of the form 6.8. The errors in emissions can be quite large even when a small error in the transport model or observation at a site is assumed, and may prevent us from obtaining a reasonable estimate of emissions.

6.4.0 Application of Inverse Method

The first application of the inverse method to determine the emissions from observational data and a transport model (using NMC winds) will use all the information we have available: the known biases in the transport model will be corrected, so that the mean observed concentration and mean modelled concentration at each site is the same in the annual average; and our best estimate of the emissions from each region is used, along with a 25% uncertainty. We will call this Case 1. Because the mean bias in the model is removed, the noise in the observational noise matrix is also reduced as discussed in section 6.2.1 The time evolution of the emission strength of

each region is shown in Figure 6.3, and the difference between the final estimate and the initial estimate is shown in Table 6.6. The final estimate of emissions suggests that the emissions from Europe and the Southern Hemisphere source regions are slightly less than the *a priori* estimate, while emissions from Asia and Japan and Korea source regions are higher than the initial estimates. The final estimate of the emissions is within the initial uncertainty in the *a priori* emission estimate, demonstrating that consistent *a priori* error estimates have been used in the problem.

Table 6.6: Percent Differences in Emission Estimates from the *a priori* Estimates

	Case 1 MATCH-NMC mean bias at sites removed; best estimate of emissions used.	Case 2 MATCH-NMC best estimate of emissions used
North America	+7	+1
Europe	-17	-27
Asia	+19	+21
Japan/ Korea	+18	+18
Southern Hemisphere	-23	-3
Total	-.1	-4

Next, the same inversion is conducted, but without removing the mean bias from the stations. We will call this inversion Case 2. Here we are checking that if we did not have an *a priori* estimate of what the mean biases were, how able would we be to obtain consistent emission estimates. The differences from the *a priori* emission estimates to the final emission estimates are shown in Table 6.6. Here the emission estimates from Europe show a decrease that is approximately equal to the uncertainty range (25%), while emissions from both the Asia and Japan/Korea source regions show a corresponding increase. Again the emission estimates are approximately within the initial uncertainty, suggesting that the error estimates in section 6.1.2 are reasonable.

These two simulations suggest that the inverse method and *a priori* error estimates have been consistently used, since the differences between the initial emissions and final emissions are within the initial estimate of the uncertainty in the emissions. The inversions also suggest a more refined emissions estimate. Since it is unclear whether the bias errors in the model simulations are due to errors in the emissions estimates, or the transport model, or the initial distributions, we will use the second case, that where the mean bias is not removed from the simulations as our best new estimate for the emissions of CCl_3F during 1990-1991. These are shown in Table 6.7. In addition, the estimated uncertainty in the emission estimate is shown. For the global total, the square root of

the squares of the uncertainties for each emission region is shown as the uncertainty (although this will overestimate the uncertainty, since the uncertainty in the regions are correlated).

Table 6.7: CCl_3F Emission Estimates

(estimated uncertainty in parenthesis)

	Case 2: MATCH-NMC best estimate of emissions used (25% uncertainty)	Case 3: MATCH-NMC best estimate of emissions used (100% uncertainty)	Case 4: MATCH-ECMWF same as Case 3	Case 5: Monthly Averaged same as Case 3
North America	92.8 (9.5)	29.9 (23.7)	-3.2 (25.5)	57.8 (43.6)
Europe	61.7 (9.7)	35.4 (12.8)	35.7 (14.5)	11.1 (29.8)
Asia	39.2 (7.7)	85.3 (39.9)	178.9 (44.5)	70.5 (55.0)
Japan/ Korea	30.2 (6.2)	97.9 (40.7)	23.1 (40.0)	96.7 (64.88)
Southern Hemi-sphere	19.7 (4.1)	14.5 (7.2)	46.9 (10.5)	41.2 (19.8)
Total	243.6 (18.8)	263.0 (63.4)	291.9 (67.4)	277.3 (102)

These also suggest that emissions from Europe are approximately 25% lower than the *a priori* estimates would suggest. This estimate of lower emissions of Europe could be closer to the true than the *a priori* estimate, since the *a priori* estimate is based on emissions in 1988, and by 1990 the emissions from Europe should be decreasing due to the signing of the Montreal Protocol. The inversion also suggests that the proportion of emissions from the Asia and Japan/Korea regions have increased by 20%. This result is also not surprising, since emissions from these regions will not be reduced at the same rate as the global mean, due to the Montreal Protocol's treatment of different counties. Developed nations are expected to cut their emissions of CCl_3F much faster than developing countries.

These above simulations have shown that the *a priori* error estimates made in the previous section are consistent, and also result in a new estimate of emissions. Next we relax the uncertainty in the initial emissions to explore what solution the inverse method would converge to, if there was little *a priori* information about the emissions from the different regions. This test will examine the feasibility of using this type of inversion study to deduce the sources of gases whose emissions are much less well known than the CCl_3F case.

First, we increase the uncertainty in the *a priori* emissions estimate to be 100% of the largest

emission region (North America) and call this Case 3. The results from this simulation are shown in Figure 6. 4, and the results presented in Table 6.7. Notice that the emissions estimates change dramatically if we no longer constrain the initial emission estimate with a 25% uncertainty. Emissions from North America and Europe decrease dramatically, while emissions from the Asia and Japan/Korean source regions increase dramatically.

Instead of using MATCH-NMC model results, we can do a similar study using the MATCH-ECMWF results, thus testing the sensitivity of the inverse method result to the transport model. This is Case 4, and is shown in Table 6.7. The global total is within 15% of the *a priori* best estimate. Similar to Case 3, emissions from North America and Europe are much smaller than the a priori estimate, while emissions from Asia are much larger. It is dissimilar to Case 3 in that emissions from the Japan/Korean source region are not much changed from the *a priori* estimate, while emissions from the Southern Hemisphere source region are much higher. These results seem worse than the results using the MATCH-NMC simulations, which is consistent with the conclusions from Chapter 5 that the MATCH-NMC simulations of CCl_3F were closer to the observations than the MATCH-EC simulations.

We can do the same tests using monthly averaged data instead of daily averaged data using the MATCH-NMC simulation. Here we assume that the errors in the observations and model transports are uncorrelated with time. Similar to the daily averaged case, the emission estimates after inversion are within the *a priori* assumptions for Cases 1 and 2 using monthly averaged data. Case 5 is the same as Case 3, except using monthly averaged input and the MATCH-NMC model simulation. Similar to Case 3, the monthly averaged data with an assumption of 100% uncertainty in the initial emissions estimate is dramatically different than the inversion with a 25% uncertainty estimate. The evolution of the emission estimate is shown in Figure 6. 5, and demonstrates that using monthly averaged data leads to higher uncertainty. This is consistent with the fact that there were fewer data used in the inversion (12 instead of 365). It also does not appear that the solutions have converged (meaning that they are still changing with each new piece of data at the end of the iteration). The qualitative behavior of the Case 3 and Case 5 solutions is similar, except for the Southern Hemisphere source region. In Case 3, the emissions from the Southern Hemisphere source region were estimated to be smaller than the *a priori* estimate, while in Case 5, the emissions were larger than the *a priori* estimate.

Note that the inverse modeling is quite successful in all Cases using the MATCH-NMC simulation diagnosing the global total emissions, as well as the total Northern Hemisphere emissions and Southern Hemisphere emissions. Since the MATCH-EC simulation did not reproduce the interhemispheric gradient, it is not surprising that the hemispheric distribution of emissions was not as good in the inversion using the MATCH-EC simulation. The inversion has a more difficult time deducing the longitudinal distributions of source regions at approximately the same latitudes using either the MATCH-NMC or MATCH-EC modelled concentrations.

Next we look at the residuals between the observed and modelled concentration at each site for each of the emission estimates calculated in the cases described above. In addition, for comparison, we calculate the residual for the case of our best *a priori* estimate of emissions. The residual is calculated by squaring the difference between the modelled and observed concentration at each site and time, then dividing by the number of observations used, and taking the square root, and so the units are ppt. The residuals are shown in Table 6.8.

Table 6.8: Residual concentration (ppt) (root mean squared difference between modelled and observed concentration)

Case	Residual concentration (ppt) using inverse method estimate	Residual concentration (ppt) using *a priori* information only
Case 1: MATCH-NMC best estimate of emissions used (25% uncertainty) and mean bias removed	2.6	3.5
Case 2: MATCH-NMC best estimate of emissions used (25% uncertainty)	3.2	3.5
Case 3: MATCH-NMC best estimate of emissions used (25% uncertainty)	2.9	3.5
Case 4: MATCH-ECMWF same as Case 3	4.7	6.3
Case 5: MATCH-NMC monthly averaged same as Case 3	2.3	3.1

As expected, the residuals using the emissions estimated from the inverse method are smaller than the residuals calculated using the *a priori* estimate of emissions. In addition, as we release the initial constraints on the emission estimate, the residuals decrease (compare Case 2 and Case 3), as expected. Case 1 has small residuals, since the mean bias is removed from the model values. The residuals are larger for the MATCH-ECMWF calculation than for the MATCH-NMC calculation, for both *a priori* emissions and emission from the inversion process. This is consistent with our earlier conclusion in Chapter 5 that the transport in the MATCH model is better using the NMC winds than the ECMWF winds. The residual concentrations are smaller when only month averaged concentrations are used, which indicates that monthly averaged values are predicted better by the transport model than daily averaged values. The residuals are less than the error estimates made in section 6.2.1.

6.5.0 Summary and Conclusions

An optimal estimator (specifically, the recursive weighted least squares, a simple form of the Kalman filter) was used to provide emission estimates for CCl_3F and to examine whether emissions of less well-defined species can be deduced. High frequency observations available at 8 stations

globally were compared to model simulations of CCl_3F using the MATCH model with NMC reanalysis winds.

The assumed errors in the input variables to the inversion procedure were rather large. We specifically calculated the accuracy in the observations and assume precision errors of 2 ppt. There are also errors in the initial state used in the transport model, errors in the transport model itself, plus errors in the temporal and spatial distribution of the emissions regions, which we estimate to be equivalent to concentrations errors of approximately 5 ppt. The difference between the observations and the model estimated initial state and averages to about 15 ppt. We have an initial estimate of the emissions, which we assume accurate to 25%. These assumptions in the errors and uncertainties may well be wrong, but using the inverse method with the above assumptions results in emission estimates which are within the *a priori* emission uncertainties, implying that the *a priori* errors are at least consistent. We have provided an improved estimate of the emissions, shown in Table 6.7 (Case 2), which implies that emissions from Europe are lower by 25% and emissions from the Asia and Japan/Korea emission regions are higher by about 20% than the initial emission estimates. These results seem reasonable considering the initial emission estimates are from 1988, before the impact of the Montreal Protocol.

Next we considered whether we can predict emission estimates which are reasonable for trace gases whose emissions are less well-known than CCl_3F. To test this, we increased the initial uncertainty so the emission estimates were largely unconstrained by the initial estimate. The resulting emission estimates for specific regions from the inverse method were dramatically different than the emission estimates using a 25% uncertainty in the initial emission estimates. However, the global total emissions, and the total Northern Hemisphere and Southern Hemisphere sources are not dissimilar.

These results suggest the total emissions of a trace gas with unknown emissions can be correctly deduced using this type of chemical transport model and inverse method. In addition, estimates of hemispheric total emissions are also reasonable. However, deducing the longitudinal distribution of sources at largely the same latitude is more difficult given the 8 available stations. Either the initial emission estimates are incorrect, or the transport model is not accurate enough to significantly improve emission estimates for regions at the same latitude

It is not clear why the inverse method was not able to capture longitudinal information. It may be that errors in the transport model, errors in the assumed emission distributions within each region or the small number and location of observation sites is responsible for the errors. The errors in the transport model could be due to the subgrid-scale parameterizations, such as boundary layer mixing or moist convective mixing. Since CCl_3F is usually fairly well mixed in the vertical, it is most likely that the analyzed wind fields are causing the errors. We should also examine the accuracy of the observations themselves for defining the appropriate spatial and temporal averages used to compare with the model runs.

The differences between the MATCH-ECMWF and MATCH-NMC simulations in Chapter 5, and the differences in the emission estimates from these two model simulations in Chapter 6 suggest that the combination of the different wind fields and different moist convective scheme can result in substantial differences in the model predictions. As seen in Chapter 6, the difference in emission estimates using the two different simulations were as much as 100% for the North American

and Southern Hemisphere source regions.

While the analyzed wind fields should be similar in regions with many meteorological observations, regions with few observations, such as east (upwind) of Barbados, most of the Southern Hemisphere and over the oceans, will differ due to the model used in the analyzed wind fields. Another difference between the ECMWF and NMC wind fields is that the ECMWF wind fields have been truncated from T106 to T42 before being used for this analysis. That may introduce errors. We saw this in the predictions of convective precipitation in Chapter 3, where the ECMWF dataset with the Tiedtke scheme did not do as well as the Pan scheme with the NMC dataset in reproducing the spatial distribution of convective precipitation. This could be indicative of truncation introducing errors which lead to bad estimates of convergence of moisture (the trigger for moist convection for the Tiedtke scheme). The convergence of air is a residual term, and would be sensitive to truncation errors. The convergence in the tropical region may well be responsible for interhemispheric transport [Hartley and Black, 1995].

In addition, we note that many of the stations used for this analysis are actually located in regions where the transport is least well-known--in remote oceanic regions. Barrow, Barbados, Mauna Loa, Samoa and Tasmania are in regions where most of the transport from the largely Northern Hemisphere sources will have to have travelled across regions which are not well defined by the meteorological observational data available. Thus transport in these regions will depend on model results from the forecast center models instead of observational data. In addition, it may be difficult for the model to capture variations at the Niwot Ridge, Colorado site, since it is in the complex terrain of the Rocky Mountains.

Additional observational sites may well improve the emission estimates gained from this type of inversion. And these observational sites could be located in a manner to reduce the errors introduced into the emission estimate. In this study, most of the errors we have assumed come from the transport model, so placing the observational sites close to the emission regions should reduce the dependence on the transport model, and thus perhaps reduce the uncertainty in the final estimate. Unfortunately, this approach might well backfire, since errors due to boundary layer mixing, moist convective mixing, and the regional distribution of emissions become more important closer to the source region.

Appendix to Chapter 6

An "averaged" partial derivative matrix for the MATCH-NMC simulation of CFC-11 as described in the text is shown in the following Table:

Partial Derivative Matrix(times 1e-2)

Observing Site	North America	Europe	Asia	Japan/Korea	Southern Hemisphere
Barrow	1.9	2.6	2.0	2.7	0.2
Ireland	3.1	6.15	1.5	2.0	0.26
Niwot	5.7	1.4	1.5	2.2	0.5
Hawaii	1.6	1.0	1.3	1.9	0.6
Barbados	2.4	2.4	1.3	1.5	0.6
Samoa	0.3	0.3	0.4	0.4	1.3
Tasmania	0.1	0.1	0.2	0.1	6.4
South Pole	0.1	0.1	0.1	0.1	1.6

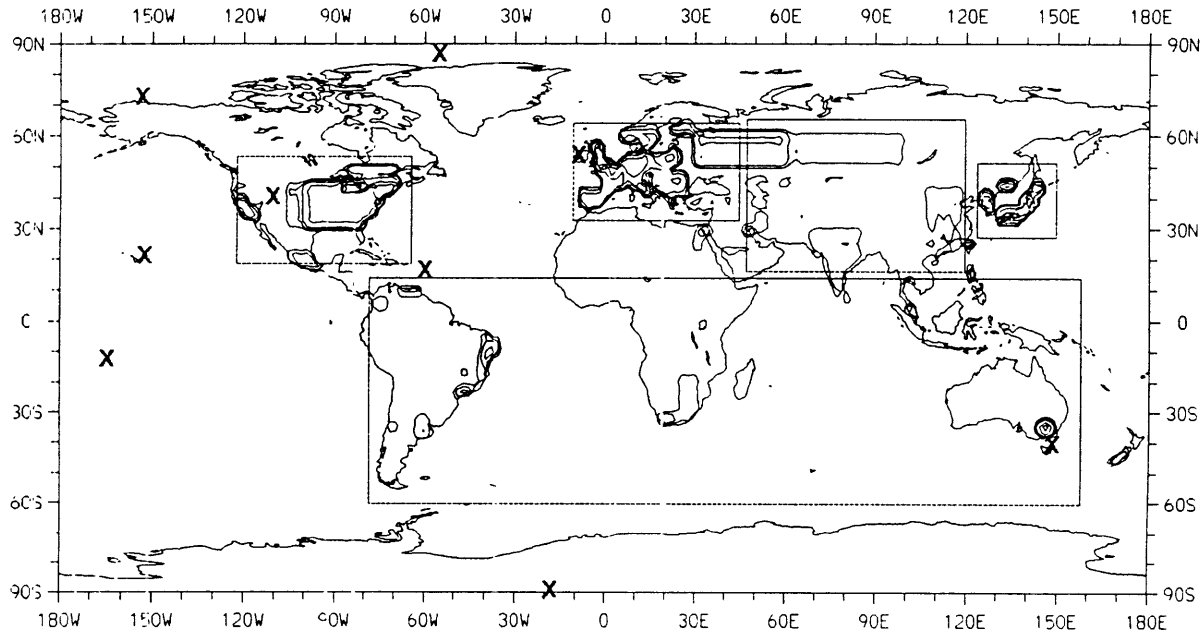

Figure 6.1: Distributions of CCl_3F emissions globally [Hartley and Prinn, 1993] as well as the location of the observing sites, and emission regions used in this study.

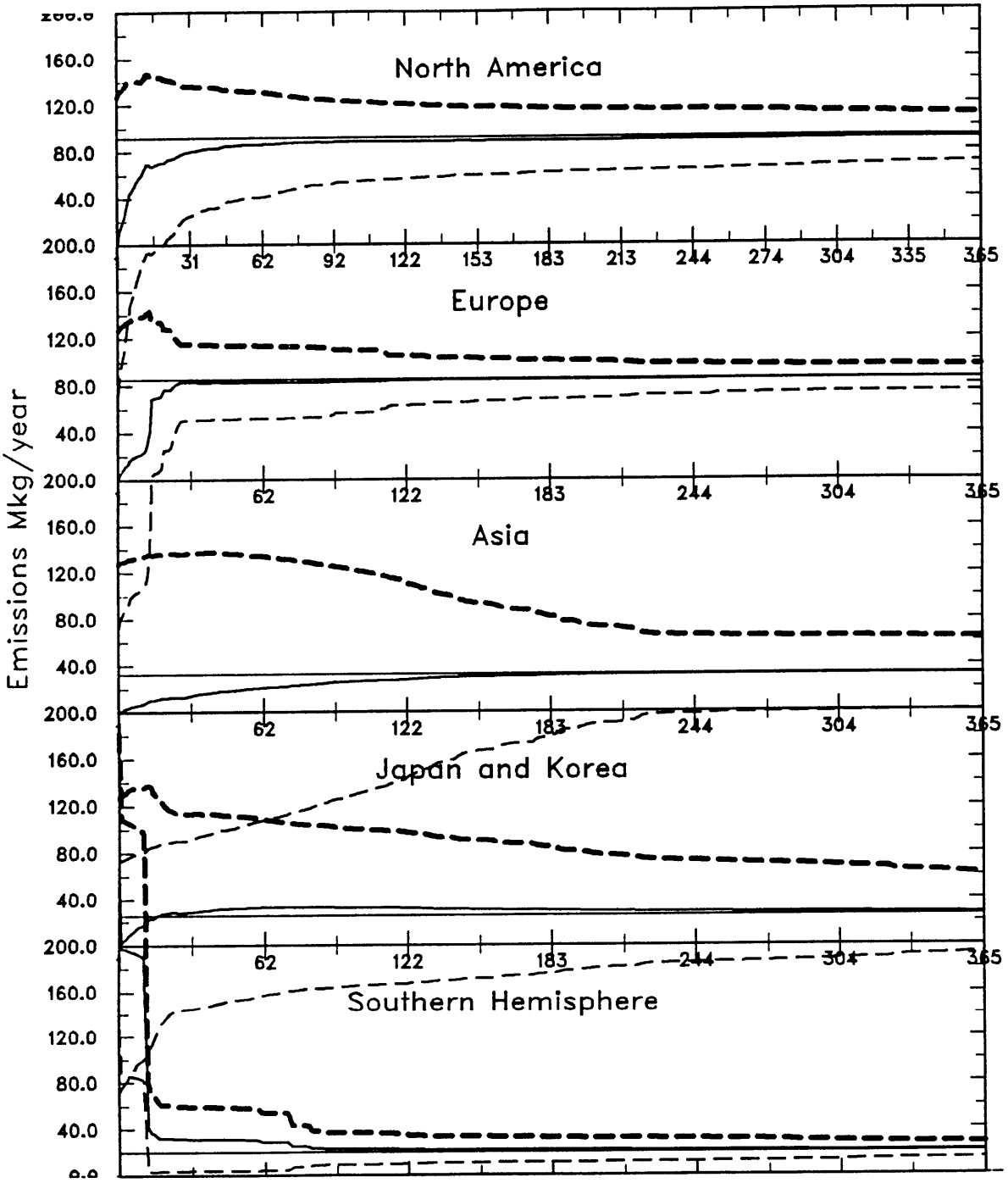

Figure 6.2: Time evolution of the emission factor for each of the emission regions and the uncertainty in the emissions for the "Pseudodata" Case described in the text. The straight solid line represents the a priori best estimate, while the time-varying solid line is the best estimate from the inverse method. The dotted line represent the uncertainty bounds for the inverse method's best estimate.

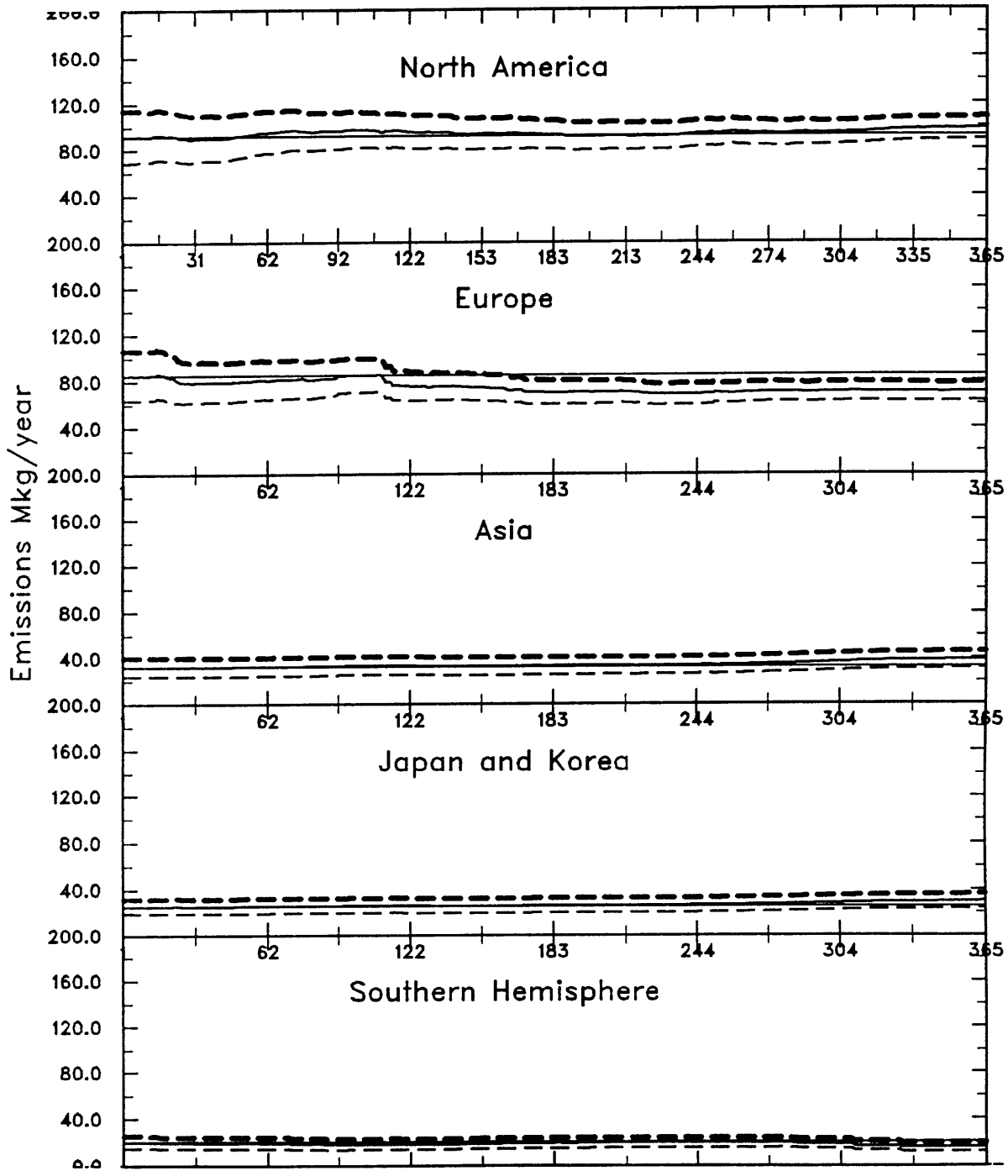

Figure 6.3: Time evolution of the emission factor for each of the emission regions and the uncertainty in the emissions for Case 1 (described in the text).

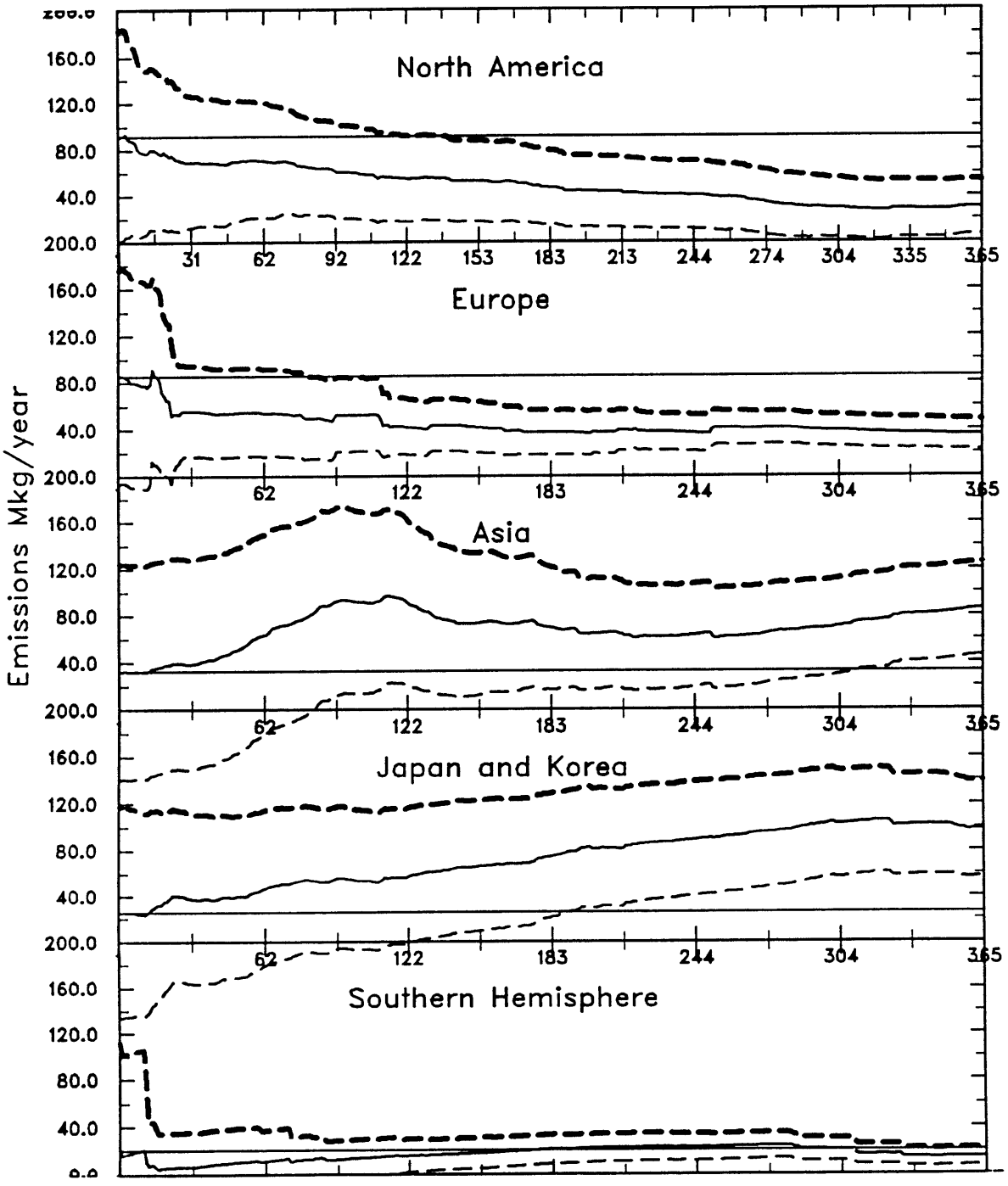

Figure 6.4: Time evolution of the emission factor for each of the emission regions and the uncertainty in the emissions for Case 3 (described in the text).

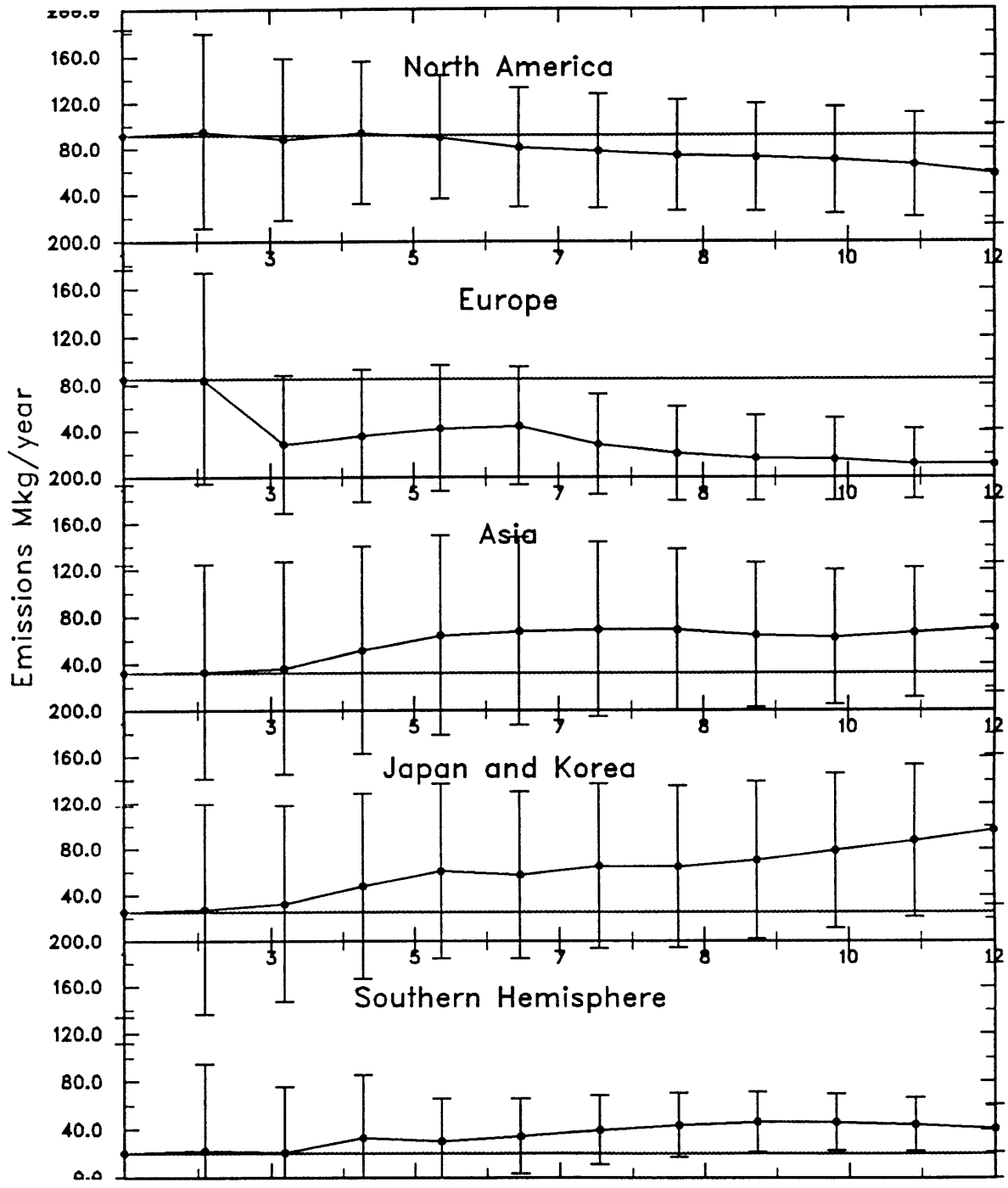

Figure 6.5: Time evolution of the emission factor for each of the emission regions and the uncertainty in the emissions for Case 5 (described in the text).

Chapter 7:
Summary and Conclusions

The goal of this thesis was to build a chemical transport model based on forecast center winds which would be accurate enough to be used to deduce the surface sources of trace gases using an inverse method. First, a cumulus convection parameterization is chosen for the chemical transport model, and implemented in MATCH (Model of Atmospheric Transport and CHemistry), which is capable of simulating transport using either ECMWF analyses or NMC reanalysis datasets. Next MATCH is used to simulate ^{222}Rn and CCl_3F and a comparison was made between observed concentrations and modeled concentrations. Finally, MATCH was used in combination with an optimal estimator technique to deduce the surface sources of CCl_3F. Here we summarize the results from each of these steps.

First, this thesis sought to define the range of behavior of moist convective schemes and point towards more reliable formulations for inclusion in chemical transport models. The emphasis was on deriving convective transport from meteorological datasets (such as from the forecast centers) which do not routinely include convective mass fluxes. Eight moist convective parameterizations were compared in a column model to examine the sensitivity of the vertical profile of trace gases to the parameterization used in a global chemical transport model. The moist convective schemes examined were the Emanuel scheme [Emanuel, 1991], the Feichter-Cruzten scheme [Feichter and Crutzen, 1990], the inverse thermodynamic scheme [Mahowald, et al., 1995], two versions of a scheme suggested by Hack [Hack, 1994], a simplified Arakawa-Schubert [1973] scheme [Pan, National Meteorological Center, personal communication, 1995], and two version of a scheme suggested by Tiedtke (one following the formulation used in the ECMWF (European Center for Medium Range Weather Forecasting) and ECHAM3 (European Center and Hamburg Max Planck Institute) models [Tiedtke, 1989] and one formulated as in the TM2 (Transport Model-2) model [Heimann, personal communication, 1992]. These convective schemes vary in the closure used to derive the mass fluxes, as well as the cloud model formulation, giving a broad range of results. In addition, two boundary layer schemes are compared: a state of the art non-local boundary layer scheme [Holtslag and Boville, 1993] and a simple adiabatic mixing scheme described in this paper. Three tests were used to compare the moist convective schemes against observations. Although the tests conducted here can not conclusively show that one parameterization is better than the others, the tests are a good measure of the ability of the schemes to transport trace gases in a realistic manner under important meteorological conditions. From these tests three moist convection schemes and one boundary layer scheme were considered as the most promising for use in CTMs such as the National Center for Atmospheric Research's (NCAR) off-line model. For moist convection the Pan scheme from the NMC reanalysis, the ECHAM3 form of the Tiedtke scheme and the inverse thermodynamic scheme performed well in the tests against observations. For the boundary layer the results of the non-local boundary layer scheme were more similar to observations than the simple adiabatic mixing scheme. Our results suggest that the middle and upper troposphere trace constituent profiles may not be sensitive to the boundary layer scheme employed in the model. The results of this one-dimensional study imply that conclusions of chemical transport modeling studies can be highly sensitive to the convective parameterization used in the transport model.

Next, the ability of an "offline" chemical transport model to recreate subgrid scale mixing and transport using forecast center winds available every 6 hours was considered. The MATCH model was developed to derive moist convective mixing parameters using either the Tiedtke [1989] or Pan [personal communication, 1995] schemes and the non-local boundary layer mixing scheme of Holtslag and Boville [1993]. Comparisons against relevant coefficients derived in the online CCM2 were compared to values calculated offline and demonstrate that the offline values are reasonable. In addition, simulations with forecast center winds seem to indicate that the model does a reasonable job with observed winds as well. Finally, a comparison of an online simulation of inert tracers with an offline simulation indicates that offline models should do a good job of advecting tracers, even when information is only available every 6 hours, as is the case with the forecast center winds.

To test the transport ability of the MATCH model, simulations of ^{222}Rn and CCl_3F were made and compared with observations. Here, winds from both the European Center for Medium-Range Weather Forecasting (ECMWF) and the National Meteorological Center (NMC) are used in simulations of ^{222}Rn, allowing a comparison of results from two datasets. The model is able to reproduce the general characteristics of the transport of trace gases, and can simulate many specific pollution events. Simulated concentrations and observed concentrations may differ by a factor of 4 in the case of a short-lived species such as radon at Mauna Loa, while at other stations, the mean simulated concentrations are much more similar to those observed. Comparisons are also made of the vertical structure of the radon concentrations, indicating that including the mixing by moist convection is important for species with e-folding lifetimes similar to Radon-222 (5.5 days). In addition, comparisons between versions of the model indicate that concentrations predicted by the models may differ by 40% in the upper troposphere on monthly and zonally averaged scales.

The MATCH model was used with both ECMWF and NMC winds to simulate CCl_3F for the year July,1990 to June, 1991. Comparisons were made with observations at 9 sites from the ALE/GAGE and CMDL networks. Both model simulations do a good job of simulating synoptic scale events and seasonal cycles, although there are discrepancies between the simulations and observations. The version of the model run with NMC winds seems to be able to simulate the observed interhemispheric gradient more accurately than the version run with ECMWF winds. Both models overpredict the concentration of CCl_3F in the mid-latitude and high latitude lower stratosphere.

Finally, the transport model was used with an optimal estimator (recursive weighted least squares, which is a simple version of a Kalman filter) to calculate the sources of CCl_3F. The surface fluxes were divided into five different emission regions: North America, Europe, Asia, Japan/Korea and the Southern Hemisphere, and the best estimate of the emissions from these regions is used as an *a priori* information to constrain the solution. *A priori* error estimates due to observational error, transport model error, error in the initial conditions in the model, and error in the distribution of emissions were made. The results suggest that these *a priori* error estimates were reasonable. In addition a "pseudodata" (where model output is used as the observations) case was conducted, demonstrating that the optimal estimator works in a perfect model.

Next, the a priori information about the uncertainty in the emissions is ignored, and the inverse method is allowed to obtain an emission estimate less constrained by *a priori* information. The emission estimates for each region in this case are very different than our *a priori* estimate, suggesting either that the *a priori* estimate of uncertainty in emissions is incorrect or that the transport model used with the optimal estimator was not able to deduce the emissions accurately given the observations available. However, the global mean emissions and the hemispheric total emissions were accurately deduced using the MATCH-NMC simulations.

This study suggests that emissions from different latitudes may be distinguishable using the MATCH model and a optimal estimator-3-dimensional inverse method, but that obtaining information about the longitudinal distribution of sources at the same latitude may be more problematic. In terms of the problem of the naturally occurring sources of greenhouse gases (e.g. carbon dioxide or methane), this type of approach may well provide valuable information about the sources, since good global estimates and latitudinal estimates are not available from emission inventories. It seems that by using daily average model and observed values, more information is available to the inverse method, and thus more information about the emissions can be extracted. Thus, a model based on forecast center winds providing reliable daily information, such as the MATCH model is a good choice for inverse modeling studies.

The reasons for the bias in the inversion emission estimates are unclear, and could be due to errors in the transport model or errors in the regional emission estimates. Sensitivity studies for the inverse method indicate an uncertainty in the emission estimates as large as 100% when the forecast center analyses is changed. Placing stations closer to the emission region would reduce the dependence of the result on the winds used, although it might increase errors due to subgrid-scale mixing and the initial distribution of emissions within each region.

This work has suggested some important future studies.

- **Improvements in transport model.** It may be possible to improve the chemical transport model, MATCH, by improving the boundary layer parameterization, moist convective parameterization or by increasing the horizontal resolution. However, there are limits to how well a chemical transport model, which must assume that concentrations are well mixed in an entire gridbox of size approximately 200 km by 200 km, can simulate concentrations at a specific station, which is often located right at the surface. In addition, improved forecast center analyses may improve the transport predictions.
- **Improvements in emission estimates**. The results of this study may be quite dependent on the spatial and regional distribution of emissions assumed for the study. A sensitivity study of the assumed emissions might suggest how important the assumed emission distribution is. For example, the Tasmania station was largely used by the inverse method to determine the magnitude of the Southern Hemisphere source region. If the emissions from Australia were off by 30%, the inverse method might well produce results with an error of 30%.
- **Implications for other gases.** This study has some implications for determining the

sources of other gases, but using the same model simulations, more information may be extractable. For example, we could examine sampling strategies for observing networks, such as whether sites should be placed upwind, downwind or in the middle of emission regions. Many of the greenhouse gases are observed at many more stations than 8, but there is only monthly mean data available. How would the inverse modeling work in that case?

References

Allen, D., R. Rood, A. Thompson, R. Hudson, Three-dimensional Rn-222 calculations using assimilated meteorological data and a convective mixing algorithm, submitted to *J. Geophys. Res.*, 1995.

Arakawa, A. and W. Schubert, Interaction of a cumulus cloud ensemble with the large scale environment, Part I, *J. Atmos. Sci.*, 31, 674-701, 1974.

Austin, P. M. and R. A. Houze, A technique for computing vertical transports by precipitating cumuli, *J. Atmos. Sci.*, 30, 1100-1111, 1973.

Balkanski, Y., D. Jacob, R. Arimoto, M. Kritz, Distribution of ^{222}Rn over the north Pacific: Implications for continental influences, *J. Atmos. Chem*, 14, 353-374, 1992.

Brost, R. A., and Chatfield, R. B., Transport of radon in a subhemispheric model, *J. Geophys. Res.* 89, p. 5095-5119, 1989.

Brost, R. A. and M. Heimann, Parameterization of cloud transport of trace species in global 3-D models, paper presented at Air Pollution Modeling and Its Application VIII, pp. 465-483, 1991.

Bartlett, K., Harriss, R., and Sebacher, D., Methane flux from coastal salt marshes, *J. Geophys. Res.*, v. 90, p. 5,710-5,720, 1985.

Brost, R. and Heimann, M., Parameterization of cloud transport of trace species in global 3-d models, *Air Pollution Models and Its Application VIII*, ed. H van Dop and D. Steyn, Plenum Press: New York, 1991.

Brost, R. and Heimann, M., The effect of the global background on a synoptic-scale simulation of tracer concentration, *J. Geophys. Res.*, v. 96, p.15,415-15,425, 1991.

Brown, M., Deduction of Emissions of source gases using an objective inversion algorithm and a chemical transport model, *J. Geophys. Res.*, 98, 12639-12660, 1993.

Chatfield, R. B. and P. J. Crutzen, Sulfur dioxide in remote oceanic air: cloud transport of reactive precursors, *J. Geophys. Res.*, 89 (D5), 7111-7132, 1984.

Cicerone, R. and Shetter, J., Sources of Atmospheric methane measured in rice paddies and a discussion, *J. Geophys. Res.*, v. 86, p.7,203-7,209, 1981.

Cicerone, R., Shetter, J., and Delwiche, C., Seasonal variation of methane flux from a California rice paddy, *J. Geophys. Res.*, v. 88, p.11,022-11,024, 1983.

Crutzen, P, Aselmann, E, and Seiler, W., Methane production by domestic animals, wild ruminants, other herbivorous fauna, and humans, *Tellus*, v. 38B, p. 271-284, 1986.

Cunnold, D., Prinn, R., Rasmussen, R., Simmonds, P., Alyea, F., Cardelino, C., Crawford, A.,

Fraser, P., and Rosen, R., The Atmospheric Lifetime Experiment 3. Lifetime methodology and application to three years of $CFCl_3$ Data, *J. Geophys.* Res., v. 88, p. 8,379-8,400, 1983.

Cunnold, D., Prinn, R., Rasmussen, R., Simmonds, P., Alyea, F., Cardelino, C., Crawford, A., Fraser, P., and Rosen, R., The atmospheric lifetime and annual release estimates for $CFCl_3$ and CF_2Cl_2 From 5 Years of ALE Data, *J. Geophys. Res.*, v. 91, p. 10,797-10,817, 1986.

Cunnold, D., P. Fraser, R. Weiss, R. Prinn, P. Simmonds, B. Miller, F. Alyea, and A. Crawford, Global trends and annual releases of CCl_3F and CCl_2F_2 estimated from ALE/GAGE and other measurements from July 1978 to June 1991, *J. Geophys. Res.*, 99, 1107-1126, 1994.

Daley, R., Atmospheric Data Analysis, Cambridge University Press, England, 1991.

Dickerson, R. R. Huffman, G. J., Luke, W. T., Nunnermacker, L. J., Pickering, K. E., Leslie, A. C. D., Lindsey, C. G., Slinn, W. G. N., Kelly, T. J., Daum, P. H., Delany, A. C., Greenberg, J. P., Zimmerman, P. R., Boatman, J. F., Ray, J. D., and D. H. Stedman, Thunderstorms: An Important Mechanism in the Transport of Air Pollutants, *Science,* 235, p. 460-5, 1987.

ECMWF Research Department, *Research Manual 1: ECMWF Data Assimilation Scientific Documentation,* 1987.

ECMWF Research Department, *Research Manual 3: ECMWF Forecast Model Physical Parameterization,* 1991.

Elkins, J., T. Thompson, T. Swanson, J. Butler, B. Hall, S. Cummings, D. Fisher, and A. Raffo, Decrease in the growth rates of atmospheric chlorofluorocarbons 11 and 12, *Nature,* 364, 780-783, 1993.

Emanuel, K. A., A scheme for representing cumulus convection in large-scale models, *J. Atmos. Sci.*, 48 (22), 2313-2335, 1991.

Emanuel, K. and D. Raymond (Ed.), The representation of cumulus convection in numerical models, *Meteorological Monographs,* 24, 1993.

Emanuel, K.A., *Atmospheric Convection.* Oxford Univ. Press, New York. 580 pp., 1994.

Enting I., and J. Mansbridge, Seasonal sources and sinks of atmospheric CO_2 by direct inversion of filtered data, *Tellus*, v. 41B, p. 11-126, 1989.

Enting I., and G. Newsam, Atmospheric constituent inversion problems: implications for baseline monitoring, J. Atmos. Chem., 11, 69-87, 1990.

Fabian, P., Borchers, R., Flentje, G., Matthews, W., Seiler, W., Giehl, H., Bunse, K., Muller, F., Schmidt, U., Volz, A., Khedim, A., and Johnen, F., The vertical distribution of stable trace gases at mid-latitudes, *J. Geophys. Res.*, v. 86, p. 5179-5184, 1981a.

Fabian, P., Borchers, R., Penkett, S., and Prosser, N., Halocarbons in the stratosphere, *Nature*, v. 294, p. 733-735, 1981b.

Feichter, J. and P. J. Crutzen, Parameterization of vertical tracer transport due to deep cumulus convection in a global transport model and its evaluation with ^{222}Radon measurements, *Tellus*, 42B, 100-117, 1990.

Fraser, P., D. Fisher, P. Bloomfield, S. Sander, M. Ko, Report on concentrations, lifetimes, and trends of CFCs, halons and related species, NASA Reference Publication 1339, ed. J. Kaye, S. Penkett, F. Ormond, January 1994.

Fung, I., John, J., Lerner, J., Matthews, E., Prather, M., Steele, L., and Fraser, P., Three-dimensional model synthesis of the global methane cycle, *J. Geophys. Res.*, v. 96, p. 13,011-13,065, 1991.

Garstang, M., J. Scala, S. Greco, R. Harriss, S. Beck, E. Browell, G. Sachse, G. Gregory, G. Hill, J. Simpson, W. -K. Tao and A. Torres, Trace gas exchanges and convective transports over the amazonian rain forest, *J. Geophys. Res.* 93 (D2), 1528-1550, 1988.

Gelb, A., Applied Optimal Estimation, MIT Press, Cambridge, 1988.

Goldan, P. W. Kuster, D. Albritton, and A. Schmeltekopf, Stratospheric $CFCl_3$, CF_2Cl_2, and N_2O height profile measurements at several latitudes, *J. Geophys. Res.*, 85, 413-412, 1980.

Golombek, A. and R. Prinn, A global three-dimensional model of the circulation and chemistry of $CFCl_3$, CF_2C_2l, CH_3CCl_3, CCl_4 and N_2O, *J. Geophys. Res.*, 91, 3985-4001, 1986.

Grell, G., Prognostic evaluation of assumptions used by cumulus parameterizations, *M. Weather R.*, 121, 764-787, 1993.

Hack, J., B. Boville, B. Briegleb, J. Kiehl, P. J. Rasch, and D. L. Williamson, *Description of the NCAR community climate model (CCM2)*, NCAR Tech. Note, NCAR/TN-382+ STR, NTIS PB93-221802/AS, 108 pp., Natl. Cent. for Atmos. Res., Boulder, Colo., 1993.

Hack, J. J., Parameterization of moist convection in the National Center for Atmospheric Research community climate model (CCM2), *J. Geophys. Res.* 99 (D3), 5551- 5568, 1994.

Harris, J., P. P. Tans, E. J. Dlugokensky, K. A. Masarie, P. M. Lang, S. Whittlestone, and L. P. Steele, Variations in atmospheric methane at Mauna Loa Observatory related to long-range transport, *J. Geophys. Res.*, 97, 6003-6010, 1992.

Hartley, D., *Deducing Trace Gas Emissions Using an Inverse Method in Three-Dimensional Chemical Transport Models*, Ph.D., MIT, 117 pgs, 1992.

Hartley, D., R. Black, Mechanistic Analysis of interhemispheric transport, Geophys. Res. Let., 22, 2945-2948, 1995.

Hartley, D. and Prinn, R, Feasibility of determining surface emissions of trace gases using an inverse method in a three-dimensional chemical transport model, *J. Geophys. Res.*, v.98, p.5183-5198, 1993.

Hartley, D. E., D. L. Williamson, P. J. Rasch and R. G. Prinn, Examination of tracer transport in the NCAR CCM2 by comparison of $CFCl_3$ simulations with ALE/GAGE observations, *J. Geophys. Res.* 99 (D6), 12885-12898, 1994.

Heimann, M. and C. D. Keeling, A three-dimensional model of atmospheric CO2 transport based on observed winds: 2. model description and simulated tracer experiments, *Geophysical Monograph,* 55, 237-275, 1989.

Heimann, M., Keeling, C. and Tucker, C, A three-dimensional model of atmospheric CO_2 transport based on observed winds: 3. seasonal cycle and synoptic time scale variations, *Geophysical Monograph,* v. 55, p.277-303, 1989.

Heimann, M. P. Monfray, G. Polian, Modeling the long range transport of Rn222 to subantarctic and antarctic areas, *Tellus*, 42B, 83-99, 1990.

Holtslag, A. M. and B. A. Boville, Local versus non-local boundary-layer diffusion in a global climate model, *J. Clim.*, 6, 1825-1842, 1993.

Holzapzel-Pschorn, A, and Seiler, W., Methane emissions during a cultivation period from an italian rice paddy, *J. Geophys. Res.*, v. 91, p. 11,803-11,814, 1986.

Hutter, A. R., R. J. Larsen, H. Marin, and J.T. Merril, Radon-222 at Bermuda and Mauna Loa: local and distant sources, *J. Radioanalytical and Nuclear Chemistry,* 193, 309-318, 1995.

Intergovernmental Panel on Climate Change, *Climate Change 1994,* Cambridge University Press, 1995.

Jacob, D., M. Prather, P. Rasch, J. Reichter, I. Kohler, P. Kasibhatla, G. Verver, P. Van Velthoven, J. Dignon, J. Penner, D. Bergmann, C. Genthon, Y. Balkanski, M. Ramonet, P. Zimmermann, S. Beagley, J. de Grandpre, W. Blackshear, W. Greose, D. Rotman, M. Chiba, M. Chipperfield, Z. Stockwell, R. Shia, K. Law, O. Wild, C. Reeves, M. Brown, H. Yang, Intercomparison of global atmospheric transport model using ^{222}Rn and other short-lived tracers, submitted to *J. Atmos. Sci,* 1995.

Jacob, D. J. and M. J. Prather, Radon-222 as a test of convective transport in a general circulation model., *Tellus,* 42B, 118-134, 1990.

Kalnay, E., M. Kanamitsu, R. Kistler, W. Collins, D. Deaven, L. Gandin, M. Iredell, S. Saha, G. White, J. Woollen, Y. Zhu, M. Chelliah, W. Ebisuzaki, W. Higgins, J. Janowiak, K. C. Mo, C. Ropelewski, J. Wang, A. Leetmaa, R. Reynolds, R. Jenne, and D. Joseph, The NCEP/ NCAR 40-Year Reanalysis Project, *Bull. of the Amer. Met. Soc.*, 77,437-471, 1996.

Kanamitsu, M., Description of the NMC global data assimilation and forecast system, *Weather and Forecasting*, v.4, p.335-342, 1989.

Khalil, M. R. Rasmussen, The potential of soils as a sink of chlorofluorocarbons and other man-made chlorocarbons, Geophys. Res. Let., 16, 679-682, 1989.

Kuo, H. L., Further studies of the parameterization of the influence of cumulus convection on large-scale flow, *J. Atmos. Sci.*, 31, 1232-1240, 1973.

Lambert, G. G. POlian, D. Taupin, Existence of periodicity in Radon concentrations and in the large scale distribution at lower altitudes between 40 and 70 South, *J. Geophys. Res.*, 75, 2341-2345, 1970.

Larson, R. E. and Hoppel, Radon 222 measurements below 4 km as related to atmospheric convection, *Pure Appl. Geophys.*, 105, 900, 1973.

Liu, S. C., J. R. McAfee and R. J. Cicerone, Radon-222 and tropospheric vertical transport, *J. Geophys. Res,.* 89 (D5), 7291-7297, 1984.

Lord, S., W. Chao, A. Arakawa, Interaction of a cumulus cloud ensemble with the large-scale environment. Part IV: the discrete model, *J. Atmos. Sci.*, 39, 104-113. 1982

Mahowald, N. M, P. J. Rasch, R. G. Prinn, Cumulus parameterizations in chemical transport models, *J. Geophys. Res.*, 100, 26173-16189, 1995.

McCulloch, A., P. Midgley, D. Fisher, Distribution of emissions of chlorofluorocarbons (CFCs) 11, 12, 113, 114, 115 among reporting and non-reporting countries in 1986, Atmospheric Environment, 28, 2567-2582, 1994.

Moore, H. E., S. E. Poet, and E. A. Martell, ^{222}Rn, ^{210}Pb, ^{210}Bi, and ^{210}Po profiles and aerosol residence times versus altitude, *J. Geophys. Res.*, 78, 7065, 1973.

Mulquiney, J.E., Global atmospheric $CFCl_3$ Flux Estimation, Thesis, Australian National University, Canberra, 1995.

Pan, H.-L. and W.-S. Wu, Implementing a mass flux convection parameterization package for the NMC medium-range forecast model, NMC Office Note, No. 409, 40pp.

Parrish, D. F. and J. C. Derber, The National Meteorological Center's spectral statistical- interpolation analysis scheme, *Mon. Weather Rev.*, 120, 1747-1763, 1992.

Pickering, K. E., A. M. Thompson, J. R. Scala, W. -K. Tao and J. Simpson, Ozone production potential following convective redistribution of biomass burning emissions, *J. Atmospheric Chemistry*. 14, 297-313, 1992.

Plumb R. and X. Zheng, Source determination from trace gas observations, an orthogonal function approach and results for long-lived gases with surface source, submitted to *J. Geophys. Res.*, 1995.

Polian, G. G. Lambert, B. Ardouin, A. Jegou, Long-range transport of continental radon in subantarctic areas, *Tellus*, 38B, 178-189, 1986.

Prather, M., M. McElroy, S. Wofsy, G. Russell and D. Rind, Chemistry of the fluorocarbons as tracers of air motion, *J. Geophys. Res.*, 92, 6579-6613, 1987.

Prinn, R., Cunnold, P., Alyea, F., Boldi, B., Crawford, A., Fraser, P., Gutzler, D., Hartley, D., Rosen, R. and Rasmussen, R., Global average concentration and trend for hydroxyl radicals deduced from ALE-GAGE Trichloroethane (Methyl Chloroform) Data for 1978-1990, J. *Geophys. Res.*, v.97, p.2445-2462, 1992.

Prinn, R., Cunnold, D., Rasmussen, R., Simmonds, P., Alyea, F., Crawford, A., Fraser, P., and Rosen, R., Atmospheric emissions and trends of nitrous oxides deduced From 10 Years of ALE-GAGE Data, *J. Geophys. Res.*, v.95, p.18,369-18,385, 1990.

Prinn, R. and Golombek, A., Global atmospheric chemistry of CFC-123, *Nature,* v. 344, p.47-49, 1990.

Ramonet, M., J. C. LeRoulley, R. Bousque, P. Monfray, Radon measurements during the Tropoz II campaign and comparison with a global atmospheric transport model, *J. Atmos. Chemistry,* 23, 107-136, 1996.

Rasch, P., and D. Williamson, Computational aspects of moisture transport in global models of the atmosphere, *Q. J. R. Meteorol. Soc.,* 116, p. 1071-1090, 1990.

Rasch, P., B. Boville, G. Brasseur, A three-dimensional general circulation model with coupled chemistry for the middle atmosphere, J. Geophys. Res., 100,9041-9071, 1995.

Roeckner, E., K. Arpe, L. Bengtsson, S. Brinkop, L. Dmenil, M. Esch, E. Kirk, F. Lunkeit, M. Ponater, B. Rockel, R. Sausen, U. Schlese, S. Schubert, M. Windelband, *Simulation of the Present-Day Climate with the ECHAM Model: Impact of Model Physics and Resolution,* Max-Planck-Institut fur Meteorologie Report No. 93, Hamburg, FRG, 1992.

Schmidt, U., C. Jebsen, F. Johnen, A. Khedim, E. Klein, D. Knapska, G. Kulessa, J. Rudolph, G. Schumacher, and E. Schunck, Stratospheric observations of long-lived trace gases at midlatitudes 1982-1985 (data report), *Spezielle Berichte der kernforschungsanlage JHlich-Nr 375,* KFA Julich, 1986.

Schmidt, U., R. Bauer, A. Khedim, E. Klein, G. Kulessa, and B. Schubert, *In situ* observations o long-lived trace gases in the Arctic stratosphere during winter, *Ozone in the Atmosphere,* ed. R. D. Bojkov and P. Fabian, 298-301, A. Deepak Publishing, Hampton, VA, 1989.

Schmidt, U., R. Bauer, A. Khedim, G. Kulessa, and C. Schiller, Profile observations of long-lived trace gases in the arctic vortex, *Geophys. Res. Let.*, 18767-18770, 1991.

Schutz, H., Holzapzel-Pschorn, A., Conrad, R. Rennenberg, H., and Seiler, W., A 3-year continuous record on the influence of daytime, season and fertilizer treatment on methane emission rates from an Italian rice paddy, *J. Geophys. Res.,* v. 94, p. 16,405-16,416, 1989.

Seiler, W., Conrad, R., and Scharffe, D., Field studies of methane emission from termite nests into the atmosphere and measurements of methane uptake by tropical soils, J. *Atmos. Chem.,* v. 1, p. 171-186, 1984.

Seiler, W., Holzapzel-Pschorn, A., Conrad, R., and Scharffe, D., Methane emissions from rice

paddies, *J. Atmos. Chem.*, v. 1, p. 241-268, 1984.

Steele, L., Fraser, P., Rasmussen, R., Khalil, M., Conway, I., Crawford, A., Gammon, R., Masarie, K., and Thoning, K., The global distribution of methane in the troposphere, *J. Atmos. Chem.*, v. 5, p. 125-171, 1987.

Strang, G. Introduction to Applied Mathematics, Cambridge Press, Wellesley, 1988.

Tans, P., Conway, T., Nakazawa, T., Latitudinal distribution of the sources and sinks of atmospheric carbon dioxide derived from surface observations and an Atmospheric Transport Model, *J. Geophys. Res.*, v. 94, p. 5151-5172, 1989.

Tiedtke, M., A Comprehensive Mass Flux Scheme for Cumulus Parameterization in Large-Scale Models, *Mon. Weather Rev.*, 117, 1779-1800, 1989.

Trenberth, K. E., *Global analyses from ECMWF and atlas of 1000 to 10 mb circulation statistics,* National Center for Atmospheric Research, NCAR Tech. Note, NCAR/TN- 373+STR, Boulder, Colo., 191 pp., 1992.

Turekian, K., Y. Nozaki and L. Benninger, Geochemistry of atmospheric radon and radon products, *Annual Review of Earth and Planetary Sciences*, pp. 227- 255, 1977.

Wang, C. and J. Chang, A three dimensional numerical model of cloud dynamics, microphysics and chemistry, 1, concepts and formulation, *J. Geophys. Res.* 98 (D8), 14827-14844, 1993.

Wang, C., P. J. Crutzen, V. Ramanthan, and S. F. Williams, The role of a deep convective storm over the tropical Pacific Ocean in the redistribution of atmosphere chemical species, submitted to *J. Geophys. Res.*,1994.

Webster P., J. Holton, Cross-equatorial response to middle-latitude forcing in a zonally varying basic state, J. Atmos. Sci., 39, 722-733, 1982.

Wilkening, M. H., Radon 222 concentrations in the convective patterns of a mountain environment, *J. Geophys. Res.*, 75, 1733, 1970.

Williamson, D. and Rasch, P., Two Dimensional Semi-Lagrangian Transport with Shape Preserving Interpolation, *Monthly Weather Review,* v. 117, p. 102-129, 1989.

Yanai, M., S. Esbensen and J. -H. Chu, Determination of bulk properties of tropical cloud clusters from large-scale heat and moisture budgets, *J. Atmos. Sci.*, 30, 611-627, 1973.

Zhang, G. Z., McFarlane, N.A., Sensitivity of climate simulations to the parameterization of cumulus convection in the Canadian Climate Centre general circulation model, *Atmosphere-Ocean,* 33, 407-446, 1995.